AD-A009 343

STICK-SLIP OF LIGHTLY LOADED ROCK. PART I. DILATANCY AND SHEARING BEHAVIOR OF ASSEMBLAGES OF RODS. PART II

Clarence B. Drennon, et al

Iowa State University
Ames, Iowa

4 February 1975

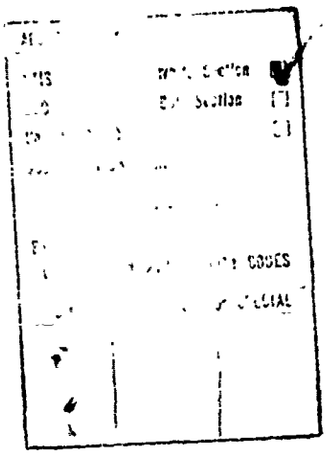

Destroy this report when it is no longer needed.
Do not return to sender.

The views and conclusions contained in this document are those of the authors and should not be interpreted as necessarily representing the official policies, either expressed or implied, of the Defense Advanced Research Projects Agency of the U.S. Government.

UNCLASSIFIED

SECURITY CLASSIFICATION OF THIS PAGE (When Data Entered)

REPORT DOCUMENTATION PAGE		READ INSTRUCTIONS BEFORE COMPLETING FORM
1 REPORT NUMBER DNA 3371F	2. GOVT ACCESSION NO.	3. RECIPIENT'S CATALOG NUMBER AD-A009 343
4 TITLE (and Subtitle) STICK-SLIP OF LIGHTLY LOADED ROCK, Part I DILATANCY AND SHEARING BEHAVIOR OF ASSEMBLAGES OF RODS, Part II		5. TYPE OF REPORT & PERIOD COVERED Final Report for Period 1 Sep 70– 31 Aug 73 6. PERFORMING ORG. REPORT NUMBER ISU-ERI-AMES 74187
7 AUTHOR(s) Clarence B. Drennon and R. L. Handy, Part I Kulbhushan L. Logani and R. L. Handy, Part II		8. CONTRACT OR GRANT NUMBER(s) DASA 01-69-C-0148
9 PERFORMING ORGANIZATION NAME AND ADDRESS Engineering Research Institute Iowa State University Ames, Iowa 50010		10. PROGRAM ELEMENT, PROJECT, TASK AREA & WORK UNIT NUMBERS
11. CONTROLLING OFFICE NAME AND ADDRESS Director Defense Nuclear Agency Washington, D.C. 20305		12. REPORT DATE 4 February 1975 13. NUMBER OF PAGES 210
14 MONITORING AGENCY NAME & ADDRESS(if different from Controlling Office)		15. SECURITY CLASS. (of this report) UNCLASSIFIED 15a. DECLASSIFICATION/DOWNGRADING SCHEDULE

16. DISTRIBUTION STATEMENT (of this Report)

Approved for public release; distribution unlimited.

17 DISTRIBUTION STATEMENT (of the abstract entered in Block 20, if different from Report)

18 SUPPLEMENTARY NOTES

19 KEY WORDS (Continue on reverse side if necessary and identify by block number)

Rock Mechanics	Rock
Sliding Friction	Rock Creep
Stick-slip	Activation Energy
Dilatancy	Shear Testing

20 ABSTRACT (Continue on reverse side if necessary and identify by block number)

Part I of the report deals with stick-slip of selected rocks at different temperatures and under normal stresses up to 20 kg/cm^2. Stick-slip dominated the sliding behavior of roughly ground surfaces of limestone, basalt, and quartzite, but tests of lightly loaded limestone below 100°C almost inevitably involved smooth slip. This was attributed to absorbed water indicated by creep data and rate process theory. Smooth slip was less readily obtained under higher normal loads, and in the harder rocks, suggesting penetration of

DD FORM 1 JAN 73 1473 EDITION OF 1 NOV 65 IS OBSOLETE

PRICES SUBJECT TO CHANGE

UNCLASSIFIED

SECURITY CLASSIFICATION OF THIS PAGE (When Data Entered)

20. ABSTRACT (Continued)

absorbed water films by mineral contact asperities. Because of the strong temperature dependence, stick-slip is attributed to asperity-to-asperity bonding.

Part II presents results from a simple but carefully controlled laboratory experiment to study the relation between dilatance, sliding friction, and resistance to deformation of densely packed assemblages of steel or Teflon rods. Results did not follow the current theories of dilatant behavior, but suggested a simpler model: (a) sliding first occurs along the path of lowest cumulative sliding friction, (b) such sliding brings new surfaces into contact, increasing friction and causing arrested slip, (c) through repetition of this process a failure zone grows and continues to grow in thickness until the number of potential shear paths is depleted and catastrophic failure becomes imminent. Stages of primary secondary and tertiary creep are predicted if time is expressed as cumulative probability. The arrested slip model, while yet unverified in the field, appears preferable to the usual assumption of cohesive or clay-like behavior of joints in rocks.

SUMMARY

This Final Report consists of two sections which, while involving distinctively different research methods and analysis, are closely interrelated in their significance for the stability of rock masses, e.g. rock slides, underground blast caverns, etc.

Part I deals with stick-slip of selected rocks at different temperatures and under normal stresses up to 20 kg/cm^2. Stick-slip was found to dominate the sliding behavior of paired roughly ground surfaces of limestone, basalt, and quartzite. An alternating short-and-long slip with intermediate creep occurred uniquely with the basalt, attributed to slow dissipation of highly localized high temperatures developed from sliding. Tests of lightly loaded limestone below 100^{o}C almost inevitably involved smooth slip, attributed to adsorbed water, supported by creep data and rate process theory. Smooth slip was less readily obtained in limestone under higher normal loads, and in the harder rocks under any loading, suggesting penetration of adsorbed water films by mineral contact asperities.

The coefficient of sliding friction nearly always was initially low and increased with sliding to approach a stable value; higher temperatures increased friction and caused longer sticks and larger slips. Because of this strong temperature dependence, stick-slip is attributed to asperity-to-asperity bonding. The effect of rock debris added between the sliding surfaces was in general to simulate tests under lower normal pressures, and to speed up sliding equilibration.

Part II of this report presents results from a simple but carefully controlled laboratory experiment to study the relation between dilatancy, sliding friction, and resistance to deformation of densely packed assemblages of steel of Teflon rods. The experiment is intended to model the behavior of fractured rock masses deforming under load; but the results also may apply on a smaller scale to sliding of rock grains along incipient fractures of grain contacts. Both occurrences of dilatancy have been confirmed in nature.

Shearing tests were conducted with controlled stresses and monitored movements and volume changes. Results did not follow the current theories of dilatant behavior, but suggested a much simpler model based on probability: (a) As the ratio of principal stresses increases, sliding occurs first along the path of lowest cumulative sliding friction. (b) Since sliding along the path of least resistance brings new surfaces into contact, the new contacts almost inevitably have a higher cumulative sliding friction, causing arrested slip. (c) Sliding then will occur along the next least resistant path, and probably in turn will become arrested. (d) Through repetition of this process a failure zone grows and continues to grow in thickness until the number of potential shear paths is depleted and catastrophic failure becomes imminent.

It is shown by theory and by experiments that arrested slip of cohesionless assemblages can deliver an increasing, decreasing or constant stress ratio, the latter being characteristic of rock creep. A classical time-deformation curve showing stages of primary, secondary and tertiary creep is developed based on an assumed equal likelihood of occurrence of any combination of 1, 2, 3...n slip planes where n is a discrete number. A distinction from viscous creep is the requirement for an increasing shear zone which might be monitored in field situations. The arrested slip model explains rock "noises" preliminary to failure, and appears preferable to the usual assumption of cohesive or clay-like behavior of joints in rocks. The model is sustained by the experiments in Part I of the Report, in that stick-slip dominates in widely varying rock types, and friction tends to increase with slip distance.

PREFACE

The authors gratefully acknowledge the support given by the Defense Nuclear Agency (Defense Atomic Support Agency) and Defense Advanced Research Project Agency, Department of Defense. Especially helpful was the assistance of Col. Lewis Reign and Lt. Col. Louis Circeo.

The authors also acknowledge the generous suggestions and criticisms of Dr. Turgut Demirel, Professor of Civil Engineering, particularly with regard to design of the rock shear apparatus and the application of rate process theory.

Dr. Glen Ferguson deserved a special acknowledgement of his dominant role in design, fabrication, and calibration of the biaxial shear tester, and countless moments of assistance throughout the experiments.

Many others have assisted in and at times have occupied important roles in this research. They are (alphabetically) Major W. W. Badger, Dr. Donald Biggs, Dr. Shyam Bahadur, Mr. Lyell Henry, Professor J. M. Hoover, Dr. R. A. Lohnes and Professor W. F. Riley.

This work was also supported by the Engineering Research Institute at Iowa State University, Ames, Iowa 50010.

TABLE OF CONTENTS

PART II: DILATANCY

Part I

STICK-SLIP OF LIGHTLY LOADED ROCK

C. B. Drennon and R. L. Handy

INTRODUCTION

Statement of the Problem

In naturally occurring bodies of rock, movement of engineering significance does not normally occur in the body of intact rock, but along joints and fracture planes. These features may be part of the geologic structure of the rock, or may be induced by the engineering construction effort in the vicinity of the rock. Whether the joints are caused by earth stresses or by blasting, stress relief, or some other mechanism, these planes of weakness control the strength of a rock body.

As a result of engineering construction work such as cuts in rock or underground excavation, previously heavily loaded rock undergoes a stress relief in the direction of excavation. This may provide a sufficient imbalance of forces to cause movement along the joint planes. This movement will be, initially at least, at a very slow rate. The mode of sliding of relatively smooth rocks over one another is stick-slip. The purpose of this investigation is to determine the mechanism of the stick-slip mode of frictional sliding in rocks with relatively light normal stresses.

Scope

Stick-slip movement occurs when loading systems are soft; that is, the stiffness k in the equation $F = kx$ (F = frictional force, x = distance moved) is small (Jaeger, 1971). Gravity is such a loading system. A loading system was therefore devised in the laboratory to allow the production of stick-slip under controlled conditions. The study included variations in several parameters which were believed to influence a strong effect on stick-slip. Particular emphasis was placed on temperature, since this variable had not been included in previous studies by others. Other important variables included are rock type and effect of debris or gouge created by sliding. Other variables were kept constant in order to isolate those believed to be critical. Relying on preliminary tests and the experience of others, the nominal rate of movement was held constant at about

1.5×10^{-3} centimeters per minute. Also held constant was the surface roughness of the three rock types: All were ground with a number-45 grit aluminum oxide grinding wheel.

The following parameters of stick-slip by use of force and distance transducers and oscillograph recorders: slip times, slip distances, shear load relaxation upon slip, time between slips, and coefficient of static friction.

BACKGROUND AND LITERATURE REVIEW

Sliding Friction

A review of past and current concepts of sliding friction seems necessary in order to understand the various concepts which have been advanced regarding stick-slip of rocks. That an effort is required to move an object along another object, including the earth itself, has been apparent ever since the first sub-human tried it. For a long time we have called the force opposing such movement friction. In the examination of sliding friction, some historical background will be briefly examined. The modern concept of sliding friction will then be presented, as will some alterations and modifications to the theory which have been proposed to handle objections caused by the nature of rock.

Historical background

A review of the historical background of current concepts of sliding friction up to about 1830 is given in Bowden and Tabor (1954, 1964). They include an extensive bibliography of the original sources.

Leonardo daVinci seems to have been the first to correctly observe the relationship between friction and normal load. However, he confined his experiments and observations to his notebooks. The first man to publicly proclaim the basic laws of friction was Guillaume Amontons (1663-1705), a French architect. In a paper presented to the French Academy in 1699, Amontons described the two main laws of friction. These are:

1. Frictional force is proportional to normal load. Amontons said that in most cases it is about one-third of the applied normal load.
2. Friction is independent of the size of the bodies in contact. Amontons viewed surface irregularities as the cause of frictional force.

Leonhard Euler (1707-1773), the Swiss mathematician and physicist, was the first to point out that there is a difference between static and dynamic (or kinetic) friction.

One of the great names in the study of friction is that of Charles Augustine Coulomb (1736-1806), a French engineer. In between his electrical experiments

and his earth pressure experiments and discoveries he also, in 1781 and 1785, published papers which revived Amontons' work, which had sunk into obscurity. Coulomb considered that friction could arise from lifting over asperities, bending of asperities, and breaking of asperities. He described the angle of friction as the slope of the steepest asperity. He also considered the possibility of cohesion, but rejected it because he thought that cohesion would have to be proportional to the gross contact area. Coulomb's explanation remains enshrined in basic engineering mechanics books, and it has some passionate defenders in the ranks of adhesion physicists (Bickerman, 1970).

During approximately the same period, scientists in England were discovering cohesion. Jean Theophile Desaguliers (1863-1744), an English physicist, discovered cohesion between clean, like solids. Samuel Vince (17 9-1821), a theologian and physicist, considered the difference between static and kinetic friction to be due to adhesion.

In the late nineteenth century, dissatisfaction with the "up-and-over" concept of the mechanism of friction grew with the spread of thermodynamic considerations of surfaces. With many contacts, what slides up must slide down, and Coulomb's concept would result in a zero energy loss. This is clearly contrary to the obvious experience of the creation of heat by energy loss during frictional sliding. As a consequence, a molecular adhesion theory of friction began to draw attention with the works of Ewing in 1892, Sir William Hardy in 1919 and in 1936, and especially Tomlinson in 1929. Karl Terzaghi (1915) came to the conclusions of the modern theory independently and intuitively. The real development of the modern adhesion theory of friction came with the work of Bowden and Tabor and their associates from 1939 until the present. It is the Bowden and Tabor theory which is now considered the "classical" theory of friction (see Byerlee, 1967, and Lambe and Whitman, 1969).

The adhesion theory of friction

Area of contact. At least on a microscopic scale, all solid surfaces are rough and contain asperities (Maurer, 1965), projections of material farther

away from an "average" surface location than other points on the surface. Contact between even smooth surfaces is thus made only at the contacts of the asperities. Obviously, true contact area bears very little relationship to apparent contact area. How can true contact area be calculated? Terzaghi (1925), suggested that the area of true contact would be related to the normal load and to the yield stress of the material. Some measurements of the true contact area of metals have been made by electrical and optical means. The results of these measurements seem to confirm the following theoretical analysis (Bowden and Tabor, 1954):

By the Hertzian elastic analysis the area of contact A of a solid deforming elastically is:

$$A = kW^{2/3} \qquad (1)$$

i.e., proportional to $W^{2/3}$ where W is the normal load. As the load W is increased, the mean pressure p_m increases until a critical point is reached within the softer of the materials in contact. When the mean pressure has become high enough to cause the regions in contact to flow plastically, the mean pressure is directly proportional to the elastic limit Y

$$p_m = cY. \qquad (2)$$

Mean pressure is therefore independent of the size of the asperities, and so is independent of the load. This makes p_m the yield pressure p. At the point below the surface where $p_m = 1.1Y$, plasticity is initiated at the most stressed point. The corresponding load is:

$$W = 13.1\, p_m^3\, r^2 \left(\frac{1}{E_1} + \frac{1}{E_2}\right)^2 \qquad (3)$$

for a spherical asperity pressing on a flat plate. The radius of the sphere is denoted by r, the elastic moduli of the sphere and the plate by E_1 and E_2. If the asperity is of a conical or pyramidal shape, the tip can be considered as a sphere with a very small radius. Therefore a small load is sufficient to deform the asperities beyond the elastic limit. Thus, at least for more ductile

materials, the tips easily deform plastically.

Since the yield pressure is independent of the amount of deformation which has already occurred, the area of real contact is directly proportional to the load W. That is:

$$A_r = \frac{1}{p} W. \qquad (4)$$

Equations (1) and (4) show that while elastic deformation is occurring on a macroscopic scale, and the apparent area of contact is increasing with $W^{2/3}$, plastic deformation is occurring in the asperities, and the area of real contact increases with W. This has been demonstrated experimentally in an indirect manner by the measurement of the conductivity of metals.

Archard (1961) points out that most asperity-asperity contacts seem to occur with no visible damage. He concludes that, while a single contact would deform with $A = kW^{2/3}$, as the number of contacts increases A approaches kW. Thus, many asperities may deform elastically under some circumstances. Archard earlier concluded (1957) that, in metal, initial contacts are plastic, but repeated contacts are elastic. He deduced that the average size of the real area of contact of asperities is a constant, but that the number of contacts increases with an increase in normal load. This may be true especially under relatively low normal loads. Still, plastic deformation of asperities seems to offer the best general explanation for frictional phenomena, as will be shown below.

Upon application of a tangential force in addition to the normal force, the area of real contact, at least of ductile materials, increases (Merchant, 1968). By analogy with the von Mises yield criteria for an ideal two-dimensional model of an intermetallic junction, the yield criteria may have the form:

$$p^2 + \alpha s^2 = p_o^2 \qquad (5)$$

where p_o is static contact pressure, s is tangential force, and α is a constant with a value of about 10. The material in the asperity is initially subjected to a normal stress equal to its yield pressure $p = p_o$. Thus as soon as

the slightest tangential stress is applied, equation (5) is satisfied only if p diminishes. This means that the area of contact must increase as p decreases, following equation (4). This process might go on indefinitely if it were not for the presence of surface contaminants, which stop junction growth and permit slip. Tangential stress may cause asperities which deform elastically under normal load to deform plastically. Tangential stresses in brittle materials may generate fracture in or below the sliding interface (Tabor, 1968).

Once sliding has begun, the temperature of the area in real contact increases greatly (Bowden and Tabor, 1954). This allows the areas of real contact to grow more rapidly than indicated by movement of the gross block.

Adhesion theory. Two effects seem to predominate when "smooth" surfaces are slid across one another. One, the equivalent of interlocking of the Coulomb theory, causes plowing in metals and may cause either brittle fracture or dilatancy in non-metals. This plowing term is estimated to cause a "friction coefficient" of about 0.1 (Merchant, 1968). The other effect, which causes what early experimenters called "true friction" though their explanations were exactly opposite to today's, is called "shearing" by Bowden and Tabor (1954). This is the action of one asperity lodged against another in the direction of shear.

Experiments and photomicrographs by Bowden and Tabor show that the shearing component of friction is caused by actual "cold welding" of metals to each other. This bonding or rather the force required to shear the bonding comprises sliding friction.

> It is clear that when similar metals are in contact the local high pressure must cause an equal flow of both surfaces as that they both contribute equally to the formation of welded junctions and when sliding takes place, both surfaces will be distorted and torn. Moreover, since the metal will be hardened at the interface, the junction will be stronger than the underlying metal, so that the break will occur in the bulk of the metal (Bowden and Tabor, 1954).

Similar effects are found in non-metals (Bowden and Tabor, 1964). The breaking point is different in materials other than metals, and at very small

loads the experimental results were similar to those at high loads.

In metals the actual bonding is believed to be of the same nature as alloying, although results by Johnson and Keller (1967) throw doubt upon this conclusion. When two asperities come close together, the approaching bodies have equal effects on the tip atoms. Thus, the forces at the interface are the same as the forces in bulk. Because of mismatch between crystal lattices it would be the greatest of coincidences if the adhesion were as strong as in the bulk metal (Merchant, 1968). The same general interaction occurs with dissimilar metals, except that the junction should be much weaker. Some non-brittle non-metallic crystalline substances such as NH_4Cl and sulphur seem to behave in the same manner as metals. Even some brittle materials such as rock salt and, under high pressure, sapphire, seem to show adhesion between asperities (Bowden and Tabor, 1964). Contamination generally present on any solid body in air will act to reduce bonding (Merchant, 1968).

Laminar solids apparently adhere to each other due to Van der Waals forces. In experiments on mica (muscovite) cleaved to present molecularly smooth surfaces on cleavage faces, Bowden and Tabor (1964) found that the attractive energy of the flat, plateau-like asperities was quite high over a relatively small separation distance when chemically clean.

Amontons' laws by the adhesion theory. If we consider only hard materials that make contact only at the tips of the asperities, i.e., a polished surface with no interlocking, the "plowing" term can be ignored. In this case, the real area of contact is, according to equation (4):

$$A_r = \frac{W}{p}.$$

If s is the mean tangential stress required to shear the junction, then the shearing force (the friction force) is:

$$F = As \qquad (6)$$

Since the real area of contact A_r depends only on W and p then:

$$F = W\frac{s}{p}, \qquad (7)$$

and thus F is proportional to the normal load. This is Amontons' (Coulombs) first law. Since frictional force F is directly proportional to load W, the proportion, the coefficient of friction μ, is independent of both load W and of apparent area of contact. In fact, the coefficient of friction

$$\mu = \frac{F}{W} = \frac{s}{p} . \qquad (8)$$

Since s and p are material properties, they do not depend upon the size of the body. This is Amontons' second law.

Bowden and Tabor (1954) emphasize that intimacy of contact and strength of adhesion at points of contact will be greatly influenced by the presence of surface films. With metals, these films are usually oxides of the metal; with non-metals, the films are adsorbed fluids and gases. The contaminant molecules will also touch and will develop a shear strength s_2 over a real contact area of $A(1 - \alpha)$, if α is the fraction of direct non-contaminated contact area. The friction force will therefore be:

$$F = A(\alpha s_1 + (1 - \alpha) s_2). \qquad (9)$$

Since α and s_2 are variables, μ is somewhat variable even for similar materials with identical surface geometry.

Removal of load. If true adhesion occurs across boundaries of bodies in contact, why do the bodies not remain adhered when the normal load is removed? Terzaghi (1925) hypothesized that the bonds would be broken by elastic rebound of the macroscopic portion of the deformation. Bowden and Tabor agree that elastic rebound of asperities and macroscopic portions of bodies in contact are sufficient to break the bonds formed (1954).

Johnson and Keller (1967) discovered no evidence of elastic rebound in soft metals under ultra-high vacuum. With contaminated (real) surfaces and with harder materials, rupture of the always-present contaminant layer is necessary for good bonding. Bonding is therefore weaker, and rupture of bonds by elastic relief seems possible.

Summary. To summarize the Bowden and Tabor theory of friction in a few words:

> The experiments show that, under the intense pressure which acts at the summits of surface irregularities, a localized adhesion and welding together of the metal surfaces occurs. When sliding takes place, work is required to shear the welded junctions and also to plough out the metal (Bowden and Tabor, 1954).

This theory has been extended to non-metals and is now the generally accepted "classic" theory of friction. Under this definition of friction, studies such as those of Patton (1966) and of Ripley and Lee (1961) which concentrate on macro-irregularities along joint planes are really studies of dilatancy and shear strength and not of friction.

Friction of Rock

Compared to the amount of study done on metals, the amount of research on friction of rocks and minerals is very small. Most of the pertinent literature (Jaeger, 1959, 1971) concerns itself with the approach of rock to Coulomb's shear strength criteria:

$$\tau = \mu\sigma_n + c. \qquad (10)$$

It must be kept in mind in this section that friction along separated planes and joints in rock is the topic of discussion. The "internal friction" of the intact rock body is not considered.

Horn and Deere (1962) experimented on the coefficient of friction of individual minerals. They found that the static coefficient of friction depended upon whether the minerals were massive crystalline (quartz, feldspars, calcite) or laminar (micas, talc, clay minerals). They found that up to a critical roughness the coefficient of friction of massive minerals depends upon the amount of water present, water acting as an anti-lubricant. The laminar minerals, on the other hand, were lubricated by water in all cases. Water seemingly separated the plates and reduced Van der Waals forces from plate to plate. Coulson (1970) has done similar work on rock systems, investigating coefficient of friction or rocks with different grinds and polishes, and moisture conditions.

Rock is normally taken to be a brittle material. With rock, along with other brittle materials, objection has been taken to the applicability of the adhesion theory of friction. Greenwood and Williamson (1966) concluded that the behavior of a surface was absolutely determined by a plasticity index:

$$\Psi = \left(\frac{E'}{H}\right)\left(\frac{\sigma}{\beta}\right)^{\frac{1}{2}} \qquad (11)$$

where $E' = \frac{1}{2}E/(1-\nu^2)$ for similar materials and H = hardness, σ = standard deviation of height of asperity, and β = radius of the asperity tip. Increase of load would not make a material with Ψ less than 1 behave plastically at any point.

Jaeger (1971) suggested that the mechanism of Bowden and Tabor and of Archard is not applicable to brittle materials. He suggests use of the Coulomb criteria, or a modification thereof in the form

$$\tau = \tau_o + k\,\sigma_n^m \qquad (12)$$

with k and m experimentally determined constants. This criteria has been advocated by Maurer (1965) and others. Jaeger does not suggest the source of the cohesion (c) in the basic Coulomb equation, but he states that it ranges from 0 to 200 pounds per square inch in natural joints.

Patton (1966), Ripley and Lee (1961), Coulson (1970), and other investigators have concentrated on the effect of macro-irregularities with the resulting equation (in the absence of cohesion) of

$$\tau = \sigma_n \tan(\theta + \phi), \qquad (13)$$

where θ is the inclination of a slope in the direction of τ.

Some experimenters, especially Byerlee (1967, 1969) and Brace and Byerlee (1970) have contended that the mechanism of friction in brittle materials such as rock differs from that of the Bowden and Tabor adhesion theory. Byerlee believes that the experimental evidence showing cracking of quartz and granite in indentation hardness tests proves that with such l[illegible] tens[illegible] strength materials, plastic

flow at the asperities is not possible. Byerlee agrees with the classic theory in postulating asperities of basically conical or wedge shape. His conclusion is that failure is more likely to be by brittle fracture due to the low tensile strength of the material.

Byerlee (1967) assumes normal and tangential stresses at the tip of a conical asperity of vanishingly small tip radius. The asperities break when the shear-induced tensile stress along the outer edge of the asperity equals the tensile strength. He can calculate a theoretical initial coefficient of friction by calculating the strength of an asperity on its outer edge as it crushes. The calculated theoretical coefficient of friction is 0.10. The predicted value of coefficient of friction for massive crystalline materials is quite similar to that found experimentally by Horn and Deere (1962) for a clean, dry surface. Experiment also showed no variation of coefficient of friction with apparent area of contact. The coefficient of friction does vary with gross roughness, and Byerlee assumes that with rough surfaces the theory will not apply due to interlocking of asperities predominating over asperity to asperity contact.

The greatest objection to Byerlee's assumption of independence of this theory from the adhesion theory is the tangential shear forces assumed present at the tips of asperities. No cause is given for the existence of a friction or shear force between asperity tips. Even with brittle material, the adhesion theory of friction cannot be excluded. Tabor (1968) considers that the shearing of asperity to asperity contacts in brittle materials may occur by tensile failure in the bulk material below the contact, but that adhesion will exist at the contact.

Stick-Slip

Stick-slip is the movement of a sliding element across a stationary element in abrupt, rapid movements alternating with periods of no movement. The applied tangential force seems to build up to a critical value required to cause movement, then to suddenly relax with an accompanying forward movement of the sliding element. The sliding element then stops moving (sticks) and the cycle begins anew. The variation of frictional force with time is shown in Figure 1, a tracing

of an actual test. The velocity of the sliding element fluctuates greatly during movement.

Stick-slip is a phenomenon which has been observed in most friction studies, particularly at light normal stresses. Such self-induced vibrations were recognized in the nineteenth century as the source of music from violin bows and strings, and of the squeak of chalk on the blackboard. Some noises in natural materials such as noises in rocks before apparent breakage, and the squeakiness when walking across some sands may be the result of stick-slip. Wells (1929) was the first experimenter to notice the phenomenon scientifically. Most of the research on stick-slip has been with metals, where stick-slip at high velocity of slider movement is a troublesome phenomenon in the machine tool industry (Brockly et. al. 1967, Derjaguin et. al. 1956). Much of this work has been of a mathematical nature, seeking to solve the general equation:

$$m\frac{d^2x}{dt^2} + A\frac{dx}{dt} + F\left(\frac{dx}{dt}, x, t_o\right) + k(x - vt) = 0 \qquad (14)$$

where $m\frac{d^2x}{dt^2}$ is the inertial force of an accelerating slider of mass m, $A\frac{dx}{dt}$ is the damping factor, $F(dx/dt, x, t_o)$ is the frictional force which is a function of velocity, time of contact between surfaces, and relative displacement, and $k(x - vt)$ is the driving or retarding force, with k the system stiffness. Attempts are usually made to solve the equation in terms of the natural frequency of the sliding system or to determine the critical velocity or the critical stiffness or other conditions under which stick-slip can be eliminated. An emphasis has been placed on the discovery that stick-slip can be eliminated by making the system stiffer. Gravity-driven systems under light normal loads, such as rock joints in open cuts, are a soft system (Jaeger, 1971).

Less work has been done in attempting to define mechanisms of stick-slip. Outstanding has been the work of Rabinowicz (1965). He states "All stick-slip processes are caused by the fact that the junction force does not remain constant as a function of some other variable." Irregular and harmonic stick-slip vibrations can occur in machine systems. In natural systems, self-induced

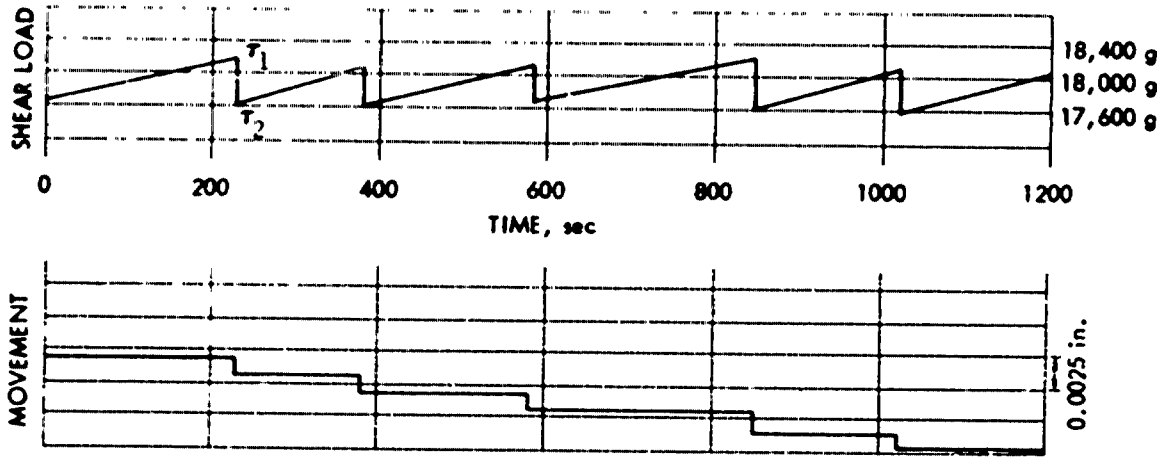

Figure 1. Typical limestone stick-slip pattern - Test L7C - σ_n = 3.0 kg/cm² - Temperature 125°C

vibrations, or regular stick-slip, is the common type found.

Bowden and Tabor (1954) note that if static friction is higher than kinetic friction, and one of the sliding surfaces has a certain degree of elastic freedom, the motion will be intermittant and characterized by stick-slip. An analysis of the equations of motion show that stick-slip under these conditions must occur when the static coefficient of friction μ_s is greater than the kinetic coefficient of friction μ_k, and that the magnitude of stick-slip reduces as μ_k approaches μ_s. Under stick-slip conditions, μ_k is determined by the shear load at one-half the slip distance. Tolstoi (1967) showed that stick-slip is dependent on the degree of freedom normal to the surface of sliding. When dilatancy is not possible, stick-slip disappears. This might be significant under geologic conditions.

Why should the static coefficient of friction be larger than the kinetic coefficient? Rabinowicz (1951), following the initial suggestion of Ishlinski, proposed that the static coefficient of friction varies with the time of contact between the sliding elements, building up exponentially within a short time of contact to be higher than kinetic friction. He suggested that junction growth was the producer of high values of static friction. He equated junction growth with creep in a vertical direction, and suggested that μ_s is controlled by (1) the creep rate in compression of asperities resulting in increase of junction area and (2) shear strength of junctions formed. As suggested previously, contaminants cause junction growth to cease and tangential stress to build up faster than shear strength. The concept of time dependency of static friction has been supported by the research of Kosterin and Kraghelsky (1962) who derived an equation relating duration of contact to stress and strain in the contacted surfaces and thus to friction. Static friction was experimentally determined to follow the equation in metals and plastics. Brockley and Davis (1968) used controlled stick-slip to investigate postulated time dependence of static friction in metals. They found that the static friction coefficient does increase with time of stick if there is a difference between μ_s and μ_k. Simkins (1967) and Tolstoi (1967) deny that there is a

difference between static and kinetic coefficients of friction. They claim that the apparent differences are caused by observing the statistical maximum and minimum of the same physical property.

A result of the equations of motion is that with a small average velocity of sliding (total distance moved/total time), the maximum velocity achieved during slips may be quite large (Derjaguin, 1956). This may influence the surface properties, especially temperature. The temperature rise upon slip is more marked with poor thermal conductors (Bowden and Tabor, 1954).

Most of the above-cited work has concentrated on the elimination of stick-slip as a nuisance. Brockley, Cameron, and Potter (1967) determined that stick-slip will be eliminated by:

1. A small load and a large stiffness.
2. A small difference in values of μ_s and μ_k.
3. A large damping ratio.
4. A small value of static friction growth constant (junction growth).

Stick-Slip of Rock

Little previous work has been done on stick-slip as applied to rocks. Jaeger, in his pioneering study of the frictional properties of rocks (1959), encountered violent stick-slip on bare, flat surfaces of plaster. Small plaster fragments, frequently arranged in slickensides, were present after slip at high stresses. Jaeger speculated from the high calculated energy release, that high temperature at points of contact had occurred during stick-slip.

Horn and Deere (1962) in their study of friction of specimens of pure minerals encountered stick-slip in many of their tests on quartz. To them, as to most other investigators of the friction of rocks, the phenomenon was a nuisance in attempts to obtain static friction coefficients.

Coulson (1970) in a study of friction of rocks with varying surface roughness found that stick-slip occurred within a wide range of normal stresses in several rock types in a direct shear type test. Stick-slip was most common in smooth-ground specimens (number-600 grit) at high normal stresses. Coulson experienced

stick-slip principally in rocks containing quartz, but also found it in a basalt. Interestingly, he did not obtain stick-slip in tests on the same Indiana limestone used in part of this study. He did encounter conditions reflecting that the static coefficient of friction is a function of duration of stick. Some effort was made by Coulson to eliminate stick-slip by increasing the stiffness of his loading system.

Dieterich (1970) conducted experiments to determine the time dependence of static friction in stick-slip sliding. In a series of experiments on sandstone, graywacke, quartzite, and granite with normal stress of from 0.02 to 0.85 kilobars (1 bar = 14.5 psi = 1.02 kg/cm^2), he found that sliding on clean rough-ground surfaces was initially stable. However, as rock debris accumulated on the surfaces, stick-slip became the dominant mode of sliding. Dieterich found that change of the interval between slips from 15 seconds to 24 hours had about a 10% influence on μ_s. He related stick-slip to periodicity of shallow earthquakes.

An investigation into friction of rocks by Hoskins et. al. (1968) included some specific study of stick-slip. These investigators determined that stick-slip occurred with smooth surfaces tested (35 $\pm$ 5 microinches roughness), and that rougher blocks demonstrated a smooth increase of frictional force up to a value controlled by the normal stress. Hoskins et. al. observed a small displacement occurring before the main slip. The time length of slip was very abrupt, usually less than 2 milliseconds. They concluded that the stick-slip observed fit the mathematical pattern of even oscillation described by Derjaguin et. al. (1956) and other mathematical investigators quite well. They made no comments relative to the mechanism of stick-slip.

In experiments on artificial joint systems made of blocks of precisely smooth-ground plaster, Brown and Trollope (1970) discovered that sliding along joints normally occurs in a stick-slip mode. With joints oriented at 45^o to principal stress directions, stick-slip occurred regardless of confining pressure. At other orientations, stick-slip occurred at high pressures (over 200 psi).

The only investigation to emphasize mechanisms of stick-slip has been that of Byerlee (1970), who concentrated on stick-slip which can occur at very high pressure deep in the earth. His investigations led him to propose a theory of stick-slip of rock which is dependent on the mechanism of brittle fracture. Basically, stick-slip is seen as a process whereby the irregularities on the surface become locked, fail by brittle fracture, and then lock again. When sufficient fault gouge builds up, the sliding becomes stable at low confining pressures, but remains unstable at high pressure due to the dense packing of the debris grains. Failure of one grain then leads to a high stress in adjoining grains, and the system becomes unstable again. This system has been seen as the explanation for shallow focus earthquakes (Brace and Byerlee, 1970).

In his recent survey of friction of rock, Jaeger (1971) states that stick-slip is a complex phenomenon related to surface roughness, average rate of sliding of the rocks, time between slips, wetness of the surface, and the amount of gouge present. The present study adds temperature as an additional variable pertinent to the mechanism for stick-slip of rock.

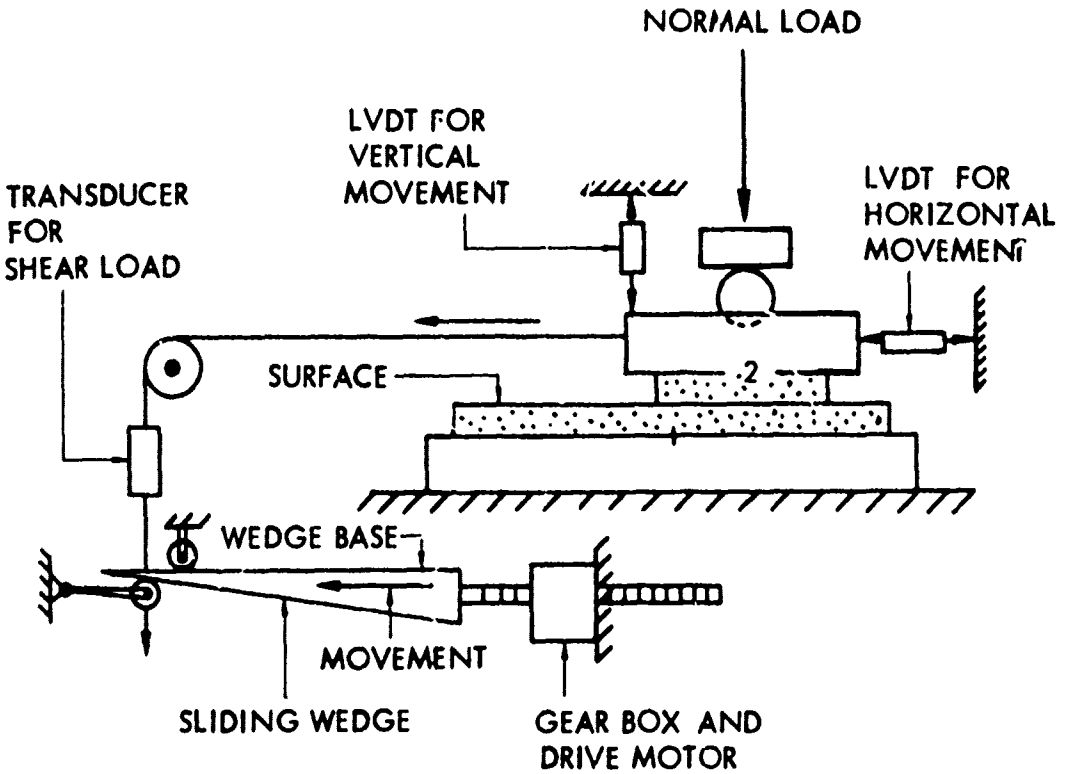

Fig. 2. Schematic of shear apparatus: (1) stationary block and holder; (2) sliding block and holder.

TEST METHODS AND PROCEDURES

Apparatus

Direct shear testing was performed on prepared, separated rock specimens to determine the mechanism of stick-slip. Hoskins et. al. (1968) presented objections to the use of pre-cut triaxial specimens for low normal-stress friction investigations. Lajtai (1969) has shown that the direct shear mode of test most closely resembles the actual condition of state of stress along a fault or joint after the faulting has taken place. Gravity is a low-stiffness mechanism (Jaeger, 1971) and the direct shear mode most closely resembles the gravity-induced case of movement along a joint.

The equipment used to conduct the stick-slip tests is a temperature controlled, constant-rate-of-strain direct shear device. Figure 2 is a schematic of the device, omitting the temperature control features. The direct shear mechanism is comprised of a 15-cm by 10-cm stationary rectangular specimen holder, with a smaller rectangular moveable holder measuring internally 8.3 cm by 7.5 cm placed on top. An insert into the moveable holder will hold smaller, 2 cm by 2 cm, rock specimens. The rock specimens are placed in these holders and held in by set screws against metal plates. Approximately one inch of travel is possible with no change in apparent contact area. A normal load is transferred to the upper block by a ball and socket, which allows a free-hanging load to travel with the moving block.

The upper block is pulled across the lower block at a constant nominal rate of strain by a screw and wedge mechanism driven by an electric motor. The screw advances the wedge at a very slow rate. A pulley impinging on the wedge is pulled downwards along the wedge. This causes the upper block to move by means of an attached steel wire. The upper block moves at a nominal rate of 1.5×10^{-3} centimeters per minute.

The shear box is enclosed in a double-walled asbestos oven. Temperature is controllable within the oven from room temperature to 275^{o} Centigrade by an Athena Model 63 temperature controller. The controller is connected to a

thermocouple placed through the lid of the oven, and to electric heating coils within the oven which activate when the temperature falls below the set value. Air temperature in the oven is controllable to within about $2^{o}C$. Closer control was difficult due to slots cut in the base of the oven to allow the normal load to move with the moving specimen holder. A fan was also provided inside the oven, but seldom used.

Instrumentation

The shear load required to move the block is measured by a strain gage direct-load transducer mounted as part of the pulling mechanism. Two arms of a wheatstone bridge are mounted so as to be additive on a thin strip of metal. As the metal strains, the load is measured by previous direct calibration on an oscillograph. Three different transducers were used during the tests, but all limestone tests with normal stress of 3 kg/cm^2 and over and all tests on the other rocks were performed using the same copper transducer. This transducer is accurate to within 100 grams. The transducers used on the lighter normal stress tests of the limestone are accurate to within 300 grams. Temperature compensation is provided by mounting dummy gages on material identical to that of the transducer.

Horizontal movement of the upper block was measured by a linear variable differential transformer (LVDT) Schaevitz Model 1000HR. The core of the transformer is attached by a metal rod directly to the moveable upper shear box. The LVDT body is Teflon lined to insure smooth sliding, and the LVDT is accurate to within 0.0005 inches (0.0013 cm). The LVDT had to be reset by hand in its holder whenever the total movement exceeded 0.02 inches (0.0508 cm) at the normal attenuation used. Calibration was by a micrometer accurate to 0.0001 inches. A second LVDT was arranged to measure vertical movement of the upper block. Though this LVDT was accurate to within 0.0002 inches, the blocks were ground too smooth for any vertical movement to be recorded, and use of this LVDT was discontinued later in the program.

The horizontal LVDT signal was conditioned by a Schaevitz Model SCM signal conditioner and further amplified by a Brush Model RD 4215-10 DC amplifier. The load transducer was activated and amplified by a Brush Model 4212 carrier amplifier. The information gathered was recorded on a Brush Mark 200 ink-writing oscillograph. The chart was usually run at speeds of 20 or 50 seconds per centimeter, though faster rates were sometimes used. Times, movements, and loads were read directly from the oscillograph record. Temperature was read from the set-dial and deviation dial of the temperature controller.

Specimen Preparation

Each block was saw-cut to the appropriate size, then ground "smooth" with a number-45 grit aluminum oxide grinding wheel on an automatic grinder. This degree of smoothness is much rougher than the "rough" quartz block of Horn and Deere (1962), which was ground to 240 grit; slightly rougher than Coulson's (1970) rough blocks (number-80); but smoother than the rough blocks of Hoskins et. al. (1968) and the natural fracture surfaces tested by Byerlee (1970). The grinding was believed necessary to minimize dilatancy (interlocking) and to give some degree of uniformity to the block surface structure so that tests run on different blocks could be compared. The number-45 grit surface is smooth enough to be controlled experimentally, but rough enough to be out of the realm of purely ideal jointing.

After grinding, the blocks were carefully washed in water to remove all grinding debris. The blocks of rock were then oven dried at 110^{o}C, removed from the oven, and allowed to cool and air-equilibrate with moisture at room temperature. For subsequent test runs on blocks already run once or more, the blocks were again carefully washed, oven dried, and air-moisture equilibrated.

Conduct of the Tests

Test series were performed on limestone with normal stresses of 0.75, 1.52, 1.95, 3.0, 5.0, 10.0, and 20.0 kilograms per square centimeter.

On the basalt, tests were run with normal stresses of 0.75, 1.50, 3.0, 5.0, 10.0, and 20.0 kilograms per square centimeter, and on the quartzite, 1.5, 3.0, 5.0, and 10.0 kilograms per square centimeter. Two series were run on limestone at 0.75 and 3.0 kg/cm^2, and on basalt at 10.0 kg/cm^2. Generally, each test series is a group of tests performed on one set of rock blocks. This series is given a number, prefixed L for limestone, Q for quartzite, or B for basalt. Each run across a block uninterrupted by unload of the normal stress is regarded as a test, and is identified by a letter suffixed to the series number. Each day's run on a block is identified by a number added behind the test letter. Thus the third test series on basalt, first test, second day's run is Test B3A2.

The series attempted to establish temperature ranges for the initiation and cessation of stick-slip, and to determine the effect of temperature change on the stick, slip, and shear load relaxation. Additionally, an attempt was made to ascertain the effect of the introduction of preground rock debris between the two test blocks.

In order to examine the stick-slip properties of the rock with respect to temperature, movement of the blocks was begun at 30^{o}C. After observation of the mode of movement at the lower temperature, the temperature was raised incrementally. For example stick-slip had initiated at 30^{o}C, the temperature was raised to 125^{o}, and subsequently to 200^{o} to study the effect of increased temperature.

Observations were made of time between slips (i.e., time of stick), amount of slip, shear load relaxation during slip, and total shear load required to initiate each slip. From these measured parameters the coefficient of static friction at the instant prior to slip, and the cumulative movement were calculated. The character of the slip in terms of time length of slip, abruptness, shape of the slip curve, and existence of creep between slips was also observed. The temperature was then reduced, and observations were made of movement quantities at various temperatures during unloading. The temperature of cessation of stick-slip was noted.

In some light load tests on limestone, the most accurate means of quantifying the stick-slip results was time between slips. While an absolute one-to-one correlation of length of slip and time between slips was not observed, for the limestone tests the correlation coefficient between the means is 0.85 to 0.98, and means were used in all quantifications in order to observe patterns. In limestone tests with normal stress of over 3.0 kg/cm^2, and in all tests on basalt and quartzite, test results will usually be presented using values of the length of slip. This parameter is preferred because there are fewer gaps in the record, and because it presents a better picture of the pattern in basalt. Shear load relaxation data parallels that for slip, but is not as complete in the limestone tests.

DESCRIPTION OF ROCKS TESTED

Three types of rocks were used in the testing program, all being from commercial quarry sources.

Salem Limestone

The limestone tested was the familiar building limestone from the vicinity of Bedford, Indiana. This rock is from the Salem Limestone formation of Mississippian age. The Salem Limestone is a very light gray, slightly porous, bioclastic limestone, the clastic particles being composed of rounded fossils shells of foraminifera, with measured sizes up to 0.82 mm, occasional fragments of bryozoans, and possibly fragments of other organisms. The fossil fragments lie in a cement of optically continuous calcite. Quarry information stated that the formation contains up to two percent quartz, but the specimens examined petrographically were 100% calcite. The measured mean fragment diameter is 0.61 mm with a standard deviation of 0.20 mm. Unconfined compressive strength was evaluated as 400 kilograms per square centimeter.

Basalt

This material is a basalt of Tertiary age from Sonoma County, California, supplied by Smith's Granite and Marble Works, Napa, California. It is a dark gray, massive basalt with interlocking crystalline texture. Altered zones which probably represent flow boundaries are spaced about one centimeter apart. Glass, corroded olivine crystals, microcrystalline augite, and occasional garnet and magnetite crystals are contained in a matrix of plagioclase feldspar (labradorite) laths. Mean length of plagioclase laths is 0.13 mm, standard deviation 0.03 mm. Some twinned plagioclase crystals are as large as 0.6 mm. Larger rectangular crystals of epidote, up to 0.66 x 0.23 mm, are scattered throughout the rock. The feldspar laths are arranged subparallel to the flow direction in-

dicated by the flow boundaries. Labradorite and augite were identified by X-ray diffraction; the other minerals did not show up in the X-ray. Mineral composition as determined by the integrating stage is: plagioclase 87%, glass 4%, epidote 1.5%, garnet 0.5%, olivine 3%, augite 4%, magnetite, trace.

The average unconfined compressive strength perpendicular to the flow boundaries was 1369 kg/cm^2, with a standard deviation of 138 kg/cm^2. Two specimens were tested with the major principal stress axis parallel to the slow boundaries. One broke along the boundary with an unconfined compressive strength of 1181 kg/cm^2, the other broke within the unaltered rock with a strength of 1785 kg/cm^2. The altered zones are not believed to be extensive enough to affect the surface properties of the rock. Tests were run parallel and perpendicular to the flow boundary zones, and also on blocks with very weakly developed altered zones.

Sioux Quartzite

The Sioux Quartzite is a dense, fine grained, very hard pre-Cambrian quartzite which outcrops in extreme northwestern Iowa and southwestern Minnesota, where it is quarried for aggregate and for monument stone. The pink to red color is attributed to iron oxide coatings on the clastic grains, which in turn are overgrown by authigenic quartz in crystallographic continuity with the adjacent sand grains. The result is a characteristic quartzite interlocking structure with minimum voids. The mineralogical content is primarily quartz with accessory zircon, anatase, rutile, hematite, and orthoclase (Beyer, 1897). The rock was not examined petrographically or tested for strength.

TEST RESULTS

Results will be discussed in several categories: temperature for initiation of stick-slip (from smooth slip), character of stick-slip, changes in stick time or slip distance with time, changes in surface character, temperature as a controlling factor, and changes in the coefficient of sliding friction. Detailed test results are given in Drennon (1972) and Drennon and Handy (1972).

Initiation of stick-slip

Initiation of stick-slip was found to depend upon four factors: (1) material, (2) previous frictional history of the specimen, (3) temperature, and (4) normal stress. The most extensive series comprising sixty tests was performed on the limestone, in which temperature and normal stress were found to have a pronounced effect on the initiation of stick-slip. In thirteen tests with a normal load of 0.75 kg/cm^2, no stick-slip occurred below a temperature of 100°C (Table 1). Under higher applied normal stresses stick-slip became more likely below 100°C, but still occurred at this low temperature in only about one-fourth of the tests. On the other hand, stick-slip always was initiated when the temperature was increased, usually (58% of the tests) beginning in the range 100-179°C. Extended movement or debris artificially added between the limestone blades usually increased the likelihood of smooth slip extending to higher temperatures.

Table 1. Temperature of initiation of stick-slip in limestone

Normal stress	Temperature range	Number of tests
0.75 kg/cm^2	30 - 99°C	0
	100 - 179	9
	180 - 205	4
	over 205	0
1.52 kg/cm^2	30 - 99°C	2
	100 - 179	5
	180 - 205	0
	over 205	0
1.95 kg/cm^2	30 - 99°C	1
	100 - 179	0
	180 - 205	6
	over 205	2
3.00 kg/cm^2	30 - 99°C	5
	100 - 179	7
	180 - 205	0
	over 205	0
5.00 kg/cm^2	30 - 99°C	1
	100 - 179	6
	180 - 205	0
	over 205	0
10.00 kg/cm^2	30 - 99°C	1
	100 - 179	5
	180 - 205	2
	over 205	0
20.00 kg/cm^2	30 - 99°C	1
	100 - 179	3
	180 - 205	0
	over 205	0

Initiation of stick-slip in basalt is more irregular in pattern as well as more frequent in occurrence than in limestone. Most tests on basalt produced stick-slip immediately upon initiation of movement regardless of normal stress or previous frictional history. These factors do seem to have some influence on the initiation of stick-slip in basalt, but certainly less than in limestone.

Smooth slip occurred at the initiation of movement mostly at higher normal stresses. Three tests with a normal stress of 10 kg/cm^2 began smooth slip on washed blocks at 30^o, whereas the initial basalt test at 0.75 kg/cm^2 went into stick-slip after a short period of irregular smooth slip on initiation of movement. These two test runs continued and ended in smooth slip.

Basalt tests with debris introduced between the blocks tended to begin sliding with a chaotic sticking, slipping, and sliding in an extremely irregular manner. Sometimes long periods of smooth slip would alternate with stick-slips which were more likely to be all pervasive in basalt in the middle range of the normal stresses tested. However, with the exception of Test Series B5, the high normal stress groups which began in smooth slip moved into stick-slip without any alteration of temperature or other test condition. Stick-slip seems to be the normal mode of frictional sliding for the basalt in the range of normal stresses and with the testing machine used.

Quartzite began movement in the stick-slip mode immediately upon initiation of movement at 30^{o}C, and the smooth slip mode of movement occurred in the three more lightly loaded tests after the blocks had remained overnight (approximately fifteen hours) at a temperature of 200^o. In those three cases, movement began with smooth slip and retained that mode of movement with an increase of temperature. A reduction in temperature, on the other hand, resulted in resumption of stick-slip at temperatures close to 100^{o}C, and stick-slip continued upon re-elevation of temperature to 200^o. This series of occurrences was the principal difference between results from quartzite and the other rocks tested, though it resembles some of the basalt tests wherein stick-slip reduction occurred with length of travel.

No debris tests were conducted on quartzite, since practically no debris was generated by sliding.

Character of stick-slip

At temperatures above 100° most limestone stick-slips were abrupt, with measurable time lengths from the beginning to the end of slip movement being relatively rare at normal oscillograph rates of 20 or 50 seconds per centimeter. Some random measurements at 125° ranged from 0.60 to 8.0 seconds, but long time lengths were most unusual. At 30°, limestone slips sometimes had a time length of up to 20 seconds, but such lengths were not common during regular stick-slip. They were normal when transition to smooth slip was imminent.

In limestone, slips tend to break off abruptly at the peak of load on the load - time record (Figure 3), and to gather time length by slowing down as the slip comes to a stop. The time length of limestone slips stretches out as the point of smooth slip approaches during temperature decrease.

Stick-slips in the basalt tests presented a different appearance. Figure 3 represents a common phenomena, called "30°-basalt stick-slip" because it was most often, though not exclusively, observed at that temperature. This is the tendency to alternate relatively large slips and relatively large shear load relaxations with small slips and small shear load relaxations. Creep frequently appears between slips. This phenomenon would often, but not invariably, cease when the temperature was raised.

The time length of slip of basalt slips tended to be longer than those of limestone.

All tests of quartzite were very abrupt (Figure 3), with a small amount of creep between slips. The time length of slip, where measured during Tests Q1 and Q3, was less than 0.05 second. This compares with normal limestone times of 0.6 to 8.0 seconds, and basalt time lengths which ranged from 1 to 22 seconds during a single test. As a rule, the magnitude of slip of the quartzite was larger than that of the basalt or of the limestone.

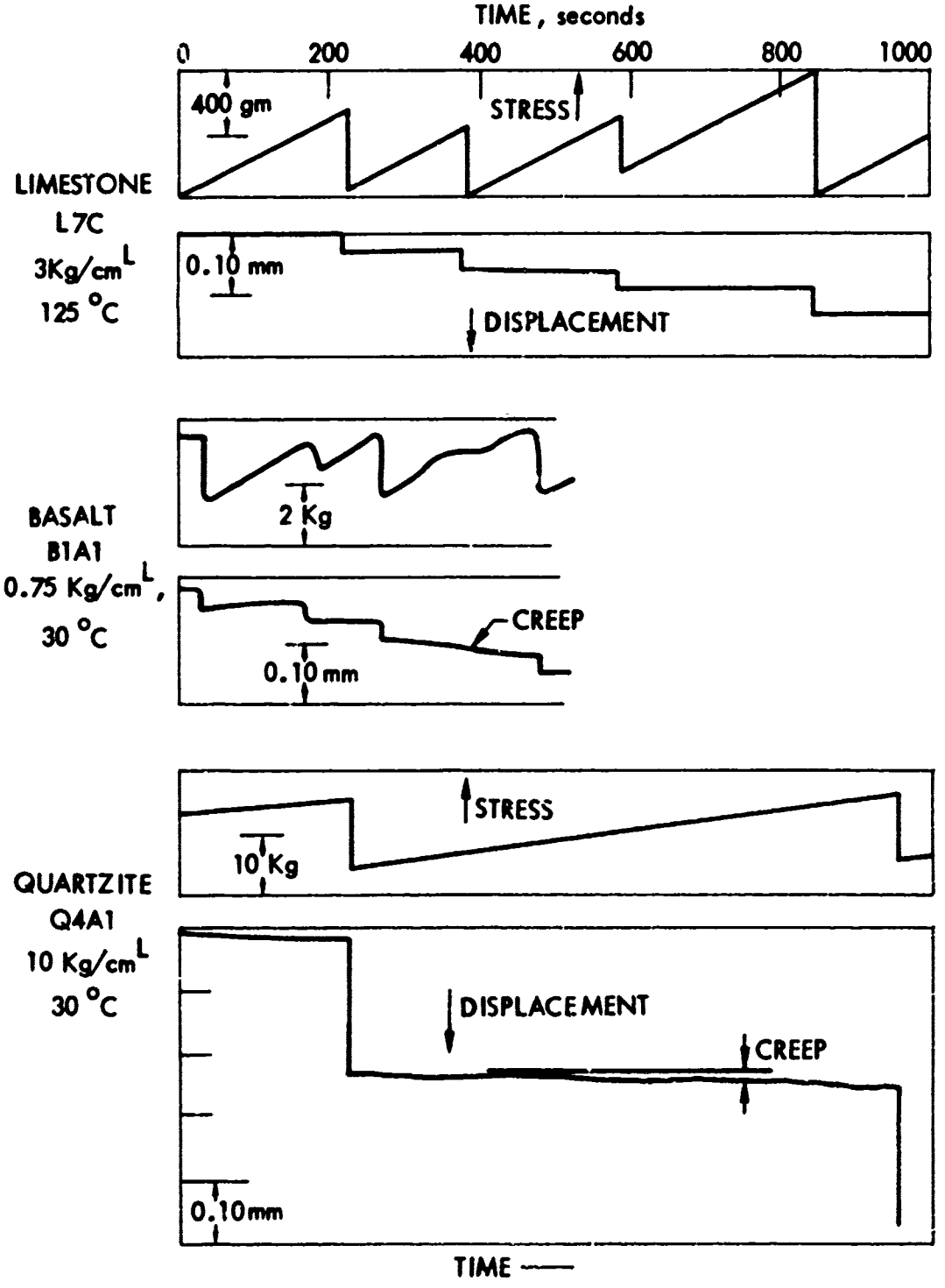

Figure 3. Typical oscillograph records of stick-slip.

A comparison of the load - time plots of Figure 3 shows clearly the abrupt break of the limestone and quartzite and the "nose over" of load of the basalt. Though this figure is one of the more exaggerated examples of "nose-over" of load and small creep movement before the major slip, a similar effect is characteristic of all basalt tests. The shape of the stick-slip curve for basalt is similar to that for silver, a very ductile material, described by Brockley and Davis (1968).

Stick-slip during long runs at constant temperature

During most of the tests the upper block was allowed to move for considerable periods of time over the lower block at a constant temperature. Measurements were made of each time between slips, slip, and shear load relaxation upon slip. Groups of ten successive slips were then averaged and studied to determine whether any trends occurred with time, or with accumulated total slip.

The most extensive constant temperature test at the lowest normal stress of 0.75 kg/cm^2 was the 190^o run during limestone Test L1B, which showed a steady increase in slip distance throughout the run. This pattern of increase of slip with time was observed in tests at 0.75 kg/cm^2 at all different temperatures. It was also the pattern of change of slip with accumulated movement at constant temperature at 1.52 kg/cm^2, but this tendency for time between slips and slip of limestone to increase with distance moved is a phenomenon restricted to small normal stresses.

In tests with normal stresses from 1.95 kg/cm^2 and up, the situation is sharply reversed. In tests beginning with clean blocks, the tendency is consistently for a reduction in time between slips, or slip, as movement progresses, approaching a constant value of about 0.0040 cm. This value would be a function of the materials, temperature, and test apparatus as well as of normal stress. In tests which were stopped at 125^o and then re-started at the same temperature, the slip value remains the same as had been attained before stopping the movement. The scatter of the first group upon resumption of movement is usually rather large.

The response of the basalt blocks to constant-rate-of-movement direct shear tests at a single temperature is in such great contrast to that of the limestone as to suggest differing mechanisms, or at least different responses to the same mechanism. As with the limestone, response of the basalt depends upon normal stress and temperature, but previous frictional history has less effect.

At the light normal stress of 0.75 kg/cm^2, little change in amount of slip occurred with continued running at a constant temperature. With an increase in normal stress 1.50 kg/cm^2, conditions begin to change slightly, and beginning at 3.0 kg/cm^2, the mode of sliding most typical of basalt tests at constant temperature takes over. Within the same test run, a steep and linear (Figure 4) or semilogarithmic (Figure 5) increase in amount of stick, slip, and shear load relaxation occurs.

In basalt tests at lower stresses, no stable value of slip was reached. At higher normal stress a tendency was observed to seek a stable value.

Continuous runs of quartzite at a single temperature tended towards constant values of slip, either increasing to the value, or decreasing to the value.

Surface changes

All blocks were prepared for sliding in a like manner, being ground with a number 45 grit aluminum oxide grinding wheel. The surface of the blocks was examined under a binocular microscope. One limestone block and one basalt block were further examined under a scanning electron microscope.

Under the binocular microscope the ground limestone, being bioclastic, gives a rough appearance. Powder-sized particles are first visible to the naked eye after sliding at a normal stress of 1.95 kg/cm^2. Examination under the binocular microscope showed some calcite chips with sharp edges apparently resulting from brittle fracture at normal stress as low as 1.52 kg/cm^2. At 1.95 kg/cm^2 normal stress all visible debris could be washed off, and no evidence of damage remained.

Beginning with a normal stress 3.0 kg/cm^2 visible chipping occurred.

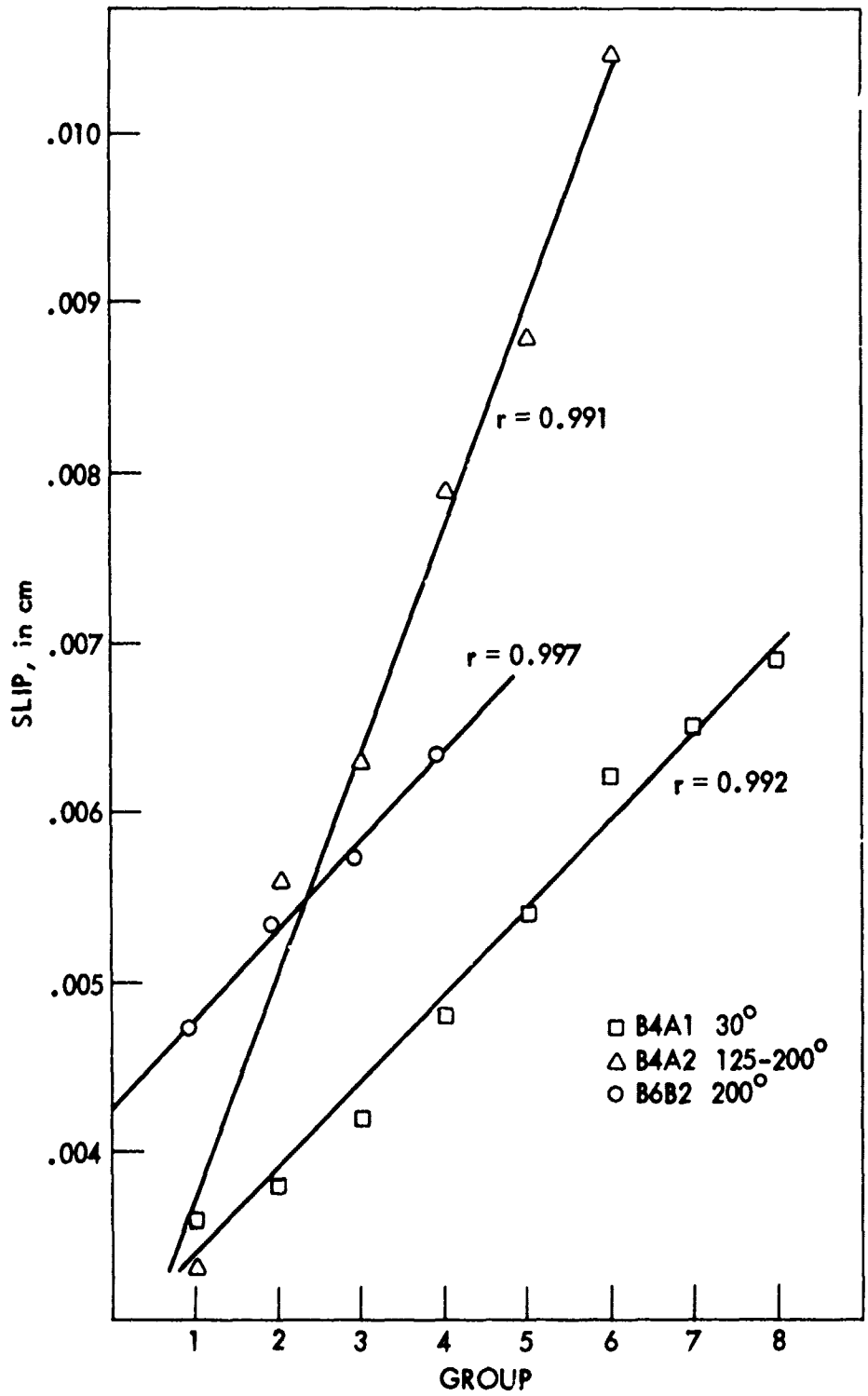

Figure 4. Increase in size of basalt slip with length of run at constant temperature. Each group represents 10 consecutive slips for which the data were averaged.

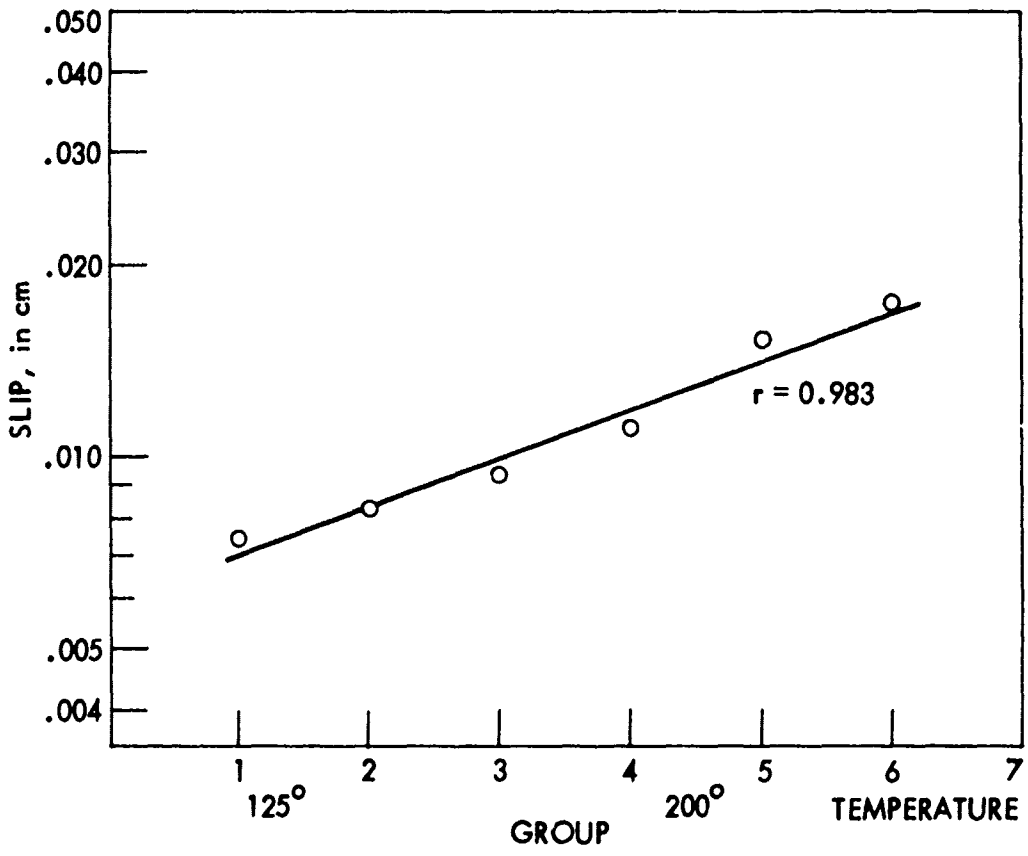

Figure 5. Semilogarithmic increase in size of slip in basalt with length of run at 125-200° temperature.

Two of the broken chips were examined under the scanning electron microscope. The surface of one chip was washed and dried according to the normal procedure before examination, and the other fragment was handled carefully to avoid disturbing the debris present on the face. The washed chip, examined at 300x showed little evidence of sliding. Some cleavage faces seemed pulled up from high points. These were usually on the rear side looking in the direction of travel. Little evidence was found in any picture for conical or otherwise sharp-peaked asperities, but, as would be expected from a limestone, the high points were relatively flat cleavage faces. These faces built up to flat contact areas which were a small percentage of the total surface of the block. The fragment examined with debris in place showed many fractured crystal fragments. Some debris is present on the higher, flat areas, but most has fallen into the lower void areas which are quite extensive in this limestone. Figure 6 and other pictures show that the debris is not created by shearing off the tops of high points which seem little affected by sliding, but by plucking of small cleavage fragments from the edges of the higher points and carrying these fragments both into voids and onto the surface of the "asperities".

The basalt, being a much harder material, showed little damage due to sliding in tests with normal stresses of less than 3.0 kg/cm^2. In the 3.0 and 5.0 normal stress tests minor striations appear on both the top and bottom blocks. In a test at 20.0 kg/cm^2, a heavy concentration of rock dust appears in parallel lineations. The striae, examined under the binocular microscope, appear much more evenly distributed and less strongly evident than with the naked eye. The fragments are visibly due to the brittle fracture of small crystals of feldspar, as they tend to be white in color, as against the black or gray augite.

Basalt fragments were also examined under the scanning electron microscope. In the clean basalt, ground with number-45 grit but never subjected to sliding, asperities appear as large, flat ground-off crystals of feldspar, (Figure 7a). The planeness of some of the flat crystal faces and their relatively large extent are remarkable. The fragment broken from an upper block

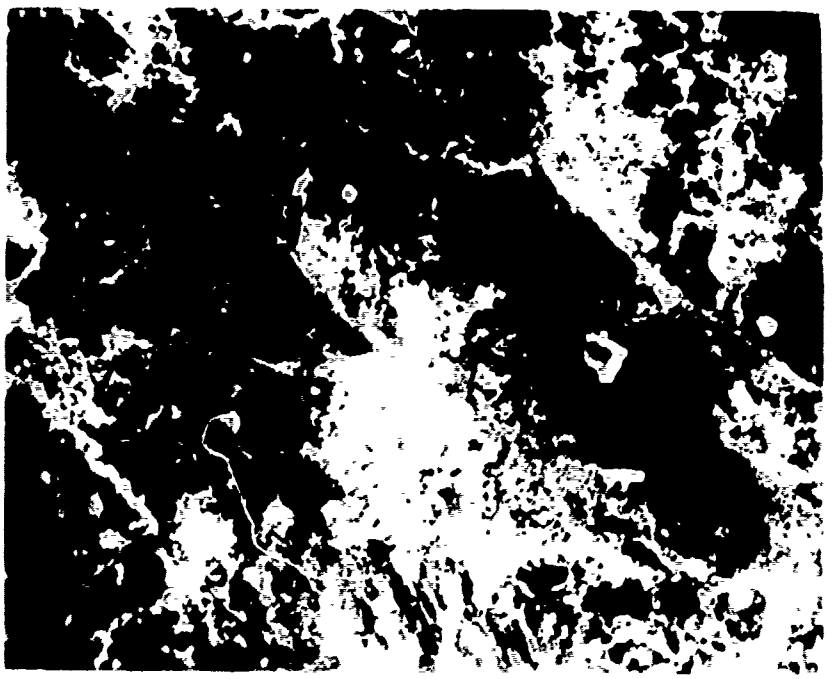

Figure 6. Scanning electron micrograph of limestone surface after sliding, debris left in place.
σ_n = 20 kg/cm², 300X.

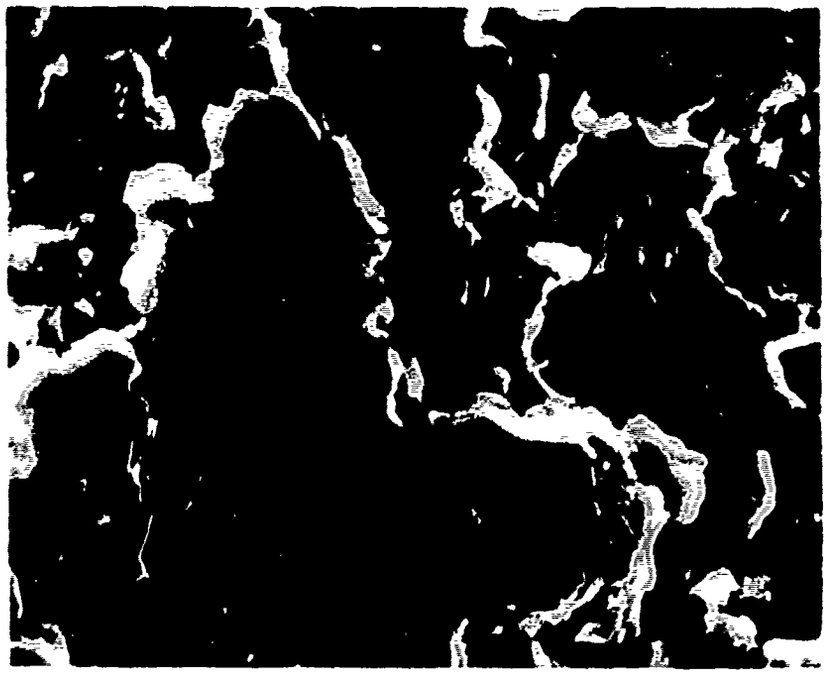

(a)

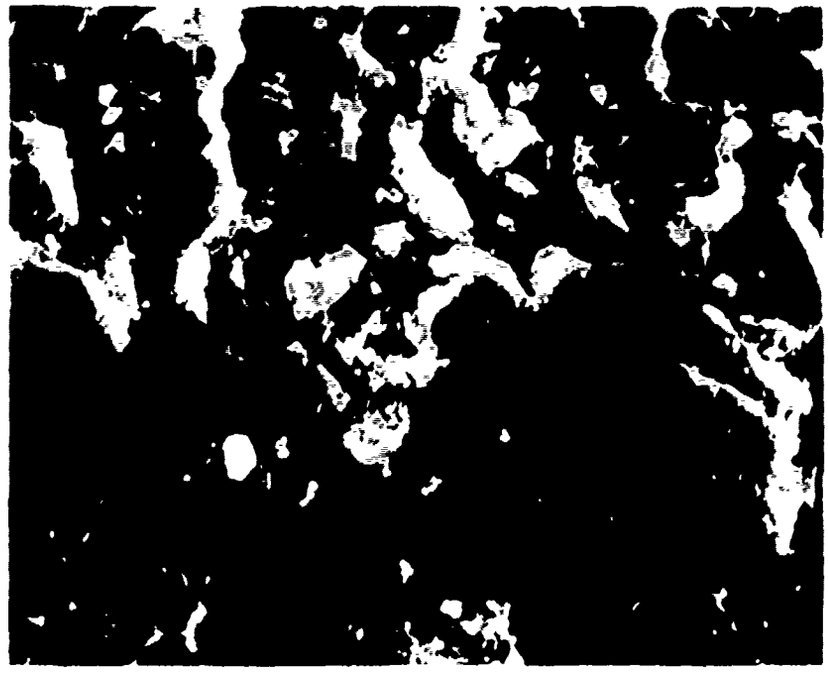

(b)

Figure 7. Scanning electron micrographs of ground basalt surfaces (a) before, and (b) after sliding, σ_n = 10 kg/cm^2. 1000X.

after sliding at 10 kg/cm^2 was also examined under the scanning electron microscope. Compared to the limestone, remarkably little debris was noted (Figure 7b). Most of the debris had fallen into lower areas, but some is present on higher areas. As with the limestone, most of the debris appears to have been removed by brittle fracture from the edges of the higher, flat crystal faces.

Because of the hardness of the quartzite, very little surface damage was noted. Two striations were observed after a test at 3.0 kg/cm^2, but the amount of damage was not sufficient to be noticeable after the dust along the marks was washed away.

Effect of added debris

Sliding obviously produced debris, and study of the stick-slip patterns in the limestone showed obvious changes in the character of slip and time between slip patterns with continued forward movement. It was thought that the debris produced upon sliding might be very influential in determining the character of stick-slip. Hoskins et. al. (1968) concluded that debris produced by the sliding would cause stick-slip to disappear, a conclusion also reached by Dieterich (1970).

It was decided, therefore, to artificially introduce debris in the form of ground rock fragments between the two sliding blocks from the beginning of sliding, in order to observe the nature of stick-slip sliding when energy was not being expended in producing the debris.

In a test at 1.95 kg/cm^2, 0.02 grams of powdered debris was added. Though this was more debris than was collected from the surface after the preceding test, no change in stick-slip pattern was noted.

In subsequent debris tests on limestone at higher normal stresses, 0.05 grams of debris were added. The added debris was not all sub-microscopic in size, as was that created by sliding, but ranged in diameter from 0.05 mm downwards. This debris had a significant effect on the nature of stick-slip, especially at the initiation of movement. In the tests with added debris, the

initial group of slips is the smallest in length of the entire test, and the amount of slip then increases rapidly to a value similar to that finally attained in the tests begun on clean blocks. Thus, addition of a finite amount of gouge between the sliding blocks appears to speed up what occurs on an initially clean joint in a longer time.

The result of adding debris between blocks of basalt is very similar to the result on limestone. In the lightest normal stress test with debris added ($3.0\ kg/cm^2$), a chaotic alternation of stick-slip, smooth slip, and creep occurred at 30^o. Upon raising the temperature to 125^o, stick-slip became established at a constant mean value, but with a standard deviation which was large and which increased with further movement. In a test B4 at $5.0\ kg/cm^2$, the debris test also seemed to reach a constant mean value of slip rapidly, but this value was accompanied by a large standard deviation.

Debris tests were not performed on quartzite, as already indicated.

The creation of addition of quantities of debris between sliding blocks of a joint system thus has a pronounced effect on stick-slip between the blocks, namely a more rapid approach to equilibrium conditions: In the amounts added, debris did not cause a cessation of stick-slip.

Effect of temperature

Temperature proved to be a major factor in controlling slip, time between slips, and shear load relaxation. In all cases, increasing the temperature of the rock while it was sliding in a stick-slip mode caused an increase in the time between slips, an increase in the length of individual slips, and an increase in the amount of relaxation of shearing load upon slip (Figures 8 and 9).

Temperature could be raised rapidly by the heaters in the temperature control enclosure of the shear box, but had to be reduced more slowly. When temperature decreased, the amount of stick, slip, and shear load relaxation all decrease with temperature until, in the limestone and sometimes in basalt, smooth slip finally became the mode of frictional movement.

The temperature of cessation of stick-slip (Table 2) varied from test to test for limestone and was lower than the temperature of initiation of stick-slip in all

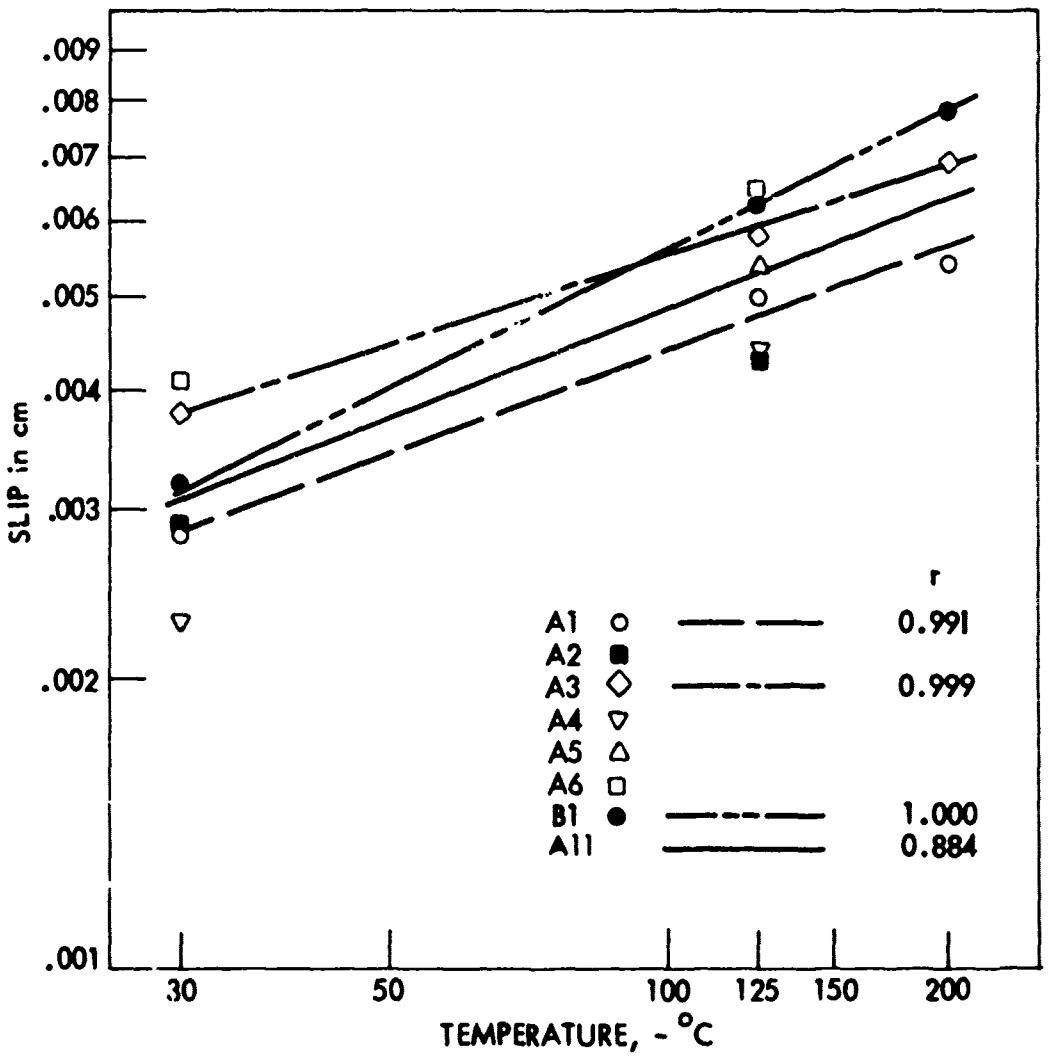

Figure 8. Change of average slip with temperature; Basalt Test B3. σ_n = 3.0 kg/cm²

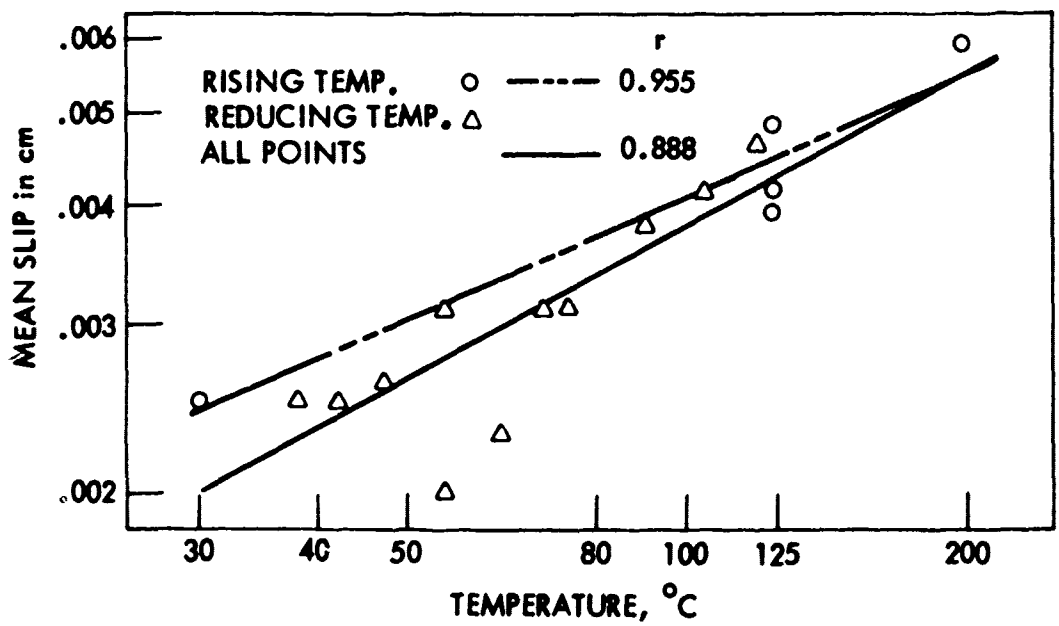

Figure 9. Change of average slip with temperature.
Limestone Test L10.
σ_n = 20.0 kg/cm^2

cases where some temperature rise from a lower temperature was required to induce the beginning of stick-slip.

Table 2. Temperature of cessation of stick-slip in limestone

Temperature of cessation Degrees Centigrade	Number of Events	
	Limestone	Basalt
30-40	0	3
40-50	7	0
51-60	3	1
61-70	1	0
71-80	4	0
81-90	2	0
91-100	9	0
101-200	2	2
200-		4
Would not stop	0	6

Generally the temperature of cessation varied with normal stress, with most of the lower temperatures representing tests with higher normal stress.

In the basalt, elimination of stick-slip by a reduction in temperature was more irregular than in the limestone, and in a number of tests, stick-slip could not be eliminated at all by temperature reduction. The few tests in which smooth slip was induced by temperatures reduction were in the higher normal stress tests, with smooth slip initiating at low temperatures (Table 2).

A peculiarity of the basalt was the frequency of the mode of sliding moving into smooth slip during continuous running at temperatures above 30^{o}. This occurred twice at 0.75 kg/cm^2 normal stress, and also occurred twice at 20.0 kg/cm^2. At 20.0 kg/cm^2 the block had moved the fairly extensive distance of 0.2677 cm when smooth sliding occurred, but the same block in the same test (B6A) subsequently continued stick-slip down to 37^{o} without going

into a smooth slip mode of sliding.

In the quartzite tests, smooth slip occurred only after a period of rest at 200°C, and lowering the temperature below 100°C caused a return to stick-slip. This is just the opposite of the reaction of the limestone and the basalt, probably reflective of a different surface property.

The coefficient of static friction was evaluated from the maximum shearing load immediately before the beginning of slip, divided by the normal load. No evaluation was made of the dynamic coefficient of friction, which in stick-slip studies is usually taken as the load at one half of slip distance divided by normal load. The behavior of the coefficient of static friction was seen to vary with rock type, frictional history, normal stress, and temperature. The evaluation of coefficient of friction was carried through temperature changes after comparison of measured values of coefficient of friction upon unloading with the calculated coefficient of friction of the last slip immediately before unloading showed the two values to be the same. Gaps in the solid lines on the plots of coefficient of friction versus cumulative distance moved represent the end of a day's run and, usually, unload of the shear load before start of the next day's run.

Under light normal loads the coefficient of friction of limestone tended to decrease to a constant value (Figure 10). This was the exception, however, because under higher normal loads (Figure 11) and in all tests on basalt and on quartzite, as the test progressed friction increased to approach a constant value. This is illustrated in Figures 12 and 13.

The final coefficient of friction for limestone tended to increase with higher normal stress (Figure 14) but not for the basalt (Figure 15) perhaps because the sliding distance was insufficient for friction to reach equilibrium value. The data for quartzite show a similar trend to limestone but are rather sparse.

The effect of temperature on friction is shown in Figures 11 and 13, an increase in temperature increasing the coefficient of sliding friction.

Debris tests showed similar characteristics of a very rapid rise from a low initial coefficient of friction to a stable value. This often is approximately maintained despite any alteration of temperature up or down or any alteration of the mode of sliding to smooth slip from stick-slip.

The values of debris-added coefficient of friction for the limestone contrasts sharply with the values for blocks which were slid with initially clean surfaces, being much higher and resembling that attained in the 20.0 kg/cm^2 normal stress test (Figure 14).

In the basalt tests, addition of debris does not change the pattern of increase of coefficient of friction with accumulated slip, but it does seem to speed is up considerably, being reached after 0.1-0.3 cm sliding. In all cases, the coefficient of static friction of debris tests in basalt is lower than the coefficient of tests begun with clean blocks, debris tests approaching a value of 0.6 while clean tests reach initial stability at 0.9 to 1.0. Temperature changes cause a greater reaction in clean tests than in debris tests.

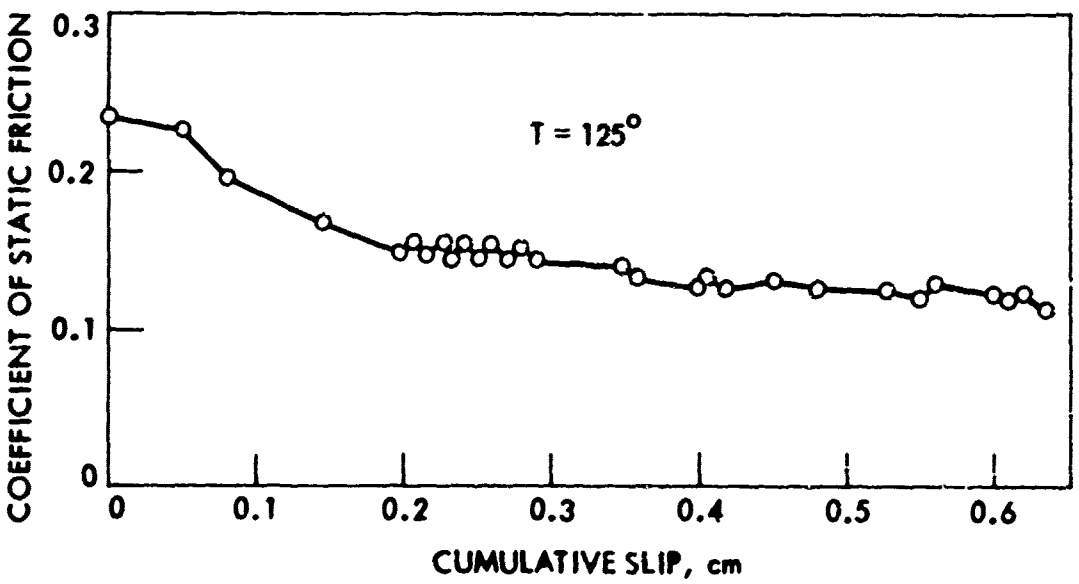

Figure 10. Pattern of coefficient of static friction for limestone. Test L7A σ_n = 3.0 kg/cm^2.

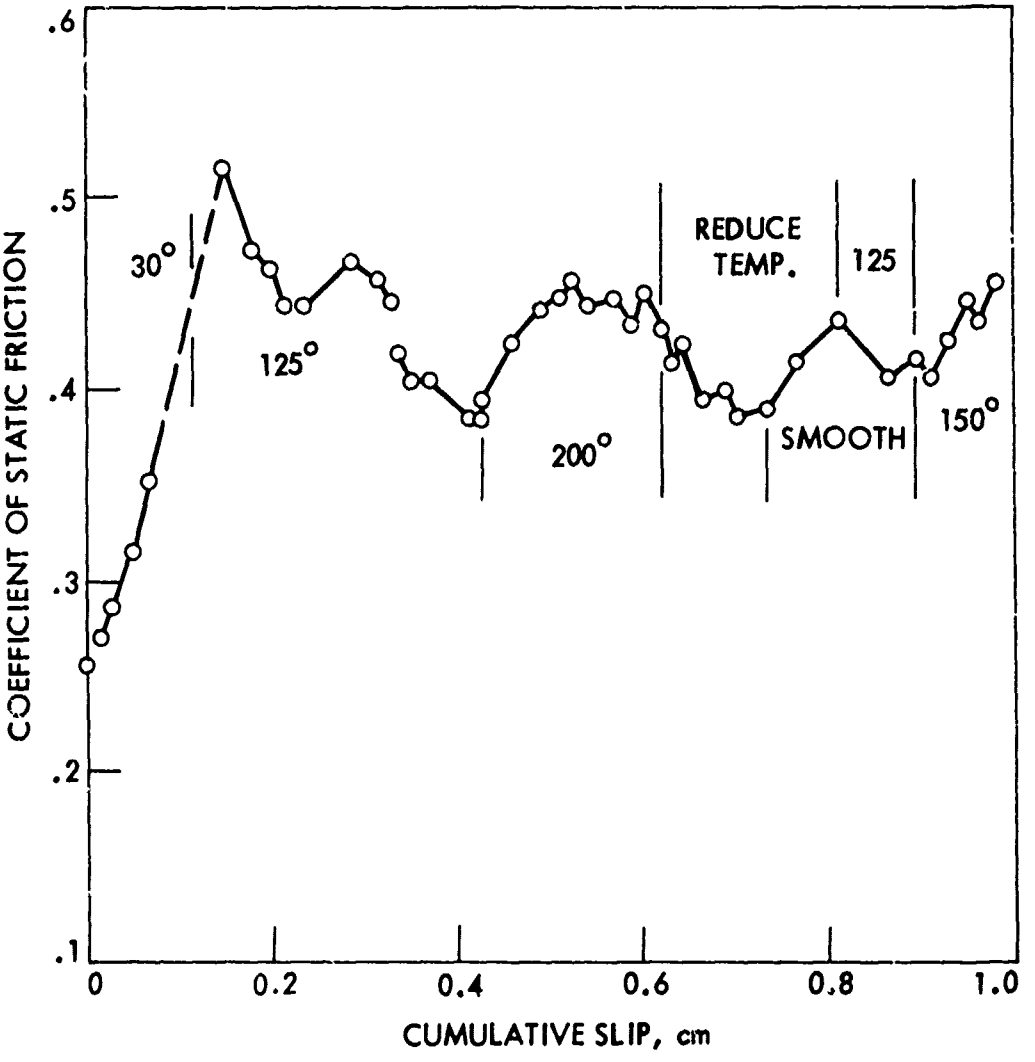

Figure 11. Pattern of coefficient of static friction.
Limestone Test L8A
σ_n = 5.0 kg/cm^2.

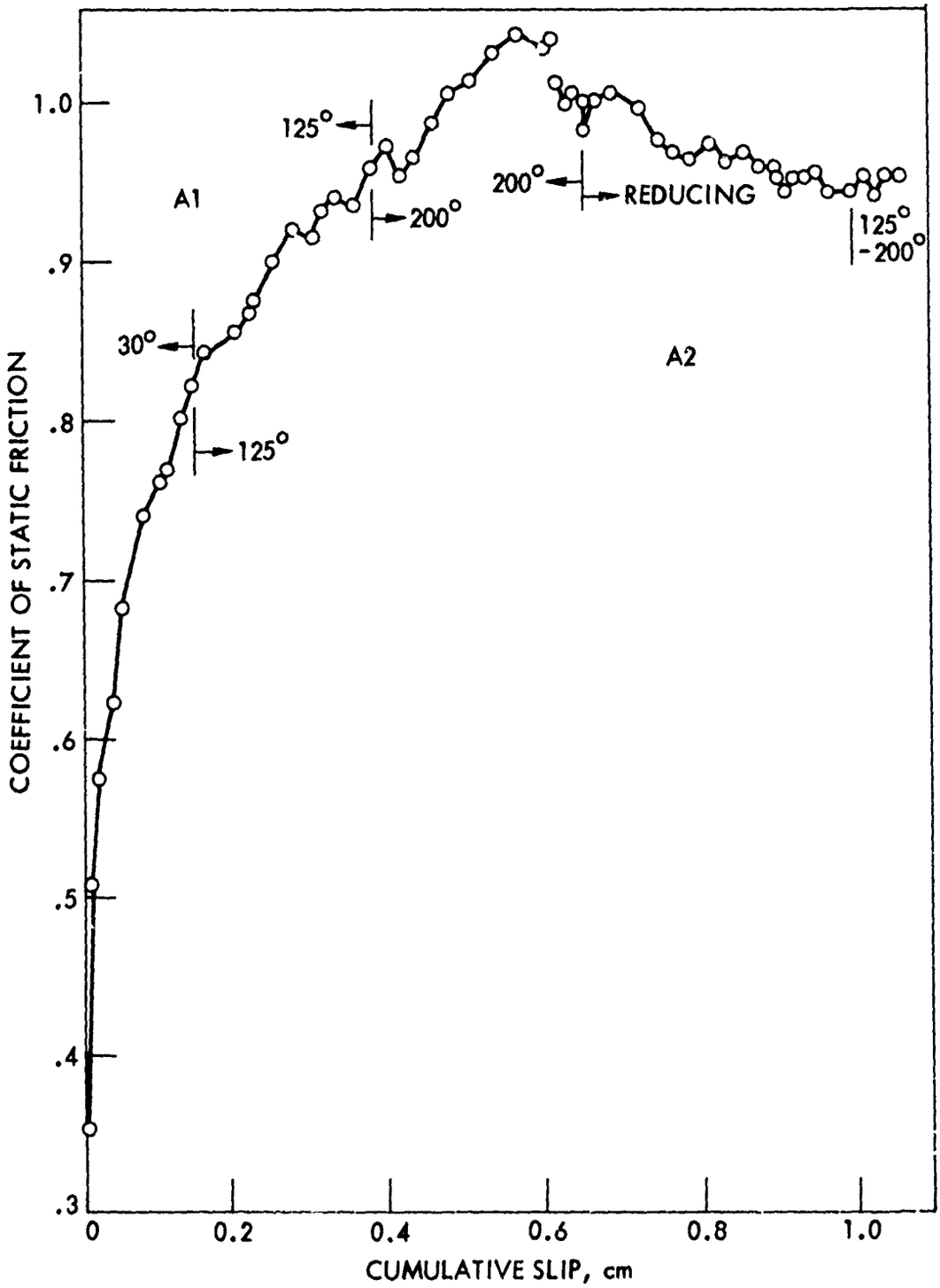

Figure 12. Pattern of coefficient friction. Basalt Test B7A.

σ_n = 10.0 kg/cm^2

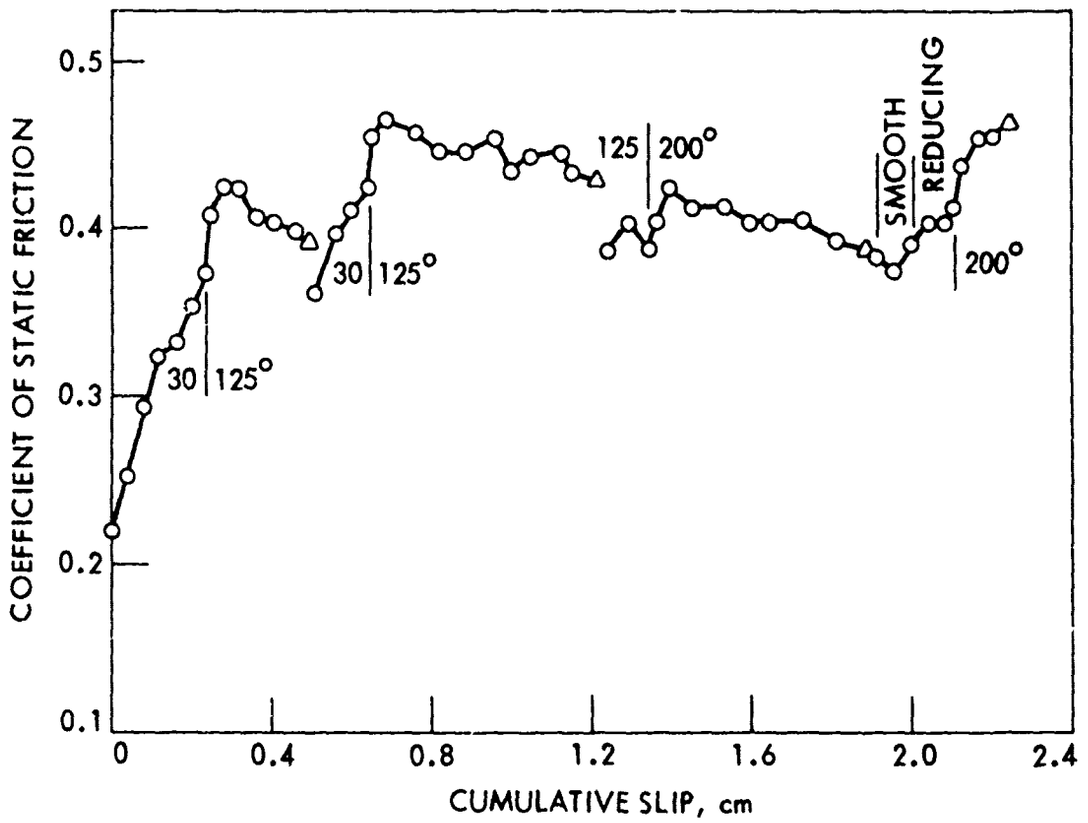

Figure 13. Pattern of coefficient of static friction. Quartzite Test Q2, σ_n = 3.0 kg/cm^2.

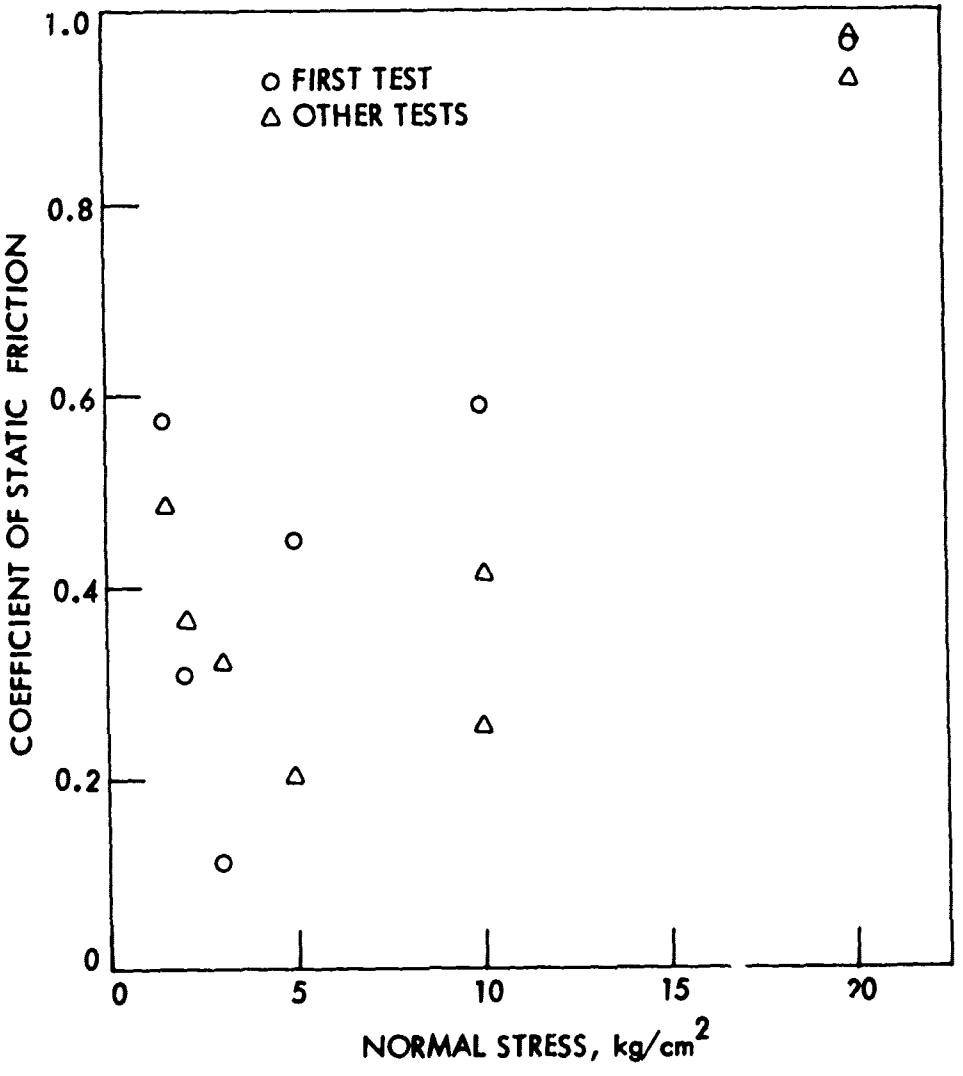

Figure 14. Limestone final coefficient of friction, non-debris tests.

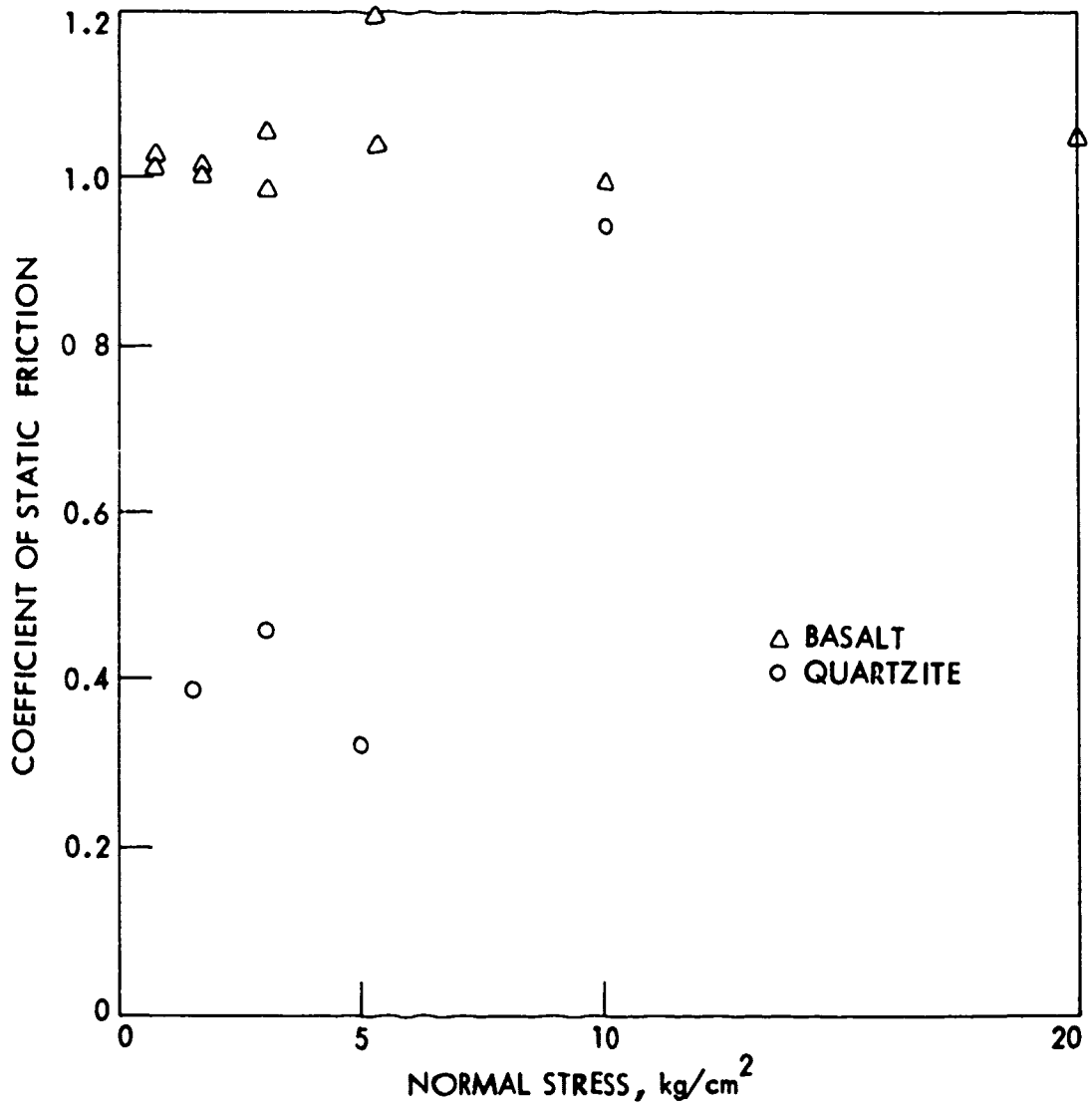

Figure 15. Basalt and quartzite final coefficients of friction.

DISCUSSION

A great deal of information on the stick-slip patterns of rock, some of it seemingly trending in opposing directions, has been gathered. It is believed, however, that most of the patterns of change in type and amount of slip and coefficient of friction with temperature, cumulative slip, and time can be integrated into a single model for the mechanism of stick-slip in rock, which, while perhaps not correct, will at least aid in organizing results.

It is obvious from these tests that stick-slip will occur in any rock, given a soft loading system such as gravity, that used in the experiments, or almost any other system with physical discontinuities allowing a degree of freedom perpendicular to the surface of sliding (Tolstoi, 1967). Stick-slip was the prevalent mode of sliding in a limestone, a basalt, and a quartzite. Only the latter contains a significant amount of quartz. Stick-slip can, then, be regarded as a universal phenomenon in rocks, given the proper conditions of movement and force.

The results of the tests on the limestone suggest that smooth slip, whenever it can be induced, may be caused by a film of adsorbed water. On the majority of low-normal-stress tests, stick-slip did not commence until the temperature was raised above 100^{o}. Even on the higher normal stress tests, reduction of temperature after a period of stick-slip at a higher temperature to a level permitting the adsorption of water resulted in the cessation of stick-slip. Temperature usually had to be raised above 100^{o} for stick-slip to reinitiate. A similar relationship between friction and adsorbed water was found by Peterson and Murray (1967) for ceramic materials.

The tests with normal stress of 3 kg/cm^2 and over, and the lighter loaded blocks which began stick-slip below 100^{o} were clean blocks. The absence of debris would permit some major asperities to come into direct contact, penetrating, as it were, the intervening film of adsorbed water and thus initiating stick-slip at low temperature. At the higher normal stresses the

adsorbed water may be reduced to a monolayer or removed entirely on the higher flat asperities. The presence of this water may also cause anomalous creep (Westbrook and Jorganson, 1965) of the crystals in contact, increasing the surface area and the bonding. This is known as the Rebinder effect (Westwood et. al., 1967). Once initiated, stick-slip might continue as the asperities, and then the debris, penetrated and disturbed the film of adsorbed water.

Further support to the concept of smooth sliding at low temperature on a boundary layer of adsorbed water is given by activation energies. In one phase of these experiments, the measurement of activation energy required to initiate and maintain creep of limestone blocks separated by a joint was attempted. These experiments are described in Appendix A. The results were found to have a bearing on the current problem. The activation energies obtained were found to be temperature dependent. For creep begun below 100^{o}, activation energies ranged from -5.12 to -10.73 kilocalories per mole, averaging -7.54 kilocalories per mole. This value compares favorably to the value for activation energy of water of -4 to -5 kilocalories per mole determined by Glasstone, Laidler, and Eyring and reported by Mitchell, Singh, and Campanella (1969). Further, activation energies determined at higher temperatures show a definite increase with temperature, with an average value of -23.0 kilocalories per mole for temperature between 140^{o} and 200^{0}. This value is similar to that determined for dry sand, about -25 kilocalories per mole, by Mitchell, Singh, and Campanella (1969). According to Horn and Deere (1962), the oven dried, air-equilibrated coefficients of friction of calcite and quartz are almost identical. Thus it is believed that most adsorbed water is being driven off, with time, when temperatures reach above 100^{o}, and that limestone asperity to asperity contact is taking effect. The fact that the average value of the activation energy below 100^{o} is above that of liquid water is believed due to a higher energy of adsorption (Noble and Demirel, 1969).

In most cases, the basalt did not begin movement with smooth slip, or attain smooth slip, even at low temperature. The basalt did, however,

normally display "30° basalt stick-slip" at temperature below 100° upon initiation of movement. This irregular motion, often accompanied by creep between stick-slips, is believed to be affected by adsorbed water. The bonding between the crystals of basalt is believed to be superior to that between those of the limestone. It is entirely possible that the surface effect caused by adsorbed water causes a time-dependent reduction of surface hardness. This reduction of surface hardness occurs in many nonmetallic crystals such as MgO (Westwood et. al., 1967) and Al_2C_3 (Westbrook and Jorganson, 1965). If it occurs more readily in plagioclase than in calcite it would explain the irregular 30° basalt movement, as caused by bonding alternating with water-water contact.

The basalt did go into smooth slip upon reduction of temperature three times. In these cases, adsorbed water could be present in more than usual thickness, and smooth slip could ensue. In all basalt temperature reductions, time lengths of slip stretch out as temperature reduces and bonding fails.

The rather unique behavior of the quartzite going into stick-slip upon a reduction of temperature below 100°C suggests a stronger Rebinder effect, also indicated by the well-known property of water as an anti-lubricant on smooth surfaces of quartz (Horn and Deere, 1962).

Above 100° in the limestone and at most temperatures in the basalt and quartzite, true asperity to asperity contact probably occurs. These contacts may be plastic and/or elastic. Consideration of the characteristics and patterns of the tests leads to the belief that plasticity and adhesion by bonding of the asperities as described by Bowden and Tabor is a critical factor in the mechanism of stick-slip in rock.

The asperities involved have been shown to be small areas of flat cleavage faces which are slightly higher than adjoining areas and thus can come into contact with the opposing flat cleavage face. Above 100° the Rebinder effect of surface softening due to water does not occur but the increased temperature may encourage plastic deformation of the asperities. In limestone, confining

pressure has been shown to have a pronounced effect on ductility. At low strains and confining pressures of around 600 bars, uniform flow occurs at room temperature (Donath et. al., 1971). If the asperities occupy one percent of the apparent area of contact, which is not an unreasonable value, pressures of up to 2000 bars were applied to the limestone asperities in the present tests, fully sufficient for uniform flow and plastic deformation to occur. Upon close contact of the asperities, actual chemical bonding is believed to take place, as the atoms of the asperity are not able to distinguish between the two sides of the contact.

When bond strength is exceeded by the constantly increasing shear force of the tests, slip occurs. As the slip rate decreases, bonding can again take over at whatever asperities are in contact. With the time required for the shear load relaxation to recover to the former load level in a soft system where the load cannot follow the movement, bonding will increase with time of asperity contact. The same general effect is believed to occur in the basalt and the quartzite.

Increase of temperature allows further plastic deformation and larger areas of contact of the asperities and a longer time is required to build up the required shearing force to break the developed bonds. The strength of bonding thus increases, as shown by Kosterin and Kraghelsky (1962). The excess of static coefficient of friction over kinetic coefficient of friction then means a larger slip, a larger stick, and a larger shear load relaxation with increase of temperature.

All of the test results on limestone, basalt, and quartzite show the dependence of stick-slip quantities on temperature, yet Heard (1960) shows that the brittle shear strength of a limestone similar to that tested is not affected within the temperature and nominal normal stresses used in this experiment. Similarly, a typical basalt varied only 2% in its bulk modulus between 25° and 200° (Nafe et. al., 1968), bulk modulus being simply related to the elastic (Youngs) modulus. Since strength and elastic properties do not vary appreciably with temperature in the range tested, the internal properties

of the material do not seem to be involved in stick-slip so much as the properties and reactions in the surface and near surface; that is, the asperities and their roots and surroundings. Plastic deformation, which is affected strongly by temperature, is regarded as the probable mode of deformation in the surface.

In this connection basalt, unconfined at room temperature, is seemingly a very brittle material. The pattern of slip, however, is almost precisely that of a very ductile material. How can this be explained? One factor is alignment of the basalt crystals because of its origin as a flow. The flow boundaries gave an external lineation to the basalt which is reflected by an internal lineation, at least with the plagioclase feldspar crystals. Test series where the upper and lower blocks were arranged so the lineation was parallel gave good stick-slip, whereas one basalt test series had the flow directions of top and bottom blocks perpendicular and gave poor stick-slip. Apparently, good bonding in the basalt only occurs if the crystals are properly oriented.

Secondly, poor conductors of heat create very high temperature rises upon sliding. Even at sliding speeds as low as 1 or 2 feet per second, temperatures tend toward the melting points at surfaces in contact (Bowden and Tabor, 1954). Basalt, with a thermal conductivity of 4.1 to 6.0 x 10^{-3} cal/cm-sec ^{o}C, is a poor thermal conductor (Nafe and Drake, 1968). In metals most of the heat is diffused into the bulk of the metal, but rock heat created upon sliding is slow to diffuse, and the contact surface may reach the melting point of plagioclase feldspar, 1090^{o}C at one bar pressure, but as low as 750^{o}C at 5000 bars (Turner and Verhoogen, 1960). At these temperatures of the asperity, plastic flow easily occurs and the bonding becomes stronger. With the ambient temperature aiding in the temperature rises, intimate contact becomes even easier, and bonding even stronger. A partial melting and recrystallization of the plagioclase feldspar with each slip would shortly bring slightly misaligned crystals into good alignment with the direction of slip.

The combination of a softening crystal and shear stress would result in the same phenomenon in basalt as occurs in metals - junction growth. The tangential stress combined with the plasticity and bonding of the crystal permits a growth of the area in good bonding contact of each asperity in the direction of the shearing stress. If the increase of shear force is faster than the junction growth, slip occurs. The presence of contaminants will also inhibit junction growth. As each slip occurs, more of the asperity areas are increased. Thus as the sliding continues, asperity area increases, bonding gets better, and the stick-slip parameters become larger.

CONCLUSIONS

The tests conducted on a limestone, a basalt, and a quartzite suggest the following general conclusions:

1. Stick-slip may be a universal phenomenon in rocks, having been demonstrated in three widely divergent rock compositions.

2. Stick-slip of lightly loaded rocks is due to asperity to asperity bonding. This bonding is affected by temperature and is believed to be due to plastic deformation of asperities. Junction growth of asperities may occur in some rocks.

3. The amount and character of stick-slip relate to the loading system involved and the mineralogical composition of the rock.

4. Temperatures above those at the initiation of stick-slip result in larger slips, longer sticks, and higher shear load relaxations. The rates of change with increasing temperature depends on the material.

5. When smooth slip occurs, it will usually occur at temperatures below $100^{o}C$. Smooth slip at low temperature is due to a boundary layer of adsorbed water. As the adsorbed water is driven off, stick-slip is induced. Alternatively at low temperatures the Rebinder effect may cause a softening of the surface by water, leading to creep of asperities and increased bonding. This results in stick-slip at low temperatures.

6. Brittle fracture and the accumulation of debris both act to reduce the amount of stick-slip at a given temperature, by reducing the area of bonding of asperities and by producing weaker bonds in the system. Debris separates the crystals which must be aligned for good bonding. Smooth slip may occur below 100^{o} in blocks covered with debris in the same manner as in initially clean blocks.

REFERENCES CITED

Archard, J. F., "Elastic Deformation and the Laws of Friction," Proceedings of the Royal Society, Vol. A243, 1957, pp. 190-205.

Archard, J. F., "Single Contacts and Multiple Encounters," Journal of Applied Physics, Vol. 32, 1961, pp. 1420-1425.

Beyer, S. W. 1897. The Sioux Quartzite and Certain Associated Rocks. Iowa Geological Survey Annual Report. 6: 67-112.

Bikerman, J. J., "Thermodynamics, Adhesion, and Sliding Friction," Journal of Lubrication Technology, Trans. ASME, Vol, 92, Series F, No. 2, 1970, pp. 243-247.

Bowden, R. P., and Tabor, D., The Friction and Lubrication of Solids, Part 1, Clarendon Press, Oxford, 1954.

Bowden, F. P., and Tabor, D., The Friction and Lubrication of Solids, Part 2, Clarendon Press, Oxford, 1964.

Brace, W. F., and Byerlee, J. D., "California Earthquakes: Why Only Shallow Focus?" Science, Vol. 168, 1970, pp. 1573-1575.

Brockley, C. A., and Davis, H. R., "The Time Dependence of Static Friction," Journal of Lubrication Technology, Trans, ASME, Vol. 90, Series F, 1968, pp. 35-41.

Brockley, C. A., Cameron, R., and Potter, A. F., "Friction Induced Vibration," Journal of Lubrication Technology, Trans, ASME, Vol. 89, Series F, 1967, pp. 101-108.

Brown, E. T, and Trollope, D. H., "Strength of a Model of Jointed Rock," Journal of the Soil Mechanics and Foundations Division, ASCE, Vol. 96, No. SM 2, 1970, pp. 685-704.

Byerlee, J. D., "Frictional Properties of Granite at High Confining Stress," Journal of Geophysical Research, Vol. 72, 1969, pp. 3639-3648.

Byerlee, J. D., "The Mechanics of Stick-Slip," Tectonophysics, Vol. 9, 1970, pp. 475-486.

Byerlee, J. D., "Theory of Friction Based on Brittle Fracture," Journal of Applied Physics, Vol. 38, 1967, pp. 2928-2935.

Coulson, J. H., The Effects of Surface Roughness on the Shear Strength of Joints in Rock, Technical Report MRD-2-70, Missouri River Division, Corps of Engineers, Omaha, 1970.

Derjaguin, B. V., Push, V. E., and Tolstoi, D. M., "Theory of Slipping and Periodic Sticking of Solid Bodies "Frictional Self-Oscillation of the First Kind)," Soviet Physics - Technical Physics (English Edition), Vol. 1 (Russian Vol. 26), 1956, pp. 1299-1312.

Dieterich, J. H., "Time Dependence in Stick-Slip Sliding," (Abstract), Eos, Transactions of the American Geophysical Union, Vol. 5, 1970, p. 423.

Donath, F. A., Faill, R. T., and Tobin, D. G., "Deformational Mode Fields in Experimentally Deformed Rock, Geological Society of America Bulletin, Vol. 82, 1971, pp. 1441-1462.

Drennon, C. B., 1972. Stick-slip of Lightly Loaded Rock. Unpub. Ph.D. Thesis, Iowa State University Library. 168 pp.

Drennon, C. B., and Handy, R. L., April 1972. Stick-slip of lightly Loaded Limestone. Progress Report, Engineering Research Institute, Iowa State University, Contract DASA01-69-C-0148. Published in International Journal of Rock Mechanics Min. Science 9: 60 3-615.

Glasstone, S., Laidler, K., and Eyring, H., The Theory of Rate Processes, McGraw-Hill, New York, 1941.

Greenwood, J. A., and Williamson, J. B. P., "Contact of Nominally Flat Surfaces," Proceedings of the Royal Society, Vol. A295, 1966, pp. 300-319.

Heard, H. C., "Transition from Brittle to Ductile Flow in Solenhofen Limestone as a Function of Temperature, Confining Pressure, and Interstitial Fluid Pressure," in Griggs, D., and Handin, J., eds., Rock Deformation, Geological Society of American Memoir 79, 1960, pp. 193-226.

Horn, J. M., and Deere, D. U., "Frictional Characteristics of Minerals," Geotechnique, Vol. 12, 1962, pp. 319-335.

Hoskins, R. R., Jaeger, J. C,, and Rosengren, K. J., "A Medium-Scale Direct Friction Experiment," International Journal of Rock Mechanics and Mining Science, Vol. 5, 1968, pp. 143-154.

Jaeger, J. C., "Friction of Rocks and Stability of Rock Slopes," Geotechnique, Vol. 21, 1971, pp. 97-134.

Jaeger, J. C., "Frictional Properties of Joints in Rocks," Geofisica Pura et Applica, Vol. 43, 1959, pp. 148-158.

Johnson, K. I., and Keller, D. V., Jr., "Effect of Contamination on the Ashesion of Metallic Couples in Ultra-High Vacuum," Journal of Applied Physics, Vol. 38, 1967, pp. 1896-1908.

Kosterin, J. I., and Kraghelsky, I. V., "Rheological Phenomena in Dry Friction," Wear, Vol. 5, 1962, pp. 190-197.

Lajtai, E. Z., "Mechanics of Second Order Faults and Tension Gashes," Geological Society of American Bulletin, Vol. 80, 1969, pp. 2253-2279.

Lambe, T. W., and Whitman, R. V., Soil Mechanics, John Wiley and Sons, New York, 1969.

Maurer, W. C., "Shear Failure of Rock under Compression," Society of Petroleum Engineers Journal, Vol. 5, 1965, pp. 167-175.

Merchant, M. E., "Friction and Adhesion," in Ku, P. M., ed., Interdisciplinary Approach to Friction and Wear, NASA SP-181, Washington, 1968, pp. 181-265.

Mitchell, J. K., Campanella, R. G., and Singh, A., "Soil Creep as a Rate Process," Journal of the Soil Mechanics and Foundations Division, ASCE, Vol. 94, No. SM 1, 1968, pp. 231-253.

Mitchell, J. K., Singh, A., and Campanella, R. G., "Bonding, Effective Stresses, and Strength of Soils," Journal of the Soil Mechanics and Foundations Division. ASCE, Vol. 95, No. SM 5, 1969, pp. 1219-1246.

Nafe, J. E., and Drake, C. L., "Physical Properties of Basalt," in Hess, H. H., and Poldervaart, A., eds., Basalts, Vol. 2, Interscience, New York, 1968, pp. 483-502.

Noble, C. A., and Demirel, T., "Effect of Temperature on the Strength Behavior of Cohesive Soil," Proceedings of International Conference on Effect of Temperature and Heat on Engineering Behavior of Soils, Highway Research Board Special Report 103, 1969, pp. 204-219.

Patton, F. D., "Multiple Modes of Shear Failure in Rock," First International Conference on Rock Mechanics, Lisbon, Vol. 1, 1966, pp. 509-513.

Peterson, M. B., and Murray, S. F., "Frictional Behavior of Ceramic Materials, Materials Engineering Quarterly, Vol. 7, 1967, pp. 22-29.

Rabinowicz, E., Friction and Wear of Materials, John Wiley and Sons, New York, 1965.

Rabinowicz, E., "The Nature of Static and Kinetic Coefficients of Friction," Journal of Applied Physics, Vol. 22, 1951, pp. 1373-1379.

Ripley, C. F., and Lee, K. L., "Sliding Friction Tests on Sedimentary Rock Specimens," Communication 8, Seventh Congress on Large Dams, Vol. 4, 1961, pp. 657-671.

Simkins, T. E., "The Mutuality of Static and Kinetic Friction," Lubrication Engineering, Vol. 23, 1967, pp. 26-31.

Singh, A., and Mitchell, J. K., "A General Stress-Strain-Time Function for Soils," Journal of the Soil Mechanics and Foundations Division, ASCE, Vol. 94, No. SM 1, 1968, pp. 21-46.

Tabor, D., "Critical Appraisal and Research Opportunities - The Lubrication Research Viewpoint," in Ku, P. M., ed., Interdisciplinary Approach to Friction and Wear, NASA SP-181, Washington, 1968, pp. 385-406.

Terzaghi, K., Erdbaumechanik, Vienna, 1925, pp. 50-52, translated Casagrande, A., in Bjerrum L., et. al., ed., From Theory to Practice in Soil Mechanics, John Wiley and Sons, New York, 1960, pp. 173-174.

Tolstoi, D. M., "Significance of the Normal Degree of Freedom and Natural Normal Vibrations in Contact Friction," Wear, Vol. 10, 1967, pp. 199-213.

Tomlinson, G. A., "A Molecular Theory of Friction," Philosophical Magazine, Vol. 7, 1929, pp. 905-939.

Turner, F. J., and Verhoogen, J., Igneous and Metamorphic Petrology, 2d ed., McGraw-Hill, New York, 1960.

Wells, J. H., "Kinetic Boundary Friction," The Engineer, London, Vol. 147, 1929, pp. 454-456.

Westbrook, J. H., and Jorgensen, P. J., "Indentation Creep of Solids," Transactions of the Metallurgical Society of AIME, Vol. 233, 1965, pp. 425-428.

Westwood, A. R. C., Goldheim, D. L., and Lye, R. G., "Rebinder Effects in MgO," Philosophical Magazine, Vol. 16, 1967, pp. 505-519.

APPENDIX A.

ACTIVATION ENERGY FOR CREEP ALONG JOINTS OF LIMESTONE

Introduction

In order to allow movement of one material past another, the bonds connecting the materials must be broken. If the Bowden and Tabor theory of adhesion friction (1964) is correct, the friction of rock joints should be controlled by bonding of asperities across the joint. If the materials then slide slowly past each other, or creep, the rate of such movement should depend on the rate of making and breaking of bonds. This rate can be investigated using the postulates of the rate process theory first set forth by Eyring in Glasstone et. al. (1941) for chemical solutions and later extended to soils by Noble and Demirel (1969) and Mitchell et. al. (1968, 1969). An attempt to confirm this hypothesis was made using temperature-controlled direct-shear of limestone. The results are only preliminary because of the overwhelming domination of tests by stick-slip.

Theory

The investigation of creep of limestone along joints centered on use of the rate process assumption to determine the applicability of the rate process equation (Noble and Demirel, 1969):

$$\ln \dot{\delta} = \ln A - \frac{\Delta H}{kT} + \beta(\tau - \mu p_n) \qquad \text{(A-1)}$$

where $\dot{\delta}$ is creep rate, ΔH is activation enthalpy, k is Boltzmann's constant, T is absolute temperature during shear, $\beta = \beta'/kT$ where β' is flow unit volume and $\beta'\tau$ represents the energy applied by the shearing stress τ, μ is a coefficient representing the effect of dilatancy, p_n is normal stress, and A is a constant including the effects of structure (arrangement of crystals and grains of the rock) and of entropy. Written in exponential form:

$$\dot{\delta} = A \exp\left(\frac{-\Delta H}{kT}\right) \exp\left(\beta (\tau - \mu p_n)\right). \qquad \text{(A-2)}$$

The dilatancy of the smoothly ground limestone was not large enough to be measured with the measuring device available. Thus, under constant shear stress conditions the second exponential term may be included in the constant coefficient giving the following equation:

$$\dot{\delta} = X \exp\left(\frac{-\Delta H}{RT}\right) \qquad \text{(A-3)}$$

where $R = N_a k$; N_a is Avogadro's number and ΔH is considered as activation energy per mole.

Assuming that X is independent of temperature and that material structure is a constant included in X, activation energy can be evaluated by determination of the rate of deformation at different temperatures.

$$\frac{\ln \dot{\delta}_1 - \ln \dot{\delta}_2}{\left(\frac{1}{T_1} - \frac{1}{T_2}\right)} = \frac{-\Delta H}{R} \qquad \text{(A-4)}$$

The analysis of the relative size of flow units and thus the relative density of bonds is possible in tests conducted at a constant temperature. Bond density is analyzed by a jump-creep test which resembles a Dorn test with shear load suddenly increased instead of temperature. The rate of creep decreases with time in an approximately logarithmic manner (Mitchell et. al., 1969). Even relatively long-term "steady-state" creep is actually transient in rate. These decreasing creep rates can be analyzed according to methods developed by Singh and Mitchell (1968) and described as a stress-strain-time function for soils. The equation described by these authors is:

$$\frac{\dot{\epsilon}(\tau_2, t_j)}{\dot{\epsilon}(\tau_1, t_i)} = \left(\frac{t_i}{t_j}\right)^m + \left(\frac{t_i}{t_i - t'}\right)^m \exp\left[\alpha(\tau_2 - \tau_1) - 1\right] \qquad \text{(A-5)}$$

where $$\alpha = \frac{\ln (y + 1)}{\tau_2 - \tau_1} \qquad \text{(A-6)}$$

and $$y = \left(\frac{t_j - t'}{t_i}\right)^m \left[\frac{\dot{\epsilon}(\tau_2, t_j)}{\dot{\epsilon}(\tau_1, t_i)} - \frac{t_i}{t_j}^m\right] \qquad \text{(A-7)}$$

in which $\dot{\epsilon}$ is strain rate, for which, as dimensions do not change, deformation rate $\dot{\delta}$ may be substituted, t_i is any time during application of the initial shear stress τ_1, t' is the time after commencement of the test of application of the stress τ_2, and t_j is the time at which the strain rate $\dot{\epsilon}(\tau_2, t_j)$ is recorded under stress τ_2. The strain rates thus obtained can be related by

$$\dot{\epsilon} = A \exp(\frac{-\Delta H}{kT}) \exp(2\alpha\tau) \qquad (A-8)$$

For comparison with the rate process equation used in this investigation:

$$\alpha = \beta/2 \qquad (A-9)$$

$$\frac{\lambda}{S} = 4\alpha kT = 2\beta' \qquad (A-10)$$

where the λ component is the distance between equilibrium positions of bonds, and S is the number of flow units per unit area. The size of β' should decrease with increasing number of bonds in the same material. Therefore, β', which has volume units, should be a relative measure of the number of bonds.

Testing Procedure

The basic test apparatus is the same as that described in the body of this report. The exception is the mechanism for inducing the shear load. Since the creep tests were performed as constant stress type tests, the shear load mechanism was simply a wire running over a low-friction pulley with weights attached to the wire.

The specimens were prepared in the same manner as described for the stick-slip tests. After preparation all blocks were raised to 200°C in the testing apparatus with the normal load applied for four hours. The temperature was then decreased to the initial testing temperature. This was done so that all samples would have the opportunity to initially form the same number of bonds.

In order to check for full-shear load and prevent rapid movement upon initial creep loading, the upper block was initially loaded by slowly adding lead shot to the load device until full shear occurred. Full shear was defined as movement of the upper block across the lower block with continuous acceleration. After the full-shear load was recorded, any debris (usually none, in these cases with light normal load) was wiped off with a clean cloth. The rock was then repositioned, re-heated to 200°, and cooled to test temperature. A shear load less than that required for full shear was applied. Lead shot was then slowly added until creep was induced.

Early in the testing program it was recognized that dilatancy due to structural differences between blocks made it impossible to validly compare deformation rates on one block with those on another block. It was decided that valid data could be obtained by use of the Dorn temperature jump method, originally developed for creep studies of metals (Mitchell and Singh, 1969). In the Dorn method, the specimen is allowed to come to a steady state of deformation rate at a lower temperature T_1. The temperature is then raised as rapidly as possible to a higher temperature T_2 whereupon the strain rate increases to a second steady state deformation rate $\dot{\delta}_2$. When these values are substituted into equation (A-4), the activation energy is obtained.

Results and Interpretation

Calculation of activation energies by the Dorn method in individual blocks rapidly showed that activation energies were not temperature independent. Results are shown in Table A-1. In the table the temperature ranges represent zones within which the lower and higher temperature of the jumps are included. Individual jumps might have different beginning and ending temperatures within the ranges. The standard deviation as a percentage of the mean should be noted. This percentage is low in the temperature areas below 100°C quite irregular in the 100 - 150° range, and decreases again at higher temperature. To insure that activation energies do rise with temperature, and do not merely reflect the size of the temperature jump employed, the activation energy per

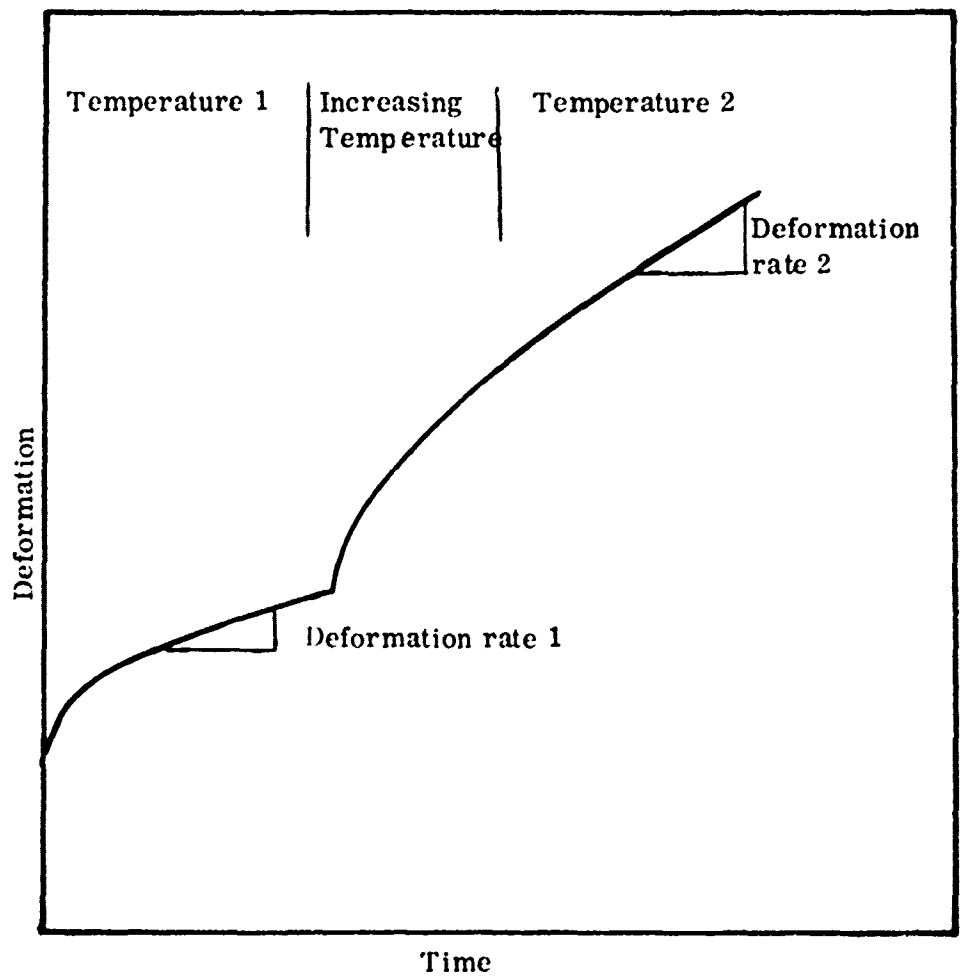

Figure A-1. Dorn temperature jump method for determination of activation energy.

Table A-1. Activation energy values for creep along limestone joints

Test	Normal stress kg/cm^2	Activation energy - kilocalories/mole Temperature ranges		
		35-100°	100-150°	140-200°
29	0.375	-9.226		
33B	0.751	-10.73		
34	0.751		-10.05	-36.43
37	0.751	-5.12		
40	0.751		-26.99	
42	1.220		-18.098	
43	1.220	-5.369	-13.917	
		-6.487		
46	1.220	-8.146		
49	1.877	-8.779	-5.590	
50	1.877		-10.599	-15.983
				-16.408
52	0.188		-8.709	-27.503
54	1.877		-5.279	-21.474
55	0.188			-12.525
56	0.188			-37.045
64	0.751	-6.466		
69D	0.751		-5.742	-28.651
69E	0.751			-24.673
69F	0.751			-11.108
Mean		-7.540	-11.664	-23.014
Standard deviation		1.991	7.129	9.849
Standard deviation as percentage of mean		26.4	61.1	42.8

degree of temperature rise during each jump was calculated, averaged according to the range of the jump, and is presented in Table A-2. The meaning of the temperature ranges if as noted above.

Table A-2. Change in activation energy per degree of temperature jump

Temperature range	Mean activation energy (kilocalories/mole/^{o}C)	Standard deviation
35 - 100^{o}	0.184	0.067
100 - 150^{o}	0.281	0.188
140 - 200^{o}	0.663	0.206

This demonstrates conclusively the dependence of activation energy upon temperature.

An attempt was made to determine if the temperature dependence could be expressed by a pre-exponential term, expressing deformation rate as:

$$\dot{\varepsilon} = BT^{m} \exp(-\Delta H/RT) \qquad (A\text{-}11)$$

Constant B and m values were not obtained. This is probably due to the importance of the structure factor in B, and the inability to separate structure factor from the items strictly dependent upon temperature.

The values of activation energies obtained seem to be indicative of different natures of sliding surfaces at different temperatures. The activation energy value at temperature below 100^{o}, -7.54 kilocalories per mole, is very similar to values for water, -4 to -5 kilocalories per mole, determined by Glasstone et. al. (1941). Values of activation energy for temperature between 140^{o} and 200^{o} is similar to the values of Mitchell et. al. (1969) for dry quartz sand. These observations lead to a conclusion that below 100^{o}C the creep of limestone is actually proceeding on a film of adsorbed water. Above 140^{o} true calcite-to-calcite bonds are obtained as all adsorbed water is driven off. An intermediate condition may prevail at intermediate temperatures until all water has had time to be removed. Chemisorbed or tightly physically adsorbed water may, indeed, remain in places, perhaps where asperities are not actually in contact. That the

activation energy value below 100^{o} is above that of water may be due to higher asperities physically squeezing out the water and permitting actual calcite-calcite bonds in limited places. It has also been speculated that the activation energy higher than that of liquid water may be due to a structural arrangement of the adsorbed water molecules which is different from that of liquid water.

Five tests conducted at 100^{o} proved amenable to analysis of the relative size of flow units by the method described in Equations (A-5) through (A-10). average values of Ω' obtained for the limestone are shown in Table A-3.

Table A-3. Flow unit volumes of limestone

Normal load (kilograms)	Normal stress (kg/cm^2)	Flow unit volume (cm^3)
100	1.88	5.493×10^{-19}
40	0.75	7.506×10^{-19}
10	0.188	592.0×10^{-19}

These values do tend to increase with decreasing normal load. Thus, the volume occupied by a single bond must decrease with increasing load. This indicates a relative increase in the number of bonds. The limited data base for this observation must be emphasized.

Conclusions

The following conclusions can be drawn from the creep tests on limestone:

1) Activation energy experiments show that ΔH is not independent of temperature but increases with increasing temperature. This does not refute the theoretical equations for activation energy, but indicates a change in the strength or nature of the chemical bonding with temperature.

2) The values of these strengths related to the test conditions and the temperatures involved lead to the conclusion that activation energies below $100^{o}C$ reflect creep occurring in a thin film of adsorbed water. Average activation energies are above that of water by a small amount. This is believed to reflect

either occasional calcite-calcite bonds, or to be a reflection of possible higher activation energy of adsorbed water compared to that of liquid water. Above 140°C, the large activation energy is believed to reflect true calcite-calcite bonding.

3) Limited data permitting calculation of flow volume units, which are proportional to the number of bonds, show that the number of bonds increases with increased normal load.

Part II

DILATANCY AND SHEARING BEHAVIOR OF ASSEMBLAGES OF RODS

K. Logani and R. L. Handy

INTRODUCTION

Statement of the Problem

The purpose of this research is to study and formulate a failure mechanism which could apply to movement of rock bodies along their joints and fracture planes. Rock bodies can acquire these features of layering, jointing, and fracturing either as a part of their geological origin or from external causes such as stress release, earthquakes, blasting, or other engineering activities. Such features in rock bodies are centers of weakness, and control strength.

Observed failures involving shear within rock or soil masses often occur in plane strain, i.e. with a relatively constant cross section normal to the failure surface. Such a two-dimensional failure can be modelled by plane-strain shear tests, whereby the rock or soil material is confined to prevent strain in the third dimension. In the present study, such strain was prevented not by confinement but by the geometry of the individual particles, which are rods lying parallel to one another in a shear box.

Scope

This research involves subjecting ideal assemblages of rods to a biaxial stress field, varying the principal stress ratio, and recording the stresses, strains, volume changes, and translocations and rotations of individual members of the assemblage. Simultaneously, a theory was developed to predict the behavior, such that the theory could be tested and revised as necessary.

The biaxial testing method used has the following advantages over the tests of natural materials.

1. A continuous photographically recorded inventory of individual particle movements in relation to assemblage stress, strain and volume changes.
2. Ready prediction of an ideal behavior, such that departures from the ideal can be identified and related to causes.

3. Controlled test conditions which minimize the sampling variable by reusing the same sample.
4. Ability of testing different regular geometrical array, affording a precise variation of void ratio and packing density.
5. An accurate visualization of failure mechanism, in that failure by sliding and/or rotation can be differentiated.

BACKGROUND AND LITERATURE REVIEW

In order to formulate a failure theory for a granular mass subjected to a biaxial stress field, it is necessary to understand the past and present concepts of dilatancy and sliding friction.

Dilatancy

Dilatancy -- "The property of granular masses of expanding in bulk with change of shape. It is due to the increase of space between the individually rigid particles as they change their relative positions" (Century Dictionary).

Dilatancy was first described and named by Professor Osborne Reynolds (1885), who showed that a dense sand mass expands upon shearing. He observed:

> . . . I would point out the existence of a singular fundamental property of such granular media which is not possessed by known fluids and solids. On perceiving some thing which resembles nothing within the limits of one's knowledge, a name is a matter of great difficulty. I have called this unique property of granular masses "dilatancy", because the property consists in a definite change of bulk, consequent on a definite change of shape or distortional strain, any disturbance whatever causing a change in volume and generally dilation.

Reynolds observed that with granular media, so long as the grains are held in mutual equilibrium by stresses transmitted through the mass, every change of relative position of the grains is attended by a consequent change in volume; and, if in any way the volume is fixed, than all change of shape in prevented. Professor Reynolds made one assumption, that the position of any internal particle becomes fixed if the positions of surrounding particles are fixed. Without frictional bridging of particles over voids, this condition would always be fulfilled. It follows that no grain in the interior can change its position in the mass by passing between the contiguous (touching) grains without disturbing them; hence, whatever alteration the medium may undergo,

the same particle will always be in the same neighborhood. If, then, such a medium is subjected to internal strain, the shape of each elementary group is determined by shape and arrangement of surrounding particles. Any distortion of the boundaries of such a medium will cause distortion of the arrangements of its particles, necessitating a change in volume and hence, the mean density. If particles are rigid, the relations between distortion and dilatancy are independent of friction; that is to say, the same distortion of any bounding surface must mean the same internal distortion whatever the friction may be. The only possible effect of friction is to render the grains stable under circumstances in which they would not otherwise be stable.

Mead (1925), while applying Reynolds' theory of dilatancy to solid rocks, concluded that incoherent, granular masses such as sand, in a condition approaching maximum density packing (rhombic packing), are dilated by deformation; whereas, in a condition of open packing (cubic packing), they deform without dilation. Prevention of free dilation by enclosing pressures induces failure by fracture or shear when the mass is deformed, and with development of joints and faults along thin zones of dilation. This manner of failure requires a minimum increase in volume and involves dilation only in the shear zone. When free dilation is not prevented, the granular mass deforms by flow. Such a deformation of closely packed grains involves the entire mass and causes a much greater volume increase than that required by failure along definite shear planes, and can be called plastic deformation or plastic flow.

Performing an experiment somewhat similar to Reynolds' experiments with a rubber balloon, sand and water, Mead (1925) observed that if the amount of fluid in the granular aggregate is only sufficient to fill the voids in the condition of maximum density packing, deformation of the mass requires an increase in volume, and the mass fails largely by fracture and not by plastic deformation. If the fluid available is slightly in excess of this amount, the aggregate is easily deformed plastically up to a point where the

increased voids absorb the available fluid, at which point the mass becomes rigid. On the other hand, when the available fluid phase is sufficient to fill the voids with grains arranged in a cubic or minimum density packing, the mass may be deformed to any extent without an increase in volume, and failure may be due to plastic flow offering very little resistance to deformation.

The mechanics of response to deformation of incoherent granular masses can be applied to solid rocks by conceiving of them as having a solid and, potentially, an ideally incompressible fluid phase. The latter may cause the rock to yield to deformation by flowing or by fracture. In simplest terms, the rocks may be regarded as granular aggregate, the hard grains the solid phase. To the extent that the rocks are porous, the pores represent the volume of fluid phase and the material that occupies the pores is the fluid phase. Alternately, the solid phase can be represented by harder, more resistant minerals of rock mass, whereas the potentially fluid phase can be represented by those constituents of rock which are relatively mobile, as evidenced by their rearrangement to schistose (foliated, i.e. capable of splitting up in thin irregular plates) structures through processes of crystallization and and recrystallization. Thus, potential fluid phases occur under certain conditions of composition, pressure, temperature, and rate of deformation.

Brown and Hawksley (1947), while experimenting with regular two-dimensional packings of equal spheres, observed a marked tendency for the spheres to move together in groups; thus, they found a third process (besides the appearance of slip lines and dilatant expansion) by which the tight regions in the array break down. They pointed out that relative movement between groups of tight packing leads to the loss of the peripheral spheres by a sort of "abrasion" between the groups which gave loose irregular packing between the groups.

In effect, their observation showed that there is a tendency for local regions in packings to become or to remain tightly packed. In general,

the tight regions did not dilate uniformly, but either failed locally in a line of slip or moved as a group. An initially uniform loose packing collapsed locally, while an initially tight packing failed irregularly along lines of slips, in either case giving a nonuniform distribution of voids. Groups of tight packing were not found to mesh with each other.

They concluded that in tight regular arrangements, dilatancy is a geometrical necessity if deformation is to occur; whereas, in irregular arrangements, dilatancy does occur, but the explanation lies in the "stability" of the packing. Moreover, since the groups of tight packing have been observed to move as a whole without dilation, or when they do dilate to fail along the line of slip (in preference to a uniform dilation), it would seem that these groups possess some rigidity. Thus an assemblage, regarded as an arrangement of fundamental units which are semirigid, may dilate through the interplay of these units. Since there can be an interchange of particles between adjacent units, such an interplay is more "flexible" than the interplay between individual particles.

Andrade and Fox (1949), while working with a two-dimensional regular (hexagonal) array of ebonite and polyethylene rods, pointed out that the dilation of a regular array is intimately connected with the mechanism of deformation. They detected two classes of dilational deformations, both of them consequences of slip on well-defined planes. In the first, the dilation was localized at the boundaries of regular areas of rods which preserved their original packing; in the second, it was more or less irregular throughout some of these areas. The first type is, in a sense, the more fundamental since the deformation necessarily involves slip which, in turn, involves the primary dilation. The occurrence of secondary dilation was ascribed to some extent, at least, to surface cohesion of the array. In the absence of secondary dilation, the primary dilation showed a fairly regular alternation corresponding to the slipping and healing of the array. The regularity of this alternation was probably disturbed by the secondary dilation since secondary dilation could not be

expected to show any regular variations. Secondary dilation was also found to be dependent on internal friction - the smaller the internal friction, the smaller the role played by secondary dilation. The result was that greater friction gave dilation which was not as regular as it was in the case of less friction. More surfaces of misfit, some of which became healed in the progressive stages, were observed with greater friction. This fact could be held as the direct consequence of secondary dilation and increased internal friction.

Apparently internal friction stabilizes the array against the onset of slip; but, when frictional forces are eventually overcome, the deformation becomes catastrophic with, consequentially, a greater tendency for the areas of rods to break up than when the deformation proceeds gradually, as in the case of low friction.

Hills (1963) notes that the relationship of dilatancy to the spacing of shear planes developed in a deformed rock may be very important. Since a considerable amount of work is done in developing a single shear plane under dilatant conditions, the principle of least work suggests that the number of planes will be small in coarse-grained materials; whereas, with a fine-grained aggregate, each shear plane involves less work and the effort may be expended with equal facility on a greater number of planes.

Friction of a Dilatant Mass

The internal friction of a soil or of any dilatant mass, may be considered to be comprised of two components: sliding friction, and dilatancy or "interlocking". Interlocking has also been recognized by later workers in metals. At the present stage of knowledge, it can be said that Reynolds' dilatancy theory superimposed on the adhesion theory of friction can roughly formulate the friction theory of dilatant masses. If F_d is the force of friction due to dilatancy (Fig. 1) and F_a is that due to adhesion, then F, the force of friction of the dilatant mass, is given by

$$F = F_d + F_a$$

$$= W \tan\phi + K W$$

$$= W(K + \tan\phi)$$

$$\frac{F}{W} = (K + \tan\phi)$$

where $\frac{F}{W}$ can be called the coefficient of friction of dilatant masses, K is a constant reflective of adhesion or sliding friction, and ϕ is the angle of sliding.

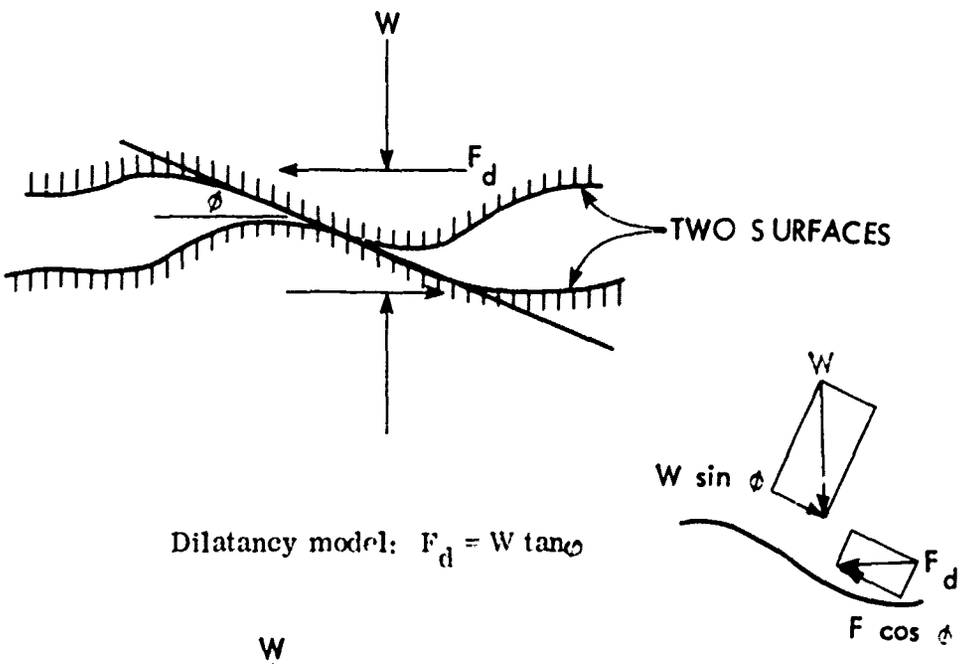

Dilatancy model: $F_d = W \tan\phi$

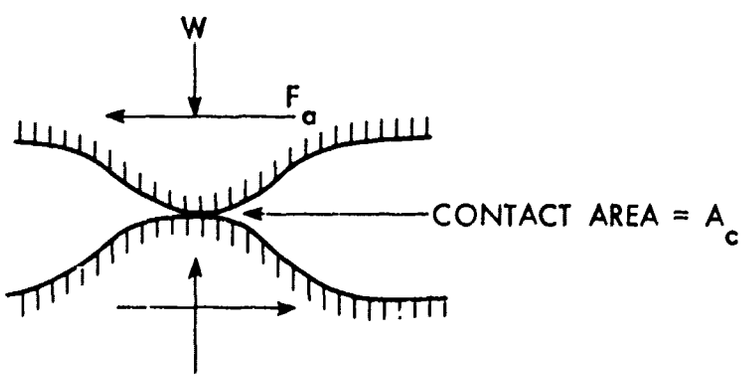

Adhesion Theory. $F_a = KW$

Figure 1. Two components of internal friction of dilatant masses.

Energy Theory of Dilatant Masses

Reynolds' energy concept

Taylor (1948) is usually credited with being the first to attempt separation of two components of friction of dilatant masses by evaluating the work done by dilatant expansion in direct shear against the normal pressure, but it seems that Reynolds (1885) had a similar energy concept in mind and which he applied to granular masses, with the difference that he neglected sliding friction. He said,

> If the particles were rigid the medium would be absolutely without resilience and hence the only energy of which it would be susceptible would be kinetic energy, so that, supposing the motion slow, the work done upon any group in distorting it would be zero. Thus, supposing contraction in one direction and expansion at right angles, then if px be the stress in the direction of contraction, and py, pz, the stress at right angles, a being contraction, b and c expansion,
>
> $$px\ a + py\ b + pz\ c = 0$$
>
> or supposing $b = c$, $py = pz$,
>
> $$px\ a + py(a + c) = 0.$$
>
> With friction the relation will be different; the friction always opposes strain, i.e. tends to give stability.

Taylor energy theory

Let σ_n be the normal stress, τ the shear stress, τ_d that portion of shearing stress which acts to supply the energy of expansion or shear stress necessary to cause the sample to dilate against the normal stress, δ_Δ the incremental displacement in direct shear test in the direction of shearing force, and δ_v the incremental volume per unit area which is incremental displacement in the direction of the normal stress. Then

Work done against normal stress = Work done by τd in moving through δ_Δ

$$\sigma_n\ \delta_v = \tau d\ \delta_\Delta$$

$$\frac{\tau_d}{\sigma_n} = \frac{\delta_v}{\delta_\Delta}$$

Shearing strength contribution by friction = $\tau - \tau_d$

$$\frac{\tau - \tau_d}{\sigma_n} = \frac{\tau}{\sigma_n} - \frac{\tau_d}{\sigma_n} = \tan \varphi_r$$

$$\frac{\tau}{\sigma_n} = \tan \varphi_r + \frac{\tau_d}{\sigma_n}$$

$$\tan \varphi_{max} = \tan \varphi_r + \frac{\delta_v}{\delta_\Delta}$$

where φ_{max} is the angle of friction of the granular mass and φ_r is the internal coefficient of friction. The above energy equation was later adapted to the triaxial test by Skempton and Bishop (1950).

Newland and Allely Theory

Newland and Allely (1957) considered that the direction of sliding of one particle relative to another is, in general, inclined at an angle to the direction of the applied shear stress. By resolving forces and displacements of particles parallel and perpendicular to their sliding surfaces, they arrived at the following expression for the direct shear test.

$$\tan \varphi_{max} = \frac{\tau_{max}}{\sigma_n} = \tan(\varphi_f + \theta)$$

$$\text{where } \tan\theta = (\delta_v / \delta_\Delta)_{max}$$

$$\text{and } \tan\varphi_f = \frac{\tau'_R}{\sigma_n}$$

where θ is the angle of sliding surface with the direction of shear stress; φ_f is the angle of internal friction, which accounts for the influence of not only the coefficient of sliding friction, but also of the mode of failure; τ'_R is the stress required to overcome frictional force, assuming sliding

planes are parallel to the direction of the shear stress; σ_n is the normal stress; and δ_v/δ_Δ if the rate of volume expansion.

They suggested that using experimental values of τ_{max}/σ_n and $\delta_v/\delta_{\Delta max}$ in the above equations, τ'_R can be obtained and in turn, compared to experimental residual stress τ_R

Newland and Allely also extended their analysis to the triaxial test.

Newland and Allely compared their equation with that of Taylor and Bishop, and considered that the difference between the energy approach method and their method lies in the tacit assumption that the work done in overcoming δWf is the same at both the peak and the residual states; whereas, according to their theory, the shear stress has a component normal to the plane of sliding which contributes to frictional strength but which decreases in magnitude as expansion occurs. In other words, the work done in overcoming frictional forces is greater at the point of maximum shear stress than at residual stress state.

Caquot (1934) derived the following expression relating angle of friction at constant volume φ_{cv} and true angle of friction φ_u between mineral surfaces:

$$\tan \varphi_{cv} = \tfrac{1}{2}\ \pi \tan \varphi_u$$

Bishop (1954) also developed an approximate solution in the form

$$\sin \varphi_{cv} = \frac{15 \tan \varphi_u}{10 + 3\ \tan \varphi_u}$$

While the precise validity of these equations is doubtful, experimental data fill the above equations closely.

Rennie (1959) studied the least stress ratio which will cause failure in a close-packed face-centered packing and obtained the approximate solution

$$\frac{\sigma_1}{\sigma_3} = 2 + 2\sqrt{6}\,u + \text{(higher terms in u)}$$

Thurston and Deresiewicz (1959) also considered a face-centered array of equal spheres with $\sigma_2 = \sigma_3$ and arrived at the following expression:

$$\frac{\sigma_1}{\sigma_3} = \frac{\sqrt{6} + 8u}{\sqrt{6} + 4u}$$

where u is a coefficient of friction.

Rowe Stress-Dilatancy Theory

Rowe considered, experimentally and theoretically, the behavior of assemblies of cohesionless, uniform rods in a parallel stack and spherical particles of uniform size, arranged initially in regular arrays. The assemblies of particles are subjected to axially symmetrical state of stress. From his analysis based on a consideration of the forces between particles, he arrived at the following findings for regular packing:

1. Whatever the geometrical arrangements of solids, the stress ratio at the peak strength and during subsequent states of deformation follows the law

$$\sigma_1 = \tan\alpha \tan(\omega_u + \varepsilon).$$

2. The energy ratio $\dot{E}$ for a fixed orientation of particle movement is given by the expression

$$\dot{E} = \frac{\tan(\omega_u + \varepsilon)}{\tan\rho} = \frac{\sigma_1}{\sigma_3\left(1 + \frac{d\dot{v}}{v\dot{\epsilon}_1}\right)}$$

3. Slip occurs well past the peak stress ratio at failure, thus establishing that the slip plane is not the cause but the result of failure.

In the above findings, α is the angle which the imaginary plane of particle interlocking makes with the direction of the minor principal stress, φ is the angle of deviation of the tangent at the contact point from the direction of major principal stress, and φ_u is the angle of sliding friction.

Rowe extended his analysis to a random mass of irregular particles by suggesting that the form of law which applies to any individual packing may be expected to apply to mixture of packings. He observed that the angle α characteristic of the particular packing arrangements, disappeared in the expression for E; thus, he concluded that the energy equation applies to random assemblages of particles, as well as to regular arrays. Since in random, the values of φ vary initially throughout the mass, the angle of sliding must also be determined. He then shows that there exists a critical angle of φ

$$E = \tan^2 \left(\frac{\pi}{4} + \frac{1}{2}\varphi_u\right) = \frac{\sigma_1}{\sigma_3 \left(1 + \frac{dv}{v \cdot \epsilon_1}\right)}$$

Departure from the stress dilatancy behavior given by the energy ratio equation is explained by Rowe in terms of a process he refers to as rearranging. In a loose sand, and in an initially dense sand when it reaches a point near the maximum stress ratio σ_1/σ_3, the length of the individual slide paths of one particle over another becomes appreciable with respect to the dimensions of the particles; hence, according to Rowe, sliding is no longer restricted to a value of φ which gives the minimum rate of expenditure of energy in internal friction. The effective value of φ_u then becomes φ_f, where $\varphi_f > \varphi_u$.

At the ultimate state of deformation when the sample reaches the state at zero rate of volume change, the effective value of φ_u at this ultimate constant volume condition, denoted by φ_{cv}, is obtained from the equation

$$\frac{\sigma_1}{\sigma_3} = \tan^2 (1/4\pi + 1/2\varphi_{cv}),$$

by using the observed stress ratio.

Rowe (1963) applied the stress dilatancy theory to the stability of earth masses behind retaining walls, in slopes, and in foundations.

The stress dilatancy theory of granular masses postulated by Rowe was discussed by Scott et al. (1964), Gibson and Morgenstern (Trollope et al., 1963), Scott (1963), and Trollope et al. (1963). Their main criticism was directed towards:

1. the assumed mechanism of deformation,
2. the assumed absence of rolling,
3. the assumption that the energy ratio E is minimum in a random assembly, and
4. the significance of the α-plane.

Horne confirmation

A more general derivation was presented by Horne (1965) who did not restrict his analysis to ideal packing. He obtained exactly similar results to that of Rowe, and thus substantiated his theory. Horne built up his analysis on the basis of the following hypotheses:

1. The assembly consists of rotund, rigid, cohesionless particles with a constant coefficient of sliding friction. Elastic and plastic deformation, crushing, and cracking are all ignored.

2. Deformation occurs as a result of relative motion between groups of particles. Motion is not facilitated by the presence of individual particles acting as rollers between groups.

Horne obtained the expression for the energy ratio E by writing a virtual work equation for the input $\sigma_1 \dot{\epsilon}_1$. Then he minimized this ratio to obtain a value of $\phi_c = 45 - \frac{1}{2}\phi_u$ which then led to

$$E = \frac{\sigma_1 \dot{\epsilon}_1}{\sigma_2 \dot{\epsilon}_2 + \sigma_3 \dot{\epsilon}_3} = \tan^2 (45 + 1/2\phi_u)$$

For the triaxial compression test with $\sigma_2 = \sigma_3$ and $\dot{\epsilon}_2 = \dot{\epsilon}_3$, this reduces to Rowe's equation. Horne thus established the limitation of the stress dilatancy theory and concluded that the equation of energy ratio $\dot{E}$ that provides a relationship between work quantities $\sigma_1\dot{\epsilon}_1$, $\sigma_2\dot{\epsilon}_2$, and $\sigma_3\dot{\epsilon}_3$ does not provide a relationship between stress and strain rates separately. He also concluded that the relationship may not apply to a highly compacted assembly with a high degree of interlocking.

Tinoco and Handy Theory

Tinoco and Handy (1967) considered a random particle assemblage and the possibilities for either sliding or rolling. They demonstrated that sliding occurs at contacts where the angle of inclination - is maximized, whereupon

$$\frac{\sigma_1}{\sigma_3} \quad \frac{1 - \sin\phi_s}{1 - \sin\phi_s} \quad \tan^2(45 + \phi_s/2)$$

which is identical to the empirical Mohr-Coulomb theory. Next, considering the work of volume change, they derived an equation for principal stresses due to friction. In simplified form,

$$\frac{\sigma_1}{\sigma_3} \quad (1 - \delta_v/\delta\epsilon_1) \quad \sigma_{TC} + \left[\sigma_1/\sigma_3 - (1 - \delta_v/\delta\epsilon_1)\right] \sin\phi_s$$

where ϕ_s is the angle of sliding friction, $\delta_v/\delta\epsilon_1$ is the unit volume change per unit axial strain, and σ_{TC} is a dimensionless constant.

For triaxial compression test, they arrived at the expression

$$\sigma_{TC} = \left[(\sigma_1/\sigma_3 - 1)(1 - \sin\phi_s)\right] \delta\epsilon_{1D}/\delta\epsilon_1$$

where $\delta\epsilon_{1D}/\delta\epsilon_1$ is the axial unit strain contributing to volume change. The

equation was tested by plotting $\sigma_1/\sigma_3 + (1 + \delta v/\delta\epsilon_1)$ versus $\sigma_1/\sigma_3 + (1 + \delta v/\delta\epsilon_1)$ which should give a straight line of slope arctan $\sin\phi$ and an intercept of Ω. All the graphs showed linear portions with slopes consistent with mineralogical composition, suggesting establishment of an equilibrium interlocking parameter Ω prior to dilation. After dilatant expansion, a new line is sometimes established at a lower Ω but still with the same slope, further supporting that this gives an independent measurement of sliding friction. From the plots it becomes evident that if the coefficient of sliding friction is constant, then the interlocking function Ω first increases with increasing strain, and then decreases upon dilation and failure.

TEST METHODS AND PROCEDURES

The Biaxial Test Apparatus

Brief description

Briefly, the biaxial load test apparatus which formed the core of the experimental program consists of a horizontal load frame with an included horizontal removable Teflon-lined test bed to contain an assemblage of vertical rods. Controllable confining stresses are introduced along the sides of the bed by aluminum plates and pressure cylinders. An axial strain is applied at one end of the test bed by a screw and jack arrangement powered by a 1/6 h.p. motor, the axial force being monitored with a Dillon load cell (Fig. 2). Axial and lateral deformations are measured with 0.001-in. mechanical dial gages (known as Ames dials), a 35mm camera being used to simultaneously record the dial readings and positions of the test rods after every 0.005-in. axial strain in the beginning, and 0.010- and 0.020-in. during the later stages of each experiment. The axial deformation rate is kept constant at 0.00465-in. per minute with a $\pm$ 2.5% variation. This gives a strain rate of 0.001% per second with, of course, a $\pm$ 2.5% variation.

Collapsible box

The collapsible box (Fig. 3) consists of three aluminum 5-in. x 4-in. x 1/2-in. rectangular plates on each side of the box and a bottom plate of Teflon 16-in. x 8-in. x 1/4-in. supported by a plate of steel 16-in. x 8-in. x 1/16-in. The steel plate rests on a layer of steel ball bearings held separated by an aluminum spacer. These, in turn, rest on an adjustable horizontal rest plate supported by the main frame. With this arrangement, the bottom of the box has three degrees of freedom of motion, namely, axial, lateral and vertical, and may be accurately levelled. Each side plate of the box is connected to four pressure units through ball-and-socket joints at the ends of the piston rods to facilitate free rotation of the plate in two directions. One end of the box consists of a 5-in. x 4-in. x 1-in. steel plate rigidly connected to the main

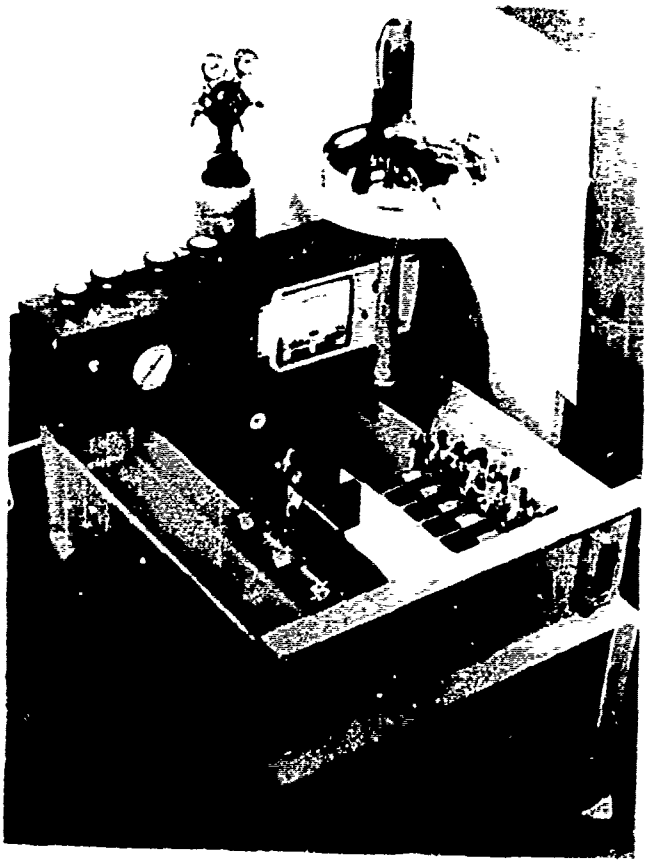

Figure 2. Biaxial test apparatus, fluorescent lights and recording camera at top.

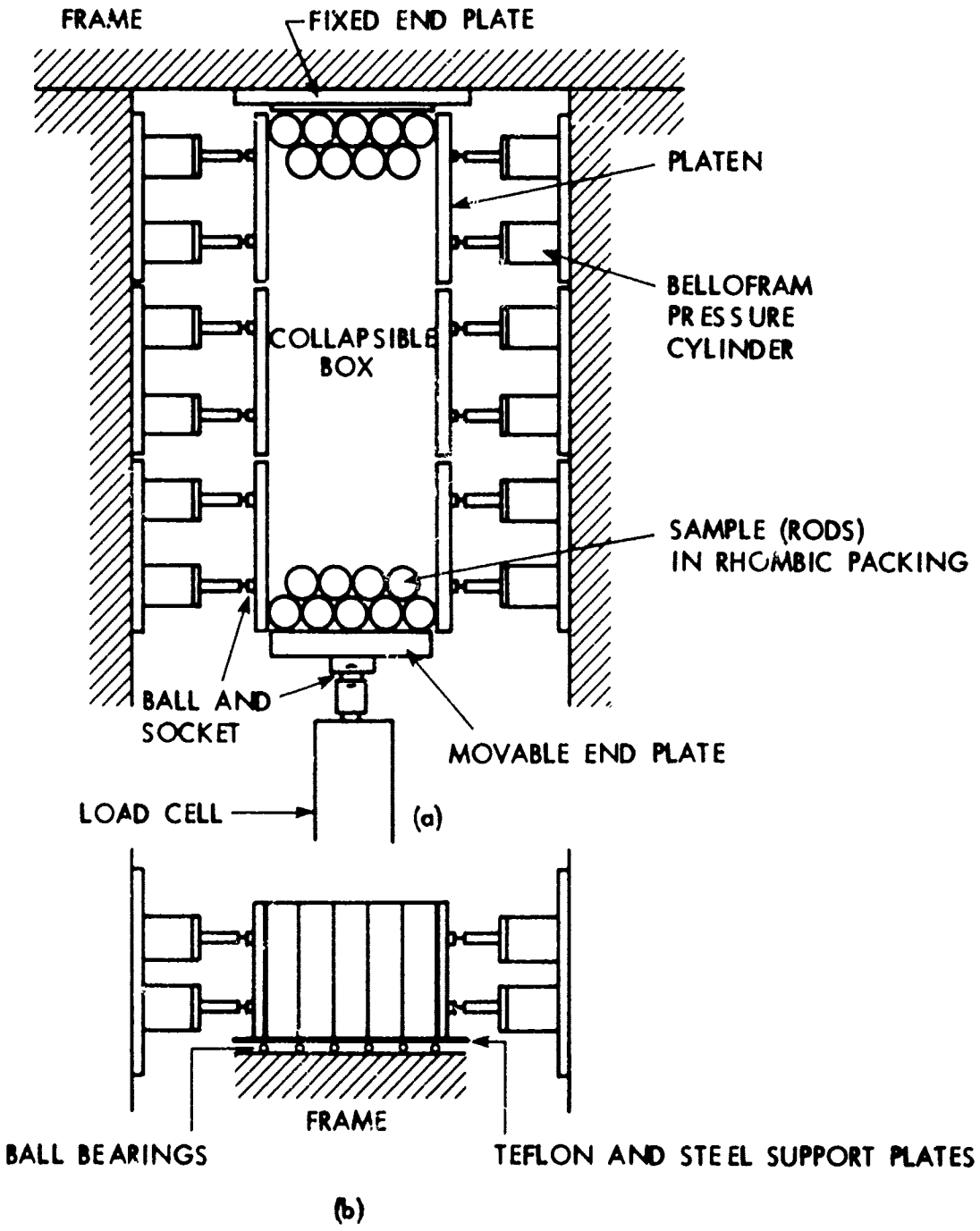

Figure 3. Collapsible box; (a) plan, (b) cross section.

frame, and the other consists of a similar steel plate which is connected to the load cell by a ball-and-socket arrangement.

Lateral stress system

Constant lateral stress is applied through a system of twelve pressure units, four for each plate, on each side of the collapsible box. Each pressure unit consists of a pressure cylinder and a piston fitted with a "Bellofram rolling diaphragm", used because it is capable of:

1. providing a leak-proof device to convert gas or liquid pressure into a linear stroke,
2. tolerating minor eccentricities and cocking of the piston rod and cylinder without affecting the operation of the unit,
3. providing a long stroke within a relatively confined area,
4. responding to small pressure variations because of very low friction and hysteresis, and
5. providing a working pressure area which is constant (within $\pm$ 1%) through its entire range.

All the pressure units on both sides of the collapsible box are connected to the same pressure source. For a low lateral pressure, upto 115 psi gage or 30 psi lateral pressure on the assemblage, compressed air is used, whereas for higher pressures, liquid carbon dioxide (CO_2) is used. Liquid CO_2 is capable of providing a constant pressure of up to 900 psi at room temperature. A maximum gage pressure of 200 psi was used in the present experimentation, dictated by the capacity of Bellofram rolling diaphragms. It has been possible to keep the pressure variations to a maximum of $\pm$1% by the use of precision pressure reuglators with operating ranges selected for the different lateral pressures used.

Calibration of Bellofram pressure units

Pressure units were calibrated in sets of two. Each set was subjected to gage pressures from 0 to 280 psi increasing at an interval of 20 psi, and from

250 psi to 0 psi decreasing at intervals of 50 or 20 psi. A previously calibrated proving ring was used to establish the relation between gage pressure and force. The proving ring was calibrated by use of a direct load, varying from 0 to 900 lbs.--increasing and decreasing at equal intervals of 100 lbs, on a calibrated platform scale. Calibration of the pressure units was repeated five times for each set to obtain average values. The lateral stress σ_3 and gage pressure correlated through the relation

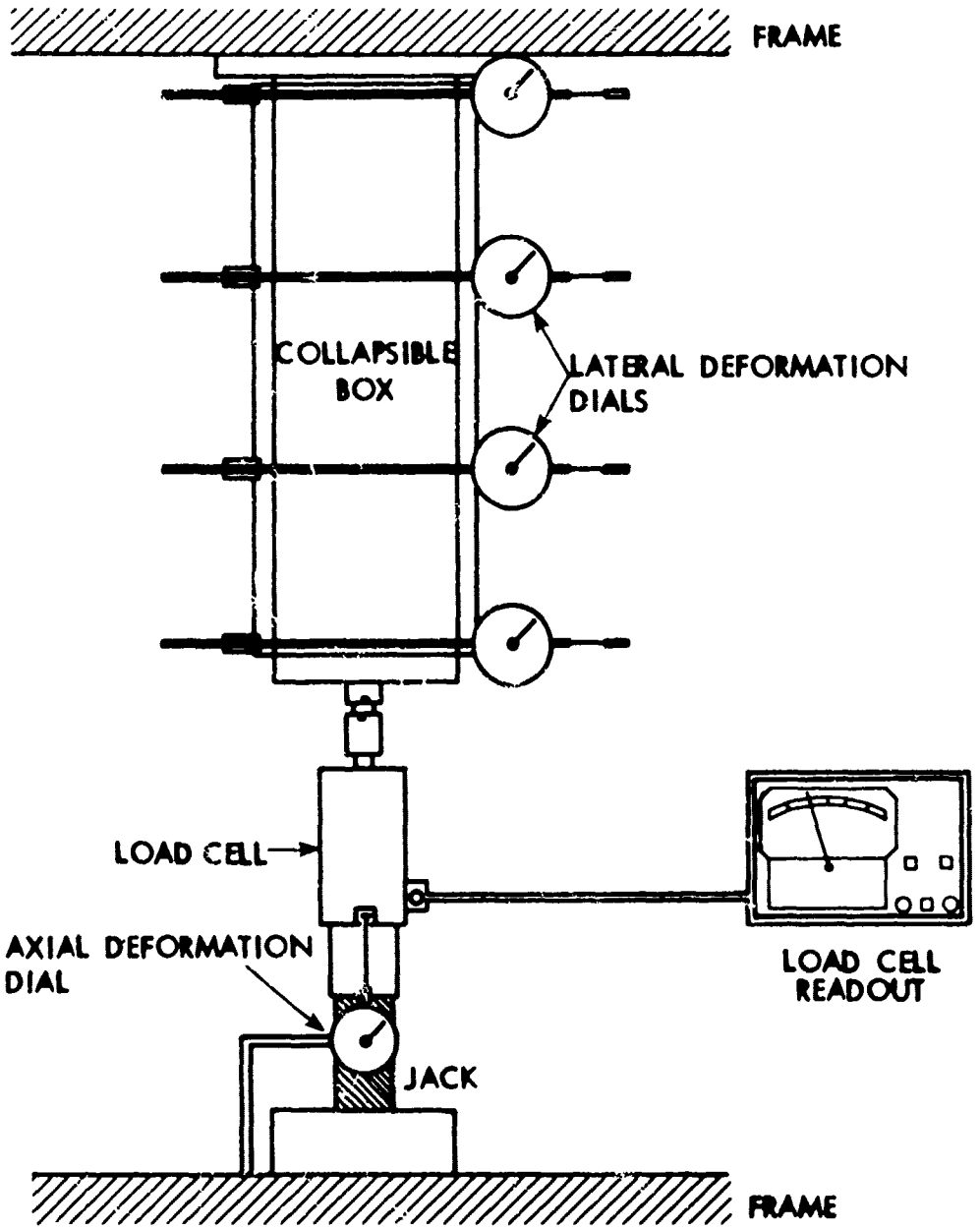

Figure 4. Lateral and axial deformation measurement and the axial load measurement system.

$$\sigma_3 = 0.2552 \text{ (gage pressure)} + 0.7188$$

$$\text{gage pressure} = 3.9185\ \sigma_3 - 2.817.$$

Lateral deformation measurement system

Lateral deformations are measured at four points - two at the ends and two in between along the length of the collapsible box (Fig. 4). Ames dials capable of reading to 0.001 in. with a total range of 1 in. were used to measure separation of points on two opposite sides of the collapsible box. The dial stems were extended by brass rods of 9-in. length and 1/8-in. diameter threaded at both ends. Coupling to the box was by two steel stops, one fixed to the bottom of the dial and the other to the brass rod. The latter stop can be fixed at any position of the rod along its length, thus giving a capability to measure across the collapsible box with variable initial width.

In order to read all four Ames dials simultaneously, along with axial deformations and loads, a photographic arrangement was made at the top of the collapsible box. The arrangement consists of two concentric neon light tubes with a 35mm Kodak f2.8/50mm camera at their center. The camera is capable of rotation is a vertical plane. The assembly of light and the camera (Fig. 2) is mounted on a horizontal leg and can slide to any position along the leg. The horizontal leg can revolve around a column which, in turn, is fixed to the main frame. The horizontal leg also can revolve in a horizontal plane and can move up and down against the column. With this arrangement, the camera can be easily focused and the light intensity can be adjusted for good photography. Photographs are made at regular time intervals, allowing all the Ames dials to be recorded, while the plan deformation of the assemblage is photographed, enabling location of the plane or zone of failure and its inclination. This also facilitates the study of translational and rotational movements of each individual rod, made possible by marking lines on the exposed rod ends prior to starting each experiment.

Axial deformation system

The axial deformation system consists of a Norton-Duff ten-ton jack driven by an electric motor of 1/6 h.p. through a complex speed reduction arrangement. Application of the axial load is thus strain-controlled.

The electric motor is fitted with a precision motor speed control which is theoretically capable of regulating the speed in 100 steps. The speed reduction system consists of two Boston reducers, five sprockets of 30, 30, 15, 9 and 112 teeth, and a worm gear jack. The Boston gears reduce the speed by 2,000 times, and the sprockets can further effect a reduction of 12 times. Thus, the whole speed reduction system, including the worm gear jack, is capable of providing an axial deformation range of 0 to 2.5-thousandths of an inch per minute. An Ames dial is connected to the worm shaft of the jack such that it directly measures the axial deformations in thousandths of an inch.

Axial load measurement

For measurement of axial load, a Dillon load cell with its readout system is used. The load cell is of a 10,000-lb. capacity and is mounted on the end of the worm shaft of the 10-ton jack. The other end of the load cell is connected to the collapsible box through a ball and socket arrangement. The Dillon readout system is in two stages, namely 0 to 5,000 lbs. and 5,000 to 10,000 lbs., which gives better precision in reading the axial load.

Main frame

The main frame (Fig. 2) was designed as a rigid closed box section for an axial load of 15,000 lbs. and a lateral load of 5,000 lbs. The maximum deflection in the box section was kept equal to one thousandth of an inch under the above load system. In practice, the maximum axial load used is less than 1,000 lbs., which gives a calculated maximum structural axial deformation equal to one-quarter of a thousandth of an inch, compared to a total axial deformation of 1/2 in. in the assemblage. The box section was rigidly welded

to a four-legged skeleton supported on rollers, which gives further rigidity to the box section.

Materials Tested

The granular assemblage is modeled by cylindrical rods of different diameters, materials, and shapes. Two different materials, namely steel and Teflon, were available in geometrical shapes of cylinders and square bars. The following five sizes of steel rods of circular cross section were experimented with:

1" diameter cold rolled steel rods
3/4" diameter cold rolled steel rods
1/2" diameter cold rolled steel rods
1/4" diameter steel welding rods
1/8" diameter steel welding rods
3/4" diameter Teflon rods

All the sizes, except the 1/8-in. diameter welding rods, were machine cut and lightly polished on a lathe with a fine emery cloth. The rods then were covered by a thin layer of light machine oil to prevent rusting. The lengths of the rods were accurately cut so as to give a reasonably smooth surface while standing with their axes vertical. The 1/8-in. steel welding rods were saw-cut, so the length could not be controlled as precisely, with the result that a smooth planar surface was not attained when they were made to stand with their axes vertical in the collapsible box.

Sample Preparation

Before testing, the rods were washed with acetone to remove any loose material and lubricant from the surface, and were then cleaned with a clean dry cloth. A second acetone bath was given to the rods before they were used for experimentation.

Countless possibilities existed for an initial arrangement of regular and random rod assemblages. To simulate a densest packing, a rhombic geometrical array was used in all tests, the long axis of the rhombus coinciding with the major principal stress direction (σ_1). Care was taken in arranging the rods in a regular geometrical array with its center line coincident with the line of application of the load, a string line being used for this purpose. In a rhombic array, the rods in alternate rows number r and r-1, and it was always seen that the first and the last rows of the assemblage had the same number (i.e., r) of rods so as to insure a symmetrical assemblage. Before application of axial strain, the assemblage was subjected to the required predetermined constant lateral stress (σ_3) and the loaded end platen moved axially with the help of the disengaged jack, so that contact with the load corresponding to $\sigma_1 = \sigma_3$ was shown by the Dillon load readout system. At this point, the axial deformation dial was set to zero. Lines making an angle of 60° with the σ_3 direction were then drawn with a felt-tipped pen through the centers of the exposed rod ends. These lines helped in establishing movements of the rods during deformation. After the linear grid was marked with black ink, the four lateral-deformation modified Ames Dials were fitted on to rest on the top of the side platens. The first lateral deformation dial was placed on the center line of the cylinders in the first row from the load side, and the last dial was placed on the center line of the last row; whereas, the second and third dials were exactly 5 inches apart on the edges of the central side platens. The camera was adjusted and focussed in such a manner that the lateral deformation dials could be read comfortably, along with a reasonably sharp picture of the deformation pattern. Special care was taken in aperture and shutter adjustment for the sake of neat photography.

Testing Technique

Five values of constant lateral stresses, namely 10, 20, 30, 40, and 50 psi, were used for the experiments. After all preparations are completed and the axial deformation dial is set for an initial zero deformation reading, a constant axial strain at the nominal rate of 0.001% per second is applied. Photographs are taken at the interval of 0.005 in. of axial deformation during the initial stage; then this interval is increased to 0.01 in. and finally to 0.02 in. Total time for which the axial deformation is applied to assemblage along with the total axial deformation itself, is noted to find the true axial strain rate. After the assemblage has been subjected to a required axial deformation, the experiment is stopped and the film is processed. Processed film is projected through an enlarger to read the lateral deformation dials and observe the movement of individual rod and failure planes. Dial readings are converted to volume change by the formulations given below:

Effective width of the assemblage

= distance between the centers of the first and last rods in the first row. With symbols as shown in Fig. 5,

$= 2\,(r - 1)\,d\,\sin\lambda$

Effective length of the assemblage

= distance between the center lines of the first and last rows

$= (n - 1)\,d\,\sin\,(90 - \lambda)$

$$\text{Axial strain } (\epsilon_1) = \frac{E}{(n - 1)d\,\sin(90 - \lambda)}$$

$$\text{Initial volume } (v_0) = 2(r - 1)\,n - 1)\,d^2L\,\sin(90-\lambda)\sin\lambda$$

$$\text{Change in volume } (dv) = \left[\frac{A + B}{2}a + \frac{B + C}{2}b + \frac{C + D}{2}e - 2(r - 1)\,dE\,\sin\lambda\right]L$$

$$\text{Volumetric strain } (dv/v_0)$$

$$= \frac{1}{2(r - 1)\,(n - 1)d^2\,\sin(90 - \lambda)\,\sin\lambda}\left[\frac{A + B}{2}a + \frac{B + C}{2}b + \frac{C + D}{2}e - 2(r - 1)dE\,\sin\lambda\right]$$

$$\text{Axial stress } (\sigma_1) = \frac{G}{2(r-1)d \sin\lambda \; L}$$

where $\lambda = 30$ in the present experimentation.

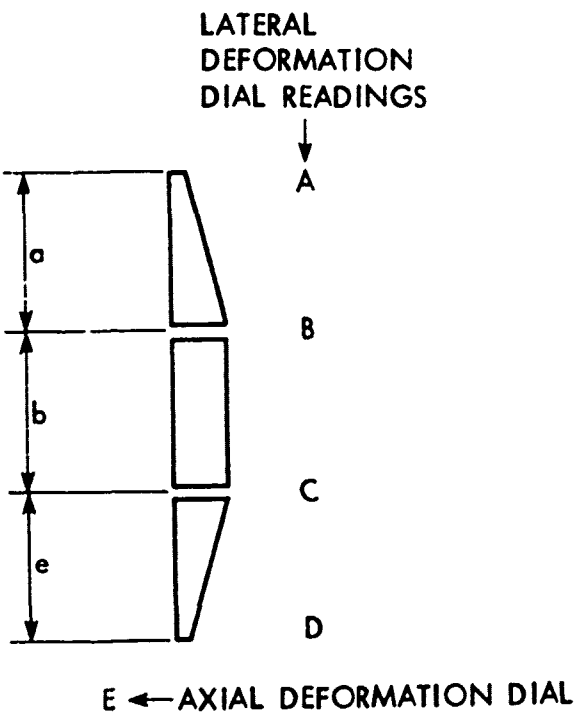

r = Number of rods in the first cross row
n = Number of cross rows
d = Diameter of rods
L = Length of rods
G = Load cell readout
λ = Distribution angle (Fig. 6).

Figure 5. Mathematics of collapsible box.

Reproducibility

The rate of application of axial strain and axial load was reproducible with a high degree of accuracy, and the use of a two-stage pressure regulator made it possible to attain an almost constant lateral pressure. The reproducibility of the regular geometrical array with its center line coincident with the line of application of load was somewhat less precise, in spite of the extreme care taken in arranging the rods. In addition, there was unavoidable variation in the surface finish of the rods.

Another important factor which may affect reproducibility is the initial zero setting of the axial deformation dial. It was observed that after application of constant stress, the axial deformation dial could not be uniquely set for load, corresponding to $\sigma_1 = \sigma_3$ on the Dillon load cell readout system. For example, after setting the axial dial at zero with the readout load corresponding to $\sigma_1 = \sigma_3$, if the assemblage was subjected to some axial load and left for some time, then after bringing the axial load to its original value, the axial deformation dial would not come to the initial zero setting. This effect was particularly pronounced in smaller diameter rods. Some of the possible reasons, in the case of the smaller diameter assemblage, can be: (1) it is extremely difficult, if not impossible, to align the center line of the assemblage along the σ_1-axis; and (2) the smaller diameter rods, being relatively more slender than the larger diameter rods, can bend more easily along their length, thus rendering the perfect fit of the assemblage impossible.

This could be a reason for a floating $(\sigma_1/\sigma_{3_{max}})$ with respect to axial strain, or a shifting dv/v_0-versus-ϵ_1 curve along the direction of the axial strain on plots. These effects were apparent from repeated tests. Flotation of the $(\sigma_1/\sigma_{3_{max}})$ point and the dv/v_0-versus-ϵ_1 curves with different lateral stresses can also be due to different initial elastic deformations, since increasing lateral stresses will induce greater initial elastic deformations.

THEORETICAL INVESTIGATIONS

General Considerations

When an assemblage of rods is subjected to a stress field, then the forces between the cylinders are at first indeterminate because each cylinder is in contact with six neighboring cylinders. Any small change in the geometry of its boundary, e.g. a change in the shape of the surrounding frame which is brought about by moving the load side platen, results in a geometrical change of pattern which always includes a series of gaps or slack contacts (this follows from Osborne Reynolds' theory of dilatancy). A very small change of shape in the boundary is sufficient to produce this effect; it needs to be only of the same order of magnitude as the elastic strain in the cylinders. The gaps are definite limits to the lines of action of the forces. Thus, creation of two gaps around a cylinder will reduce the neighboring contacts from six to four, which will make the forces between the cylinders determinate. Since dilatancy may be looked upon as a cause of gaps and also of slack contacts (no visible gaps), its intimate connection with the pressure distribution is apparent.

Forces Acting

Let us consider an assemblage of cylinders having a distribution angle equal to λ (angle for some skew arrangements such that $\lambda = 30^{o}$ gives us a hexagonal array and $\lambda = 45^{o}$ gives us a cubic array, shape factor $\tau = 1$). When it is subjected to a biaxial stress field, a sort of mass transmission of forces takes place in the axial and lateral directions. If a cylinder K (Fig. 7) in an upper layer is supported by two cylinders P and L in the lower layer, cylinder K tends to push cylinders P and L apart, tending to break the contact between them. Now consider a λ- array (distribution angle = λ) of cylinders in which cylinder P is surrounded by six cylinders, L, M, N, O, J, and K

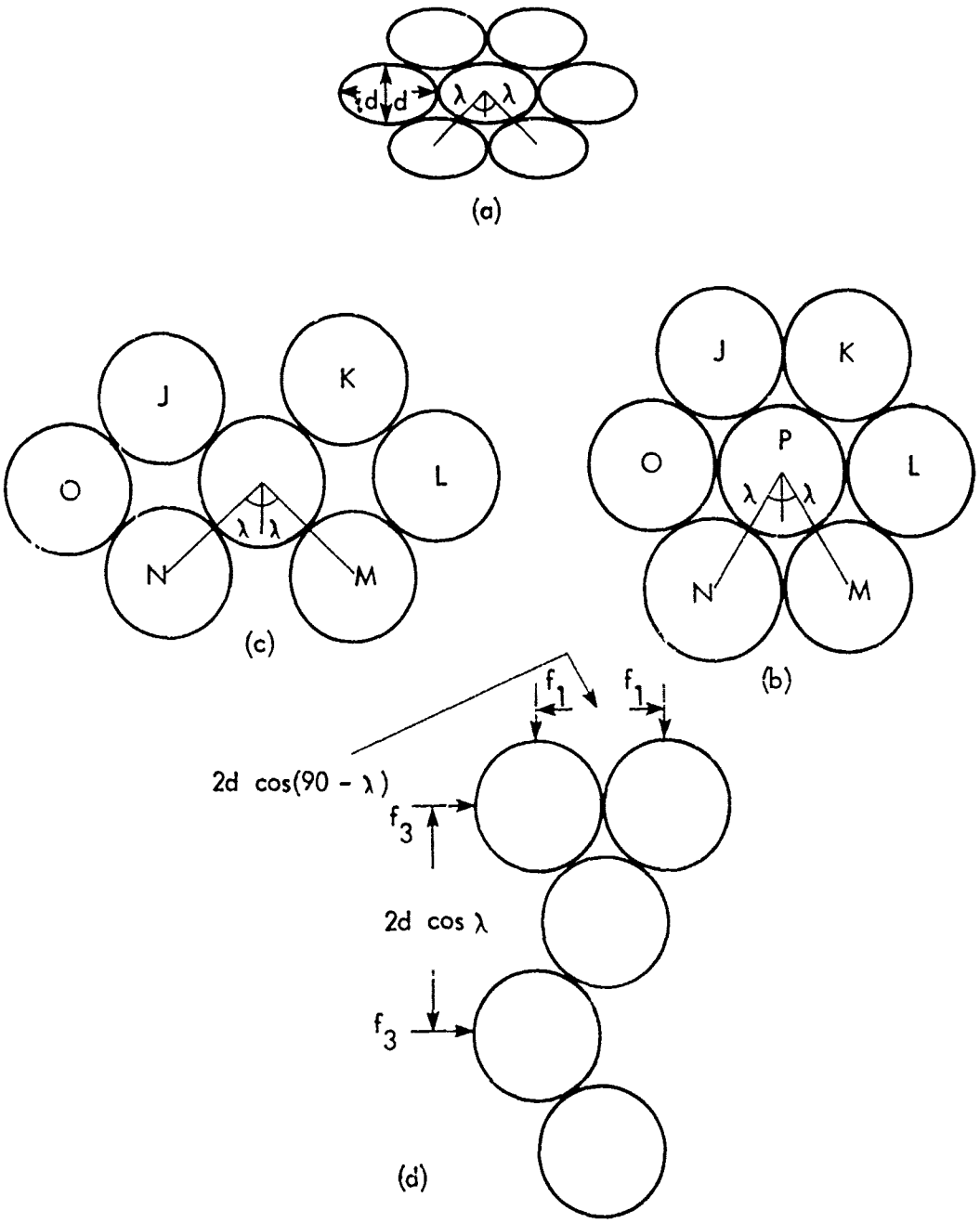

Figure 6. Regular geometrical arrays; τ is the shape factor and λ is the distribution angle; (a) hexagonal array of oval shapes, (b) hexagonal array of circular shapes, $\lambda = 30^{o}$, (c) cubic array of circular shapes, $\lambda = 45^{o}$, (d) hexagonal array shown with forces

(Fig. 7). This is the geometric arrangement which gives the minimum void ratio when $\lambda = 30^{o}$. In the axial direction, rods J and K are supported by rods O and P, and P and L, respectively. Similarly, rod P is axially supported by rods N and M. In the lateral direction, rod O is supported by rods J and N, and rod P by K and M, assuming no contacts between O and P, and P and L. This gives rise to the mass transmission of forces from cylinder to cylinder. If f_1 is the axial force on one cylinder and f_3 is the lateral force, then

$$f_1 = 2d\ \sigma_1 \cos(90 - \lambda) \tag{1}$$

$$f_3 = 2d\ \sigma_3 \cos \lambda \tag{2}$$

where d is the diameter of cylinders, σ_1 and σ_3 are axial and lateral stresses on a gross area basis, respectively, and λ is the distribution angle.

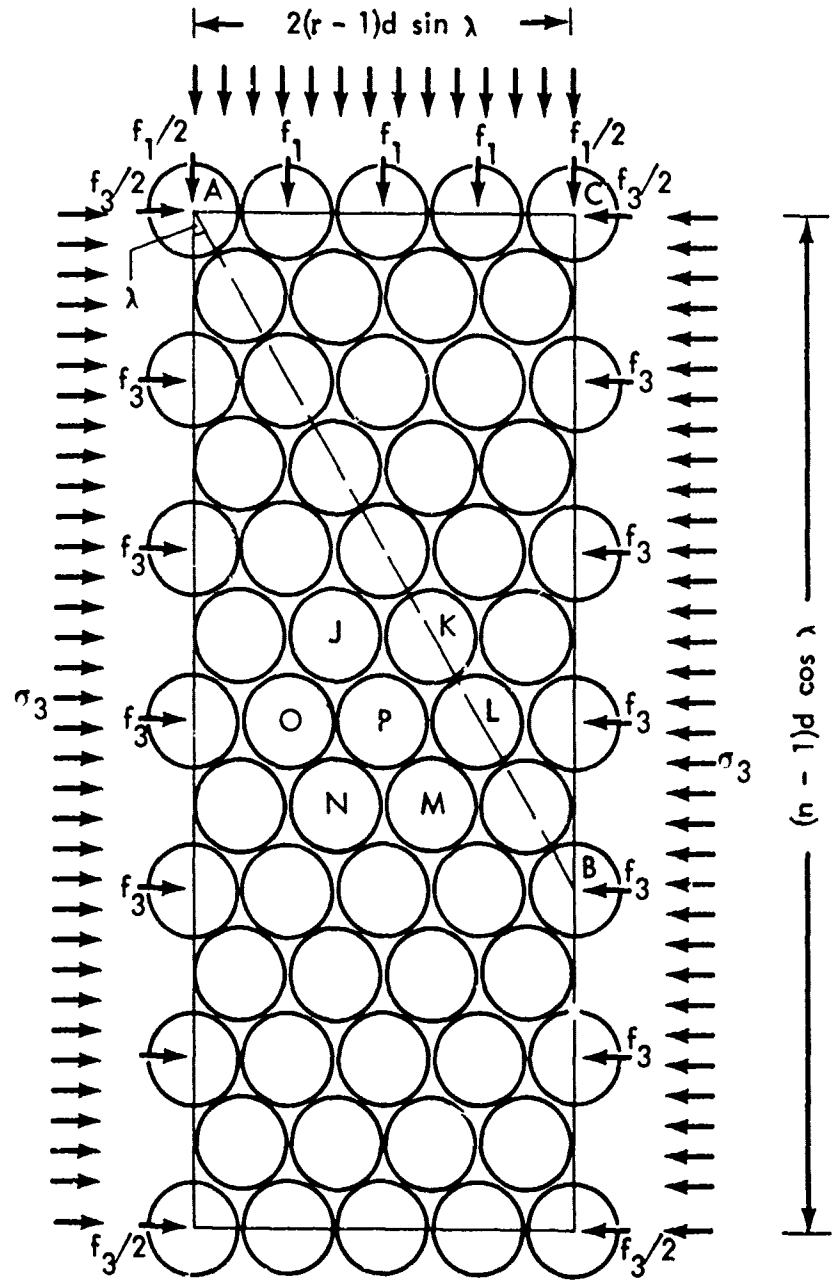

Figure 7. An assemblage of rods subjected to biaxial stresses.

Next, consider a cylinder P of the array and resolve the axial and lateral forces $f_1/2$ and $f_3/2$ to give a normal force F acting along the $(90 - \lambda)$ -direction from the σ_3 -axis, and a tangential force T at a right angle to the $(90 - \lambda)$ -direction. Then

$$F = \frac{f_1}{2}\cos\lambda + \frac{f_3}{2}\sin\lambda$$

Substituting the values of f_1 and f_3 from Eqs. (1) and (2), respectively, then

$$F = d\sigma_1 \cos(90 - \lambda)\cos\lambda + d\sigma_3 \cos\lambda \sin\lambda$$

$$= d \cos\lambda \sin\lambda (\sigma_1 + \sigma_3)$$

$$= d\frac{\sin 2\lambda}{2} (\sigma_1 + \sigma_3 \qquad (3)$$

$$T = \frac{f_1}{2}\sin\lambda - \frac{f_3}{2}\cos\lambda$$

$$= d\sigma_1 \cos(90 - \lambda)\sin\lambda - d\sigma_3 \cos\lambda\cos\lambda$$

$$= d\sigma_1 \sin^2\lambda - d\sigma_3\cos^2\lambda$$

$$= d(\sigma_1 \sin^2\lambda - \sigma^2\cos^2\lambda) \qquad (4)$$

The remainder of the theoretical development is rather long, and is presented in Appendices to this report.

The results may be summarized as follows:

Elastic Strain

$$\frac{(dv)_e}{v_o} = \frac{4(\alpha + \delta\tan\lambda)}{d^3\sin 2\lambda} \qquad (10)$$

where $(dv)_e/v_o$ is the elastic volumetric strain of the assemblage and d and δ are radial and tangential deformations at cylinder contacts.

Analytical solutions for δ and α for cylindrical rods, to the best knowledge of the authors, are not available. As previously shown,

$$F = d\frac{\sin 2\lambda}{2}\ (\sigma_1 + \sigma_3) \tag{3}$$

$$T = d(\sigma_1 \sin^2\lambda - \sigma_3\cos^2\lambda) \tag{4}$$

By definition within the elastic region, σ_1/σ_3 varies linearly with ϵ_1; this also is seen in the experiments. If σ_3 is kept constant throughout the experiment,

$$\sigma_1 \propto \epsilon_1$$

$$\sigma_1 = E_s\epsilon_1 \tag{11}$$

where E_s is a constant and can be called an elasticity modulus of the assemblage.

From the above, it can be seen that for a particular diameter d and distribution angle λ of the assemblage,

$$F = \text{some constant} \times \epsilon_1$$

$$T = \text{another constant} \times \epsilon_1$$

Thus, once a relation is found between α, δ, F, and T from the theory of elasticity, one could easily find a relation between $(dv)_e/v_o$ and axial strain ϵ_1.

Dilatancy Stress Ratio

At failure

$$\frac{\sigma_1}{\sigma_3} = (f + \sin\lambda\cos\lambda)\frac{\cos\lambda}{\sin^3\lambda} \tag{26}$$

where f is the coefficient of sliding friction.

Post failure

$$\frac{\sigma_1}{\sigma_3} = \cot\lambda\left[\frac{F}{\sin\lambda\ \sin(\lambda + \eta)} + \cot(\lambda + \eta)\right] \tag{29}$$

Thus, the stress ratio should change according to the above relation with increasing deformation after initial failure. The relation between ω and the axial unit strain ϵ_1 may be shown to be

$$\omega = \arctan\left[\frac{d}{E \sin\lambda} - \cot 2\lambda\right] - 1 \qquad (39a)$$

where

$$E = (n - 1)d\,\epsilon_1 \cos\lambda \qquad (42)$$

Example solutions of Eq. 29 for a hexagonal array of cylinders, i.e., for $\lambda = 30^{\circ}$, are given in Table 1. For a maximum stress ratio, $\omega = 0$ and Eq. 29 reduces to Eq. 26.

Complete derivations and intermediate equations are given in Appendix A.

Table 1. Theoretical maximum stress ratios for hexagonal array of cylinders

Coefficient of sliding friction, f	Maximum stress ratio, (σ_1/σ_3)
0.00	3.00
0.01	3.07
0.05	3.35
0.10	3.69
0.12	3.83
0.14	3.97
0.16	4.11
0.18	4.24
0.20	4.39
0.22	4.52
0.24	4.66
0.26	4.80
0.28	4.94
0.30	5.08

Volumetric Strain as a Function of Axial Strain

On the basis of observed failures along discrete failure planes, $dv/v_o =$

$$\frac{4}{n-1}\left\{\frac{1}{\sin 2\lambda}\sin(2\lambda + \arctan\left[\frac{2}{(n-1)\,\epsilon_1 \sin 2\lambda} - \cot 2\lambda\right]^{-1}) - 1\right\} \qquad (43)$$

Where n is the number of cross-rods. The derivation of this equation is given in the Appendix.

Effects of multiple failure planes and particle (rod) size

The coefficient of friction on the surfaces of the particles (rods) is not constant, but is randomly distributed both in space and, as slipping occurs, in time. Therefore, the resolved total friction will be different on the different possible failure planes, failure following a plane with the lowest resistance. As slipping occurs on a failure plane, which may be called the active shear plane, the coefficient of friction on that plane will change, whereas the coefficient of friction on other possible shear planes will remain constant due to absence of movement along them. Simultaneously with increasing ϵ_1, the value of axial stress σ_1 decreases (Eq. 29). Thus, in the process of slipping along the active shear plane, if the friction along it momentarily exceeds friction on another possible failure plane, slip will become arrested and shift to the plane with the lowest friction, where the process will repeat. However, as the axial strain progresses and axial stress σ_1 reduces considerably following Eq. 29, variation in friction eventually will be insufficient to trigger slipping on a fresh plane, and slipping will continue on the same plane. Hence, with increasing axial strain, the process of shifting to new failure planes slows down and ultimately stops.

Since the tendency for arrested slip to occur depends on variability of the cumulative friction along each available slip plane, it may be

affected by element size, in that the smaller the elements, the more planes are available for slipping to occur. The number of planes p may be estimated from the number of rods r in a cross row and number of cross rows n:

$$p = \frac{n - 1}{2} + r - 1 \qquad (43a)$$

This assumes no dead zones at the ends of the box, and no cross shears, which would double p. Cross-shears were occasionally observed, but were not common due to blocking. Following are the planes possible in the experiments:

d,in.	r	Slip Planes, p* End	Central	Total	Rod contacts per plane
1.0	5	8	4	12	8
0.75	7	12	5	17	12
0.50	10	18	17	35	18
0.25	20	38	34	72	37
0.125	40	78	66	144	77

*May be multiplied by 2 for cross-shears

Probabilities

The probability of a particular number of slip zones developing during a test may be calculated from the number of possible combinations. For example, let us assume that due to end restraint only the four central planes in the array of one inch rods are eligible for slip. There is an equal likelihood that slip will initiate on any one of the four - 1, 2, 3, or 4, whereupon friction will increase and slip will most likely become arrested. The second slip then may involve several combinations: 1 + 2, 1 + 3, 1 + 4, 2 + 3, 2 + 4, 3 + 4. Similarly a third slip, if it occurs, could involve 1 + 2 + 3, 1 + 2 + 4, 1 + 3 + 4, 2 + 3 + 4, whereas a fourth slip could only involve 1 + 2 + 3 + 4. In total there are 4 + 6 + 4 + 1 = 15 possibilities. If we assume that failure involved an equal likelihood for any of the 15, the probability of one plane at failure is 4 ÷ 15 = 0.27;

affected by element size, in that the smaller the elements, the more planes are available for slipping to occur. The number of planes p may be estimated from the number of rods r in a cross row and number of cross rows n:

$$p = \frac{n-1}{2} + r - 1 \qquad (43a)$$

This assumes no dead zones at the ends of the box, and no cross shears, which would double p. Cross-shears were occasionally observed, but were not common due to blocking. Following are the planes possible in the experiments:

d, in.	r	Slip Planes, p* End	Central	Total	Rod contacts per plane
1.0	5	8	4	12	8
0.75	7	12	5	17	12
0.50	10	18	17	35	18
0.25	20	38	34	72	37
0.125	40	78	66	144	77

*May be multiplied by 2 for cross-shears

Probabilities

The probability of a particular number of slip zones developing during a test may be calculated from the number of possible combinations. For example, let us assume that due to end restraint only the four central planes in the array of one inch rods are eligible for slip. There is an equal likelihood that slip will initiate on any one of the four - 1, 2, 3, or 4, whereupon friction will increase and slip will most likely become arrested. The second slip then may involve several combinations: 1 + 2, 1 · 3, 1 · 4, 2 + 3, 2 + 4, 3 · 4. Similarly a third slip, if it occurs, could involve 1 · 2 · 3, 1 · 2 · 4, 1 · 3 · 4, 2 · 3 · 4, whereas a fourth slip could only involve 1 + 2 + 3 · 4. In total there are 4 · 6 + 4 · 1 15 possibilities. If we assume that failure involved an equal likelihood for any of the 15, the probability of one plane at failure is 4 ÷ 15 0.27;

of two planes, 0.40; of three planes, 0.27; and of four planes, 0.07. Based on these assumptions the most likely number of slip planes is two, but there is still a 60 percent chance that the number involved will be other than two.

The above relation involves elementary probability theory, whereby the n number of combinations is

$$C_m^p = \frac{p!}{m!\,(p-m)!} \tag{43b}$$

where p is the number of planes available and m is the number participating. In the above example, for two active planes

$$C_2^4 = \frac{4 \cdot 3 \cdot 2 \cdot 1}{2 \cdot 1\,(2 \cdot 1)} = 6.$$

The total combinations possible is then

$$C_{p!}^p = \frac{p!}{1!\,(p-1)!} + \frac{p!}{2!\,(p-2)!} + \frac{p!}{3!\,(p-3)!} + \cdots + \frac{p!}{p!\,(p-p)!} \tag{43c}$$

Where 0! is assigned a value of 1.0. In the above example

$$C_{4!}^4 = \frac{4!}{3!} + \frac{4!}{2(2)} + \frac{4!}{3!} + \frac{4!}{4!\,(0)!}$$

$$= 4 + 6 + 4 + 1 = 15.$$

The probability of occurrence of any particular number of acting planes m may be calculated by dividing C_m^p by $C_{p!}^p$. This has been done for several values of p in Table 2. The highest probability in each column is underlined. In the case of one inch rods with p = 4, the most likely number is 2, whereas for 0.5 - inch rods, p = 12, and the most likely number is 6, predicting the typical results presented in Fig. 9.

The data of Table 2 are plotted on a cumulative basis in Fig. 18.

Table 2. Theoretical probabilities of multiple slip planes

	p					
m	4	5	12	17	34	66
1	0.267	0.161	0.003	*	*	
2	0.400	0.322	0.016	0.001	*	
3	0.267	0.322	0.054	0.005	*	
4	0.067	0.161	0.121	0.018	*	
5		0.032	0.193	0.047	*	
6			0.226	0.094	*	
7			0.193	0.148	*	
8			0.121	0.185	*	
9			0.054	0.185	0.003	
10			0.016	0.148	0.007	
11			0.003	0.094	0.015	
12			*	0.047	0.028	
13				0.018	0.048	
14				0.005	0.071	
15				0.001	0.095	
16				*	0.113	
17				*	0.120	
18					0.120	*
19					0.113	*
20					0.095	*
21					0.071	*
22					0.048	0.001
23					0.028	0.002
24					0.015	0.005
25					0.007	0.008
26					0.003	0.014
27					*	0.022
28					*	0.033
29					*	0.046
30					*	0.061
31					*	0.075
32					*	0.087
33					*	0.095
34					*	0.098
35						0.095
36						0.087
etc.						etc.
$C^p_{p!}$ =	15	31	4095	131,071	$1.951\ (10)^{10}$	$7379\ (10)^{19}$

* Less than 0.1%.

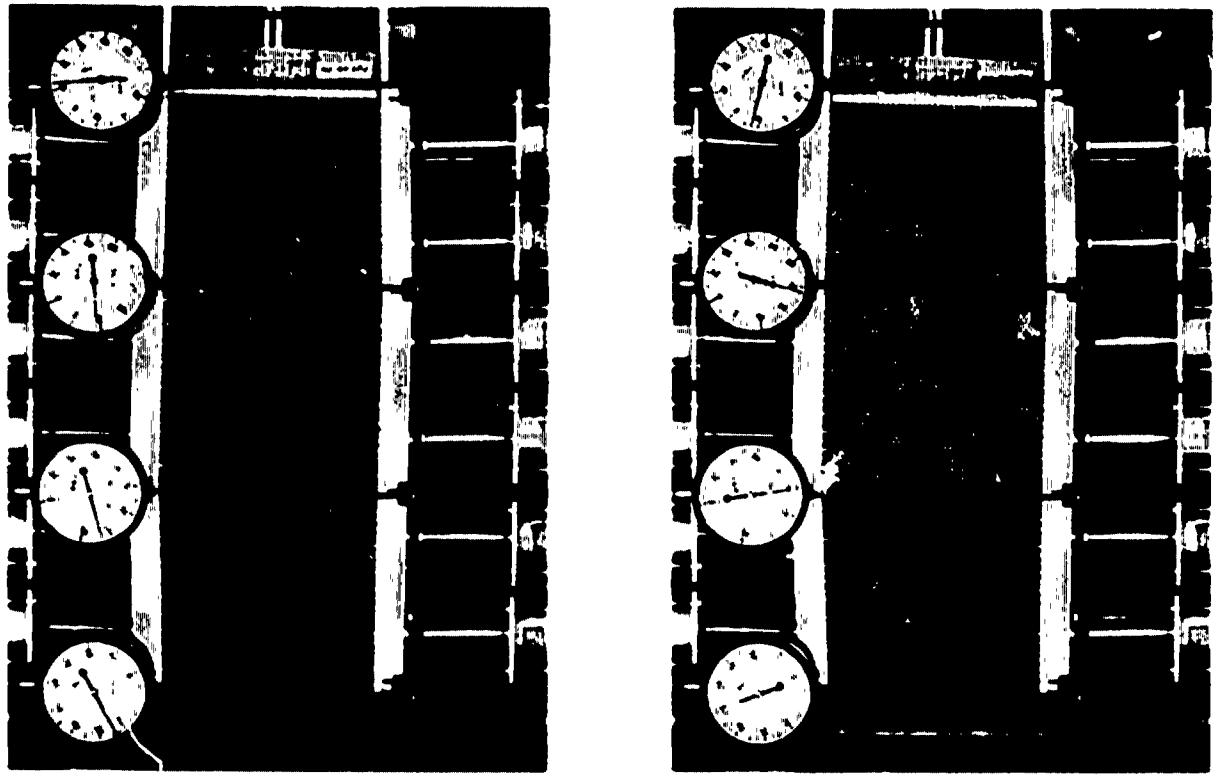

(a) (b)

Figure 8. Typical experimental slip zones. (a) 1-in. steel rods, two planes
(b) 0.5-in. steel rods, six planes

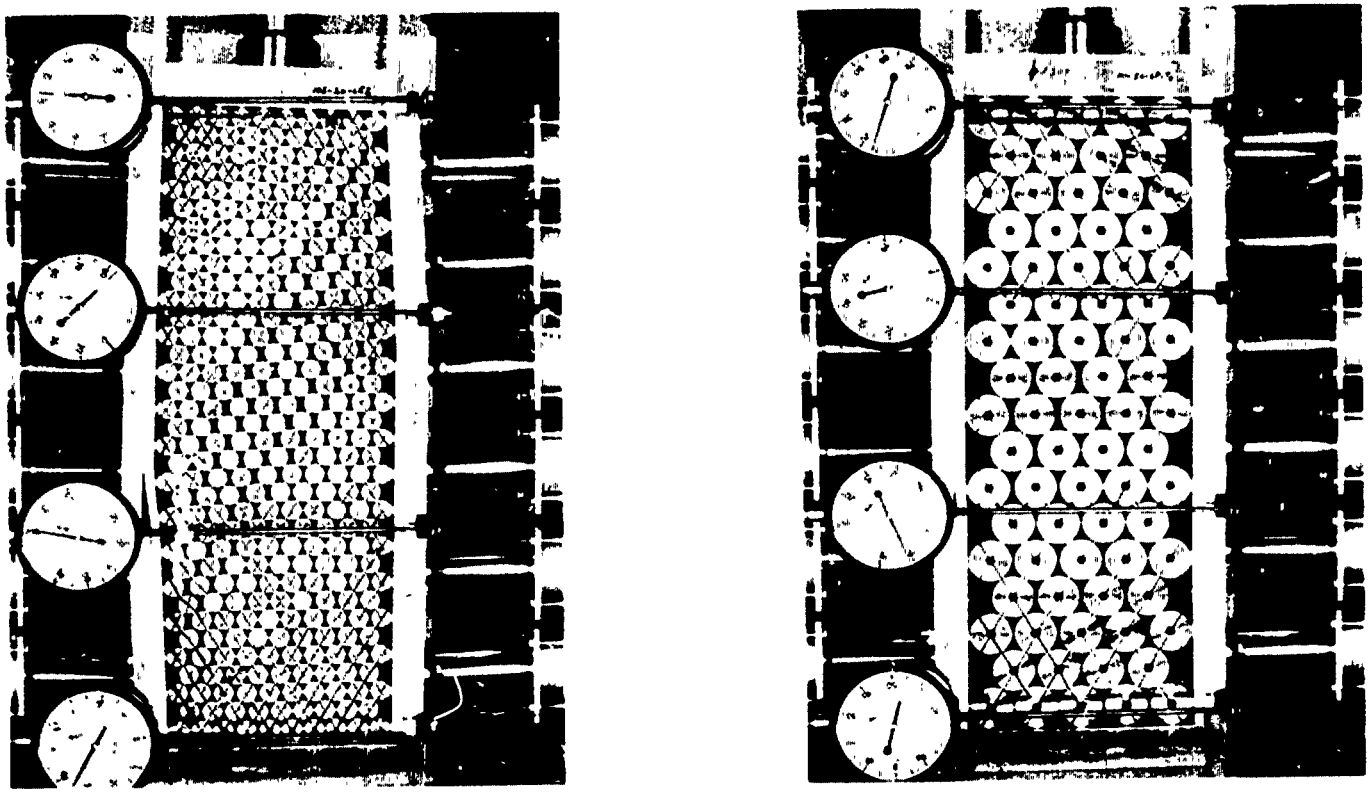

(a) (b)

Figure 9. Experimental slip zones, 0.125-in. steel rods. (a) Multiple planes. (b) Dislocation centers from continued axial strain.

TESTING OF THEORY

Experimental Measurement of Sliding Friction

The coefficient of sliding friction, f, appearing in the stress ratio equations (26) and (29) was independently evaluated by the method of Bahadur (1970), also described in Logani (1973).

The experimental coefficients of friction from a section of the 1-inch diameter steel rods varied somewhat with normal load, Fig. 10. The mean from 14 determinations was $f = 0.1922 \pm 0.0052$, the $\pm$ entry indicating 90% confidence limits on the mean from experimental error. Similar tests performed on a section of Teflon rod also indicated a tendency for the coefficient of friction to decrease with increasing normal ad , the mean and 90% confidence limits from eight tests being 0.0144 ± 0.0018. Scanning electron micrographs of the steel rod surfaces showed major irregularities indicating that the actual coeffieicnt of friction of different areas on different rods probably varies considerably more than indicated by the $\pm$ entries.

To test Eq. 29, which expresses a relation between stress ratio (σ_1/σ_3) and axial strain (ϵ_1), the equation is $\alpha = 0$. The equation is reduced for maximum stress ratio $(\sigma_1/\sigma_3)_{max}$ by substituting $\omega = 0$. The reduced equation becomes the same as Eq. 26. By substituting various values of coefficients of friction in Eq. 26, the corresponding predicted maximum stress ratios $(\sigma_1/\sigma_3)_{max}$ were found and tabulated against the coefficient of friction in Table 3. The experimental maximum stress ratios (σ_1/σ_3) are tabulated against corresponding lateral stresses (σ_3) in Table 3 for all sizes of rods tested. A very slight linear trend of increasing $(\sigma_1/\sigma_3)_{max}$ with increasing lateral stress (σ_3) has been observed, and is particularly conspicuous in the case of 1"-diameter and 1/8"-diameter rods; but, in the case of other sizes of rods, this trend is very slight. Data with the 1/8"-diameter rods are less reliable, due to the presence of Teflon side plates in early tests.

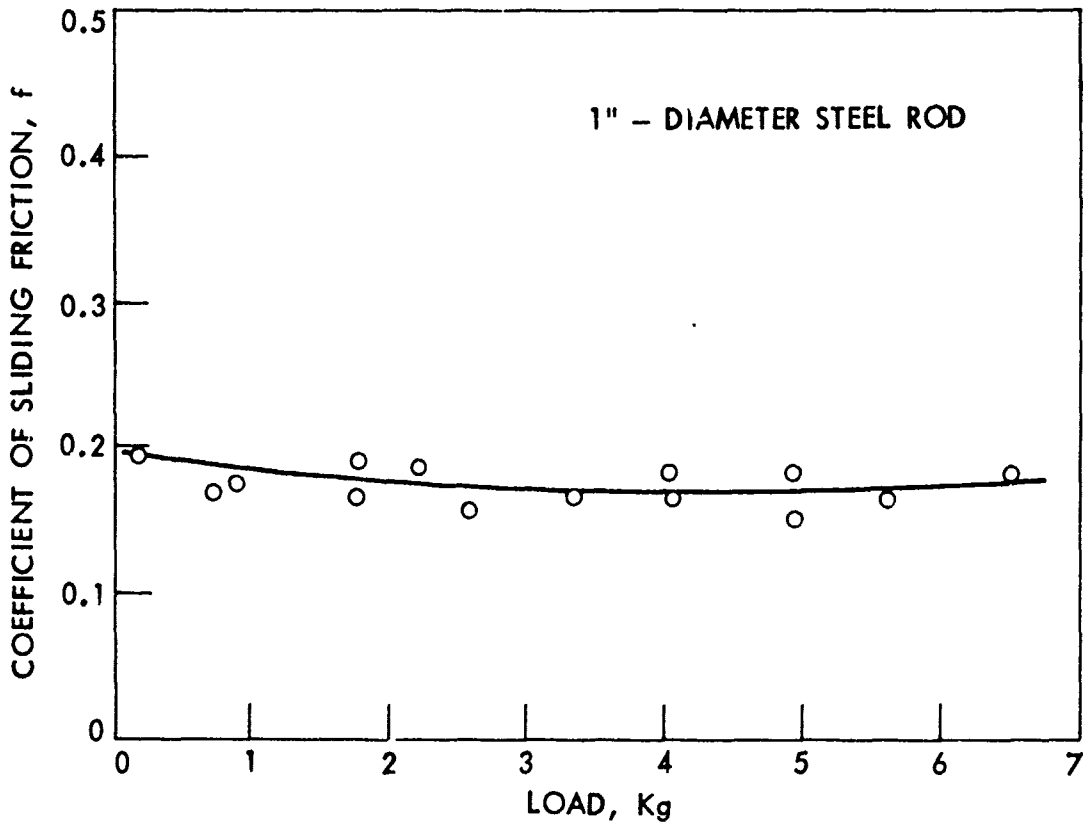

Figure 10. Experimental coefficient of sliding friction, steel on steel.

Table 3. Experimental Maximum Stress Ratio

Serial number	Material	Diameter of rods (inch)	σ_3 (psi)	$(\sigma_1/\sigma_3)_{max}$
1	Cold rolled	1	10	4.13
2	steel		20	4.62
3			30	4.40
4			40	4.53
5			50	4.72
6		3/4	10	4.20
7			20	4.00
8			30	4.27
9			40	4.28
10			50	4.28
11		1/2	10	3.60
12			20	3.90
13			30	3.93
14			40	3.95
15			50	4.00
16		1/4	10	3.80
17			20	3.60
18			30	3.93
19			40	4.08
20			50	4.00
21		1/8	10	3.6
22			20	3.7
23			30	3.9
24			40	4.1
25			50	4.0
26	Teflon	3/4	10	3.1
27			20	3.18
28			30	3.21
29			40	3.24
30			50	3.36

The mean experimental maximum stress ratios and 90% confidence limits on the means are 4.06 ± 0.15 for steel and 3.22 ± 0.05 for Teflon. Equation 26 solved for f and with $\lambda = 30^{o}$ becomes

$$f = 0.1443 \frac{\sigma_1}{\sigma_2} - 0.433 \qquad (26a)$$

Substituting the values for σ_1/σ_2 into this equation gives $f = 0.15 \pm 0.02$ for steel and $f = 0.032 \pm 0.008$ for Teflon, reasonably close to the measured values of 0.19 and 0.014, respectively, in the one case the comparative value being higher and in the other case lower.

Predicted Stress Ratio in the Post-Failure Region

To test Eq. 29 in the post-failure region, curves of the theoretical stress ratio against axial strain (ϵ_1) have been drawn for various levels of coefficient of friction. For drawing the above curves, the axial strain at the maximum stress ratio was assumed to be zero, because we are assuming that dilatancy begins after the maximum stress ratio is reached. These theoretical curves are superimposed on experimental stress ratio curves in Figs. 11 - 14, selected to illustrate different phenomena.* This superposition was done in such a way that the point on the theoretical stress ratio curve corresponding to $\psi = 0$ or, in other words, the point of maximum stress ratio coincided with the maximum stress ratio on the curve. The theoretical formulation for the stress ratio does not take into account arrested slip, which means that slip is assumed to be taking place only on a definite shear plane.

The theoretical and experimental stress ratio curves are in good agreement in the case of larger diameter rods, i.e., 1" and 3/4", where arrested slip is less probable. In Fig. 11 can be seen an initial slip at $f = 0.16$ falling to 0.14, and then suddenly increasing and stabilizing at about 0.20.

In the case of 0.5-inch diameter rods, Fig. 12, the development of new shear zones causes the experimental curve to cross the theoretical curves, which should be translated as a group to the right to account for

---

*Other experimental curves are presented in Appendix B.

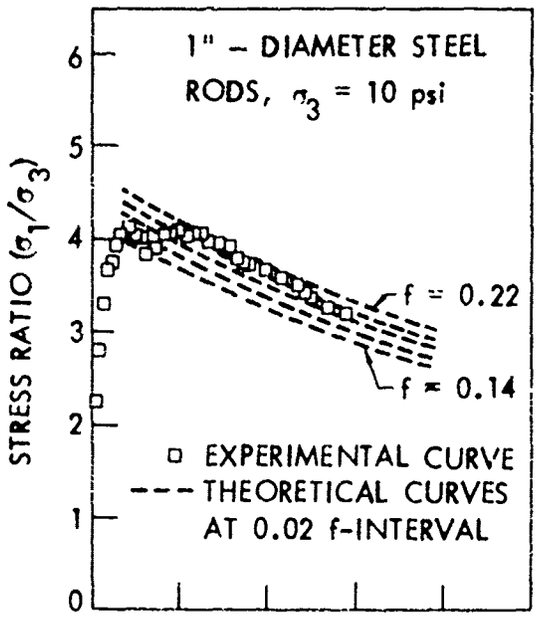

Figure 11.

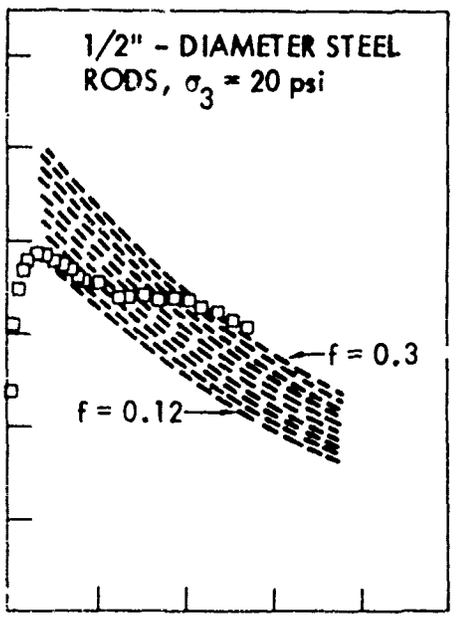

Figure 12.

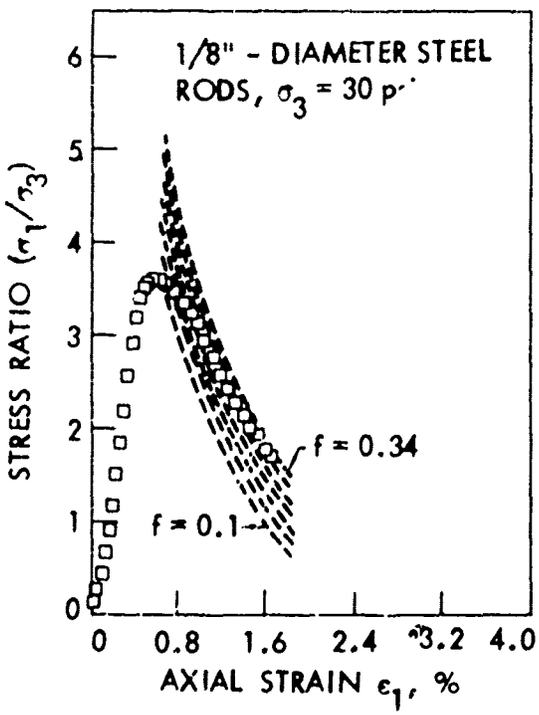

Figure 13.

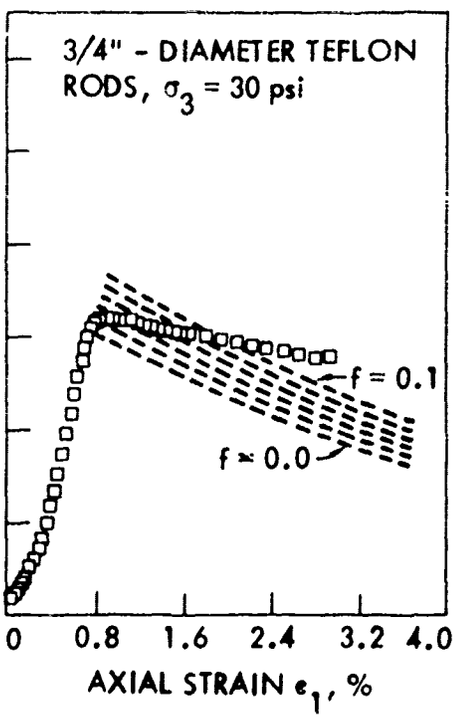

Figure 14.

Figures 11-14. Selected experimental stress-strain curves for various rods and several lateral stresses.

initiation of strain in a new location. Other curves with 0.5-inch rods were almost horizontal because of increasing shear zones. This tendency was less pronounced with the 0.25- and 0.125- inch rods, Fig. 13, because of the more rapid decrease in σ_1/σ_3 as a function of axial strain. Evidence for increasing shear planes is the unrealistically high f if the theoretical curves are not translated.

The experiments with Teflon rods were complicated by a much larger elastic strain, Fig. 14, and suggest multiple shear planes.

Figures 11-14 are representative of many tests; other curves are in Appendix B.

Two modes of failure appear to be defined by the experimental and theoretical curves. These are illustrated in Fig. 15. In the first, elastic deformation is followed by slip along a single zone, with the coefficient of sliding friction f relatively constant, and in the second, shear slip transfers from plane to plane throughout the post-maximum stress ratio dilation. That is, slip takes place on one shear plane, becomes arrested, and shifts to another, and so on. If the coefficient of friction is still relatively constant, the experimental stress ratio curve, instead of following one theoretical f-level curve, will stay more of less parallel to the axial strain axis. This can be explained by considering that, with each shear plane abondonment and formation of a new plane, the theoretical stress ratio curve starts anew, i.e., is shifted to the right along the axis of axial strain. Thus, the failure point will move parallel to the axial strain axis. In the soil mechanics literature, such a stage in the stress ratio versus axial strain curve is called a residual stage of assumed constant volume stage, whereas in the above mechanism, the coefficient of friction stays constant while the volume may go on increasing.

If the coefficient of friction does not remain constant the point P will not move parallel to the axial strain axis, but will shift (up or) down to various f-level curves at each particular axial strain.

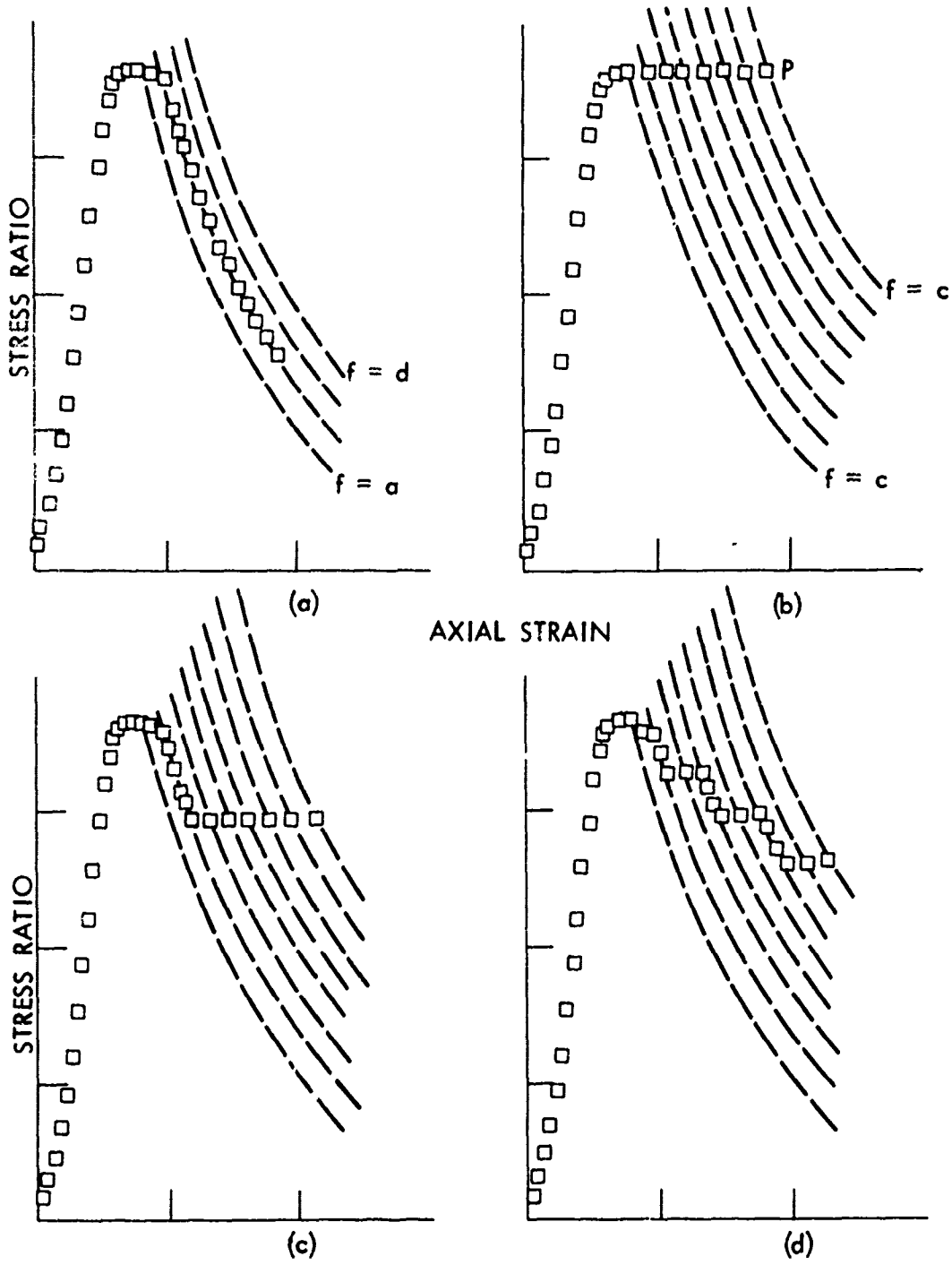

Figure 15. Axial strain to stress ratio curves; (a) failure mechanism 1, (b) failure mechanism 2, (c & d) two combinations of failure mechanisms 1 and 2

Volumetric Strain

On the basis of experimental observations, the following postulates are suggested:

1. The rate of change of the number of failure planes is inversely proportional to axial strain. This implies that the width of the failure zone increases sharply at first, and then slows down with increasing axial strain.
2. For the same strain, the smaller the diameter of the rods, the larger is the number of failure planes.

If in the first postulate dL is the change of number of failure planes, L is the number of failure plane at any instant, and $d\epsilon_1$ is the axial strain. Then the first postulate may be expressed as an equation:

$$\frac{dL}{d\epsilon_1} = \frac{1}{c}\,\frac{1}{\epsilon_1} \tag{44}$$

where $\frac{dL}{d\epsilon_1}$ is the slope of the tangent to L-versus-ϵ_1 curves and c is a constant. Rearranging and integrating Eq. 44,

$$c\,dL = \frac{d\epsilon_1}{\epsilon_1}$$

$$cL = \ln\epsilon_1 + \ln k$$

$$= \ln \epsilon_1 k$$

$$L = \frac{1}{c}\,\ln\epsilon_1 k \tag{45}$$

where k is a constant of integration, or

$$\epsilon_1 = \frac{1}{k}\,e^{cL} \tag{46}$$

Constants c and k can be found from experimental boundary conditions. A verification of the form of Eq. 46 will be shown by a linear relationship

between L and in ϵ_1 from which k was evaluated experimentally, giving

$$L = n\,417\,\epsilon_1 \tag{47}$$

where ϵ_1 is the unit strain x 10^{-3}.

To express postulate 2 in a mathematical form, a general tabulation of the number of major failure planes, i.e. those contributing significantly to volumetric strain, was made against axial strains for all the experiments. On the examination of this data, the following generalization was made:

On the average, if one failure plane is taking part in 1"-diameter assemblage, then $\frac{1}{0.9}$, $\frac{1}{0.7}$ and $\frac{1}{0.5}$ failure planes will take part in $\frac{1}{2}$", $\frac{1}{4}$" and 1/8"-diameter assemblage, respectively. Therefore, if L is the number of major failure planes and d (in inches) is the diameter of the particles (rods), the above generalization can be approximately expressed as:

$$L = (d)^{-0.33} \tag{48}$$

Combining Eqs. 47 and 48, we obtain

$$L = \frac{\ln 417\,\epsilon_1}{(d)^{0.33}} \tag{49}$$

To incorporate the requirement of postulates 1 and 2, the final relation for volumetric strain is obtained by multiplying Eqs. 43 and 49:

$$\frac{dv}{v_0} = \frac{\ln 417\,\epsilon_1}{(d)^{.33}}\left\{\frac{1}{\sin 2\lambda}\sin(2\lambda + \arctan\left[\frac{2}{(n-1)\,\epsilon_1 \sin 2\lambda} - \cot 2\lambda\right]^{-1}) - 1\right\} \tag{50}$$

which should hold outside of the region of elastic deformation. Elastic deformations have been observed to be confined to the initial region of 0-0.2% axial strain.

Equation 50 was tested by superimposing calculated and experimental volumetric strain (dv/v_0) versus axial strain ϵ_1 curves. This superposition should be done such that the point of zero volumetric strain (dv/v_0) on the theoretical curve coincides with the point on the experimental

curve where elastic volumetric strain becomes complete. This point is uncertain, and, for the sake of simplicity, it is assumed to the point of minimum volumetric strain. The difficulty is all the more problematic when one considers that elastic and dilational deformations probably overlap.

In spite of the simplifying assumptions, it can be seen from the superimposed curves that there is fairly good agreement between the theoretical and experimental date (Fig. 16 and 17). A slight deviation from the theoretical curves has been observed in the intermediate stage of axial strain in that the experimental volumetric strain exceeds the theoretical value corresponding to a particular axial strain. Deviation from the theoretical volumetric strain (dv/v_o) versus axial strain ϵ_1 curve also becomes significant at very large axial strains because of more chaotic and less predictable movements of the particles at large induced deformations.

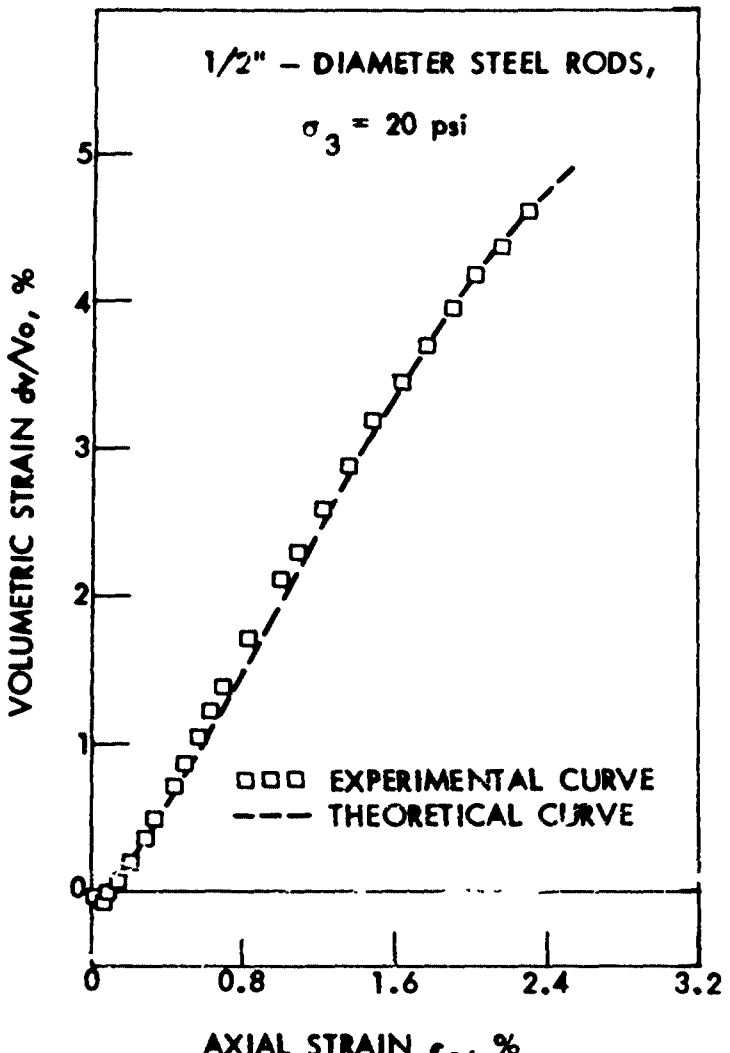

Figure 16. Volumetric strain curves

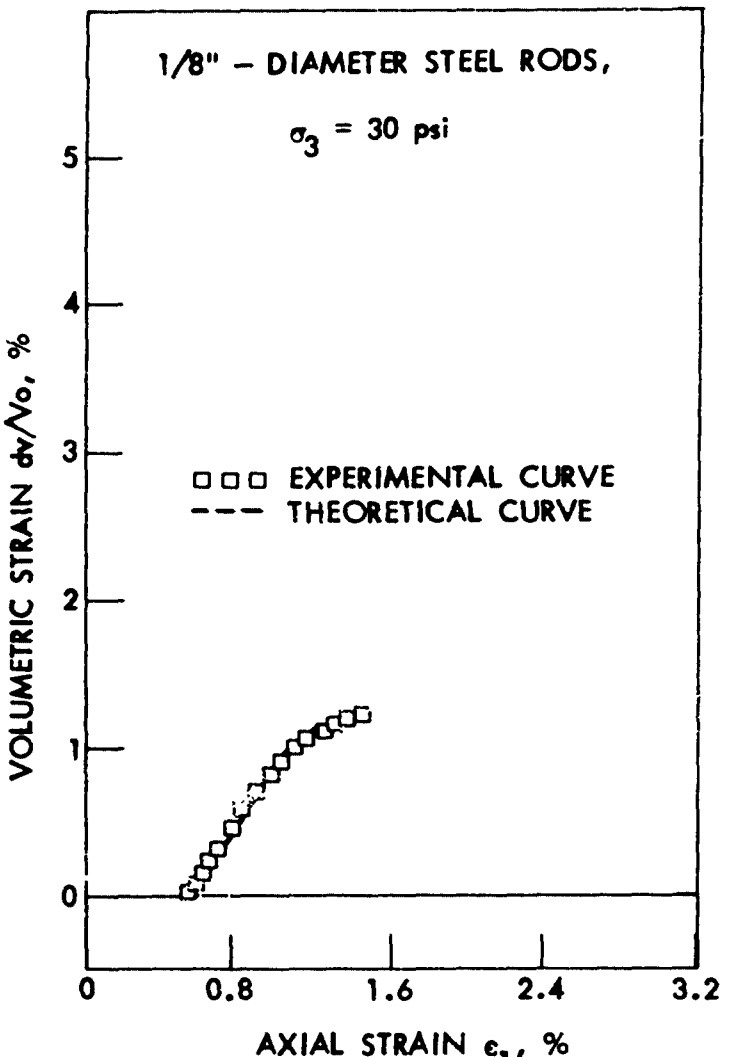

Figure 17. Volumetric strain curves

PROBABILITY IN RELATION TO ROCK CREEP AND PROGRESSIVE FAILURE

Rock Creep

Rock creep is a widely known phenomenon, descriptive of progressive movements which may lead to eventual catastrophic failure of rockslides, cavern roofs, etc. In this connection Terzaghi (1960) suggests that a randomly jointed rock behaves like a stiff clay or an impure sand with considerable cohesion. Following the behavioral analogy to clay soils, Barton (1972) relates creep to a loss of cohesion exemplified by a residual strength contrasted to a peak strength. Brawner et. al. (1972) and other authors have recognized the variable nature of friction in jointed rocks, but to our knowledge have not attempted to relate this to a creep behavior. The zonal nature of rock creep is suggested by Zischinsky (1966), who differentiates between rock sliding (Gleitung) and rock creep (Sackung) on the basis that the latter shows a velocity dependent on distance above stable rock, therefore constituting a zonal failure.

A prevailing assumption with regard to rock creep appears to be that clay in the joints must be a causal factor. For example, Cording et. al. (1971), in discussing the stability of caverns at the Nevada Test Site and other locations, suggests that strain is a function of t exp m where t is lime and m is a constant that may relate to plasticity index of the fault gouge. Broadbent and Ko (1971) also report gross semilogarithmic relationships between slope movements and time, but analyze the data with a rheological model and replot on a linear scale to show that movement actually is in a series of jumps which may or may not show a progressive increase in magnitude.

Probability and Creep Rate

The calculated probabilities for number of shear planes, Table 2, are plotted on a cumulative basis in Fig. 18. The resulting curves bear a striking resemblance to classical creep behavior, by considering that the total shear deformation is proportional to the number of shear planes, and cumulative

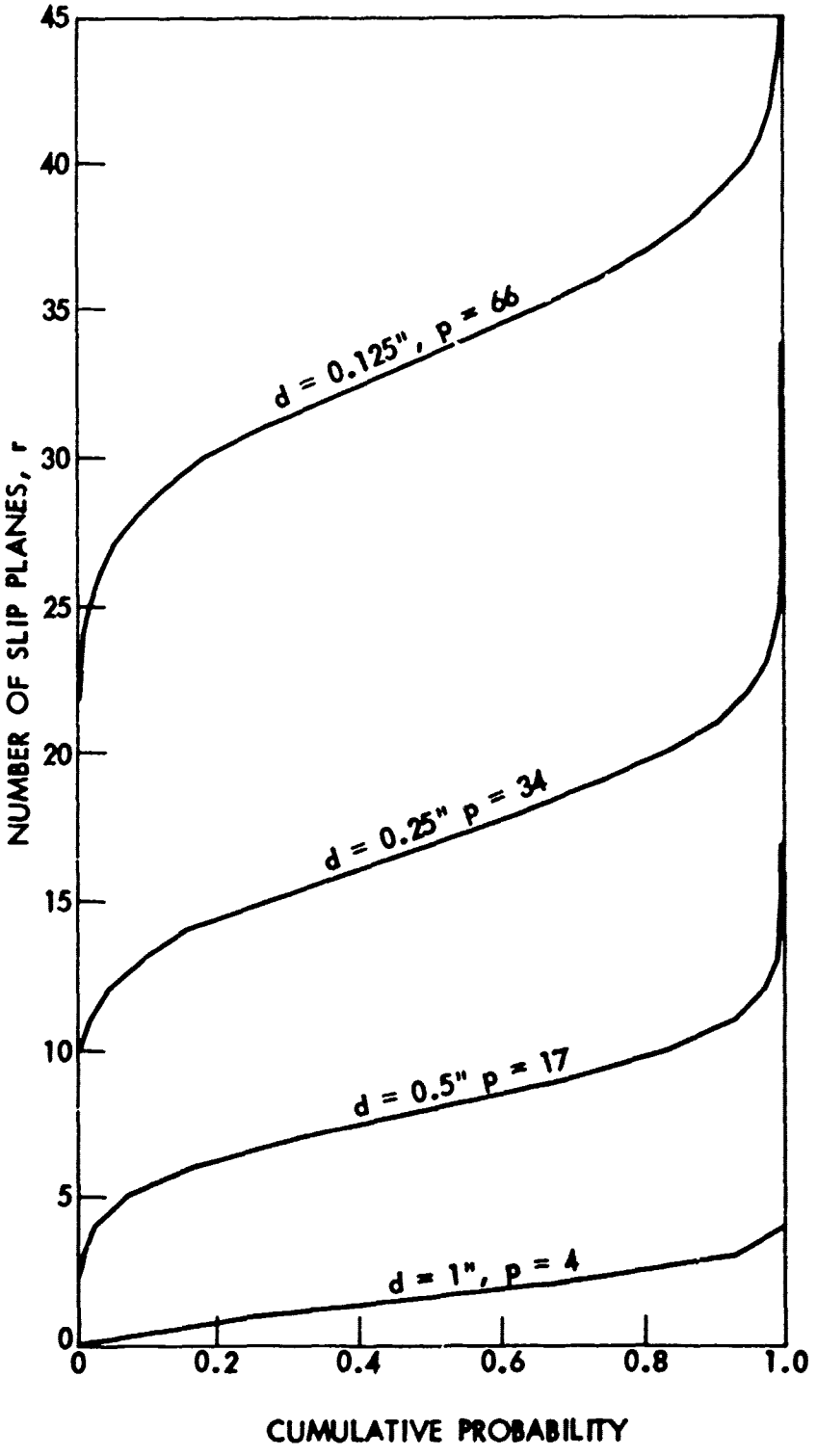

Figure 18. Theoretical slip distance (number of slip planes) vs. time (cumulative probability) curves from data in Table 2.

probability is representative of elapsed time. Both of these assumptions appear reasonable, in that in a given assemblage exhibiting the arrested slip phenomenon the cumulative slip will equal the average individual slip distance times the number of slip planes, and secondly slip results from minor fluctuations in stress or friction which are random in time, the cumulative probability of slip will bear a linear relation to time.

Let us therefore reexamine the factors and assumptions made to obtain data in Table 2 and Fig. 18:

1. Slip will initiate along the weakest plane or the surface with the lowest accumulated friction.

2. By bringing new surfaces into contact, slip will tend to induce an increase in friction, which usually will be sufficient to cause slip to become arrested and shift to the next stronger plane.

3. As a result of arrested and relocated slip, a constant stress ratio vs. strain curve may be developed.

4. Each possible combination of the potential failure planes either singly or in multiples has an equal likelihood of occurrence.

There can be little argument that the first assumption is valid for fractured rock masses, so long as frictional resistance is taken to include both sliding friction and dilatant effects.

The second assumption that sliding increases friction, appears valid so long as the reduction is not overcome by strain weakening through thixotropy or slickensiding. If the second assumption is invalid, strain will continue along the same weakest plane, with friction decreasing or remaining constant. If stress is not somehow relieved, the result can only be sudden failure.

The third factor, development of an interval of constant stress vs. strain, has been demonstrated for the steel and Teflon rods (Fig. 11, 12, 14) and is fairly common in triaxial testing of rock.

The fourth assumption affects the shape of the probability curve. While the test data are insufficient in quantity to validate this assumption they do comply with its prediction.

Perhaps most significant is that an ideal creep behavior is predicted for a fractured rock assemblage which is devoid of cohesion. The requisites include a stress level close to failure, and several planes available and engaged in arrested slip. Should such an action be involved in field occurrences of rock creep along fractures, it may also explain the subaudible, clicking "rock noises" which characterize creep and warn of an impending landslide.

Finally, if rock creep field data can be fitted to probability based curves as in Fig. 18, there should be a considerable advantage for prediction of ultimate failure, compared to empirical semilogarithmic data plots which predict a smoothly increasing rate of movement with no sudden changes. Such a plot of the right half of data in Fig. 18 shows two straight lines, Fig. 19, the second line being indicative of catastrophic failure. The lines intersect at a cumulative probability of about 0.99, where about 60-70 percent of the available planes are participating in the failure.

Thus it would appear that the time of failure may be rather accurately predictable from a changing thickness of the failure zone. This may be monitured by inserting vertical pipes through the failure zone and periodically measuring their curvature with depth. The zone thickness plotted against time may give graphs as in Fig. 18 or 19. From Fig. 18 may be seen that as a rough guide, a doubling in thickness of the shear zone should be sufficient to bring about catastrophic failure.

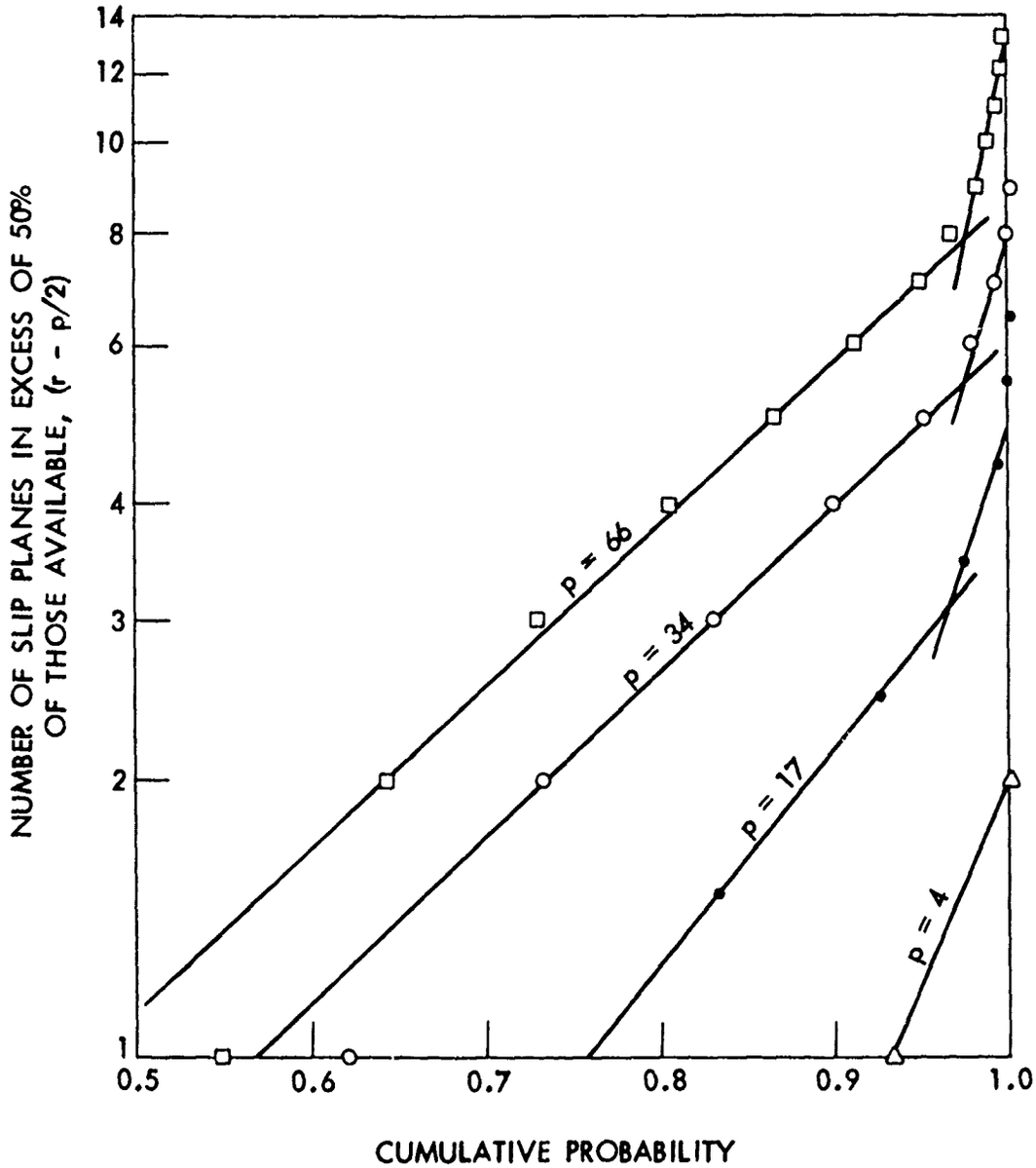

Figure 19. Semilogarithmic plot of right-half data in Figure 18.

CONCLUSIONS

Relative to Test Data

1. In a regular array representing a homogeneous, cohesionless assemblage, the stress ratio (σ_1/σ_3) is a predictable function of geometry of the array and the coefficient of sliding friction at contacts.

2. Previous dilatant work theories derived for soils do not describe the observed results because they neglect elastic deformations prior to dilatancy, and they assume sliding friction to be a constant.

3. After an elastic volumetric decrease stage, dilatancy initiates by sliding along the least resistant chain of frictional contacts. Friction in this active zone is thus less than the average. Therefore, as sliding proceeds and brings new surfaces into contact, friction in the active zone almost always increases, tending to cause slip to become arrested and relocated to a new zone.

4. A densest packed starting geometry such as the one chosen (a rhombic arrangement of cylindrical particles) gives a decreasing stress ratio (σ_1/σ_3) as strain proceeds; however, a recurrence of arrested slip will cause σ_1/σ_3 to increase, decrease less rapidly, or hold constant, (the latter simulating creep behavior), as the shear zone increases. After the maximum shear zone becomes established, the stress ratio decreases in the predicted manner.

5. For volume change of a dilating array to be predicted from geometry of the array, allowance must be made for the gradually enlarging shear zone caused by arrested slip, and the volume change usually is larger than would occur from a single slip. This violates a basic premise of the minimum-work theories.

6. The number of slip planes appears to be predictable from laws of probability, the most likely number being one-half of those available.

7. The probability model for number of shear planes reasonably simulates typical creep stress-strain behavior, the rate slowing down at first (primary creep), then remaining constant (secondary creep), then speeding up and going into rapid failure (tertiary creep). However, the mechanism differs from viscous creep in that the particulate array may be cohesionless, and the active zone is ever increasing in thickness.

8. The probability model for creep behavior requires that the thickness of the shear zone be increasing, and that catastrophic failure becomes imminent when the thickness approximately doubles its initial value.

REFERENCES CITED

Andrade, E. N. Dac., and Fox, J. W., "The mechanism of dilatancy," The Proceedings of the Physical Society, London, Section B. Vol. 62, Part 8, No. 356B, 1949, pp. 483-500.

Barton, Nicholas, "Progressive failure of excavated rock slopes" Proc. 13th Symposium on Rock Mechanics ASCE., 1972. pp. 139-170.

Brawner, C. O., Penz, D. L., and Sharp, J. C., "Stability studies of a foot-wall slope in layered coal deposit." Proc. 13th Symposium on Rock Mechanics ASCE., 1972. pp. 329-365.

Broadbent, C. D., and Ko, K. C. "Rheological aspects of rock slope failures." Proc. 13th Symposium on Rock Mechanics ASCE., 1972. pp. 573-593.

Brown, R. L., and Hawksley, P. G. W., "The internal flow of granular masses." Fuel, Vol. 26, No. 6, Nov. - Dec., 1947, pp. 159-173.

Caquot, A., Equilibre des Massifs a Frottement Inteme, Stabilite des Terres Pulverent et Coherentes, Gauthier Villars, Paris, 1934.

Cording, E. J., Hendron, A. J., and Deere, D. V. "Rock engineering for underground caverns" ASCE Symposium on Underground Rock Chambers, 1971. pp. 567-600.

Hills, E. Sherbon, Elements of Structural Geology, John Wiley and Sons, Inc., New York, 1963.

Horne, J. R., "The behaviour of an assembly of rotund, rigid, cohesionless particles. I and II," Proceedings, Royal Society of London, Series A, Vol. 286, 1965, pp. 62-97.

Logani, K. L. "Dilatancy model for the failure of rocks." Unpubl. Ph.D. Thesis, Iowa State University Library, Ames. 1972. 214 pp.

Mead, Warren J., "The geologic role of dilatancy," The Journal of Geology, Vol. 33, 1925, pp. 685-698.

Newland, P. L., and Allely, B. H., "Volume changes in drained triaxial tests on granular materials," Geotechnique, Vol. 7, No. 1, 1957, pp. 17-34.

Rennie, B. C., "On the strength of sand," Journal Australia Mathematical Society, Vol. 1, 1959, pp. 71-75.

Reynolds, Osborne, "On the dilatancy of media composed of rigid particles in contact with experimental illustrations," Philosophical Magazine and Journal of Science, Fifth Series 20, December, 1885, pp. 469-481.

Rowe, P. W., "Stress-dilatancy, earth pressure, and slopes," Proceedings of the A.S.C.E., Vol. 89, No. SM3, 1963, pp. 37-61.

Scott, Ronald F., Principles of Soil Mechanics, Addison-Wesley Publishing Company, Reading, Mass., 1963.

Scott, R. F., Meyerhof, George G., Roscoe, K. H., Schofield, A. N., Pijushkanti, Som, and Das, S., "Stress-dilatancy, earth pressure, and slopes" (discussion), Proceedings of the A.S.C.E., Vol. 90, No. SM1, 1964, pp. 133-150.

Skempton, A. W., and Bishop, A. W., "Measurement of shear strength of soils," Geotechnique, Vol. 2, 1950, pp. 90-108.

Taylor, D. W., Fundamental of Soil Mechanics, John Wiley and Sons, Inc., New York, 1948.

Terzaghi, Karl. "Stability of slopes on hard weathered rock." Geotechnique 12: 1960. pp. 251-270.

Thurston, C. W., and Deresiewicz, H., "Analysis of a compression test of a model of a granular medium," J. Appl. Mech., Vol. 26, 1959, pp. 251-258.

Tinoco, F. H., and Handy, R. L., "Shear Strength of Granular Materials," Iowa State Soil Research Lab. Contribution No. 67-9, 1967.

Trollope, D. H., Parkin, A. K., Gibson, R. E., and Morgenstern, N. R., "Stress-dilatancy, earth pressure and slopes" (discussion), Proceedings A.S.C.E., Vol. 89, No. SM6, 1963, pp. 127-133.

Zischinsky, Ulf. "On the deformation of high slopes." Proc. 1st Congress Int. Society of Rock Mechanics, Lisbon, II: 1966. pp. 179-185.

PART II

APPENDICES

Appendix A

Derivations of Equations

Elastic Strain

Consider cylinder pairs J and P, and K and P, in an array, Fig. 7. A compressive force acting through the centers of a pair will bring them closer by a distance here designated α, known as the distance of relative approach. A tangential force similarly will cause a tangential displacement δ. In a symmetrical array the lateral components of both α and δ are equal and opposite in sign and add to zero in the σ_3 direction, giving $\epsilon_{3e} = 0$. The sum of axial components of α and δ is

$$\epsilon_{1e} = \frac{2(\alpha\cos\lambda + \delta\sin\lambda)}{d\cos\lambda}$$

$$= \frac{2}{d}(\alpha + \delta\tan\lambda) \qquad (5)$$

Since $\epsilon_{2e} = \epsilon_{3e} = 0$, and the elastic volume change per unit length of one cylinder is

$$(\delta v)_e = \epsilon_{1e} + \epsilon_{2e} + \epsilon_{3e}$$

$$= \epsilon_{1e} = \frac{2}{d}(\alpha + \delta\tan\lambda) \qquad (6)$$

For a cylinder pair,

$$(dv)_e = 2(\delta v)_e \qquad (7)$$

Multiplying by the number of cylinders in the assemblage,

$$(dv)_e = (n - 1)(r - 1)\frac{4}{d}(\alpha + \delta\tan\lambda) \qquad (8)$$

The orignial volume of the assemblage is

$$v_o = (n - 1)(r - 1)d^2\sin 2\lambda \qquad (9)$$

Dividing (8) by (9)

$$\frac{(dv)_e}{v_o} = \frac{4(\alpha + \delta\tan\lambda)}{d^3\sin 2\lambda} \qquad (10)$$

At Failure

The sides of the wedge ABC, Fig. 7, are:

$$\overline{AC} = 2(r - 1)\, d \sin \lambda \tag{11}$$

$$\overline{BC} = 2(r - 1)\, d \cos \lambda$$

$$\overline{AB} = 2(r - 1)\, d$$

Then $\overline{BC}$ σ_3 and $\overline{AC}$ σ_1 are the lateral and axial forces on the wedge, giving for a resultant

$$R = 2(r - 1)d \sqrt{\sigma_1^2 \sin^2\lambda + \sigma_3^2 \cos^2\lambda} \tag{12}$$

at an angle from the σ_3 axis

$$\tan \gamma = \frac{2(r - 1)\, d \sin \lambda\, \sigma_1}{2(r - 1)\, d \cos \lambda\, \sigma_3} \tag{13}$$

Assuming an even distribution of the resultant force on cylinders along the wedge face AB, the force on one cylinder is

$$S = \frac{R}{2(r - 1)}$$

$$= d \sqrt{\sigma_1^2 \sin^2\lambda + \sigma_3^2 \cos^2\lambda} \tag{14}$$

As σ_1 increases with respect to σ_3, γ increases per Eq. (13). When γ reaches the value $(90 - \lambda)$,

$$\tan \gamma = \frac{\sigma_1}{\sigma_3} \tan \lambda = \tan(90 - \lambda) \tag{15}$$

$$\sigma_1 = \sigma_3 \cot^2\lambda \tag{16}$$

at which value of λ the force S is being transmitted along the centerline of the contacting cylinders. From Eq. (14), the four axial forces symetrically disposed in four directions around P became

$$S_1 = d \sqrt{(\sigma_3 \cot^2\lambda)^2 \sin^2\lambda + \sigma_3^2 \cos^2\lambda} \tag{17}$$

$$= d \cot\lambda \sigma_3 \tag{18}$$

As the stress ratio further increases, this condition is abandoned, and the normal component of S becomes

$$S_n = S \cos (\gamma + \lambda - 90) \tag{19}$$

The tangential component is no longer zero, but is

$$S_t = S \sin (\gamma + \lambda - 90) \tag{20}$$

Experimental data indicate that this occurs before 0.1 to 0.2% axial strain. Eventually it is observed that two contacts, as JP and PM, slide, and two, as KP and PN, roll, the remaining two contacts OP and PL becoming separated. The limiting tangential force at JP and PM when the contact stress is a maximum is

$$S_{1\,max} = f(d \cot\lambda)\, \sigma_3 \tag{21}$$

where f is the coefficient of sliding friction. The resulting couple is:

$$f(d \cot\lambda)\, \sigma_3 d \tag{22}$$

which is opposed by a couple at the other rolling contacts:

$$S \sin(\gamma + \lambda - 90) d \tag{23}$$

Equating and sutstituting for S from Equation (14) gives

$$f \cot\lambda\, \sigma_3\, d^2 = d^2 \sin (\gamma + \lambda - 90) \sqrt{\sigma_1^2 \sin^2\lambda + \sigma_3^2 \cos^2\lambda}$$

Simplifying and utilizing Equation (15) for λ gives

$$\sin \gamma = \frac{\sigma_1 \tan\lambda}{\sqrt{\sigma_1^2 \tan^2\lambda + \sigma_3^2}} \tag{24}$$

and

$$\cos \gamma = \frac{\sigma_3}{\sqrt{\sigma_1^2 \tan^2\lambda + \sigma_3^2}} \tag{25}$$

which may be substituted in the above to give

$$\frac{\sigma_1}{\sigma_3} = (f + \sin\lambda \cos\lambda) \frac{\cos\lambda}{\sin^3\lambda} \tag{26}$$

(See also Logani, 1973).

Post Failure

As the array deforms from the initial angle λ by an amount ω, the individual force S makes an angle $(\gamma + \lambda + \omega - 90)$ with a line connecting centers of pairs. The force given by Equation (18) will still be acting and may be resolved as before. The two opposing couples become

$$f(d \cot \lambda)\, \sigma_3 d \tag{27}$$

and

$$S \sin (\gamma + \lambda + \omega - 90)d \tag{28}$$

A similar development then gives

$$\frac{\sigma_1}{\sigma_3} = \cot\lambda \left[\frac{f}{\sin\lambda \sin(\lambda + \omega)} + \cot(\lambda + \omega) \right] \tag{29}$$

Volumetric Strain

Assuming the wedge ABC moves as one unit parallel to AB, the movement of gf parallel to AB relates to the axial movement by

$$gf = \frac{E}{\sin(90 - \lambda)} . \tag{30}$$

The lines connecting centers of a unit cell in the array, as JPNO in Figure 7 form a parallelogram with area $d^2 \sin 2\lambda$. The area of void involved is

$$d^2(\sin 2\lambda - \frac{\pi}{4}). \tag{31}$$

As λ increases by the amount ω, the new void area becomes

$$d^2\left[\sin(2\lambda + \omega) - \frac{\pi}{4}\right] \tag{32}$$

Subtracting and multiplying the result by the number of distorting unit cells in two shear planes, $4(r - 1)$, gives

$$dv = 4(r - 1)d^2 \left[\sin(2\lambda + \omega) - \sin 2\lambda\right] \text{x rod length} \tag{33}$$

The original volume is

$$v_o = \left[(n - 1)(r - 1)d^2 \sin 2\lambda\right] \text{x rod length} \tag{34}$$

Dividing,

$$\frac{dv}{v_o} = \frac{4\left[\sin(2\lambda + \omega) - \sin 2\lambda\right]}{(n-1)\sin^2\lambda} \tag{35}$$

Since the length of the assemblage is

$$L_o = (n-1)\, d \cos\lambda, \tag{36}$$

substituting in Equation (34) gives

$$\frac{dv}{v_o} = \frac{2d}{L_o} \frac{\sin(2\lambda + \omega) - \sin 2\lambda}{\sin\lambda}. \tag{37}$$

The angle ψ may be solved as follows: Let the distance moved by a contact be gg', the chord of an arc which for the usual two-shear-plane zone has a radium 2d. The chord length is

$$gg' = 2(2d \sin\tfrac{\psi}{2}) \tag{38}$$

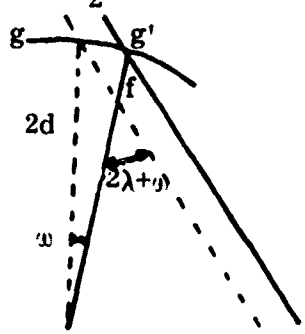

Since $\angle gg'f = (90 - \frac{\psi}{2})$ and $\angle gfg' = 2\lambda + \omega$, by the law of sines

$$gg' = \frac{gf \sin(2\lambda + \omega)}{\sin(90 - \frac{\psi}{2})}$$

Combining with Equations (30) and (38),

$$2(2d \sin\tfrac{\psi}{2}) = \frac{E \sin(2\lambda + \omega)}{\sin(90 - \frac{\psi}{2}) \sin(90 - \lambda)}$$

which simplifies to (Logani, 1973)

$$\tan \omega = \left[\frac{d}{E \sin \lambda} - \cot 2\lambda\right]^{-1}. \tag{39}$$

The value for ω may be substituted in Equation (37) to give

$$\frac{dv}{v_o} = \frac{4}{n-1}\left\{\frac{1}{\sin 2\lambda}\sin(2\lambda + \arctan\left[\frac{d}{E \sin\lambda} - \cot 2\lambda\right]^{-1}) - 1\right\} \tag{40}$$

or

$$\frac{dv}{v_o} = \frac{2d}{L_o \sin\lambda}\left\{\sin(2\lambda + \arctan\left[\frac{d}{E \sin\lambda} - \cot 2\lambda\right]^{-1}) - \sin 2\lambda\right\}. \tag{41}$$

By definition axial strain ϵ_1 = E ÷ length of the sample or

$$\epsilon_1 = \frac{E}{(n-1)\, d \cos\lambda} \tag{42}$$

which solved for E and substituted in Equation (40) gives

$$\frac{dv}{v_o} = \frac{4}{n-1}\left\{\frac{1}{\sin 2\lambda}\sin(2\lambda + \arctan\left[\frac{2}{(n-1)\,\epsilon_1 \sin 2\lambda} - \cot 2\lambda\right]^{-1}) - 1\right\} \tag{43}$$

Appendix B

Data Plots

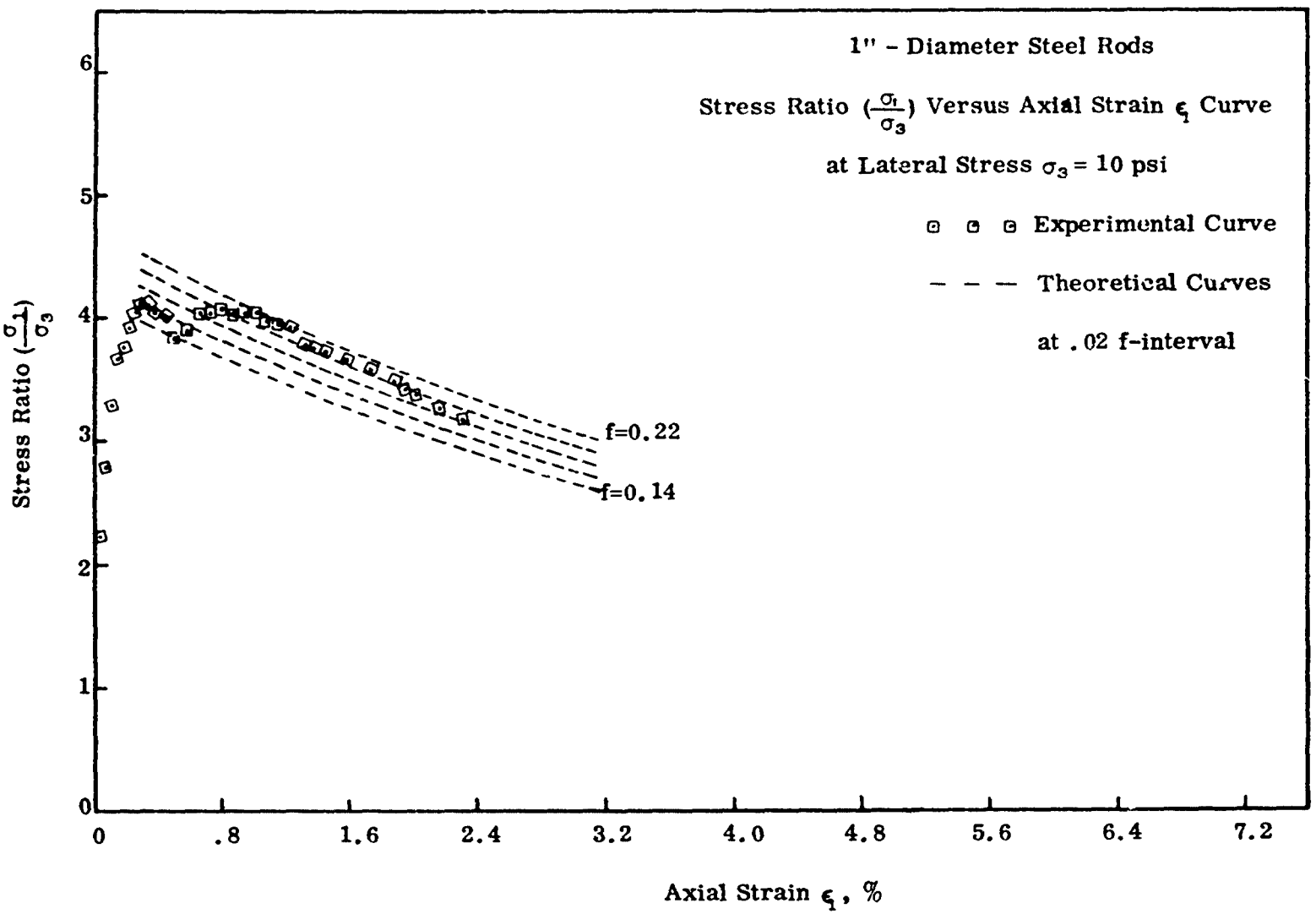
1" - Diameter Steel Rods
Stress Ratio $(\frac{\sigma_1}{\sigma_3})$ Versus Axial Strain ϵ_1 Curve
at Lateral Stress σ_3 = 10 psi
Experimental Curve
Theoretical Curves
at .02 f-interval
f=0.22
f=0.14
Stress Ratio $(\frac{\sigma_1}{\sigma_3})$
Axial Strain ϵ_1, %
0
1
2
3
4
5
6
0
.8
1.6
2.4
3.2
4.0
4.8
5.6
6.4
7.2

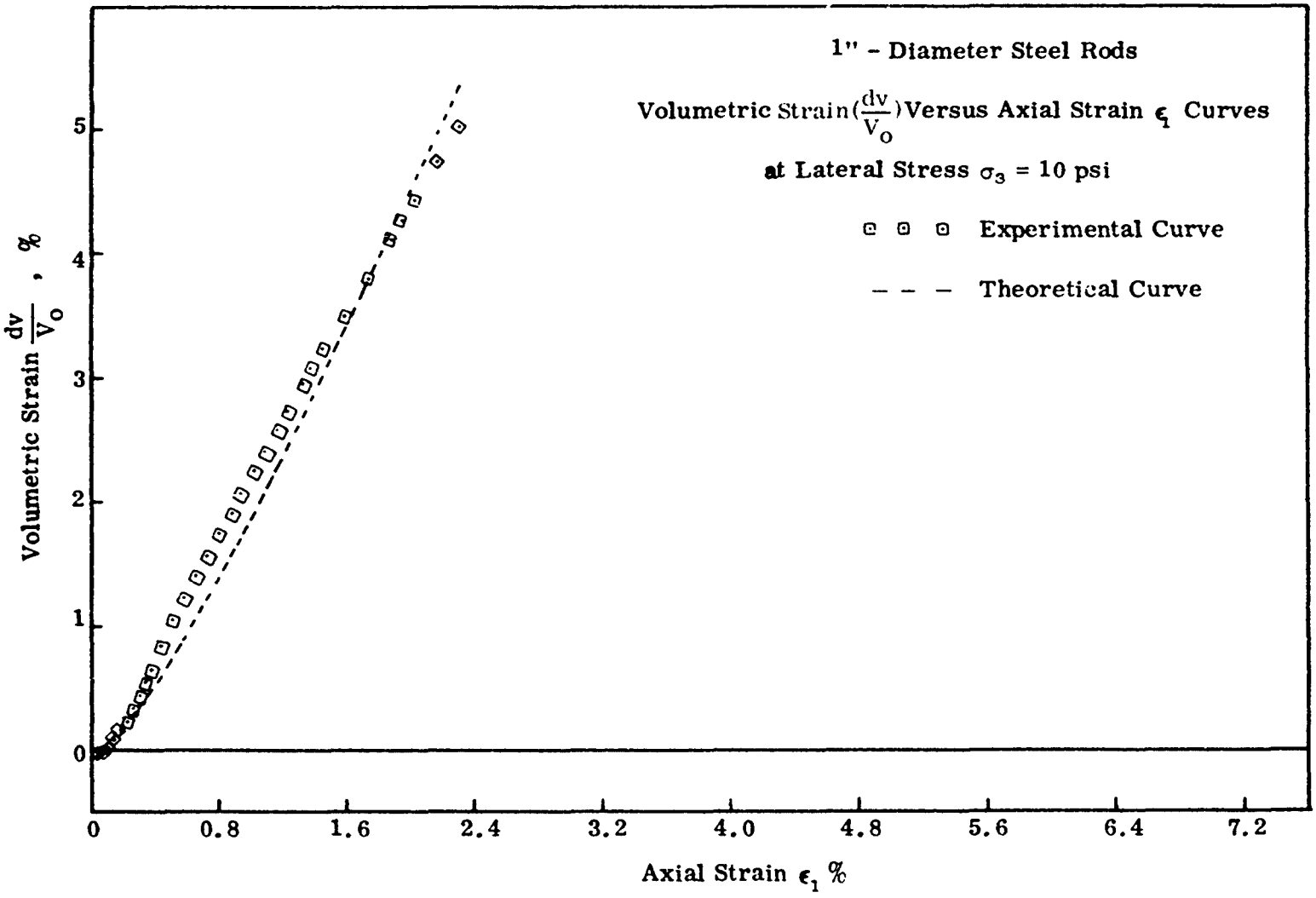
1" - Diameter Steel Rods
Volumetric Strain (dv/Vo) Versus Axial Strain ε1 Curves
at Lateral Stress σ3 = 10 psi
Experimental Curve
Theoretical Curve
Volumetric Strain dv/Vo , %
Axial Strain ε1 %
0
1
2
3
4
5
0
0.8
1.6
2.4
3.2
4.0
4.8
5.6
6.4
7.2

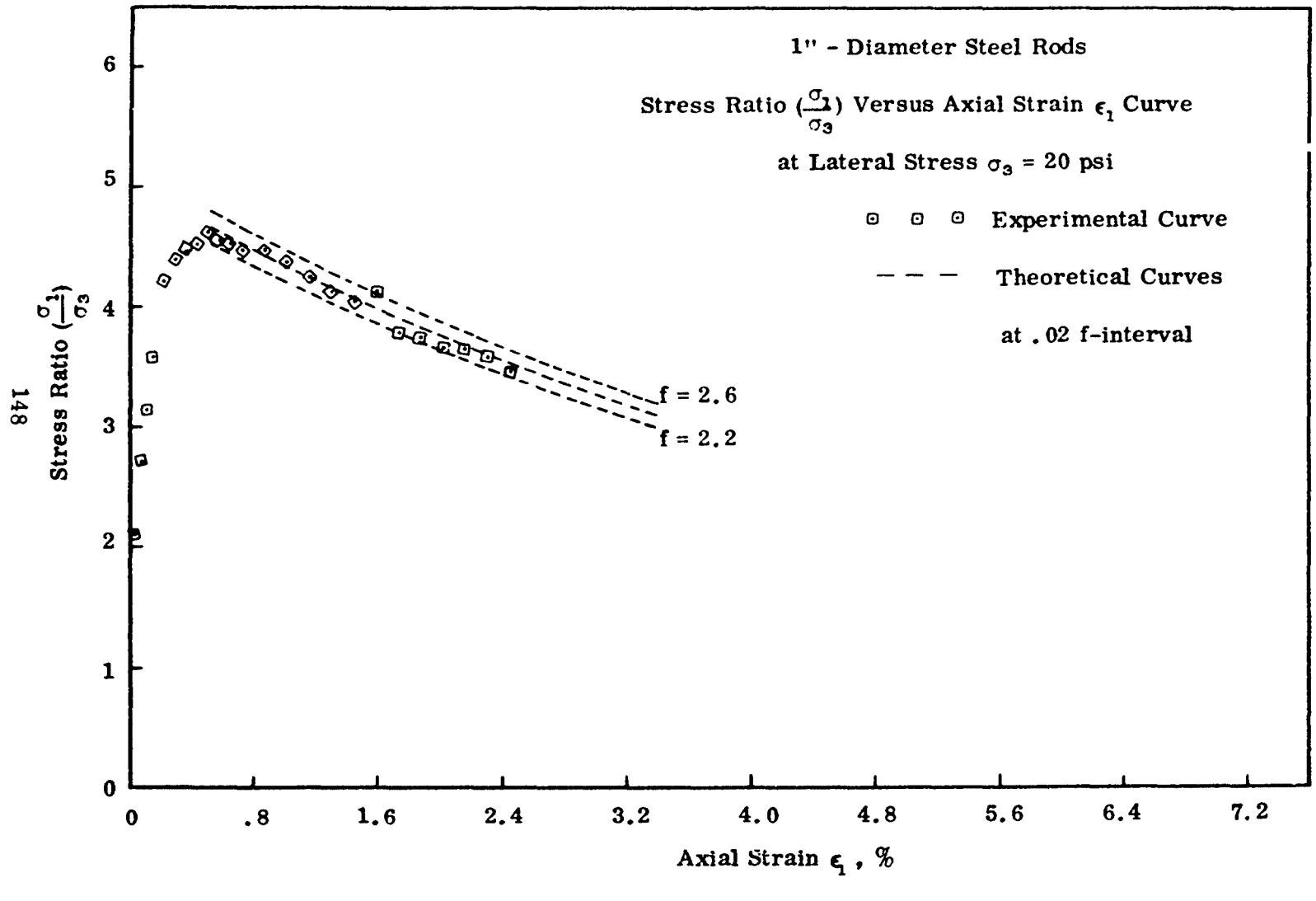
1" - Diameter Steel Rods
Stress Ratio ($\frac{\sigma_1}{\sigma_3}$) Versus Axial Strain ϵ_1 Curve
at Lateral Stress σ_3 = 20 psi
Experimental Curve
Theoretical Curves
at .02 f-interval
f = 2.6
f = 2.2
Stress Ratio ($\frac{\sigma_1}{\sigma_3}$)
Axial Strain ϵ_1, %
0
1
2
3
4
5
6
.8
1.6
2.4
3.2
4.0
4.8
5.6
6.4
7.2

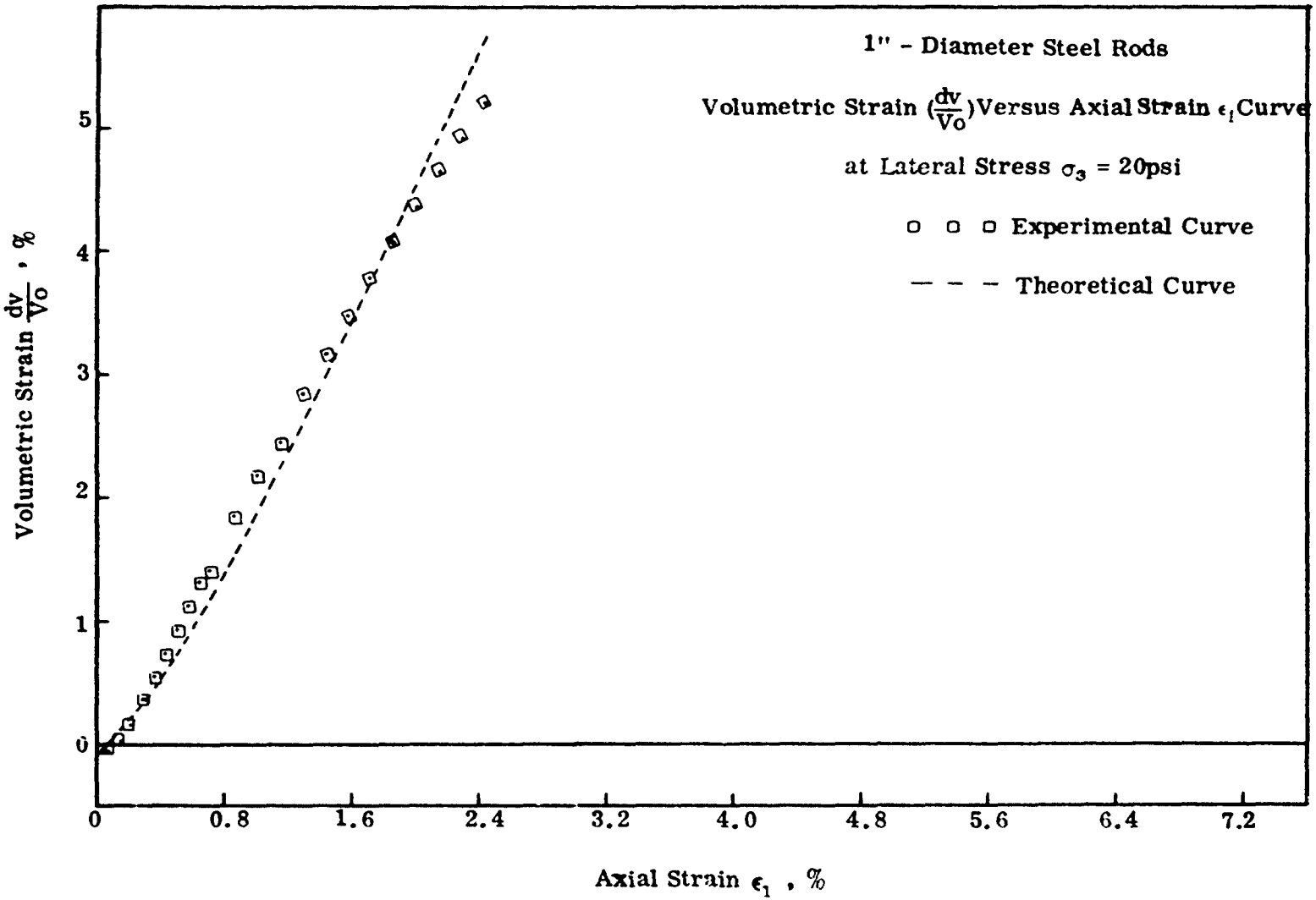
1" - Diameter Steel Rods
Volumetric Strain (dv/Vo) Versus Axial Strain ε1 Curve
at Lateral Stress σ3 = 20psi
Experimental Curve
Theoretical Curve
Volumetric Strain dv/Vo , %
Axial Strain ε1 , %
0
1
2
3
4
5
0
0.8
1.6
2.4
3.2
4.0
4.8
5.6
6.4
7.2

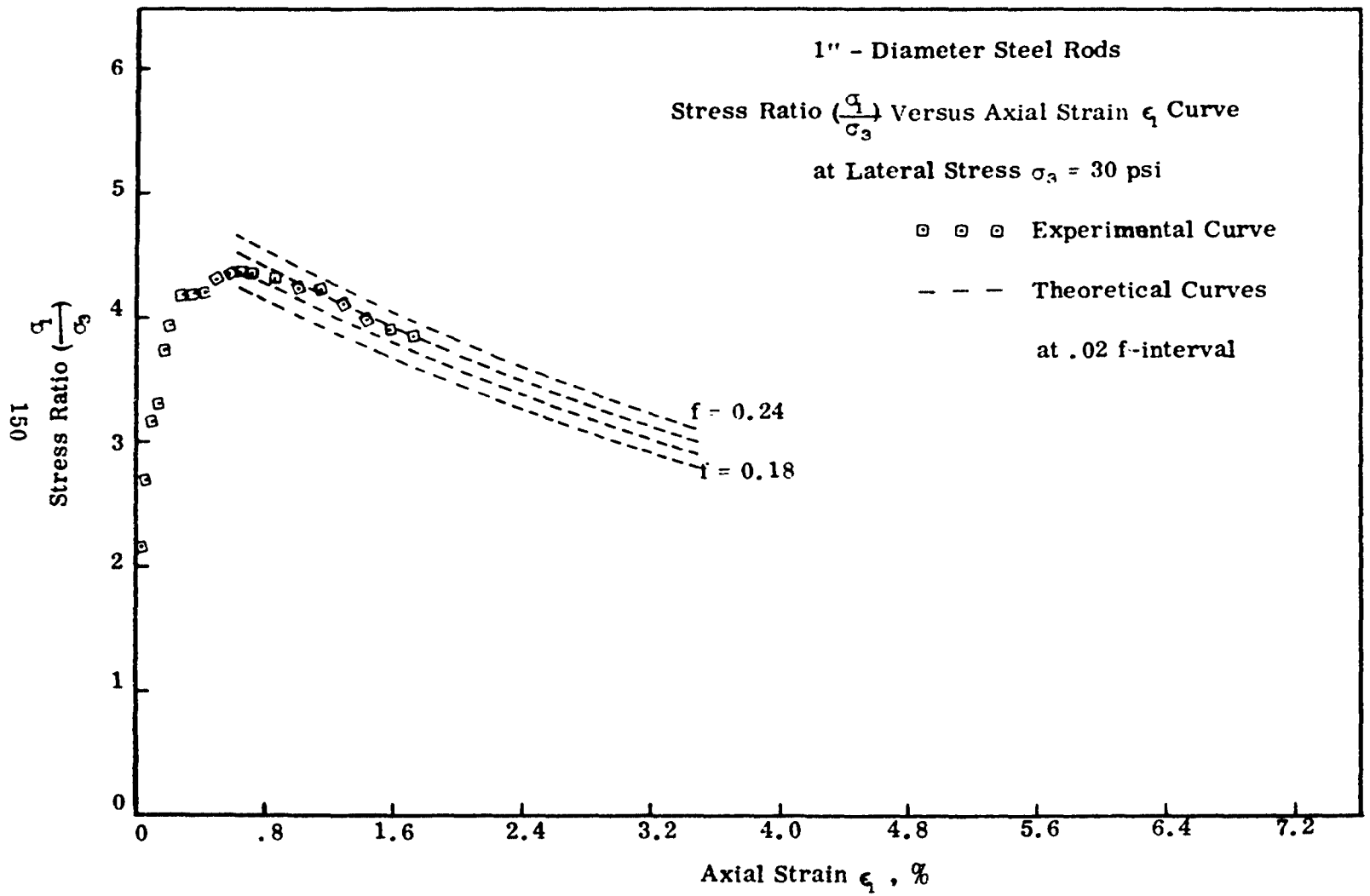
1" - Diameter Steel Rods
Stress Ratio $(\frac{\sigma_1}{\sigma_3})$ Versus Axial Strain ϵ_1 Curve
at Lateral Stress σ_3 = 30 psi
Experimental Curve
Theoretical Curves
at .02 f-interval
f = 0.24
f = 0.18
Stress Ratio $(\frac{\sigma_1}{\sigma_3})$
Axial Strain ϵ_1 , %
0
1
2
3
4
5
6
0
.8
1.6
2.4
3.2
4.0
4.8
5.6
6.4
7.2

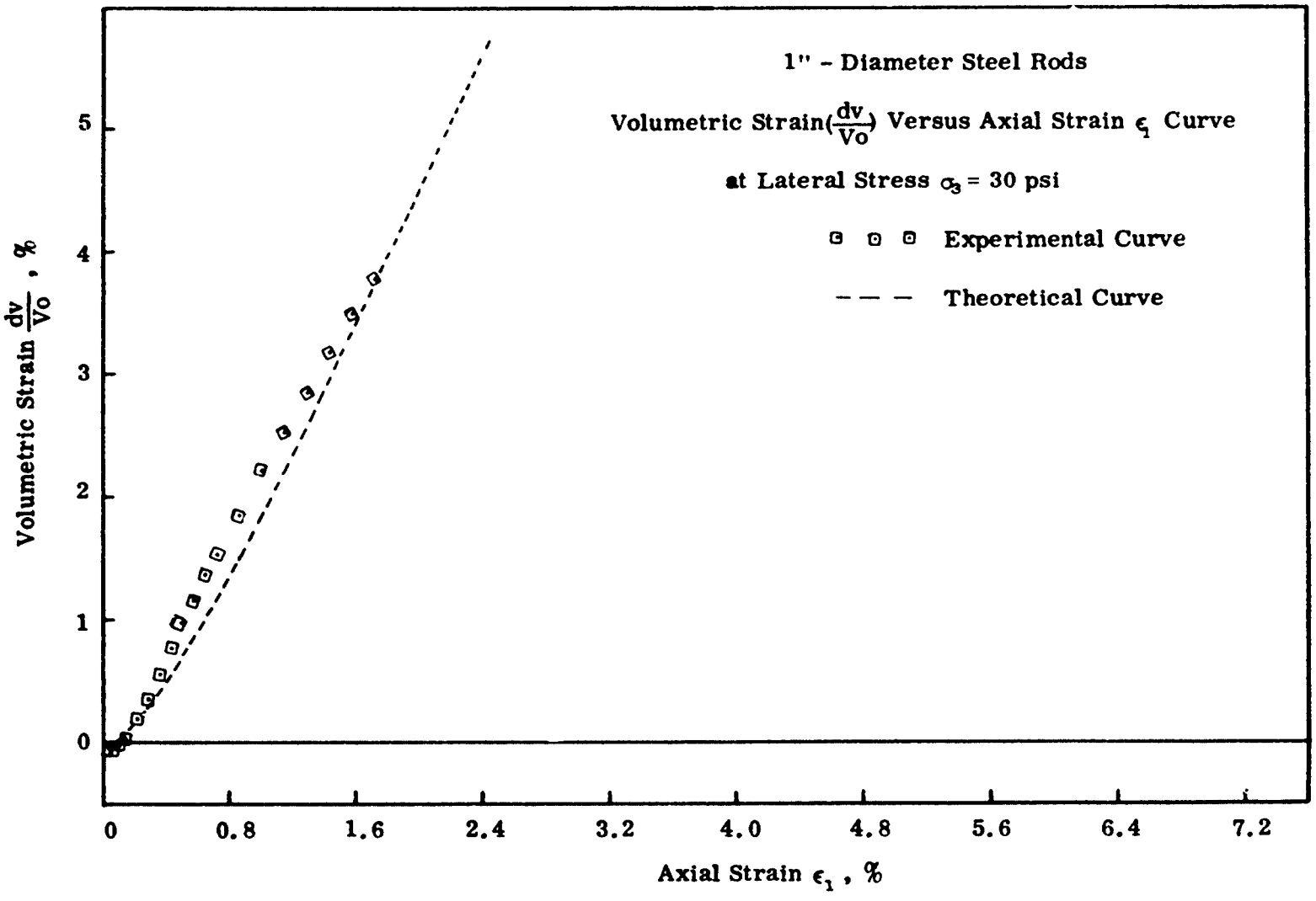
1" - Diameter Steel Rods
Volumetric Strain(dv/Vo) Versus Axial Strain ε1 Curve
at Lateral Stress σ3 = 30 psi
Experimental Curve
Theoretical Curve
Volumetric Strain dv/Vo , %
Axial Strain ε1 , %
0
1
2
3
4
5
0
0.8
1.6
2.4
3.2
4.0
4.8
5.6
6.4
7.2

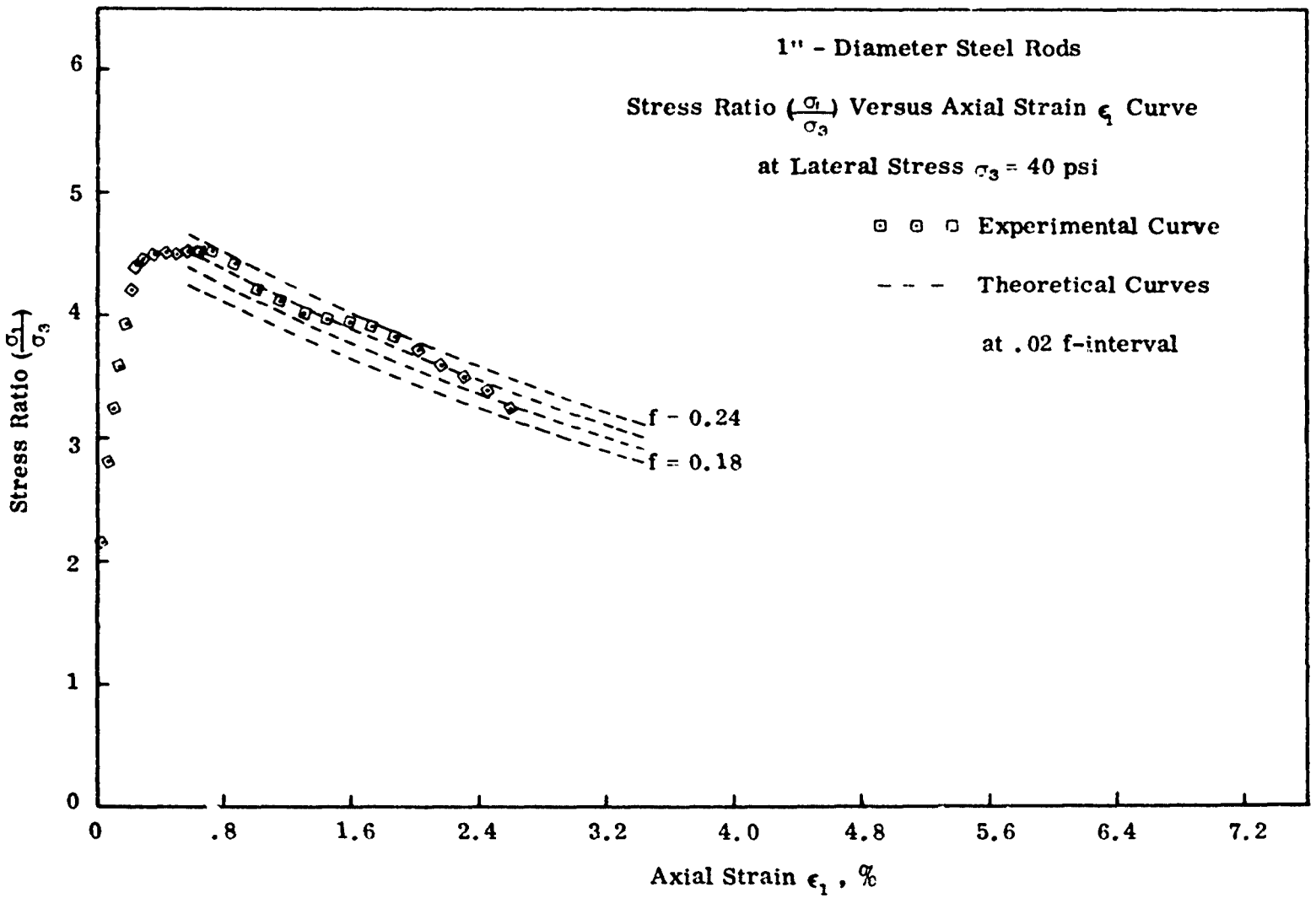
1" - Diameter Steel Rods
Stress Ratio $(\frac{\sigma_1}{\sigma_3})$ Versus Axial Strain ϵ_1 Curve
at Lateral Stress σ_3 = 40 psi
Experimental Curve
Theoretical Curves
at .02 f-interval
f - 0.24
f = 0.18
Stress Ratio $(\frac{\sigma_1}{\sigma_3})$
Axial Strain ϵ_1 , %
0
1
2
3
4
5
6
.8
1.6
2.4
3.2
4.0
4.8
5.6
6.4
7.2

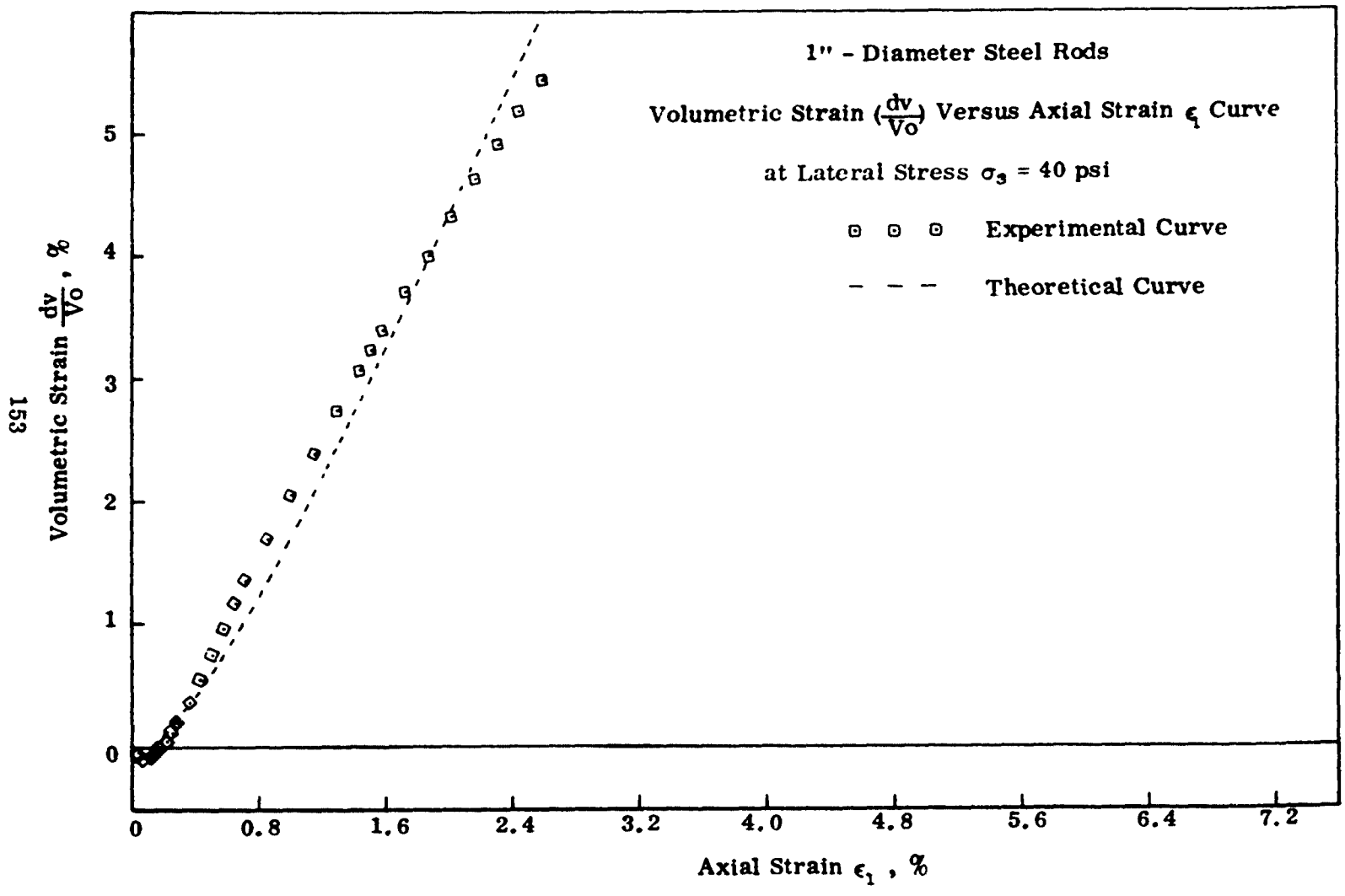
1" - Diameter Steel Rods
Volumetric Strain (dv/Vo) Versus Axial Strain ε1 Curve
at Lateral Stress σ3 = 40 psi
Experimental Curve
Theoretical Curve
Volumetric Strain dv/Vo , %
Axial Strain ε1 , %
0
1
2
3
4
5
0
0.8
1.6
2.4
3.2
4.0
4.8
5.6
6.4
7.2

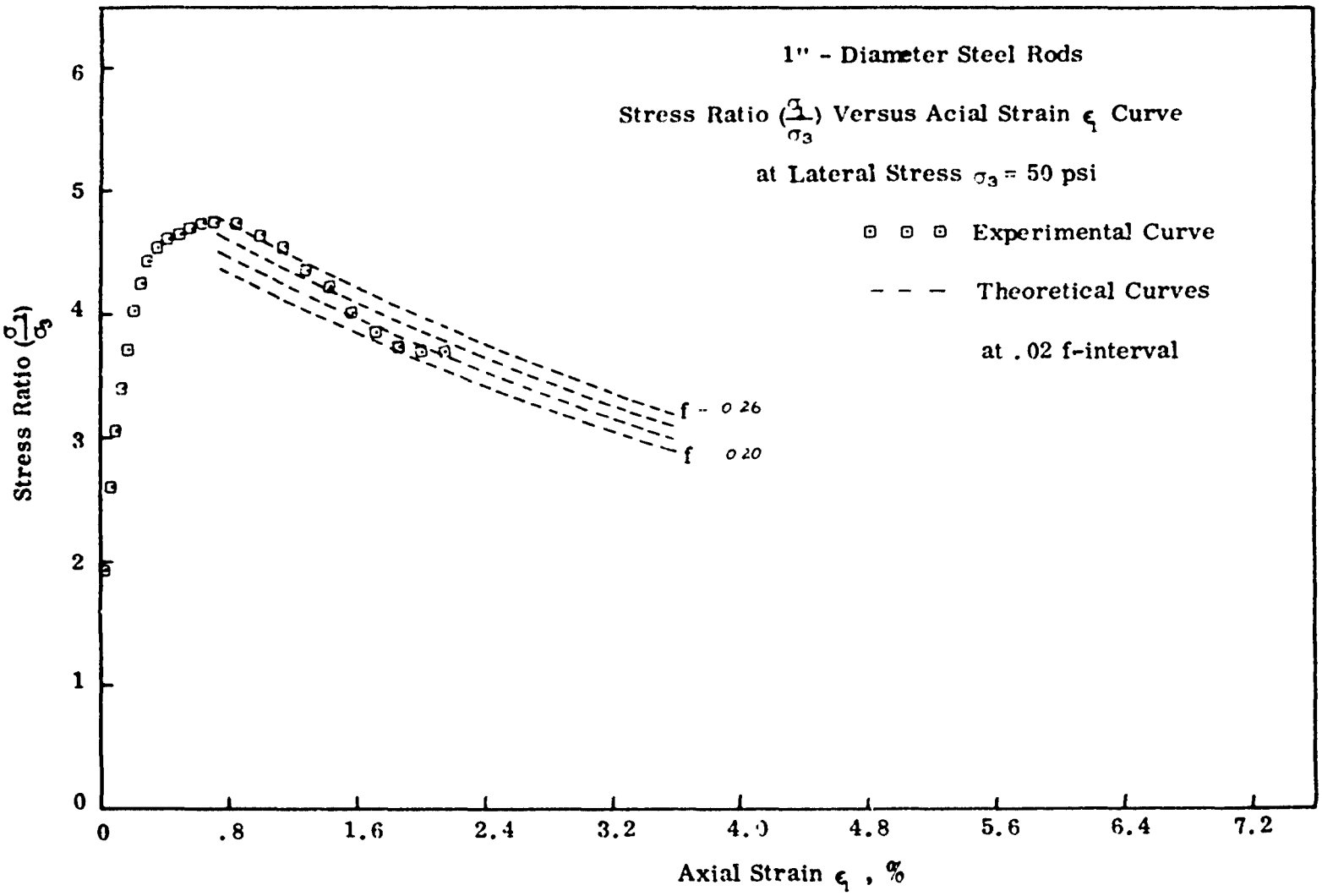
1" - Diameter Steel Rods
Stress Ratio $(\frac{\sigma_1}{\sigma_3})$ Versus Acial Strain ϵ_1 Curve
at Lateral Stress σ_3 = 50 psi
Experimental Curve
Theoretical Curves
at .02 f-interval
f = 0.26
f = 0.20
Stress Ratio $(\frac{\sigma_1}{\sigma_3})$
Axial Strain ϵ_1 , %
0
1
2
3
4
5
6
0
.8
1.6
2.4
3.2
4.0
4.8
5.6
6.4
7.2

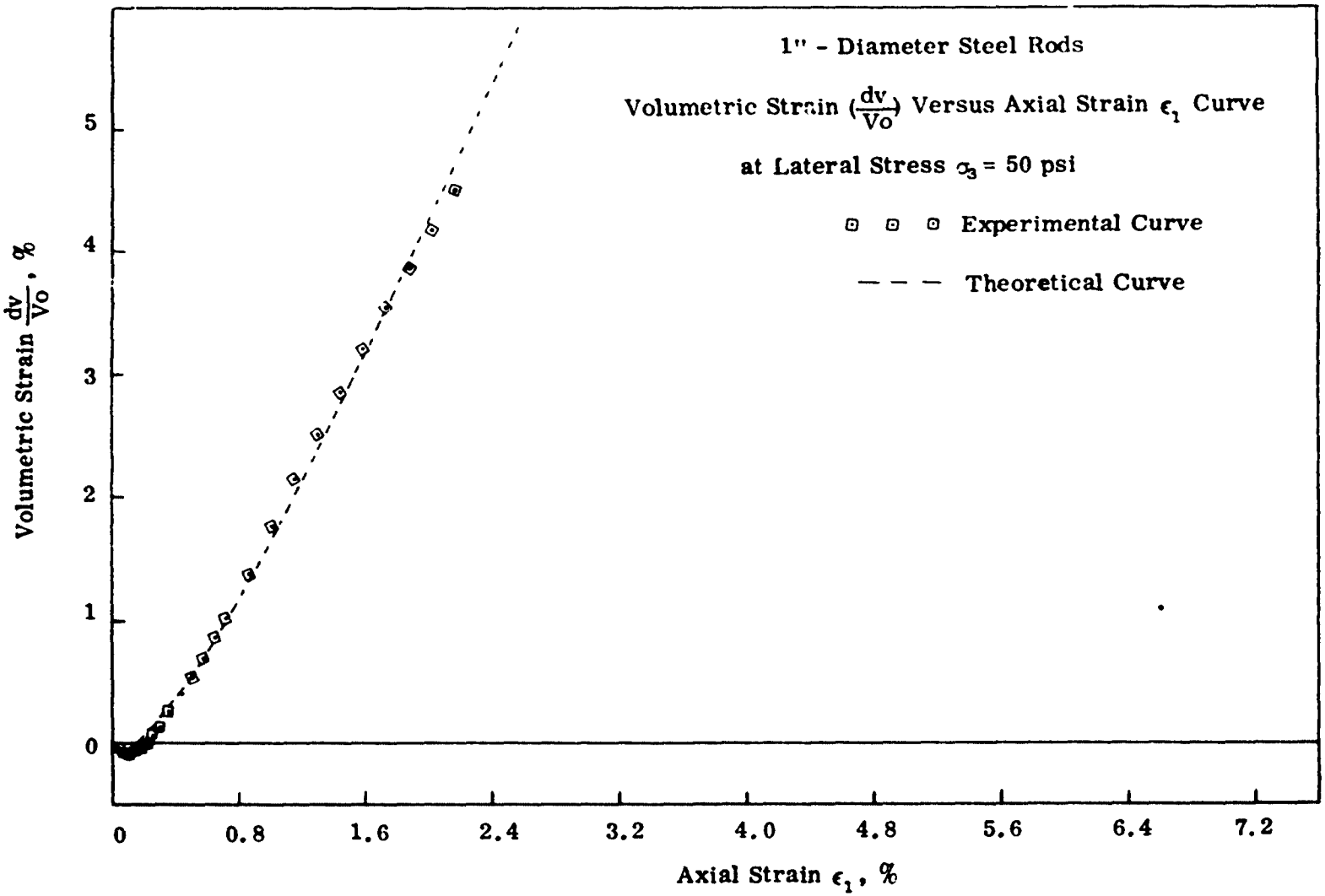
1" - Diameter Steel Rods
Volumetric Strain (dv/Vo) Versus Axial Strain ε1 Curve
at Lateral Stress σ3 = 50 psi
Experimental Curve
Theoretical Curve
Volumetric Strain dv/Vo, %
Axial Strain ε1, %
0
1
2
3
4
5
0
0.8
1.6
2.4
3.2
4.0
4.8
5.6
6.4
7.2

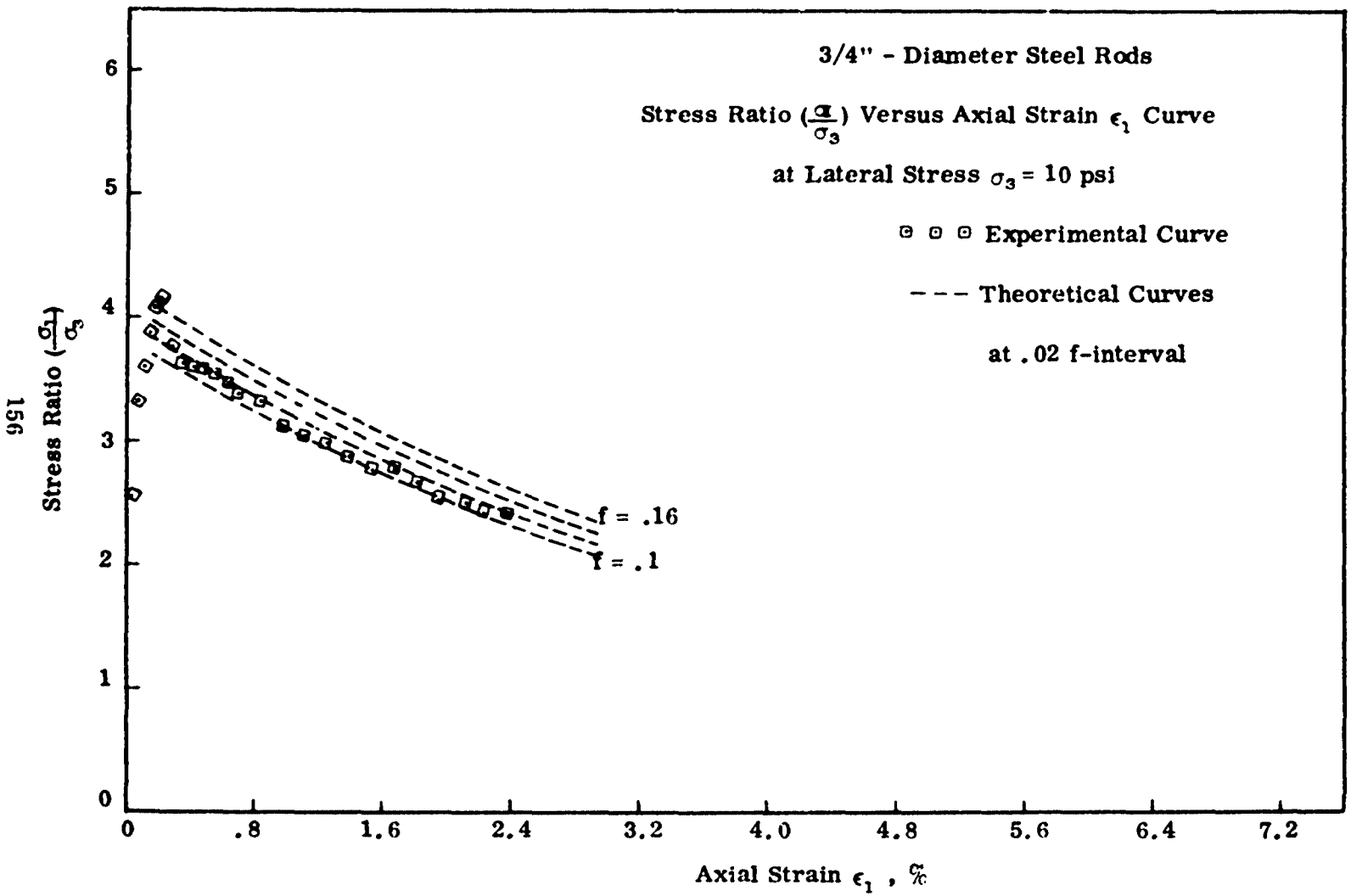
3/4" - Diameter Steel Rods
Stress Ratio ($\frac{\sigma_1}{\sigma_3}$) Versus Axial Strain ϵ_1 Curve
at Lateral Stress σ_3 = 10 psi
Experimental Curve
Theoretical Curves
at .02 f-interval
f = .16
f = .1
Stress Ratio ($\frac{\sigma_1}{\sigma_3}$)
Axial Strain ϵ_1 , %
0
1
2
3
4
5
6
0
.8
1.6
2.4
3.2
4.0
4.8
5.6
6.4
7.2

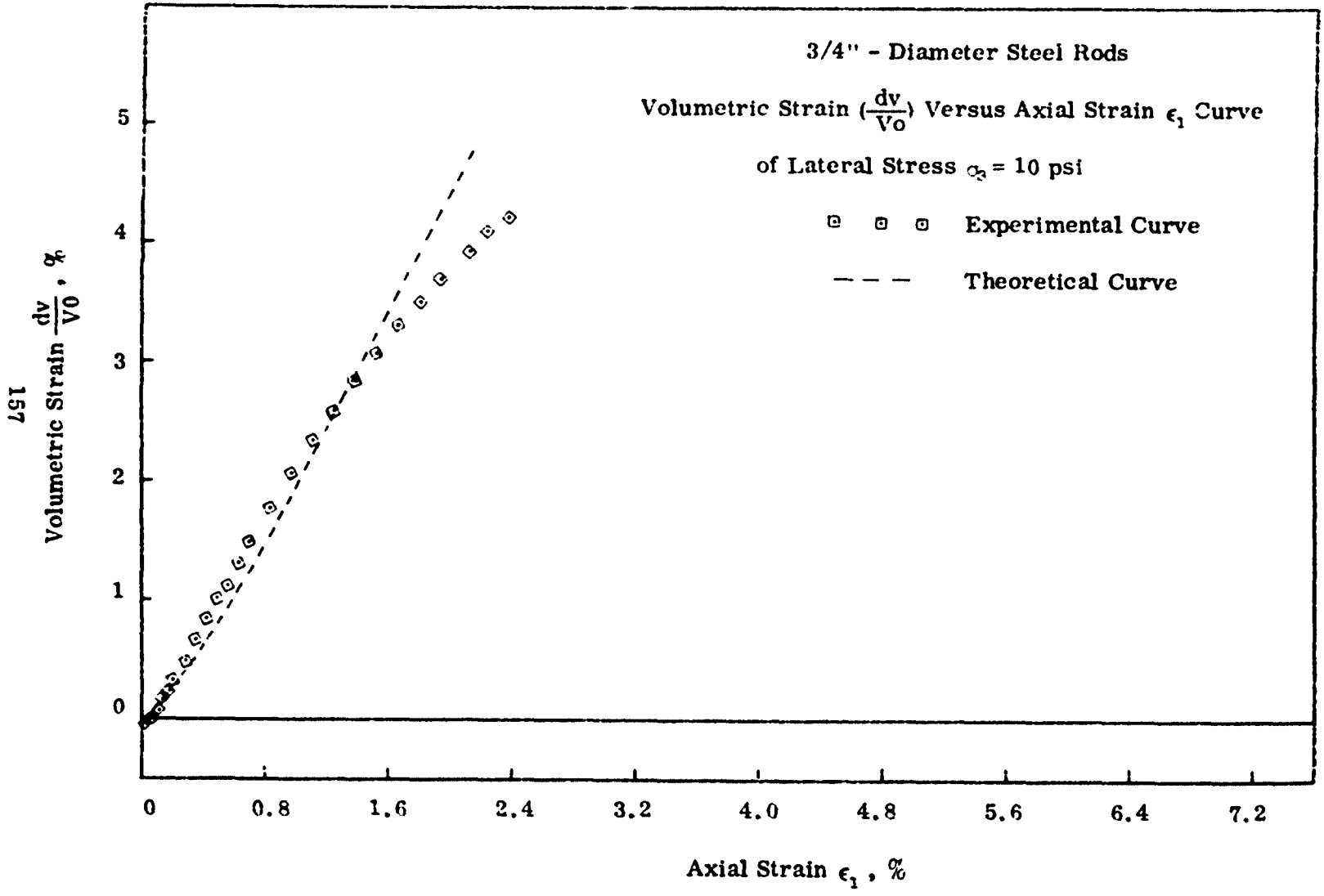
3/4" - Diameter Steel Rods
Volumetric Strain (dv/Vo) Versus Axial Strain ε1 Curve
of Lateral Stress σ3 = 10 psi
Experimental Curve
Theoretical Curve
Volumetric Strain dv/V0 , %
Axial Strain ε1 , %
0
1
2
3
4
5
0
0.8
1.6
2.4
3.2
4.0
4.8
5.6
6.4
7.2

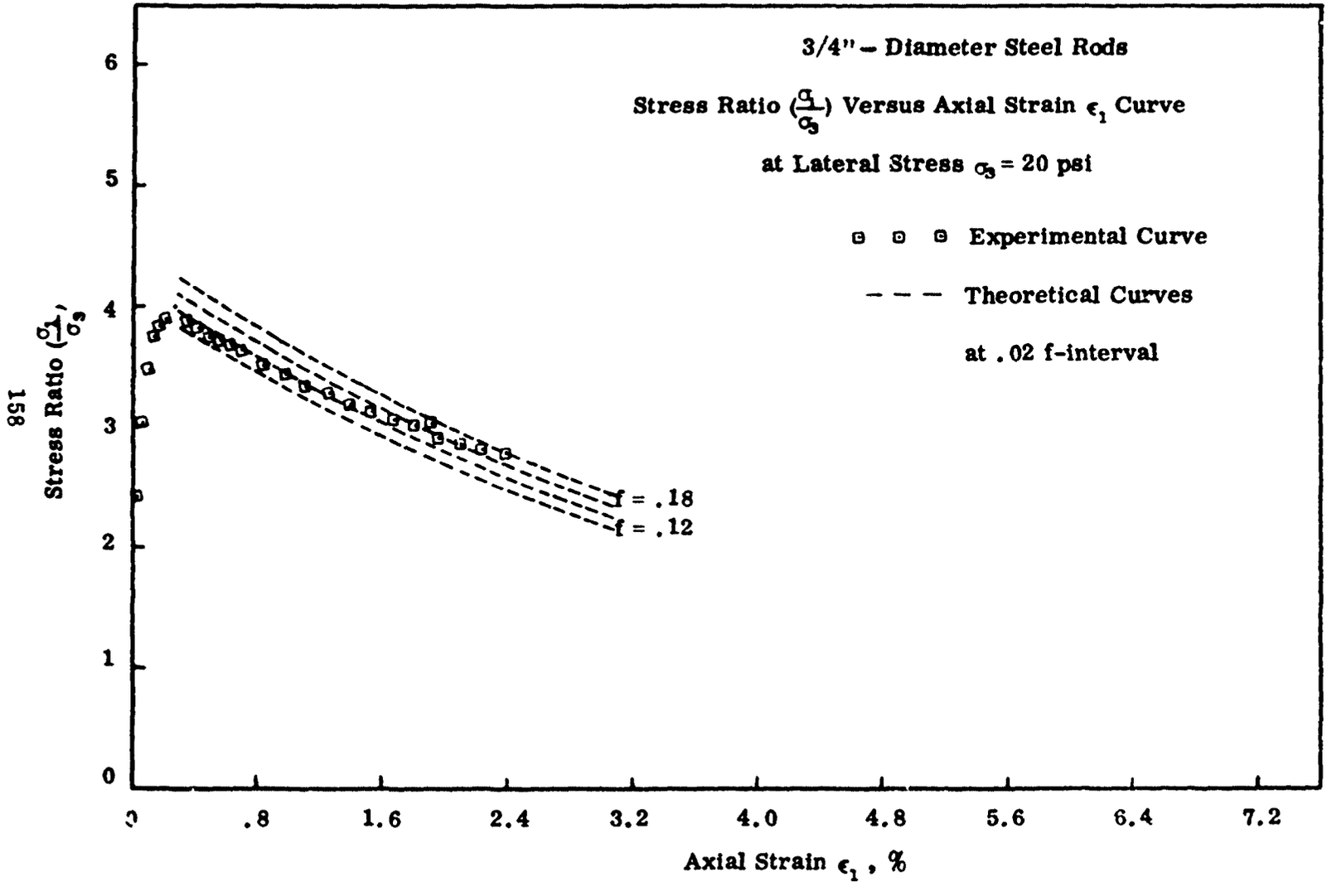
3/4" – Diameter Steel Rods
Stress Ratio ($\frac{\sigma_1}{\sigma_3}$) Versus Axial Strain ϵ_1 Curve
at Lateral Stress σ_3 = 20 psi
Experimental Curve
Theoretical Curves
at .02 f-interval
f = .18
f = .12
Stress Ratio ($\frac{\sigma_1}{\sigma_3}$)
Axial Strain ϵ_1, %
0
1
2
3
4
5
6
.8
1.6
2.4
3.2
4.0
4.8
5.6
6.4
7.2

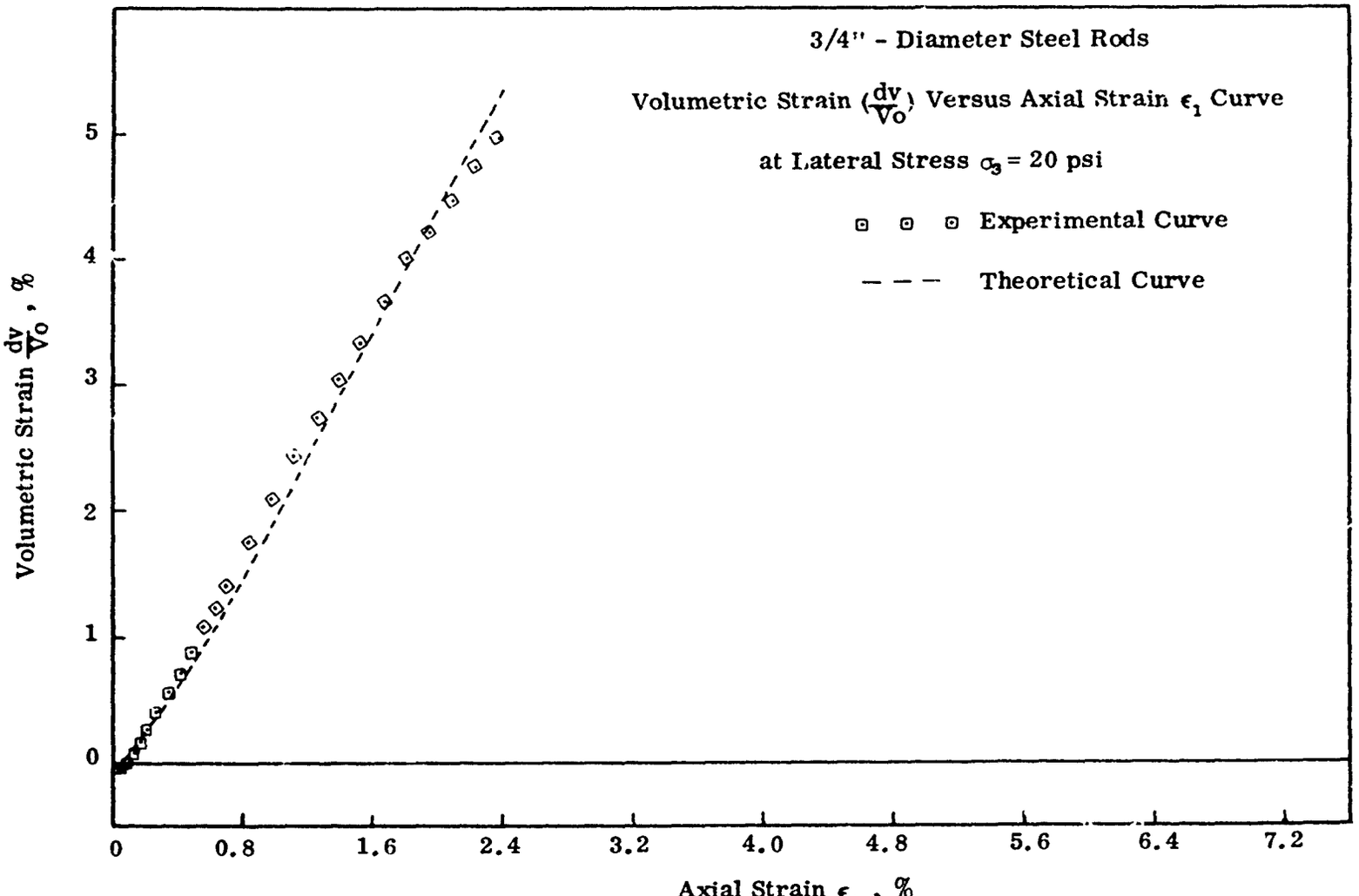
3/4" - Diameter Steel Rods
Volumetric Strain (dv/Vo) Versus Axial Strain ε1 Curve
at Lateral Stress σ3 = 20 psi
Experimental Curve
Theoretical Curve
Volumetric Strain dv/Vo , %
Axial Strain ε1 , %
0
1
2
3
4
5
0
0.8
1.6
2.4
3.2
4.0
4.8
5.6
6.4
7.2

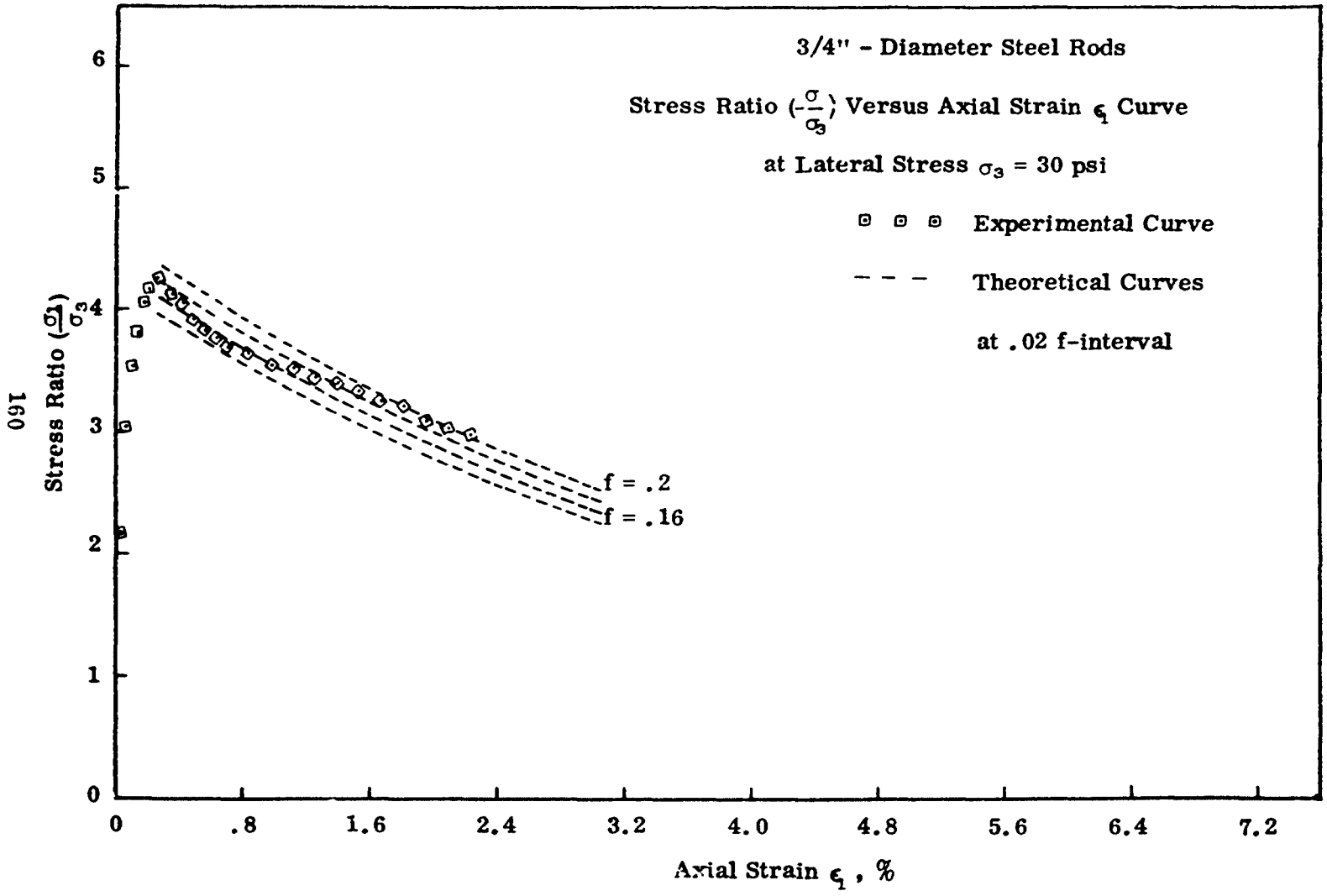
3/4" - Diameter Steel Rods
Stress Ratio $(\frac{\sigma}{\sigma_3})$ Versus Axial Strain ϵ_1 Curve
at Lateral Stress σ_3 = 30 psi
Experimental Curve
Theoretical Curves
at .02 f-interval
f = .2
f = .16
Stress Ratio $(\frac{\sigma_1}{\sigma_3})$
Axial Strain ϵ_1 , %
0
1
2
3
4
5
6
.8
1.6
2.4
3.2
4.0
4.8
5.6
6.4
7.2

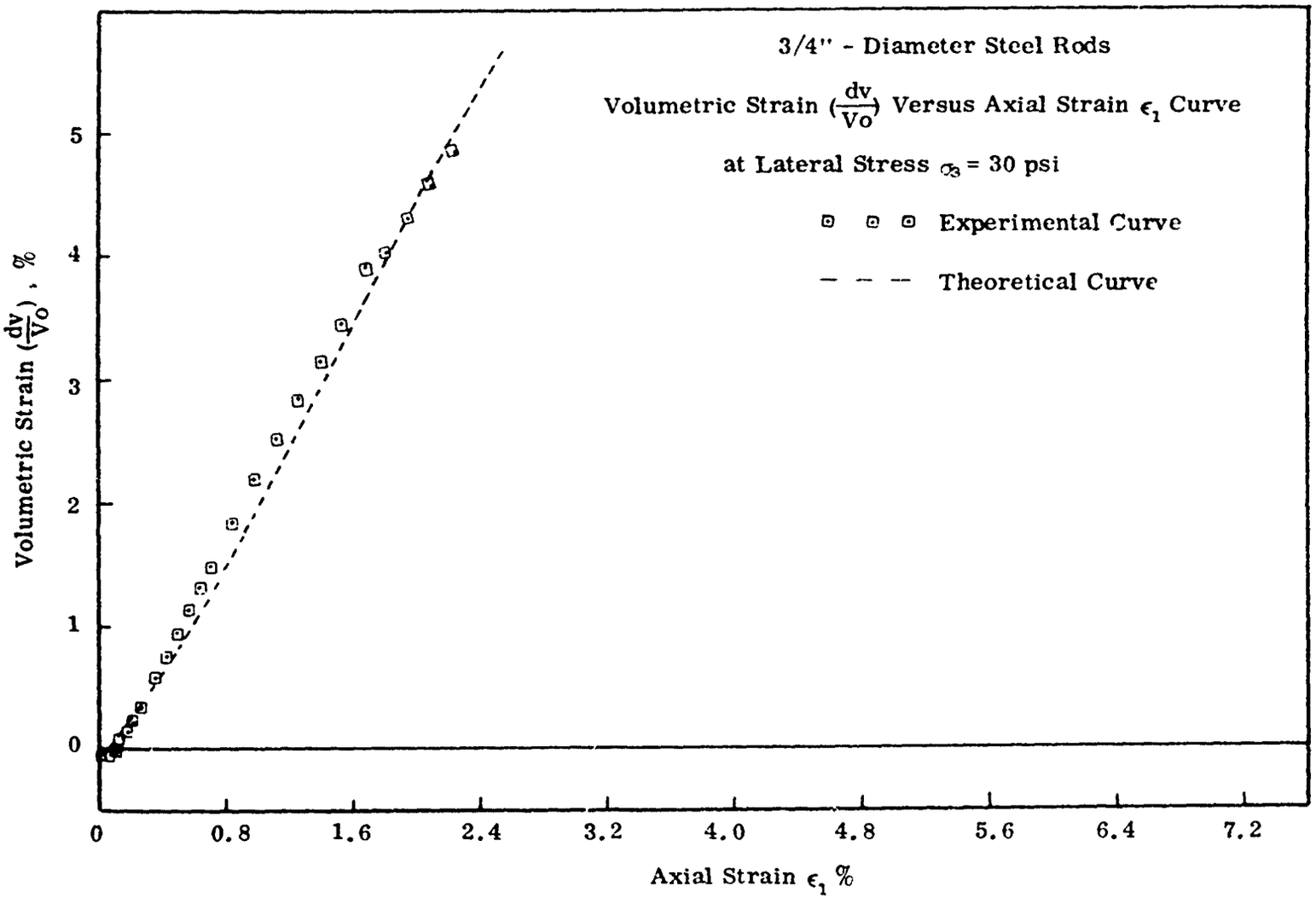
3/4" - Diameter Steel Rods
Volumetric Strain (dv/Vo) Versus Axial Strain ε1 Curve
at Lateral Stress σ3 = 30 psi
Experimental Curve
Theoretical Curve
Volumetric Strain (dv/Vo), %
Axial Strain ε1 %
0
1
2
3
4
5
0
0.8
1.6
2.4
3.2
4.0
4.8
5.6
6.4
7.2

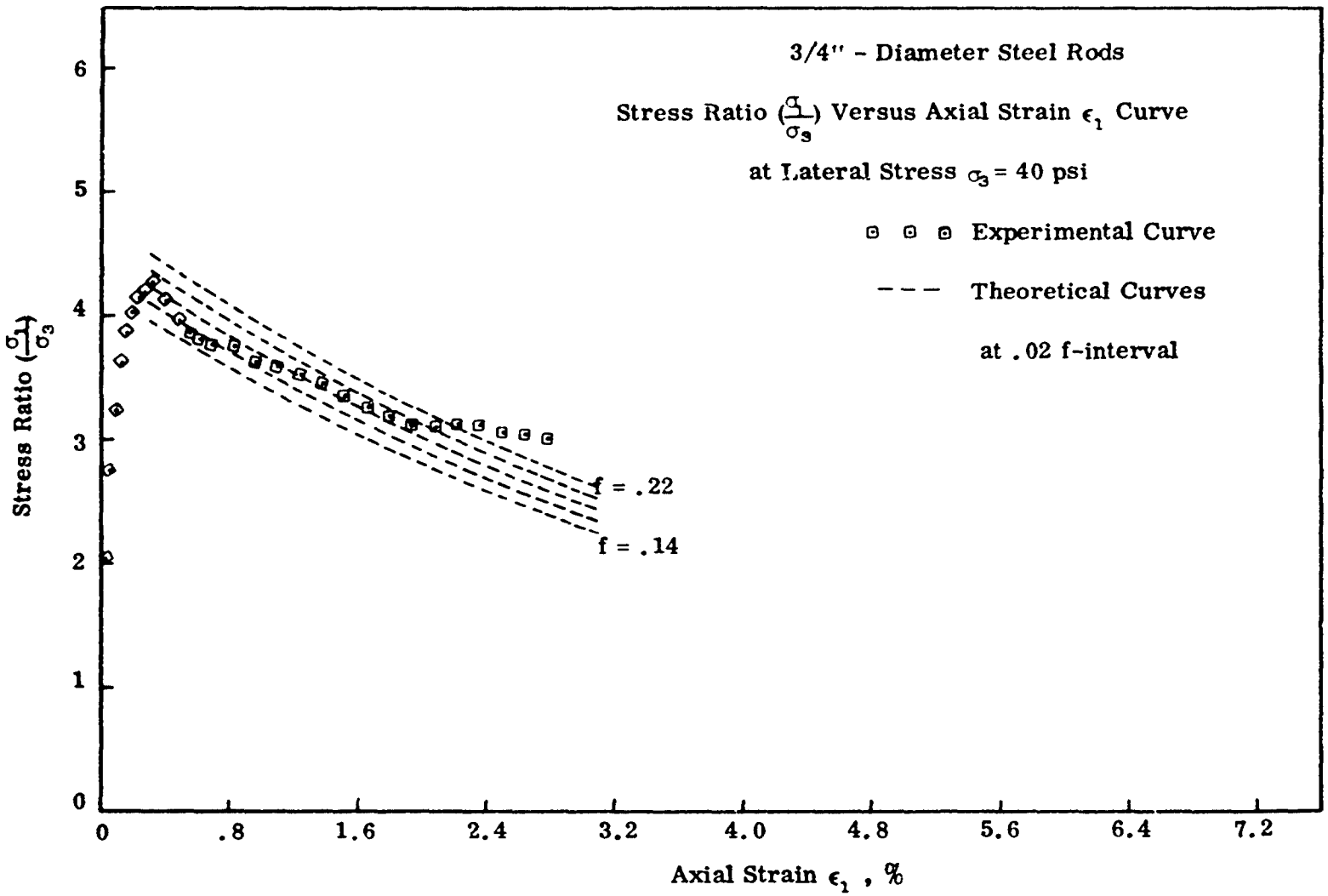
3/4" - Diameter Steel Rods
Stress Ratio $(\frac{\sigma_1}{\sigma_3})$ Versus Axial Strain ϵ_1 Curve
at Lateral Stress σ_3 = 40 psi
Experimental Curve
Theoretical Curves
at .02 f-interval
f = .22
f = .14
Stress Ratio $(\frac{\sigma_1}{\sigma_3})$
Axial Strain ϵ_1 , %
0
1
2
3
4
5
6
0
.8
1.6
2.4
3.2
4.0
4.8
5.6
6.4
7.2

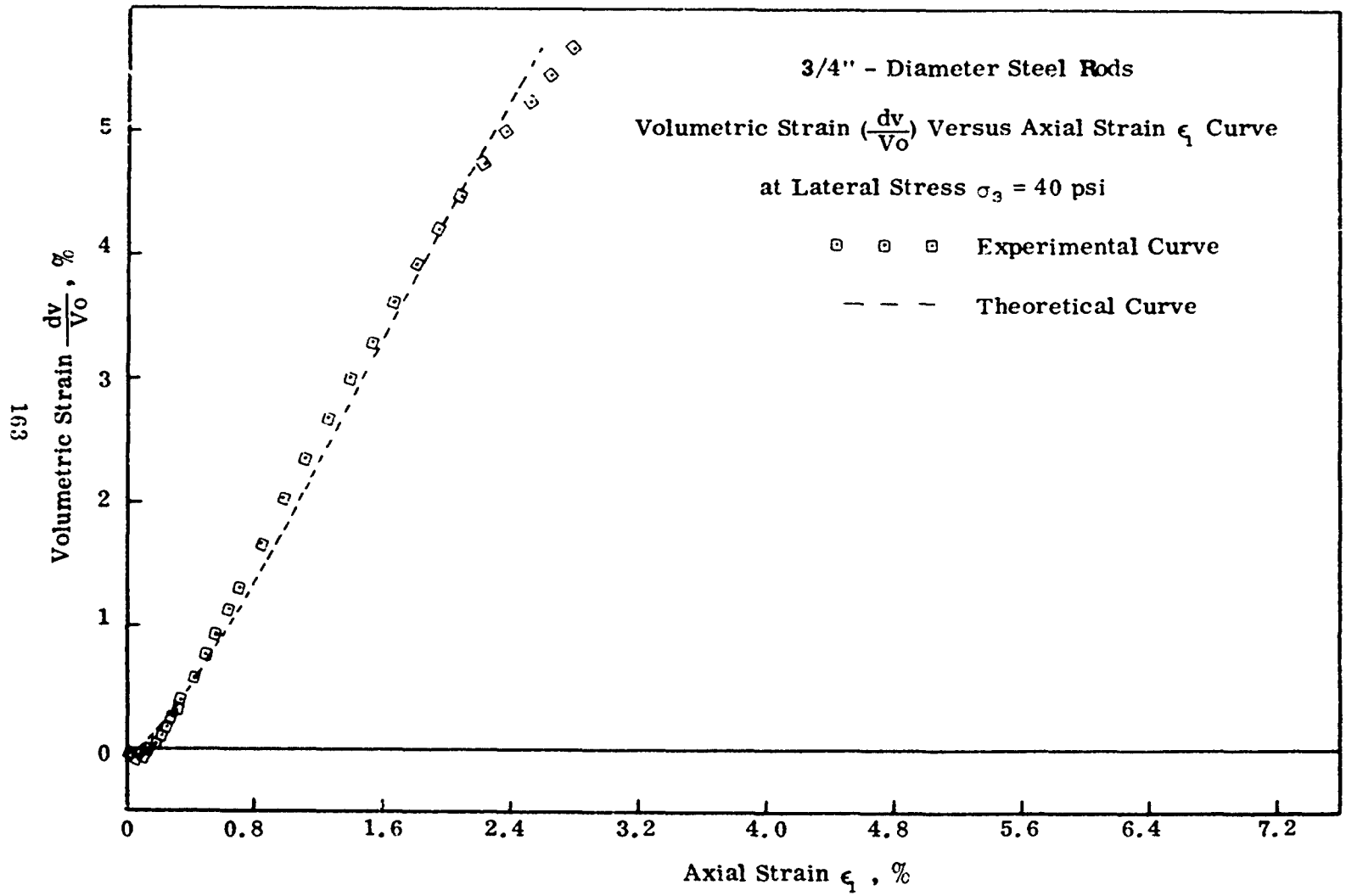
3/4" - Diameter Steel Rods
Volumetric Strain (dv/Vo) Versus Axial Strain ε1 Curve
at Lateral Stress σ3 = 40 psi
Experimental Curve
Theoretical Curve
Volumetric Strain dv/Vo, %
Axial Strain ε1, %
0
1
2
3
4
5
0
0.8
1.6
2.4
3.2
4.0
4.8
5.6
6.4
7.2

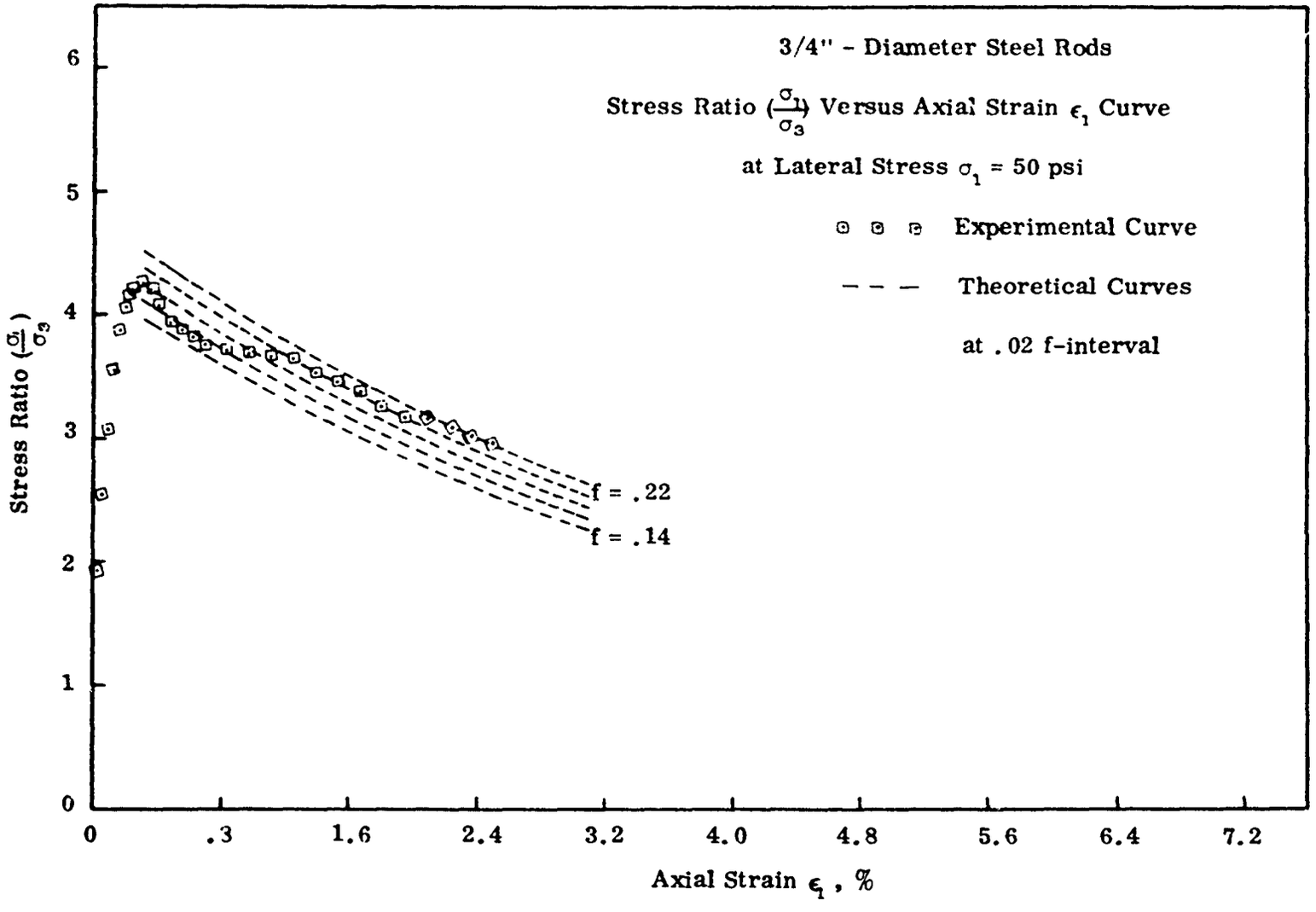
3/4" - Diameter Steel Rods
Stress Ratio $(\frac{\sigma_1}{\sigma_3})$ Versus Axial Strain ϵ_1 Curve
at Lateral Stress σ_1 = 50 psi
Experimental Curve
Theoretical Curves
at .02 f-interval
f = .22
f = .14
Stress Ratio $(\frac{\sigma_1}{\sigma_3})$
Axial Strain ϵ_1, %
0
1
2
3
4
5
6
0
.3
1.6
2.4
3.2
4.0
4.8
5.6
6.4
7.2

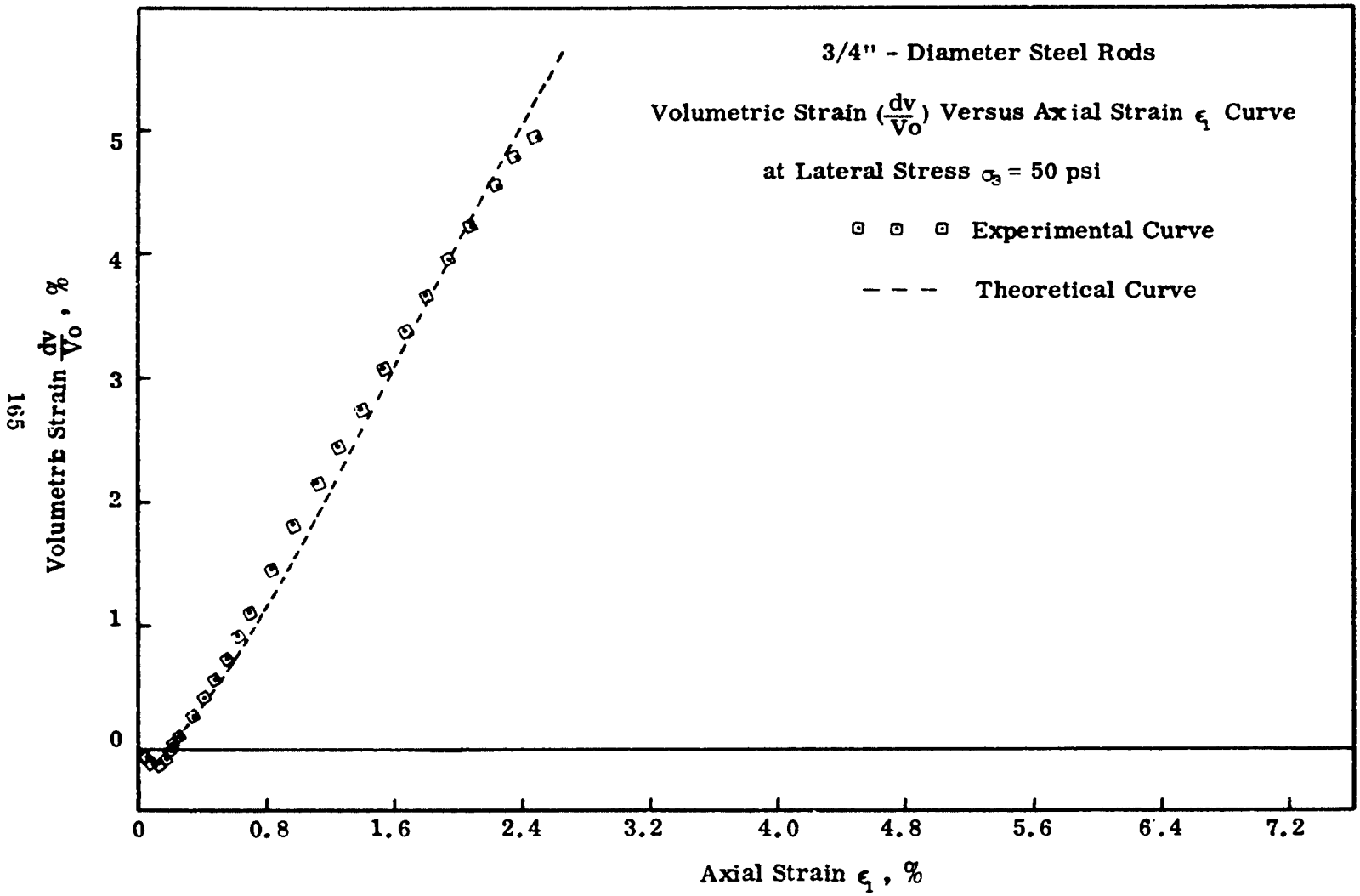
3/4" - Diameter Steel Rods
Volumetric Strain (dv/Vo) Versus Axial Strain ε1 Curve
at Lateral Stress σ3 = 50 psi
Experimental Curve
Theoretical Curve
Volumetric Strain dv/Vo , %
Axial Strain ε1 , %
0
1
2
3
4
5
0
0.8
1.6
2.4
3.2
4.0
4.8
5.6
6.4
7.2

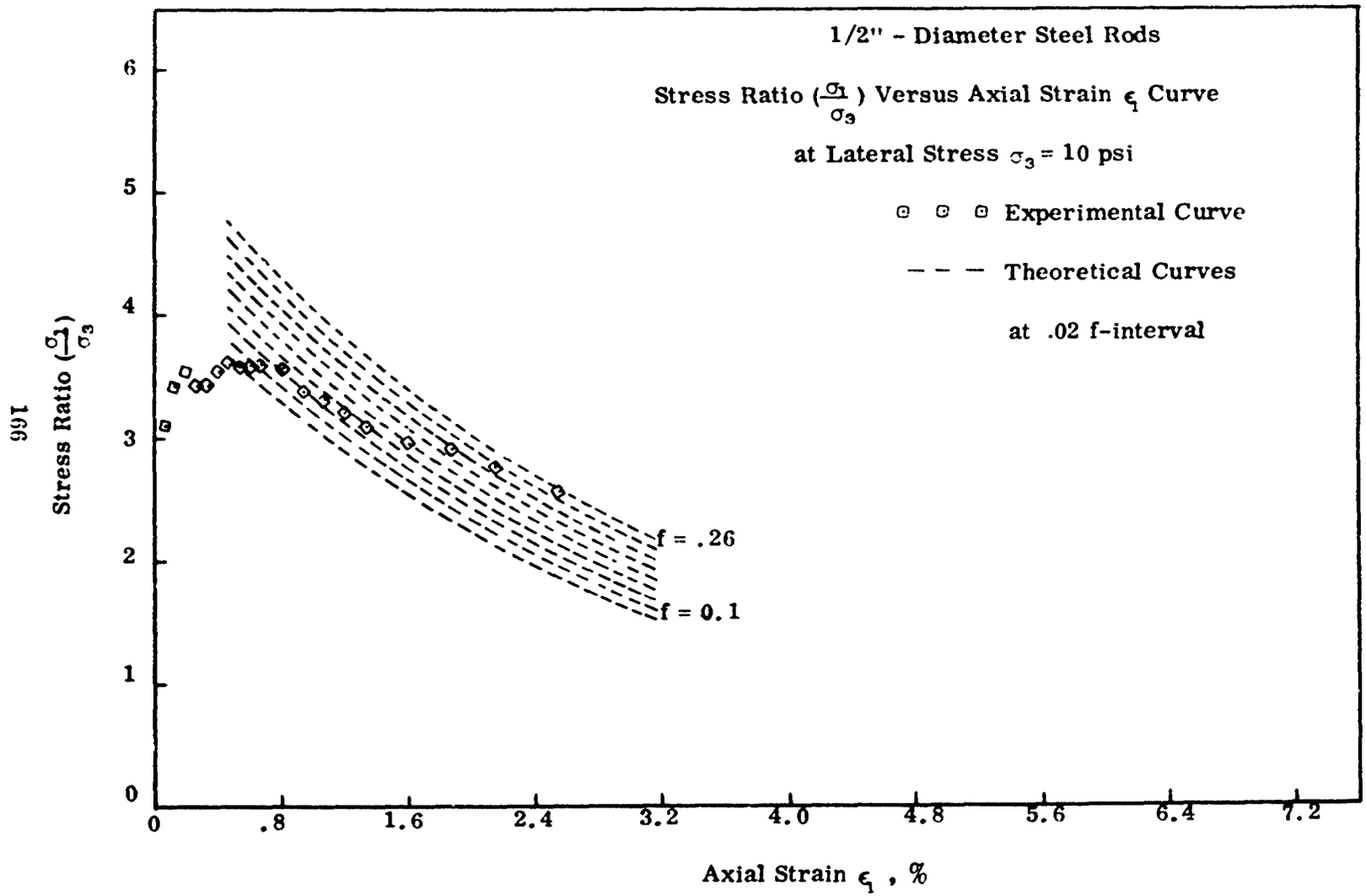
1/2" - Diameter Steel Rods
Stress Ratio ($\frac{\sigma_1}{\sigma_3}$) Versus Axial Strain ϵ_1 Curve
at Lateral Stress σ_3 = 10 psi
Experimental Curve
Theoretical Curves
at .02 f-interval
f = .26
f = 0.1
Stress Ratio ($\frac{\sigma_1}{\sigma_3}$)
Axial Strain ϵ_1 , %
0
1
2
3
4
5
6
0
.8
1.6
2.4
3.2
4.0
4.8
5.6
6.4
7.2

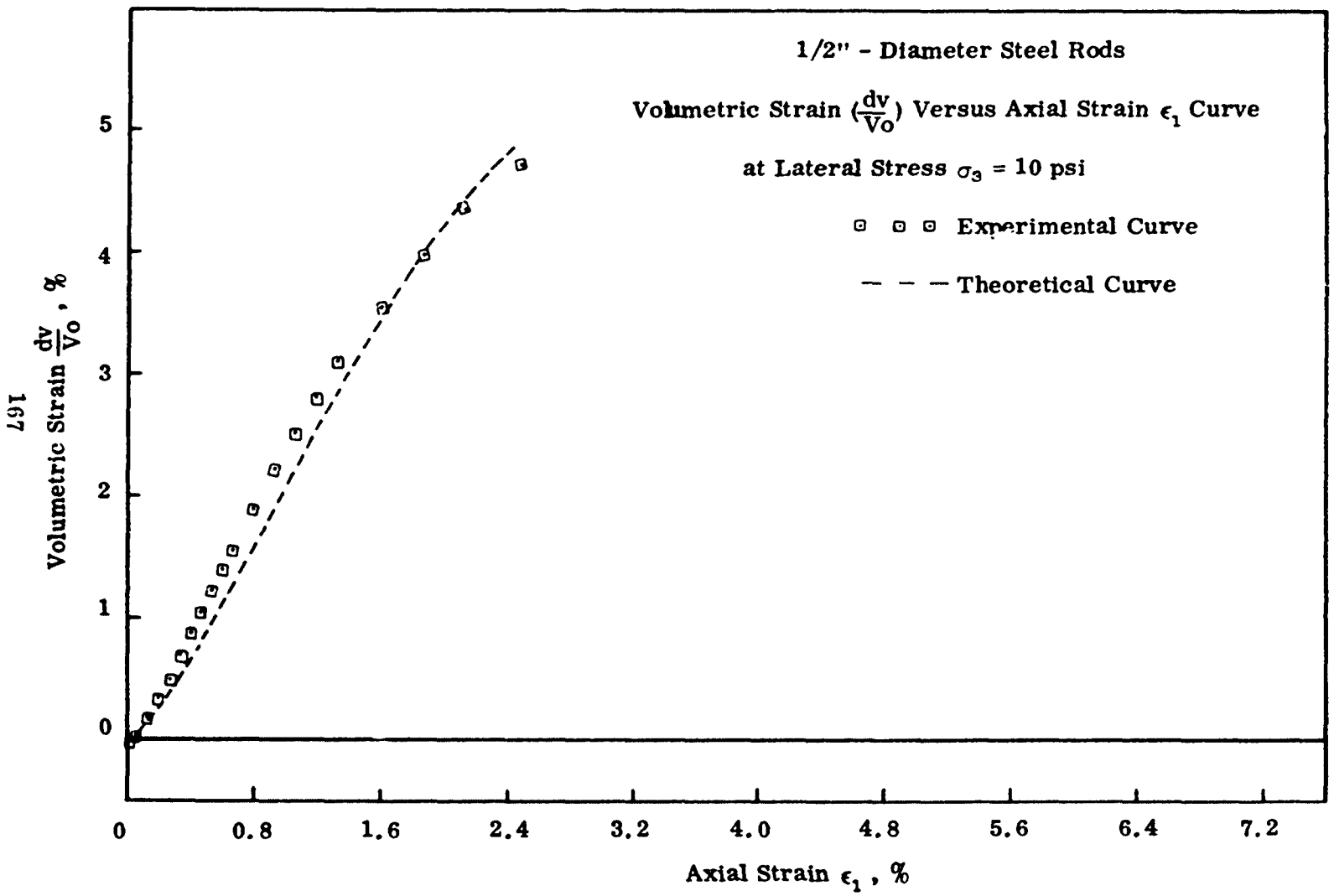
1/2" - Diameter Steel Rods
Volumetric Strain (dv/Vo) Versus Axial Strain ε1 Curve
at Lateral Stress σ3 = 10 psi
Experimental Curve
Theoretical Curve
Volumetric Strain dv/Vo , %
Axial Strain ε1 , %
0
1
2
3
4
5
0
0.8
1.6
2.4
3.2
4.0
4.8
5.6
6.4
7.2

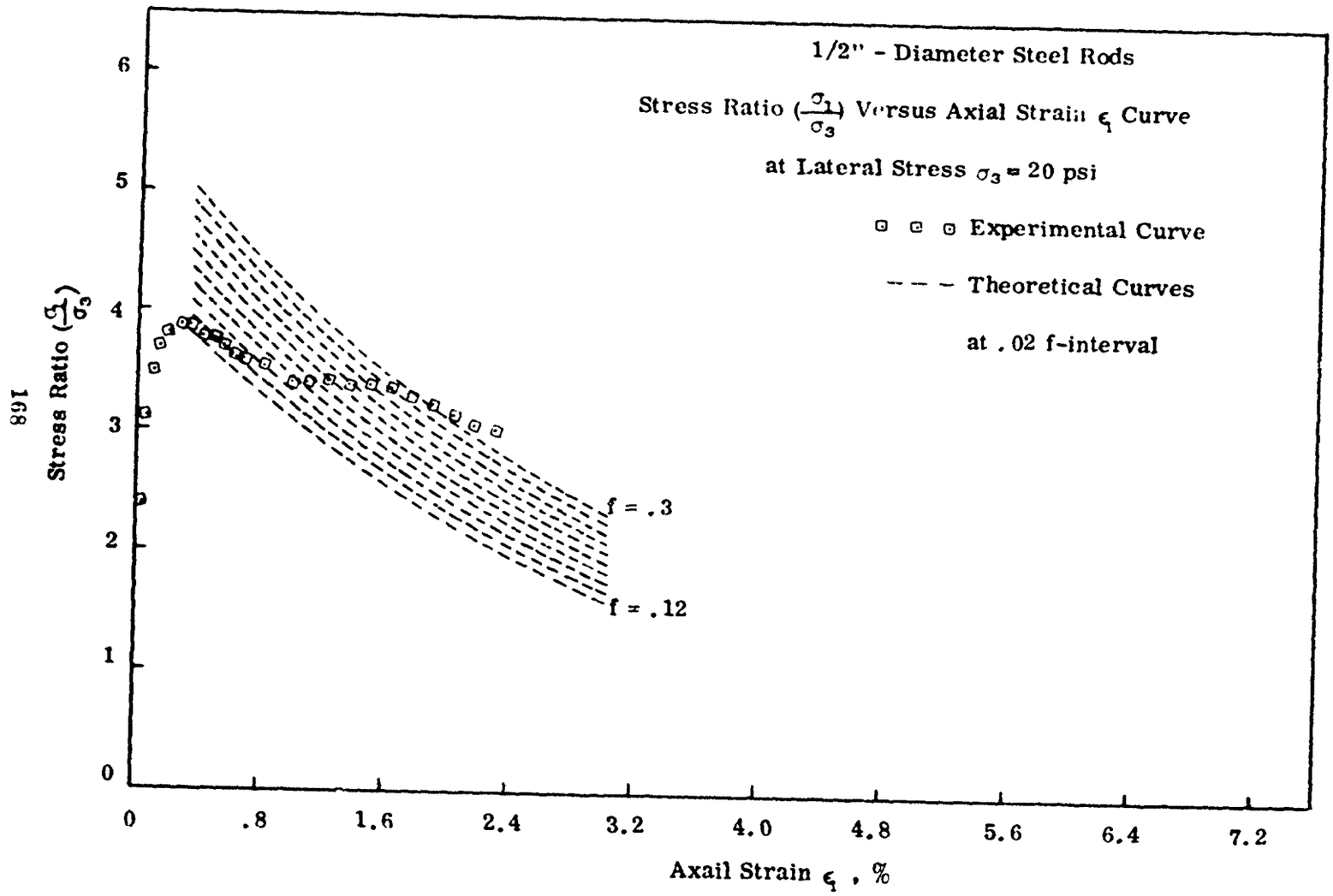
1/2" - Diameter Steel Rods
Stress Ratio ($\frac{\sigma_1}{\sigma_3}$) Versus Axial Strain ϵ_1 Curve
at Lateral Stress σ_3 = 20 psi
Experimental Curve
Theoretical Curves
at .02 f-interval
f = .3
f = .12
Stress Ratio ($\frac{\sigma_1}{\sigma_3}$)
Axail Strain ϵ_1 , %
0
1
2
3
4
5
6
.8
1.6
2.4
3.2
4.0
4.8
5.6
6.4
7.2

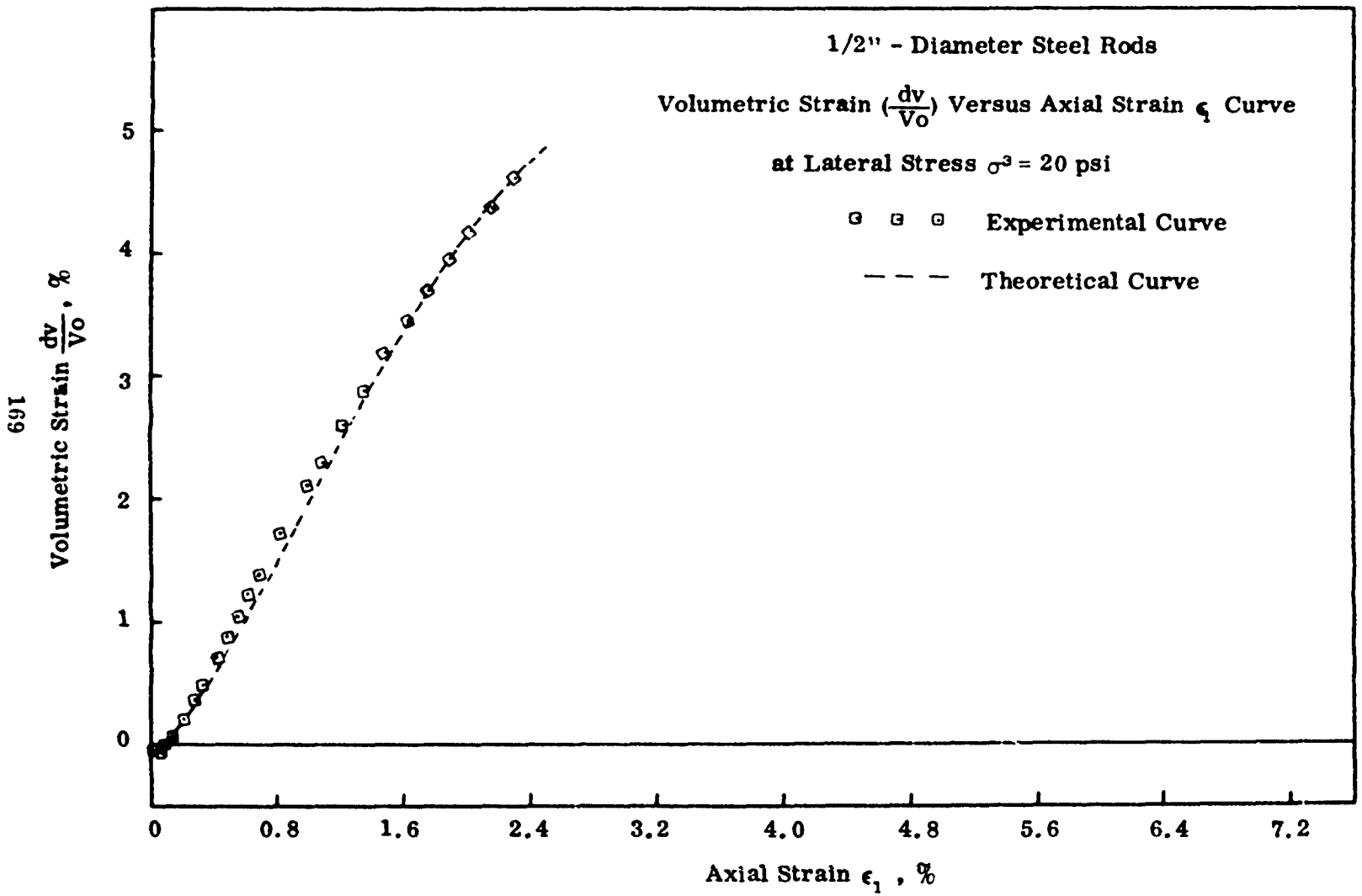
1/2" - Diameter Steel Rods
Volumetric Strain (dv/Vo) Versus Axial Strain ε1 Curve
at Lateral Stress σ3 = 20 psi
Experimental Curve
Theoretical Curve
Volumetric Strain dv/Vo, %
Axial Strain ε1, %
0
1
2
3
4
5
0
0.8
1.6
2.4
3.2
4.0
4.8
5.6
6.4
7.2

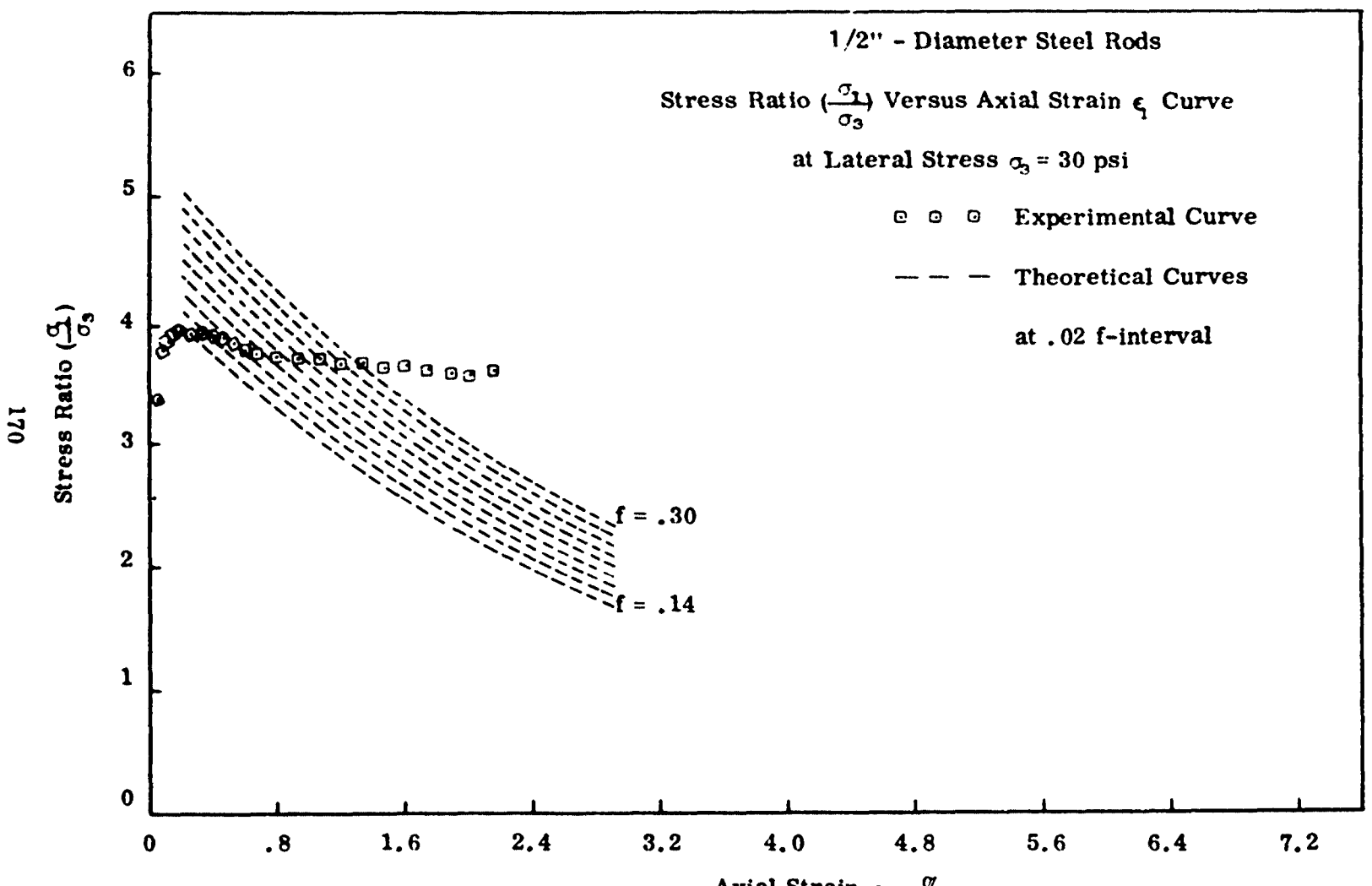
1/2" - Diameter Steel Rods
Stress Ratio $(\frac{\sigma_1}{\sigma_3})$ Versus Axial Strain ϵ_1 Curve
at Lateral Stress σ_3 = 30 psi
Experimental Curve
Theoretical Curves
at .02 f-interval
f = .30
f = .14
Stress Ratio $(\frac{\sigma_1}{\sigma_3})$
Axial Strain ϵ_1, %
0
1
2
3
4
5
6
.8
1.6
2.4
3.2
4.0
4.8
5.6
6.4
7.2

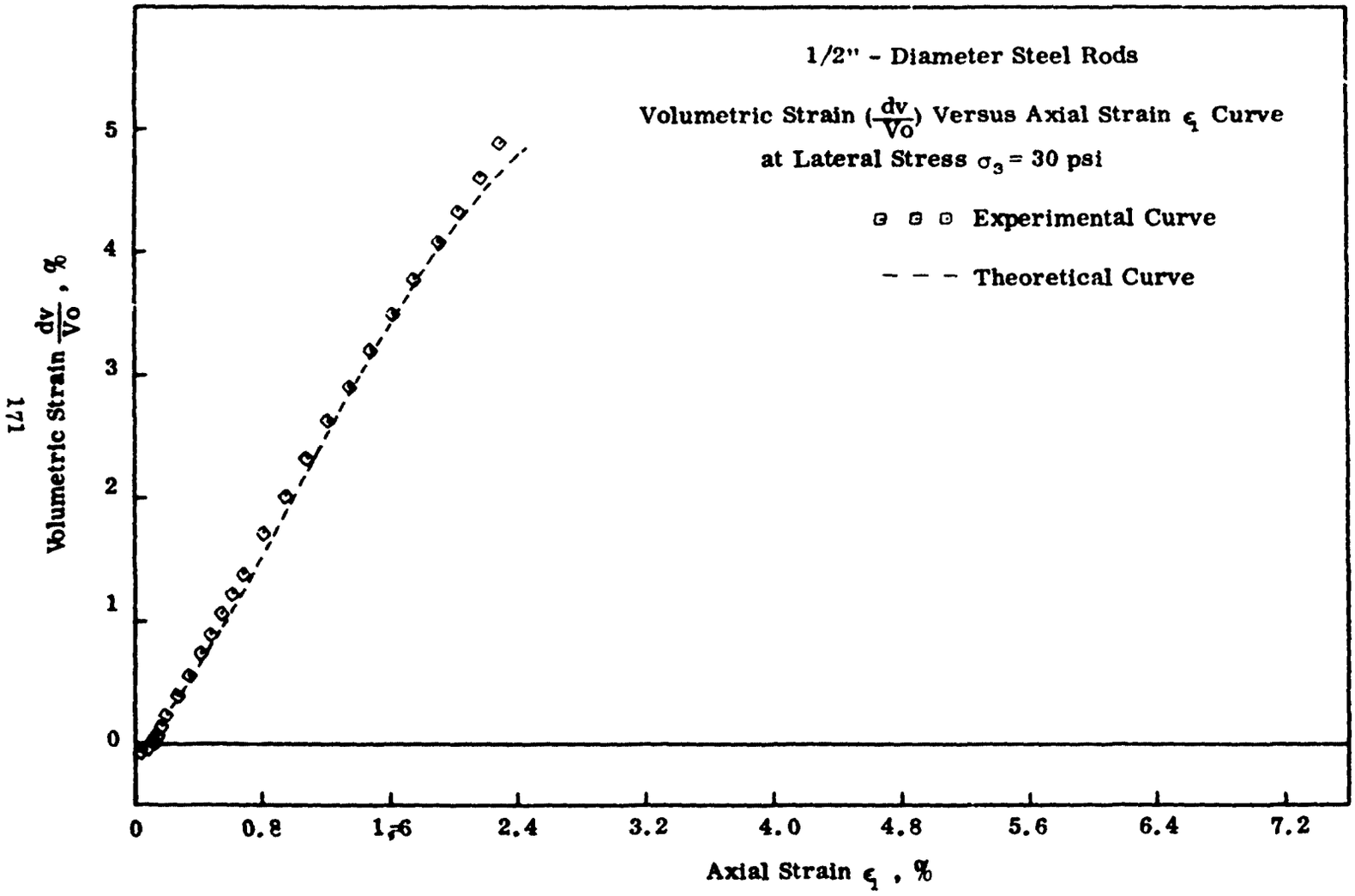
1/2" - Diameter Steel Rods
Volumetric Strain (dv/Vo) Versus Axial Strain ε1 Curve
at Lateral Stress σ3 = 30 psi
Experimental Curve
Theoretical Curve
Volumetric Strain dv/Vo , %
Axial Strain ε1 , %
0
1
2
3
4
5
0
0.8
1.6
2.4
3.2
4.0
4.8
5.6
6.4
7.2

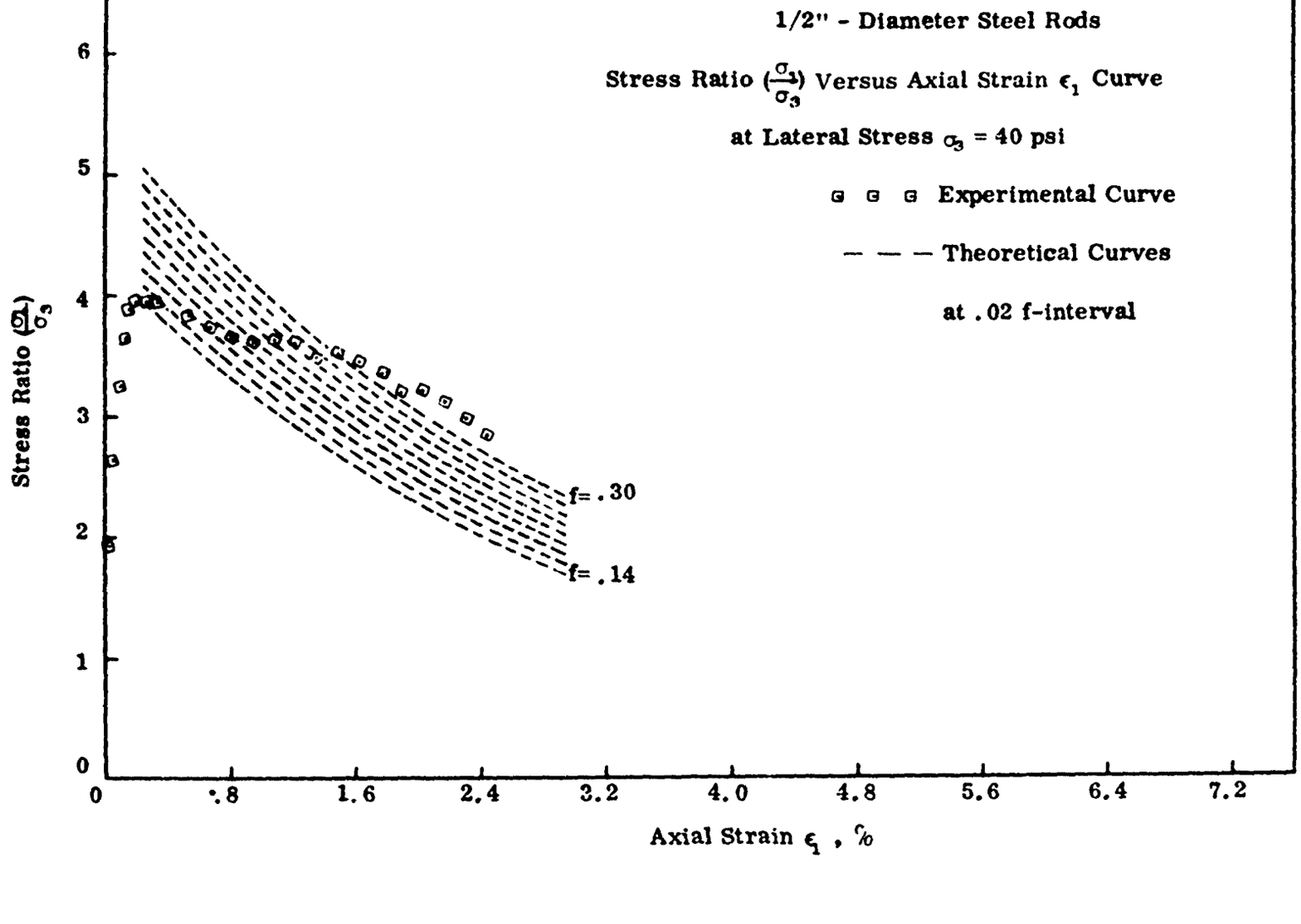
1/2" - Diameter Steel Rods
Stress Ratio $(\frac{\sigma_1}{\sigma_3})$ Versus Axial Strain ϵ_1 Curve
at Lateral Stress σ_3 = 40 psi
Experimental Curve
Theoretical Curves
at .02 f-interval
f= .30
f= .14
Stress Ratio $(\frac{\sigma_1}{\sigma_3})$
Axial Strain ϵ_1 , %
0
1
2
3
4
5
6
.8
1.6
2.4
3.2
4.0
4.8
5.6
6.4
7.2

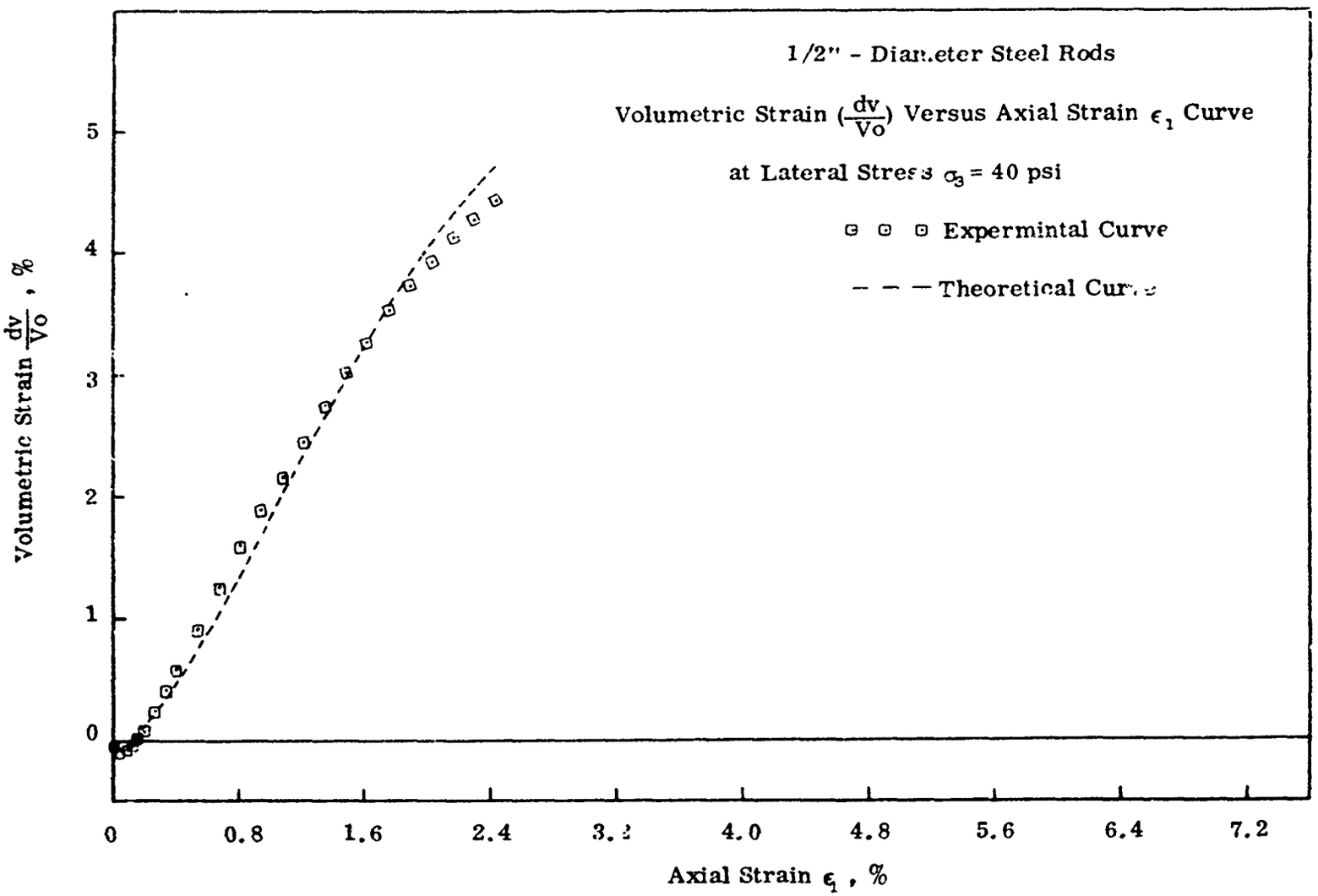
1/2" - Diameter Steel Rods
Volumetric Strain ($\frac{dv}{Vo}$) Versus Axial Strain ϵ_1 Curve
at Lateral Stress σ_3 = 40 psi
Expermintal Curve
Theoretical Curve
Volumetric Strain $\frac{dv}{Vo}$, %
Axial Strain ϵ_1 , %
0
1
2
3
4
5
0
0.8
1.6
2.4
3.2
4.0
4.8
5.6
6.4
7.2

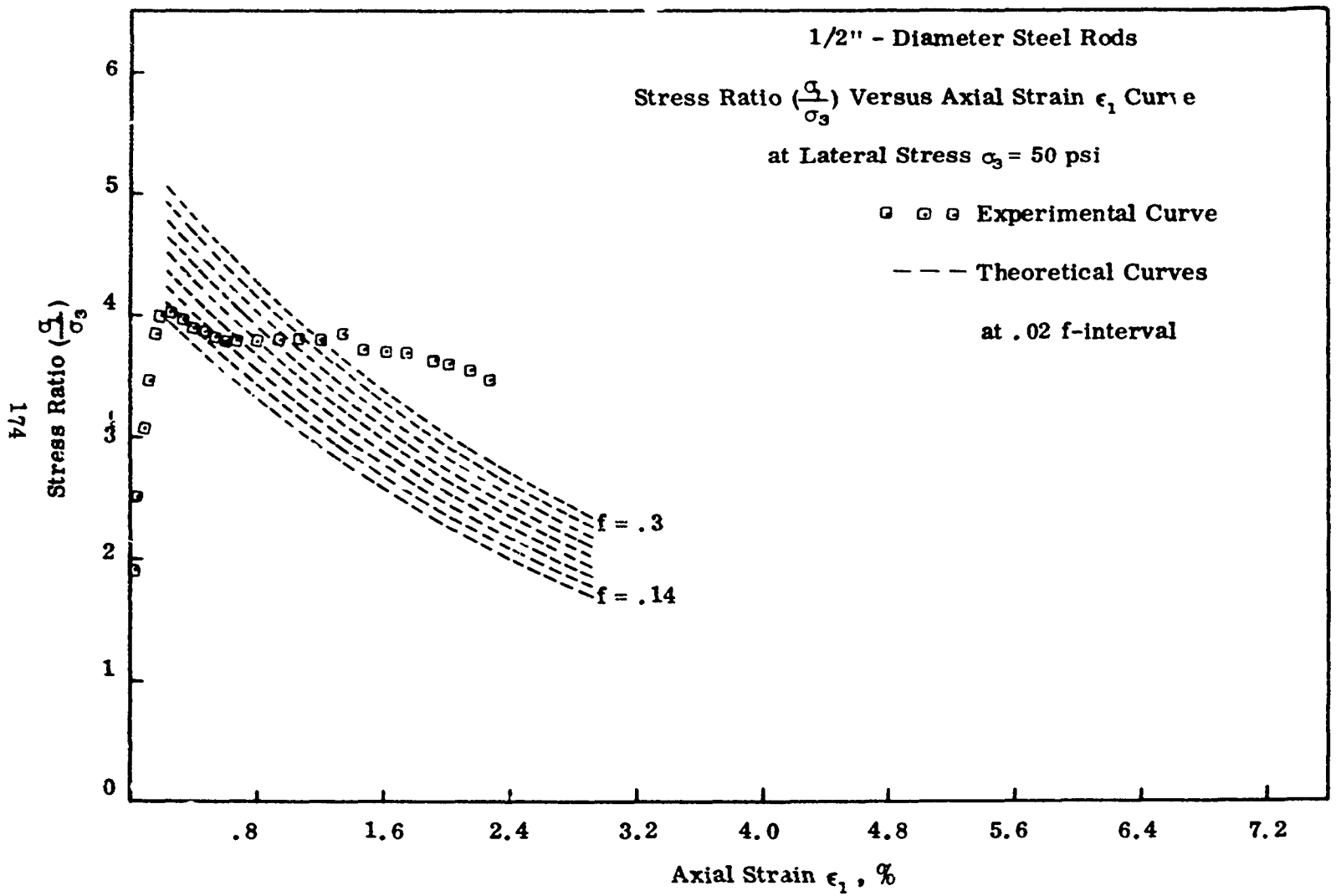
1/2" - Diameter Steel Rods
Stress Ratio ($\frac{\sigma_1}{\sigma_3}$) Versus Axial Strain ϵ_1 Curve
at Lateral Stress σ_3 = 50 psi
Experimental Curve
Theoretical Curves
at .02 f-interval
f = .3
f = .14
Stress Ratio ($\frac{\sigma_1}{\sigma_3}$)
Axial Strain ϵ_1, %
0
1
2
3
4
5
6
.8
1.6
2.4
3.2
4.0
4.8
5.6
6.4
7.2

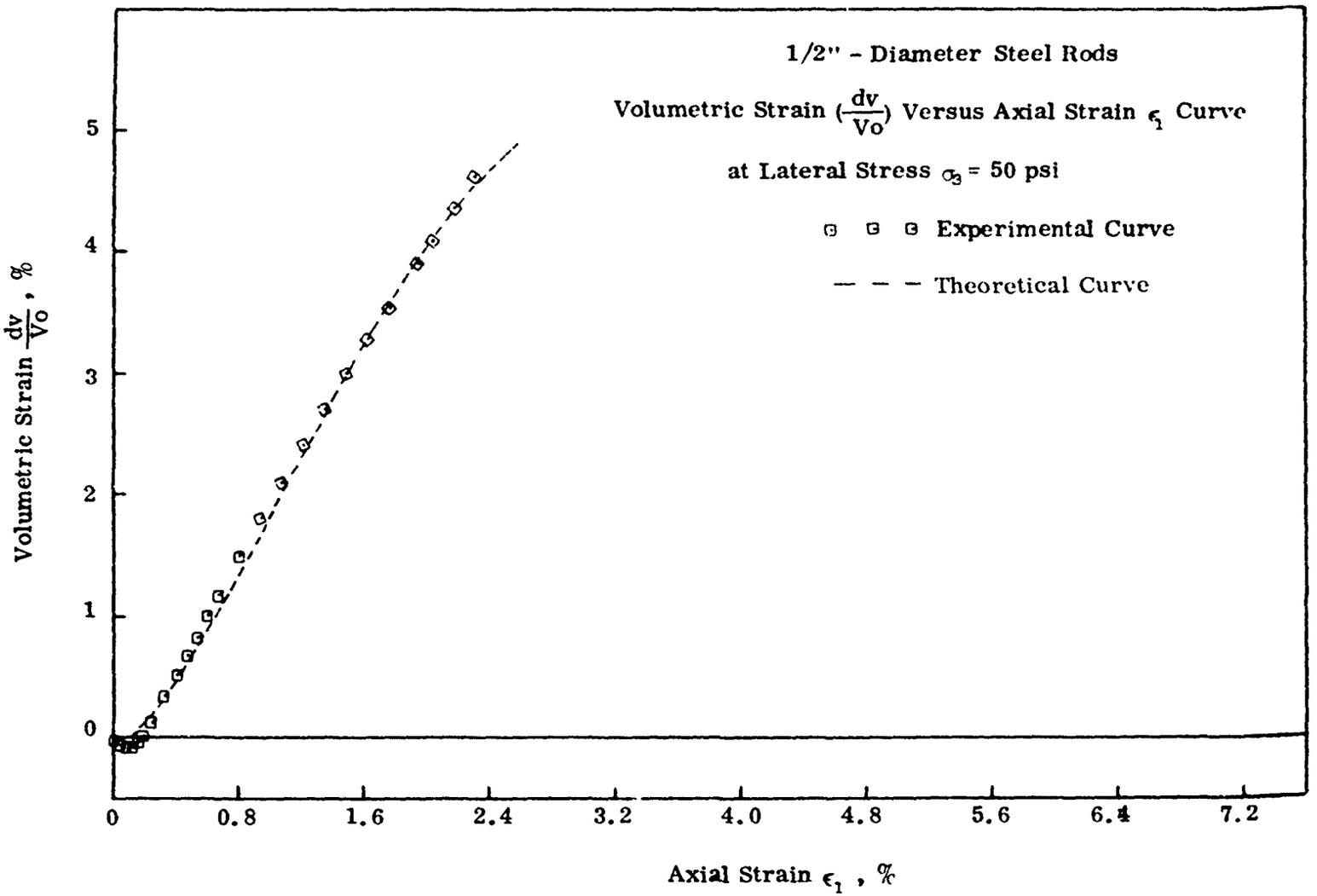
1/2" - Diameter Steel Rods
Volumetric Strain (dv/Vo) Versus Axial Strain ε1 Curve
at Lateral Stress σ3 = 50 psi
Experimental Curve
Theoretical Curve
Volumetric Strain dv/Vo , %
Axial Strain ε1 , %
0
1
2
3
4
5
0
0.8
1.6
2.4
3.2
4.0
4.8
5.6
6.4
7.2

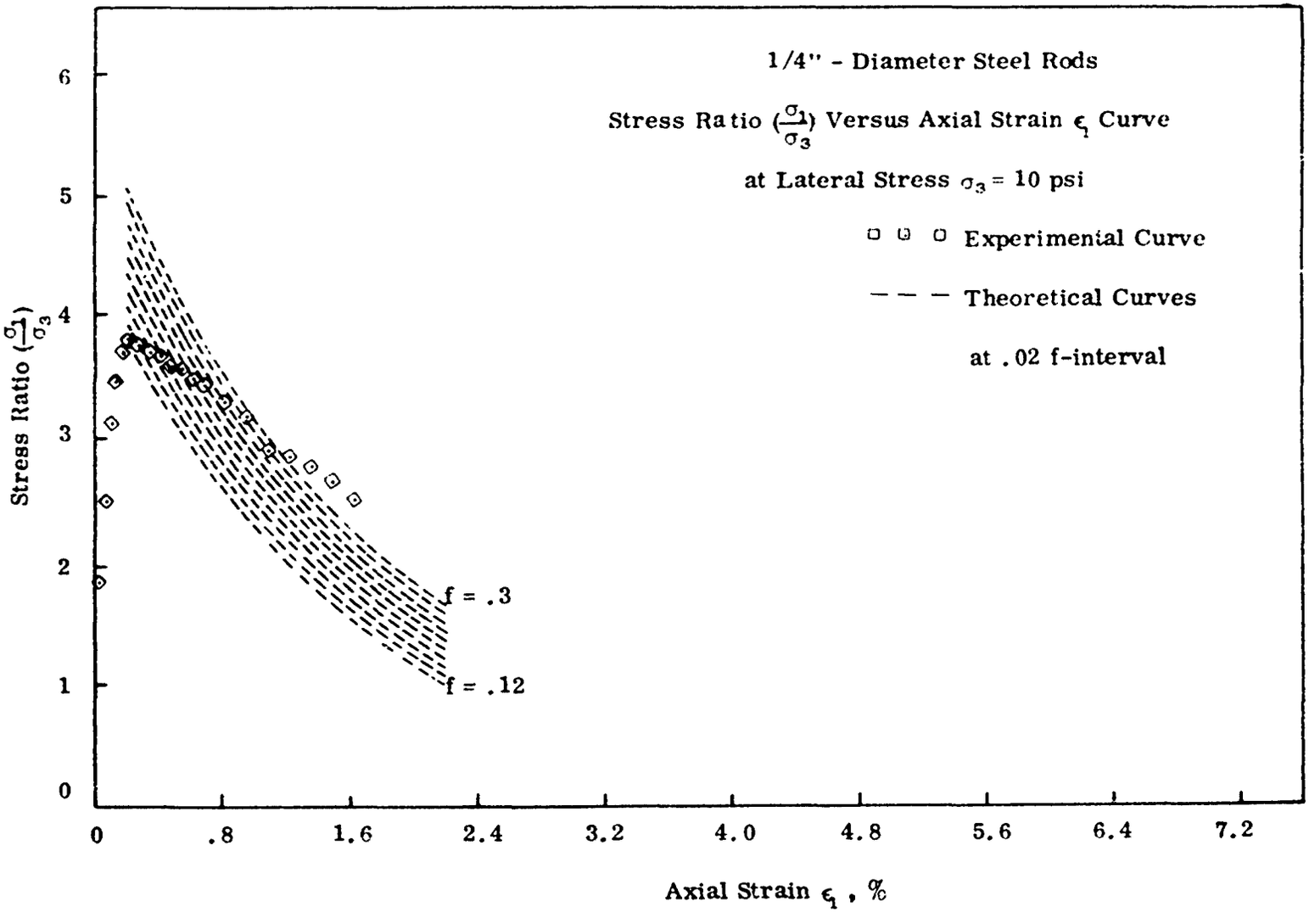
1/4" - Diameter Steel Rods
Stress Ratio ($\frac{\sigma_1}{\sigma_3}$) Versus Axial Strain ϵ_1 Curve
at Lateral Stress σ_3 = 10 psi
Experimental Curve
Theoretical Curves
at .02 f-interval
f = .3
f = .12
Stress Ratio ($\frac{\sigma_1}{\sigma_3}$)
Axial Strain ϵ_1, %
0
1
2
3
4
5
6
0
.8
1.6
2.4
3.2
4.0
4.8
5.6
6.4
7.2

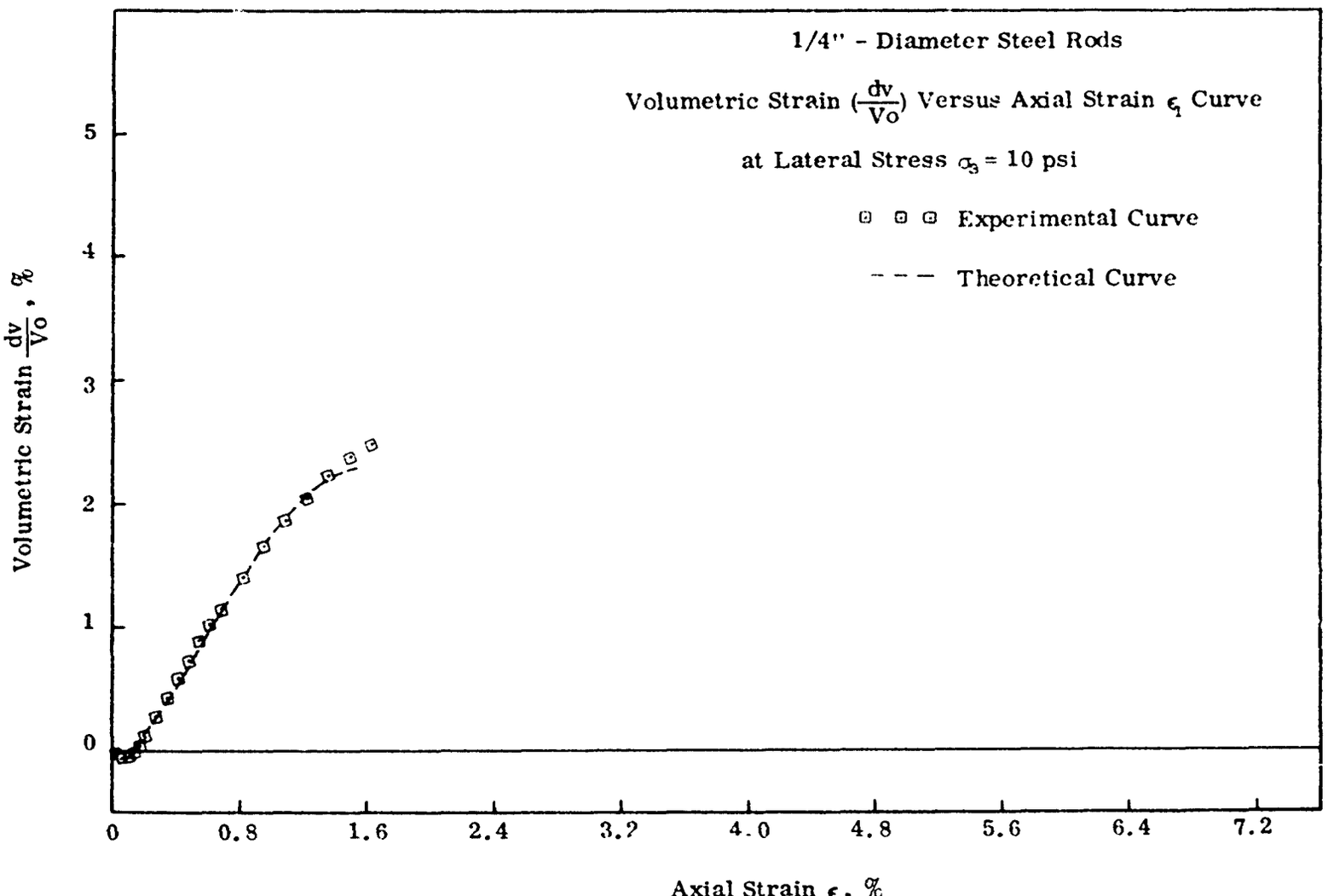
1/4" - Diameter Steel Rods
Volumetric Strain (dv/Vo) Versus Axial Strain ε1 Curve
at Lateral Stress σ3 = 10 psi
Experimental Curve
Theoretical Curve
Volumetric Strain dv/Vo, %
Axial Strain ε1, %
0
1
2
3
4
5
0
0.8
1.6
2.4
3.2
4.0
4.8
5.6
6.4
7.2

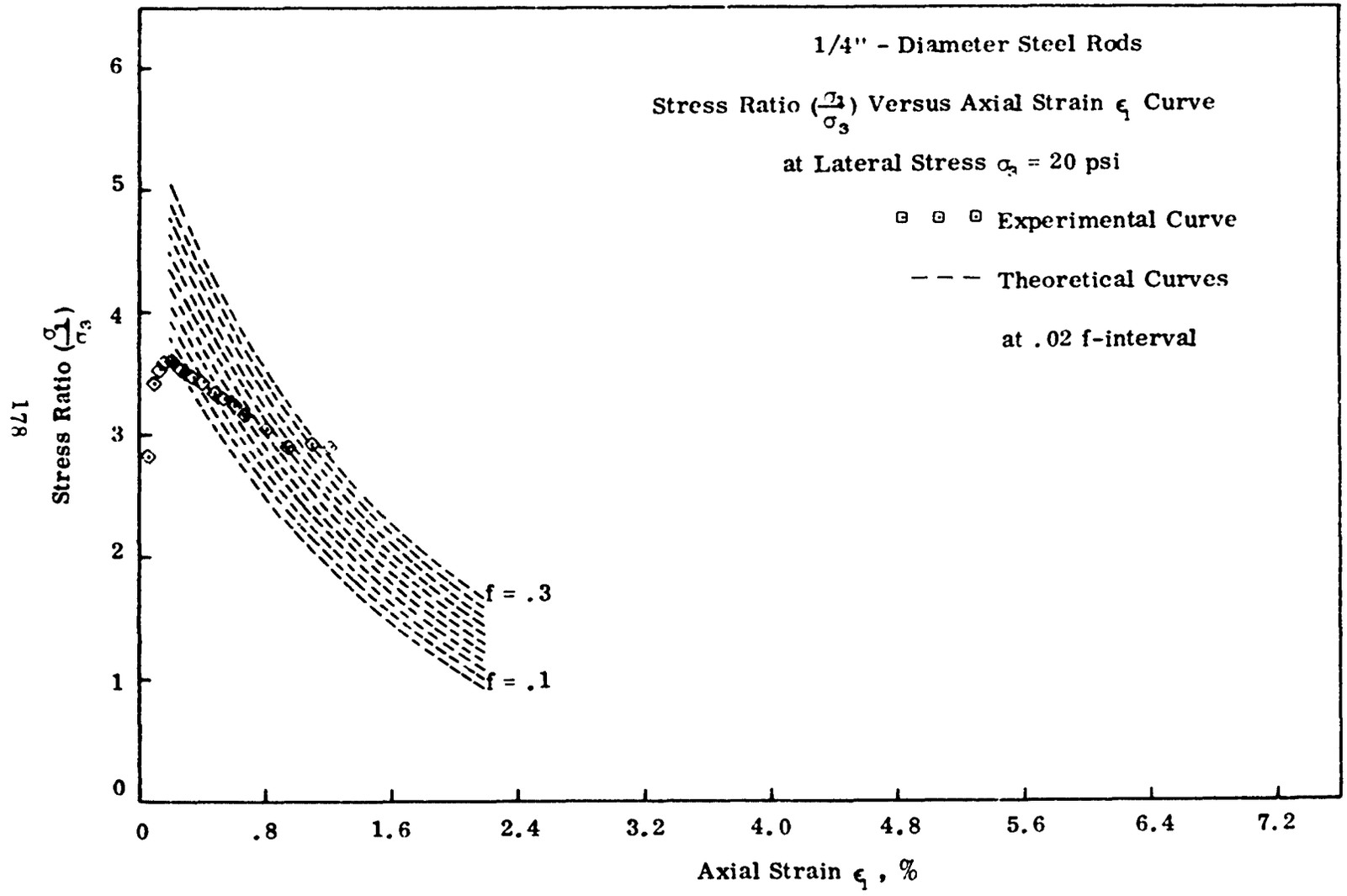
1/4" - Diameter Steel Rods
Stress Ratio ($\frac{\sigma_1}{\sigma_3}$) Versus Axial Strain ϵ_1 Curve
at Lateral Stress σ_3 = 20 psi
Experimental Curve
Theoretical Curves
at .02 f-interval
f = .3
f = .1
Stress Ratio ($\frac{\sigma_1}{\sigma_3}$)
Axial Strain ϵ_1, %
0
1
2
3
4
5
6
0
.8
1.6
2.4
3.2
4.0
4.8
5.6
6.4
7.2

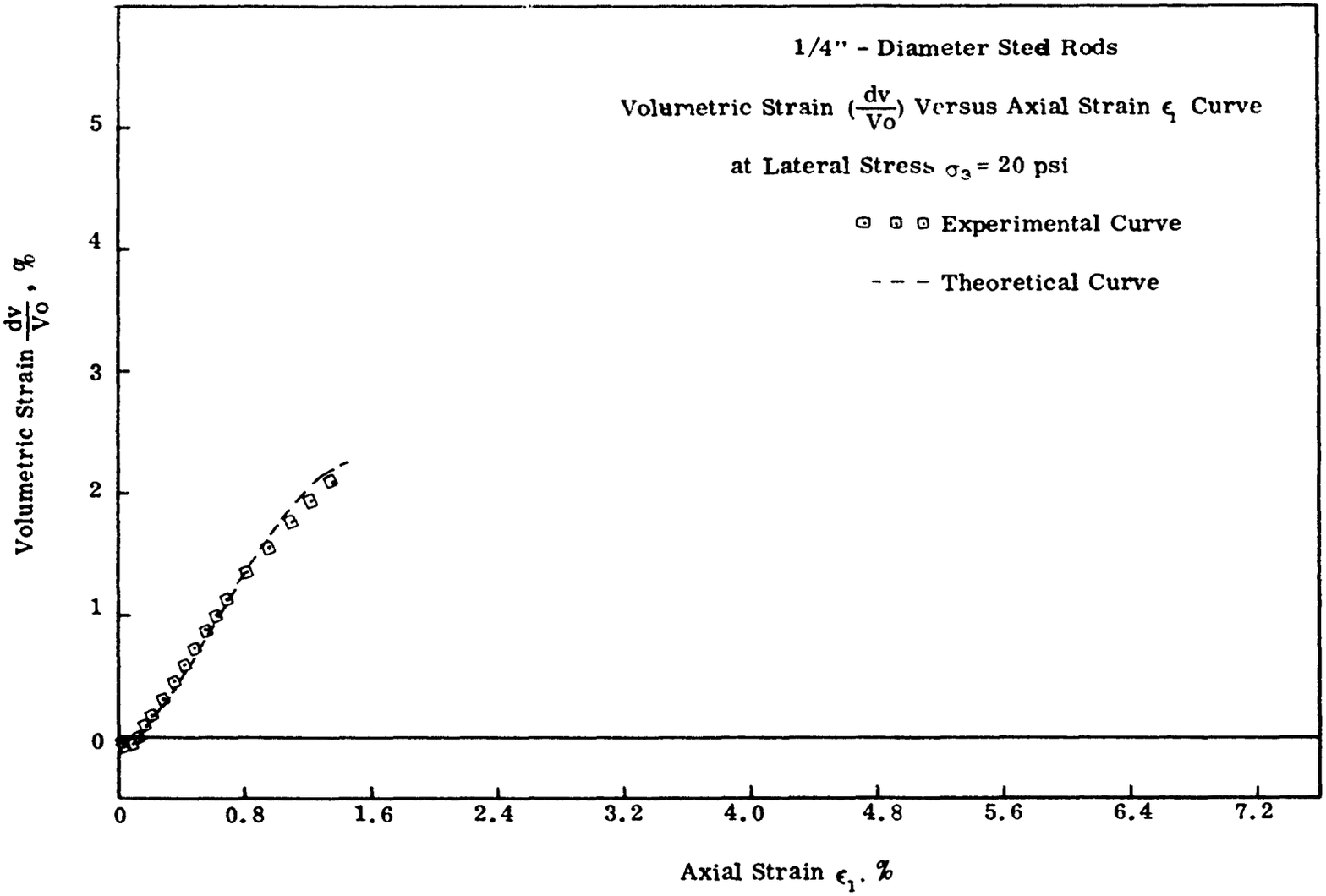
1/4" - Diameter Steel Rods
Volumetric Strain (dv/Vo) Versus Axial Strain ε1 Curve
at Lateral Stress σ3 = 20 psi
Experimental Curve
Theoretical Curve
Volumetric Strain dv/Vo, %
Axial Strain ε1, %
0
1
2
3
4
5
0
0.8
1.6
2.4
3.2
4.0
4.8
5.6
6.4
7.2

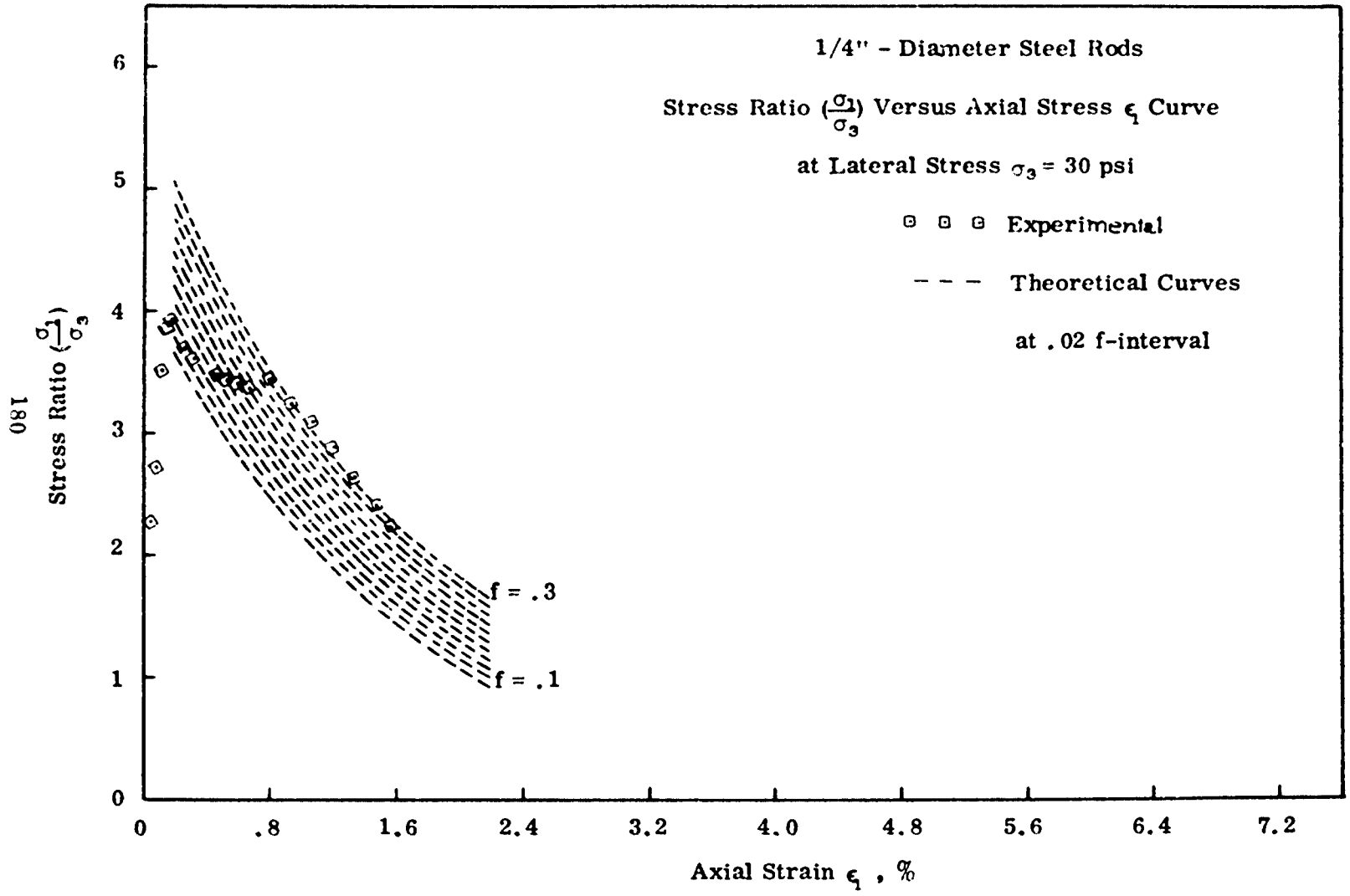
1/4" - Diameter Steel Rods
Stress Ratio ($\frac{\sigma_1}{\sigma_3}$) Versus Axial Stress ϵ_1 Curve
at Lateral Stress σ_3 = 30 psi
Experimental
Theoretical Curves
at .02 f-interval
f = .3
f = .1
Stress Ratio ($\frac{\sigma_1}{\sigma_3}$)
Axial Strain ϵ_1 , %
0
1
2
3
4
5
6
.8
1.6
2.4
3.2
4.0
4.8
5.6
6.4
7.2

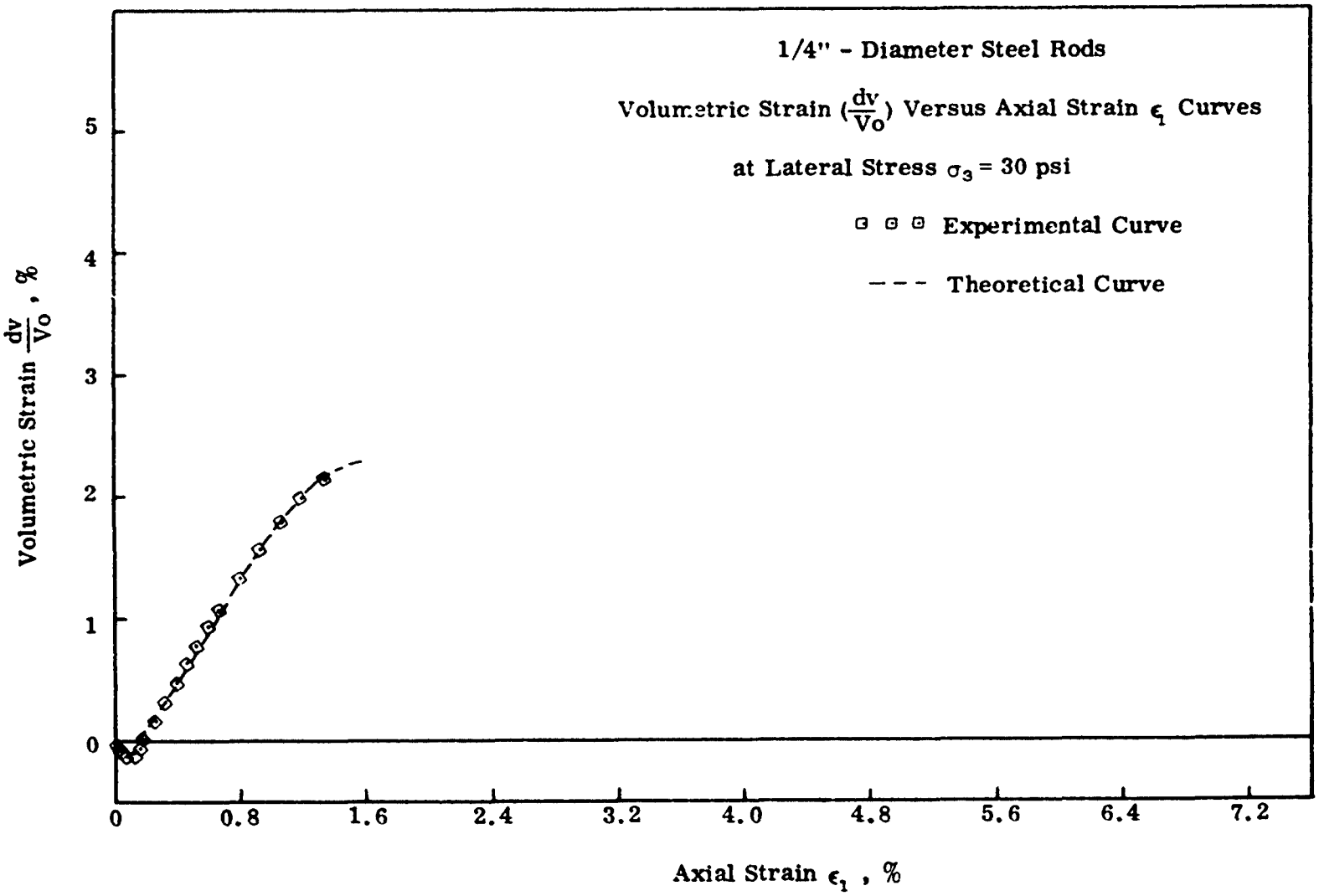
1/4" - Diameter Steel Rods
Volumetric Strain (dv/Vo) Versus Axial Strain ε1 Curves
at Lateral Stress σ3 = 30 psi
Experimental Curve
Theoretical Curve
Volumetric Strain dv/Vo , %
Axial Strain ε1 , %
0
1
2
3
4
5
0
0.8
1.6
2.4
3.2
4.0
4.8
5.6
6.4
7.2

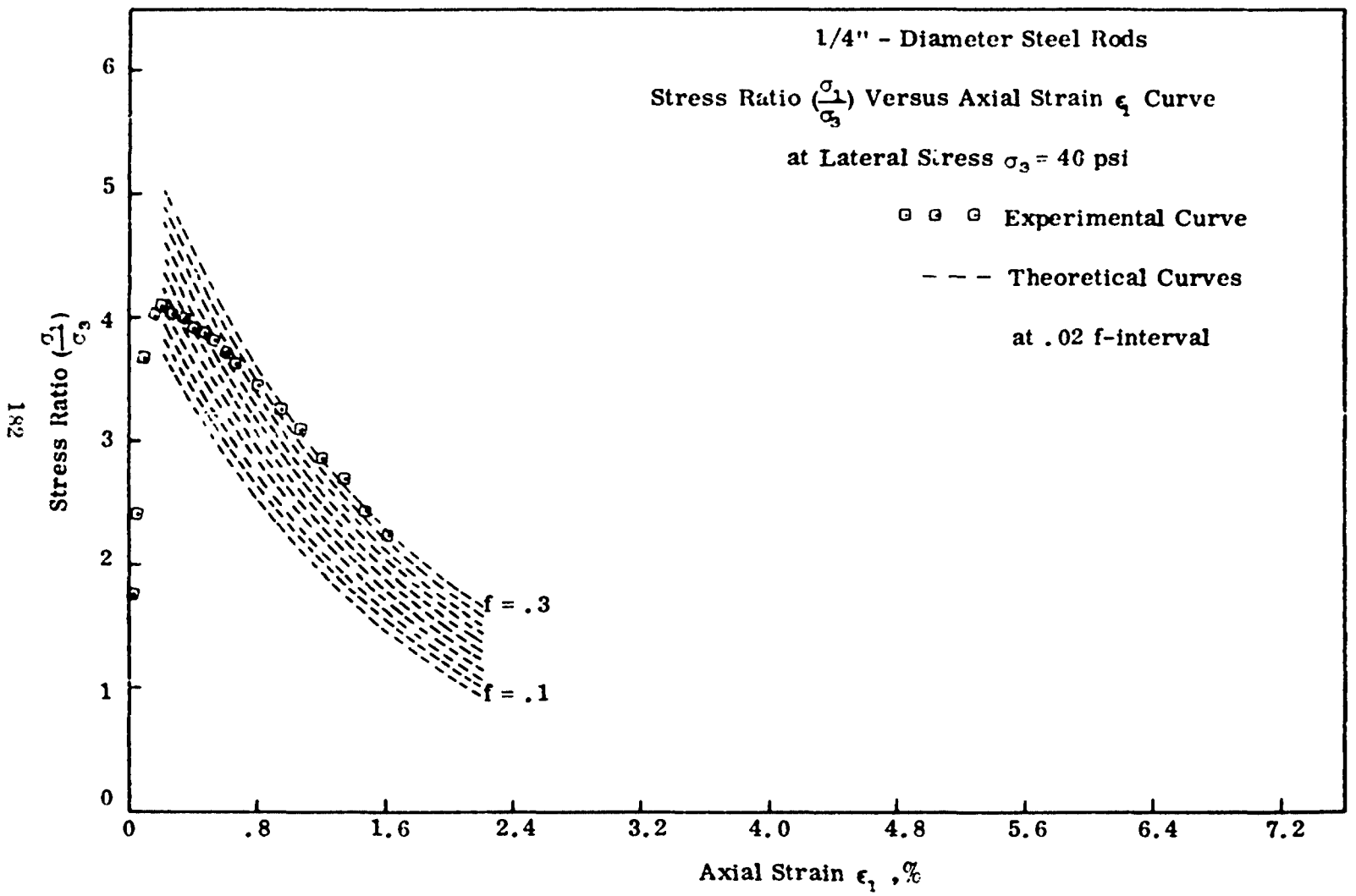
1/4" - Diameter Steel Rods
Stress Ratio $(\frac{\sigma_1}{\sigma_3})$ Versus Axial Strain ϵ_1 Curve
at Lateral Stress σ_3 = 40 psi
Experimental Curve
Theoretical Curves
at .02 f-interval
Stress Ratio $(\frac{\sigma_1}{\sigma_3})$
Axial Strain ϵ_1 ,%
f = .3
f = .1
0
1
2
3
4
5
6
0
.8
1.6
2.4
3.2
4.0
4.8
5.6
6.4
7.2

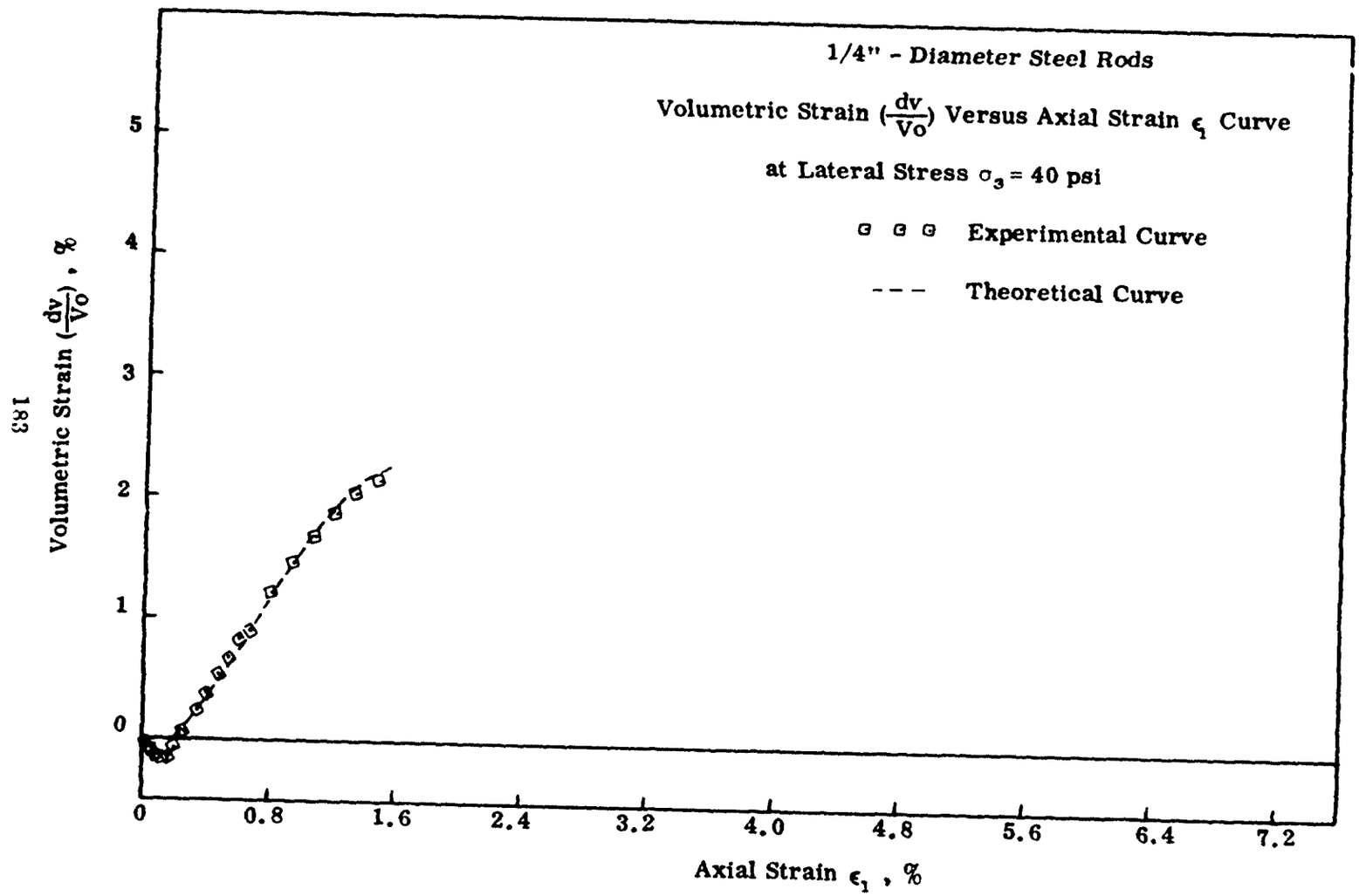
1/4" - Diameter Steel Rods
Volumetric Strain (dv/Vo) Versus Axial Strain ε1 Curve
at Lateral Stress σ3 = 40 psi
Experimental Curve
Theoretical Curve
Volumetric Strain (dv/Vo) , %
Axial Strain ε1 , %
0
1
2
3
4
5
0
0.8
1.6
2.4
3.2
4.0
4.8
5.6
6.4
7.2

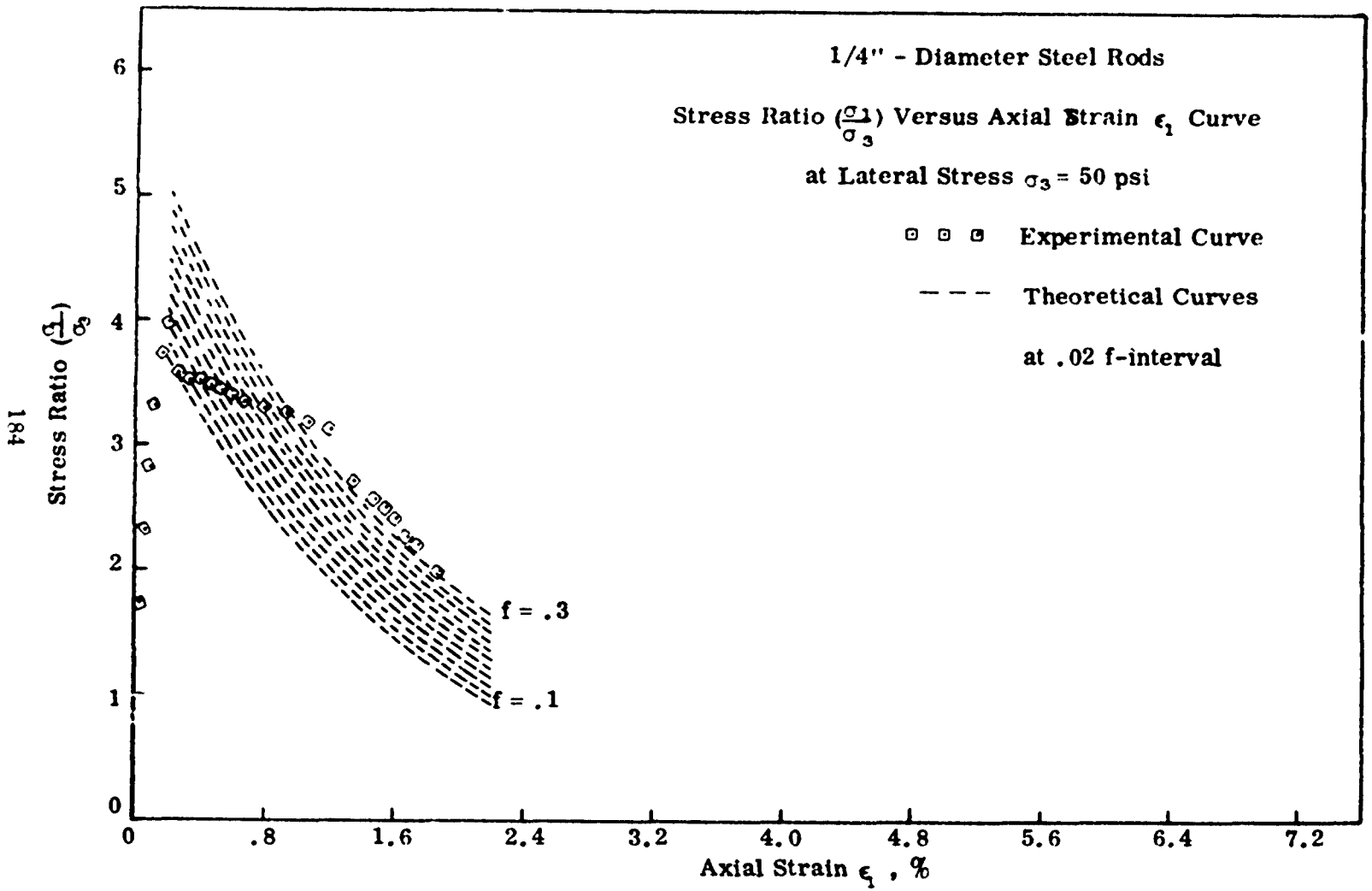
1/4" - Diameter Steel Rods
Stress Ratio $(\frac{\sigma_1}{\sigma_3})$ Versus Axial Strain ϵ_1 Curve
at Lateral Stress σ_3 = 50 psi
Experimental Curve
Theoretical Curves
at .02 f-interval
Stress Ratio $(\frac{\sigma_1}{\sigma_3})$
Axial Strain ϵ_1 , %
f = .3
f = .1
0
1
2
3
4
5
6
.8
1.6
2.4
3.2
4.0
4.8
5.6
6.4
7.2

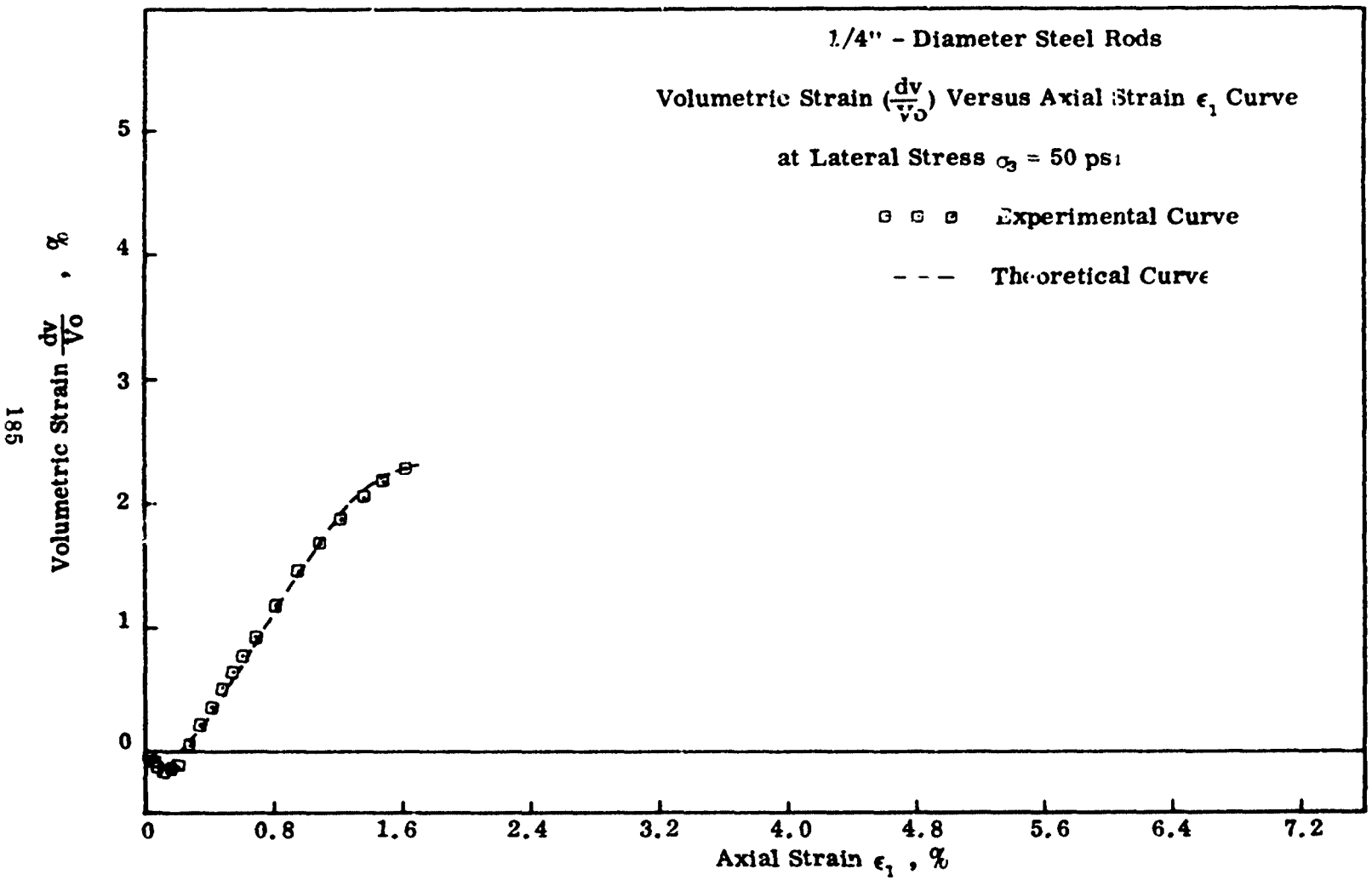
1/4" - Diameter Steel Rods
Volumetric Strain ($\frac{dv}{vo}$) Versus Axial Strain ϵ_1 Curve
at Lateral Stress σ_3 = 50 psi
Experimental Curve
Theoretical Curve
Volumetric Strain $\frac{dv}{Vo}$, %
Axial Strain ϵ_1 , %
0
1
2
3
4
5
0
0.8
1.6
2.4
3.2
4.0
4.8
5.6
6.4
7.2

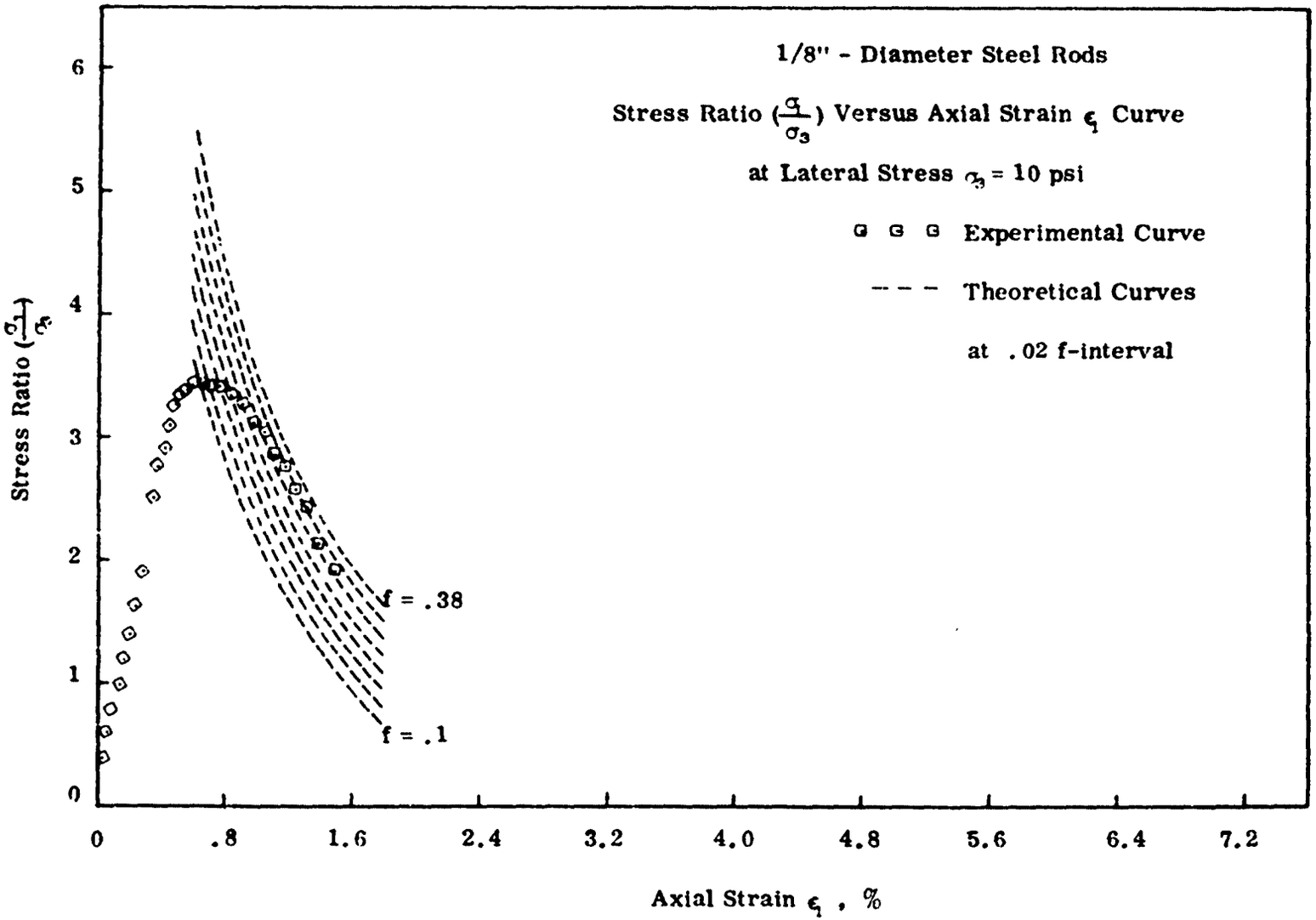
1/8" - Diameter Steel Rods
Stress Ratio ($\frac{\sigma_1}{\sigma_3}$) Versus Axial Strain ϵ_1 Curve
at Lateral Stress σ_3 = 10 psi
Experimental Curve
Theoretical Curves
at .02 f-interval
f = .38
f = .1
Stress Ratio ($\frac{\sigma_1}{\sigma_3}$)
Axial Strain ϵ_1 , %
0
1
2
3
4
5
6
0
.8
1.6
2.4
3.2
4.0
4.8
5.6
6.4
7.2

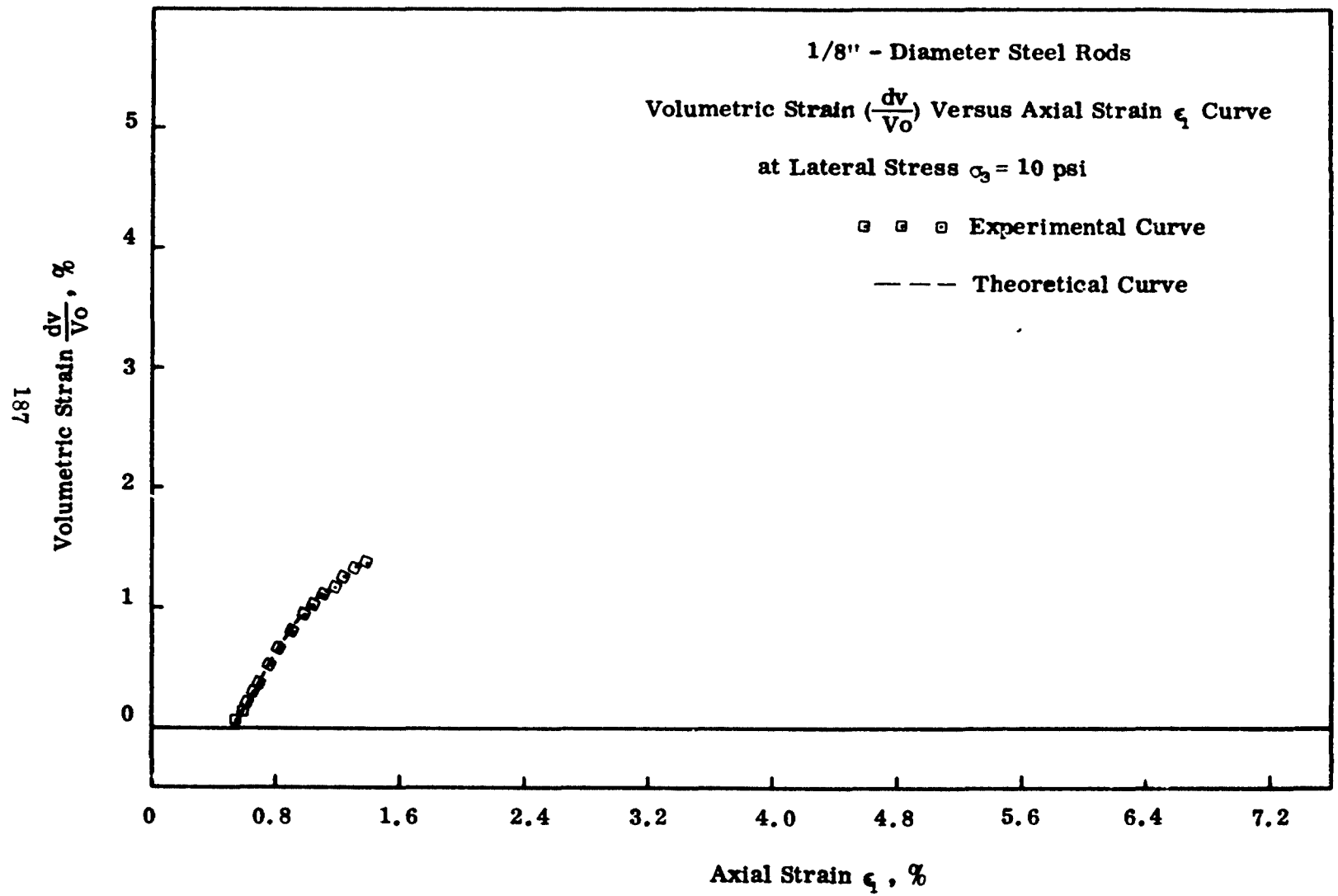
1/8" - Diameter Steel Rods
Volumetric Strain (dv/Vo) Versus Axial Strain ε1 Curve
at Lateral Stress σ3 = 10 psi
Experimental Curve
Theoretical Curve
Volumetric Strain dv/Vo, %
0
1
2
3
4
5
0
0.8
1.6
2.4
3.2
4.0
4.8
5.6
6.4
7.2
Axial Strain ε1, %

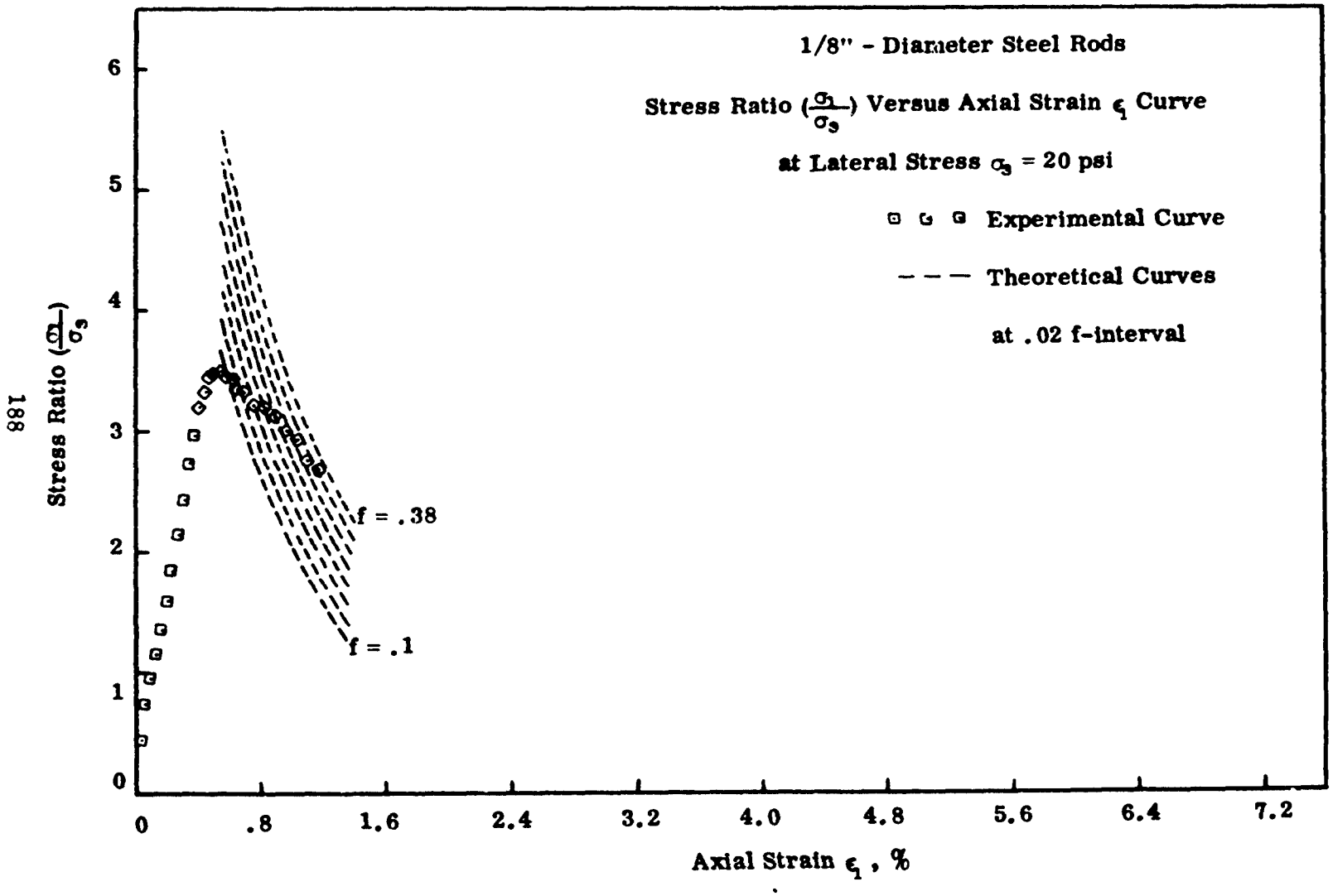
1/8" - Diameter Steel Rods
Stress Ratio ($\frac{\sigma_1}{\sigma_3}$) Versus Axial Strain ϵ_1 Curve
at Lateral Stress σ_3 = 20 psi
Experimental Curve
Theoretical Curves
at .02 f-interval
f = .38
f = .1
Stress Ratio ($\frac{\sigma_1}{\sigma_3}$)
Axial Strain ϵ_1, %
0
1
2
3
4
5
6
0
.8
1.6
2.4
3.2
4.0
4.8
5.6
6.4
7.2

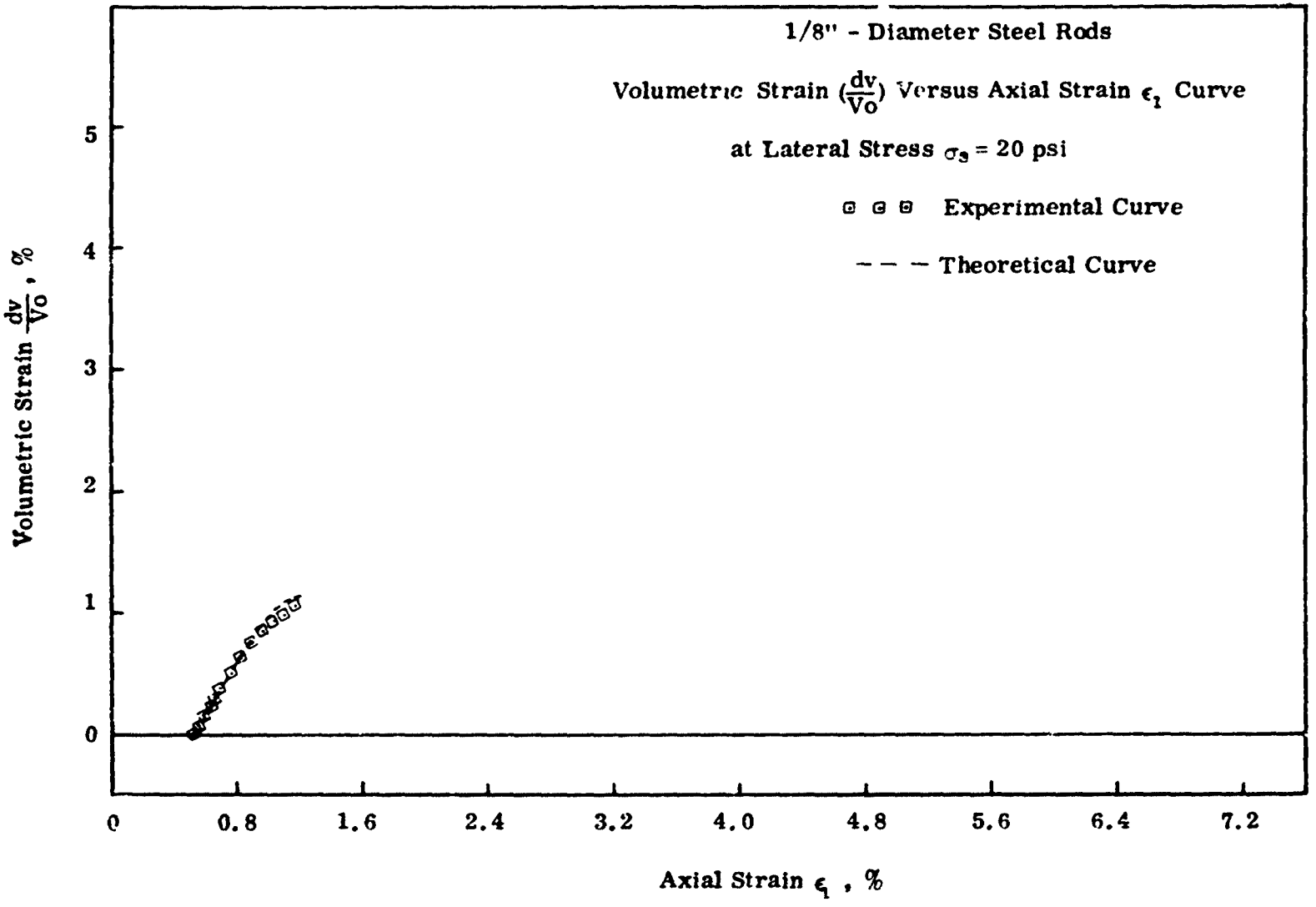
1/8" - Diameter Steel Rods
Volumetric Strain (dv/Vo) Versus Axial Strain ε1 Curve
at Lateral Stress σ3 = 20 psi
Experimental Curve
Theoretical Curve
Volumetric Strain dv/Vo , %
0
1
2
3
4
5
0
0.8
1.6
2.4
3.2
4.0
4.8
5.6
6.4
7.2
Axial Strain ε1 , %

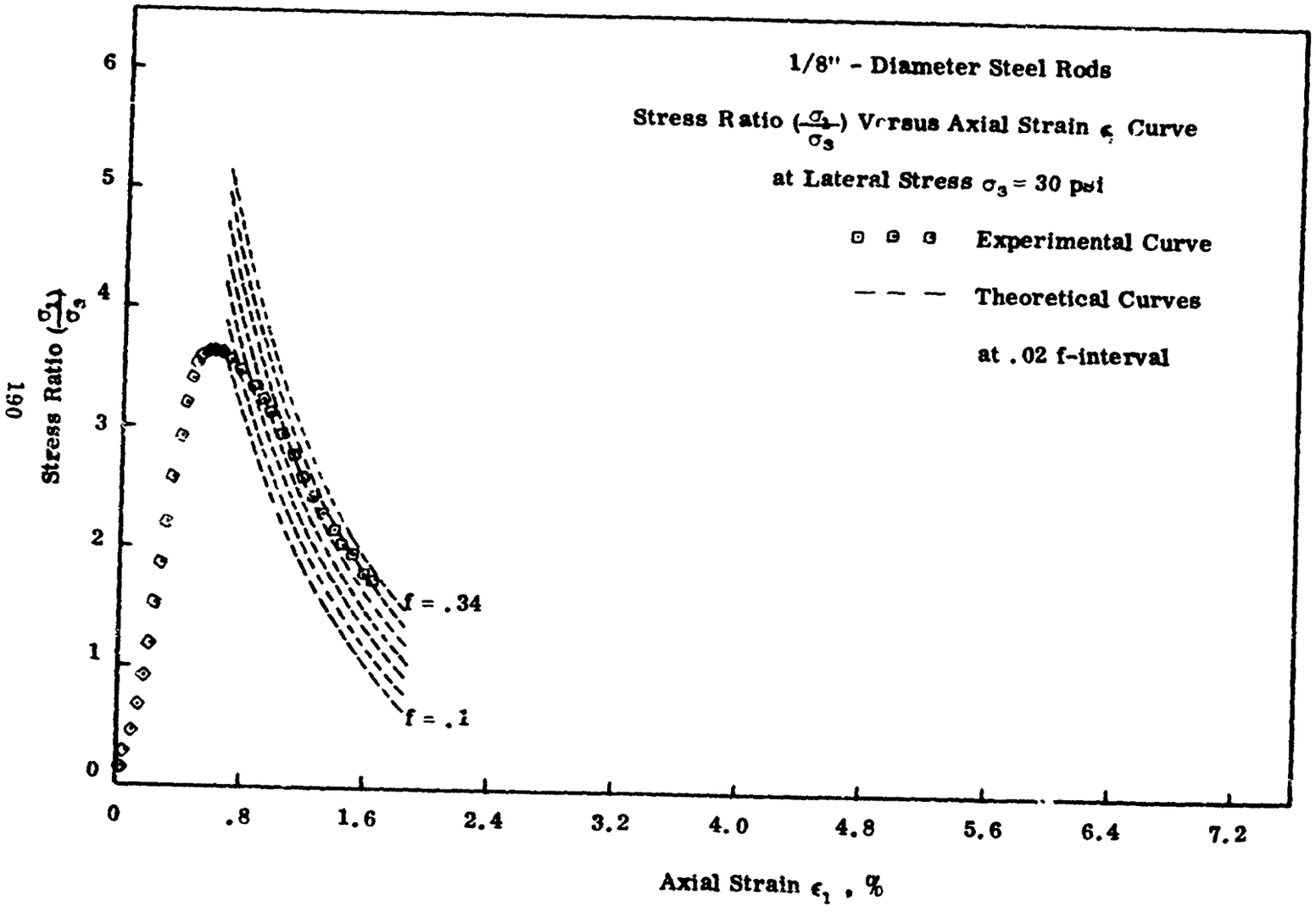
1/8" - Diameter Steel Rods
Stress Ratio $(\frac{\sigma_1}{\sigma_3})$ Versus Axial Strain ϵ_1 Curve
at Lateral Stress σ_3 = 30 psi
Experimental Curve
Theoretical Curves
at .02 f-interval
f = .34
f = .1
Stress Ratio $(\frac{\sigma_1}{\sigma_3})$
Axial Strain ϵ_1 , %
0
1
2
3
4
5
6
.8
1.6
2.4
3.2
4.0
4.8
5.6
6.4
7.2

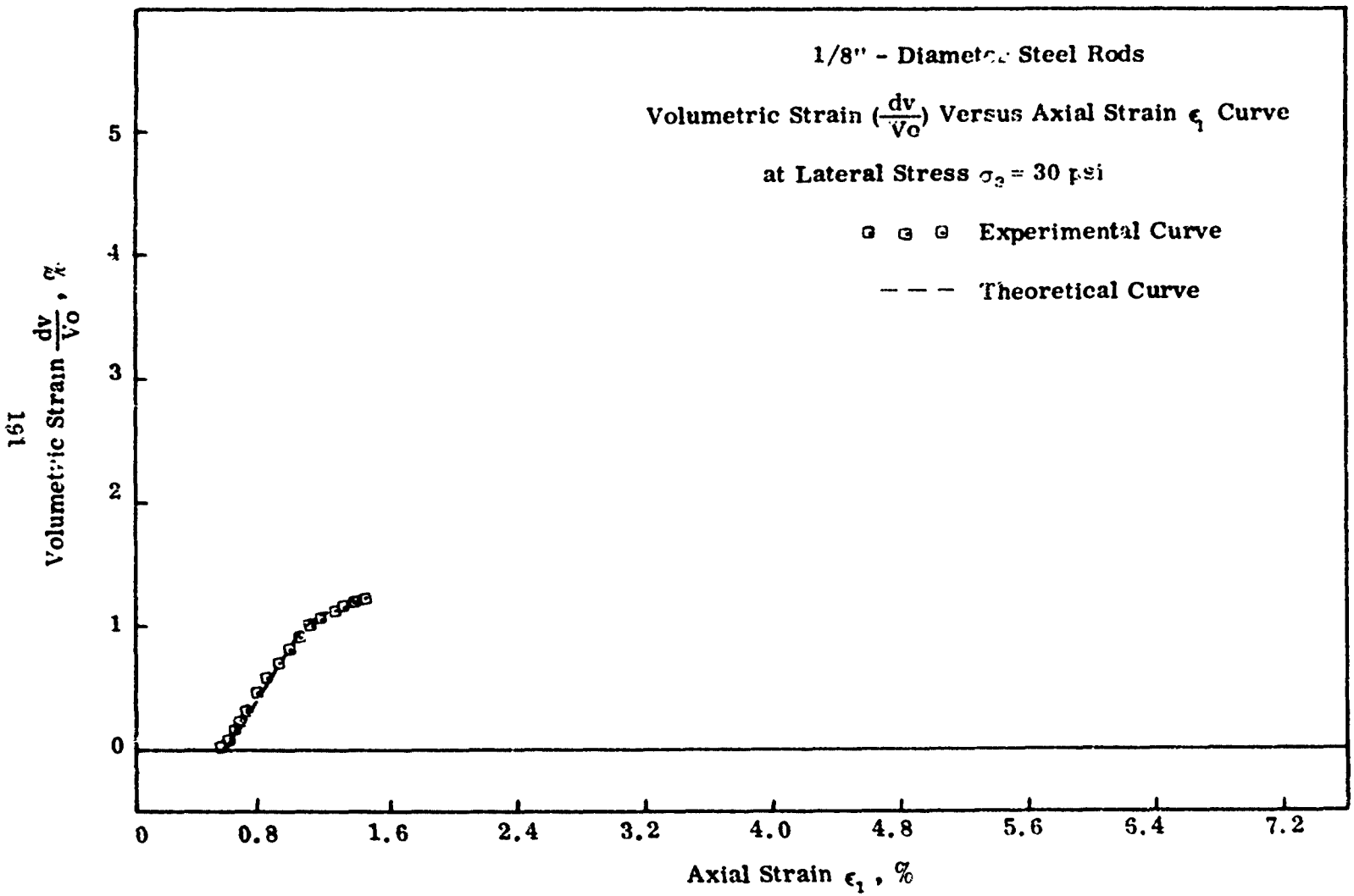
1/8" - Diameter Steel Rods
Volumetric Strain ($\frac{dv}{Vo}$) Versus Axial Strain ϵ_1 Curve
at Lateral Stress σ_3 = 30 psi
Experimental Curve
Theoretical Curve
Volumetric Strain $\frac{dv}{Vo}$, %
Axial Strain ϵ_1, %
0
1
2
3
4
5
0
0.8
1.6
2.4
3.2
4.0
4.8
5.6
6.4
7.2

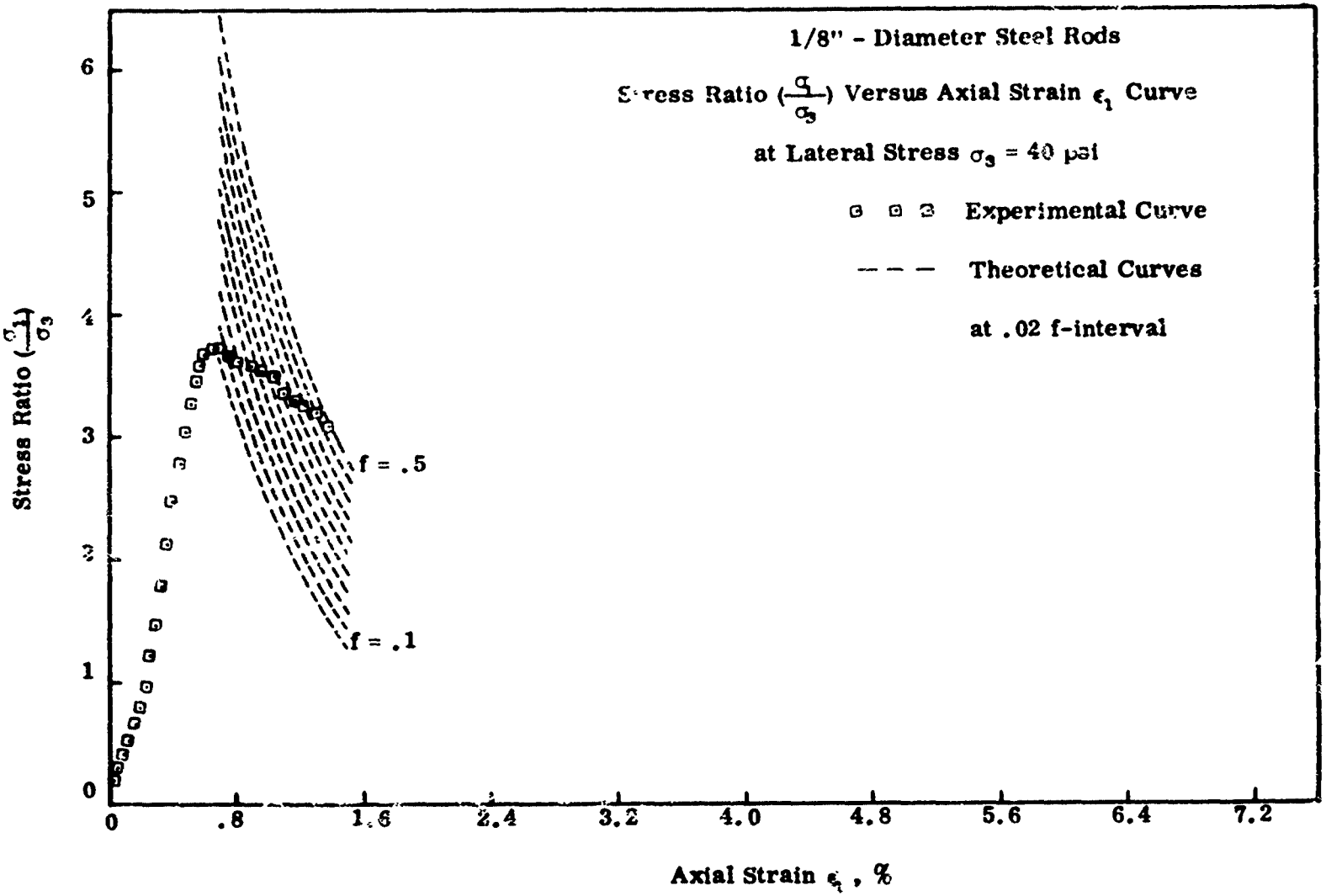
1/8" - Diameter Steel Rods
Stress Ratio ($\frac{\sigma_1}{\sigma_3}$) Versus Axial Strain ϵ_1 Curve
at Lateral Stress σ_3 = 40 psi
Experimental Curve
Theoretical Curves
at .02 f-interval
f = .5
f = .1
Stress Ratio ($\frac{\sigma_1}{\sigma_3}$)
Axial Strain ϵ_1, %
0
1
3
4
5
6
.8
1.6
2.4
3.2
4.0
4.8
5.6
6.4
7.2

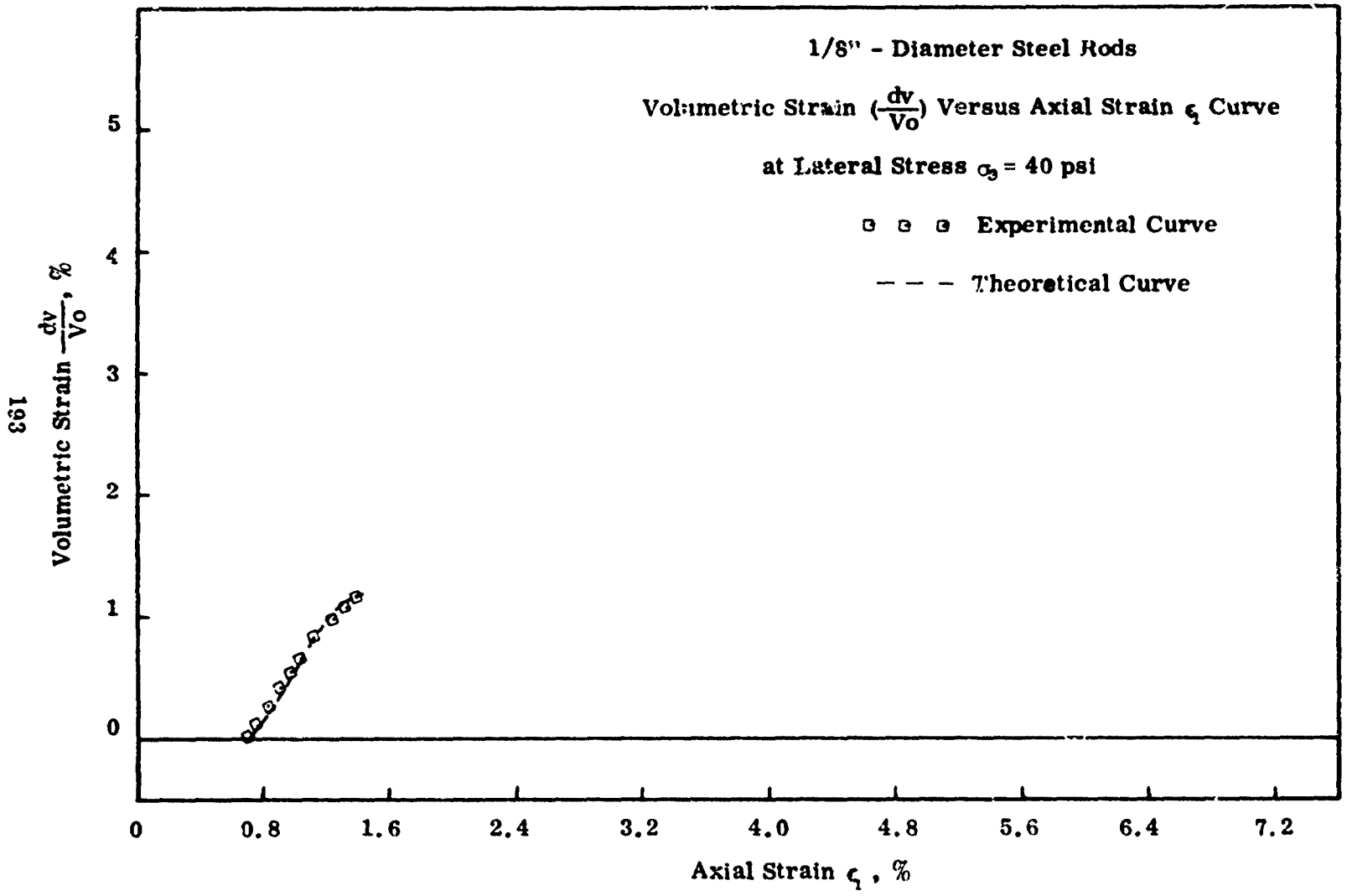
1/8" - Diameter Steel Rods
Volumetric Strain (dv/Vo) Versus Axial Strain ε1 Curve
at Lateral Stress σ3 = 40 psi
Experimental Curve
Theoretical Curve
Volumetric Strain dv/Vo, %
Axial Strain ε1, %
0
1
2
3
4
5
0
0.8
1.6
2.4
3.2
4.0
4.8
5.6
6.4
7.2

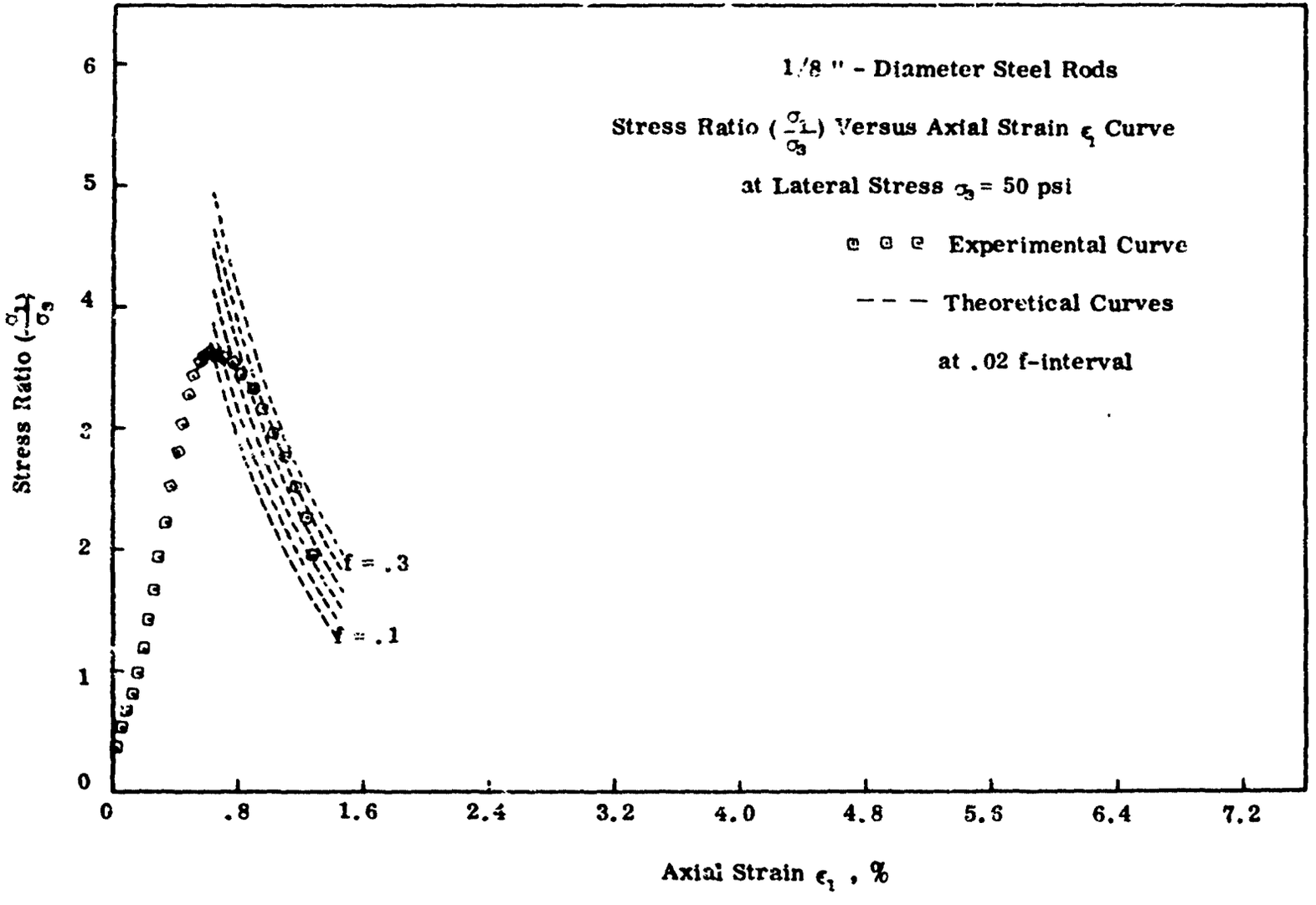
1/8 " - Diameter Steel Rods
Stress Ratio ($\frac{\sigma_1}{\sigma_3}$) Versus Axial Strain ϵ_1 Curve
at Lateral Stress σ_3 = 50 psi
Experimental Curve
Theoretical Curves
at .02 f-interval
f = .3
f = .1
Stress Ratio ($\frac{\sigma_1}{\sigma_3}$)
Axial Strain ϵ_1 , %
0
1
2
3
4
5
6
.8
1.6
2.4
3.2
4.0
4.8
5.6
6.4
7.2

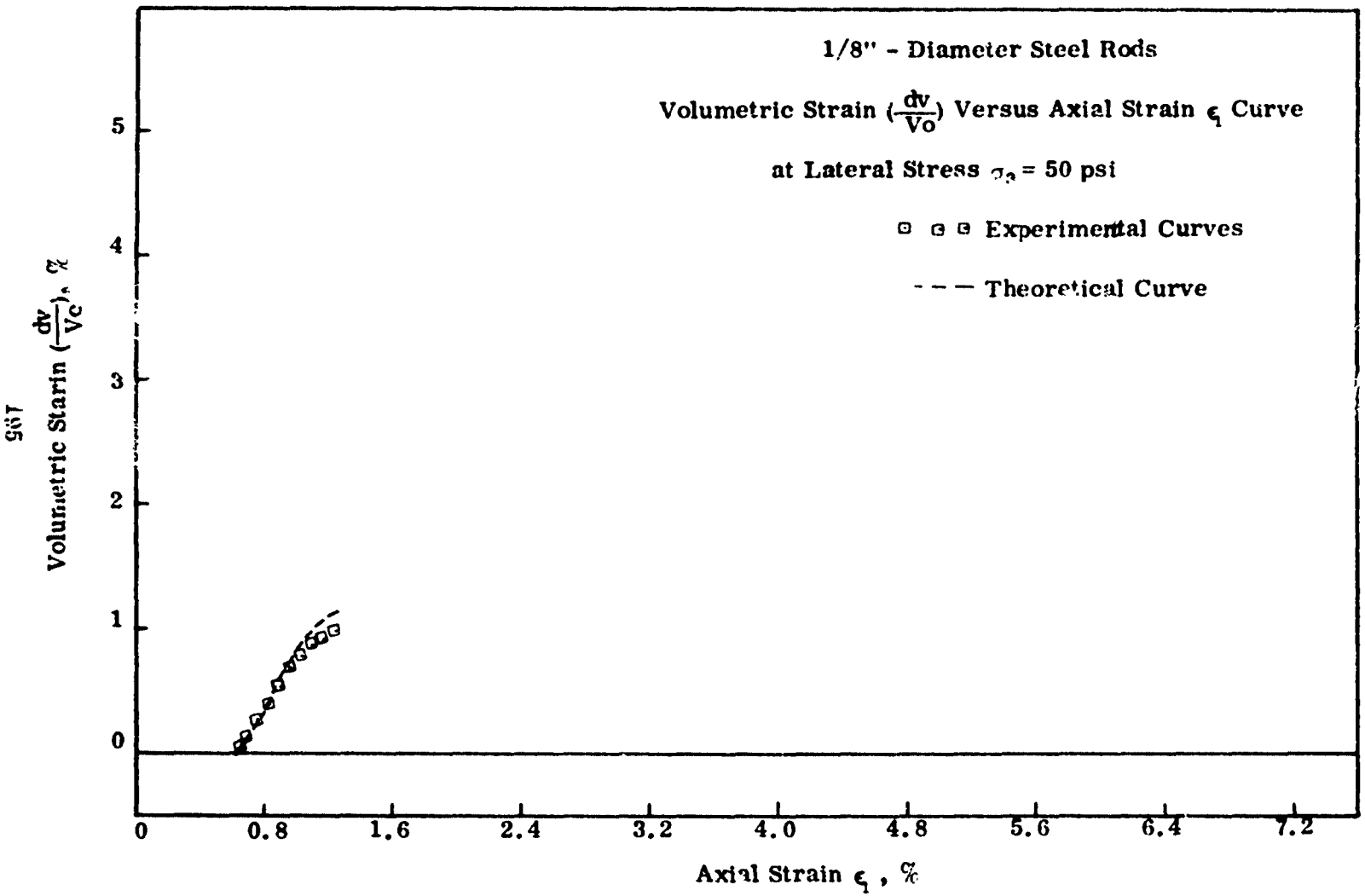
1/8" - Diameter Steel Rods
Volumetric Strain (dv/Vo) Versus Axial Strain ε1 Curve
at Lateral Stress σ3 = 50 psi
Experimental Curves
Theoretical Curve
Volumetric Starin (dv/Vc), %
Axial Strain ε1 , %
0
1
2
3
4
5
0
0.8
1.6
2.4
3.2
4.0
4.8
5.6
6.4
7.2

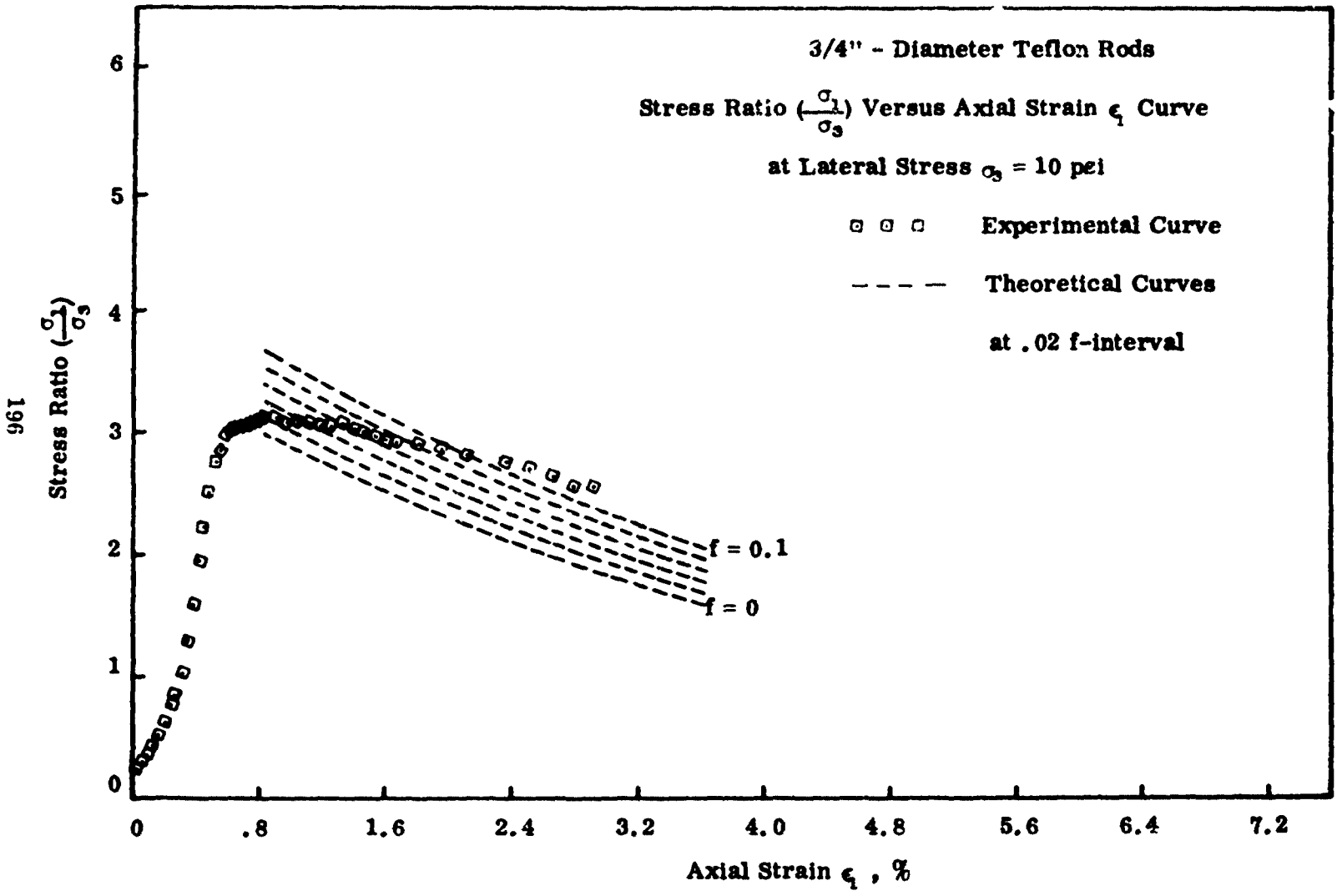
3/4" - Diameter Teflon Rods
Stress Ratio $(\frac{\sigma_1}{\sigma_3})$ Versus Axial Strain ϵ_1 Curve
at Lateral Stress σ_3 = 10 psi
Experimental Curve
Theoretical Curves
at .02 f-interval
f = 0.1
f = 0
Stress Ratio $(\frac{\sigma_1}{\sigma_3})$
Axial Strain ϵ_1 , %
0
1
2
3
4
5
6
.8
1.6
2.4
3.2
4.0
4.8
5.6
6.4
7.2

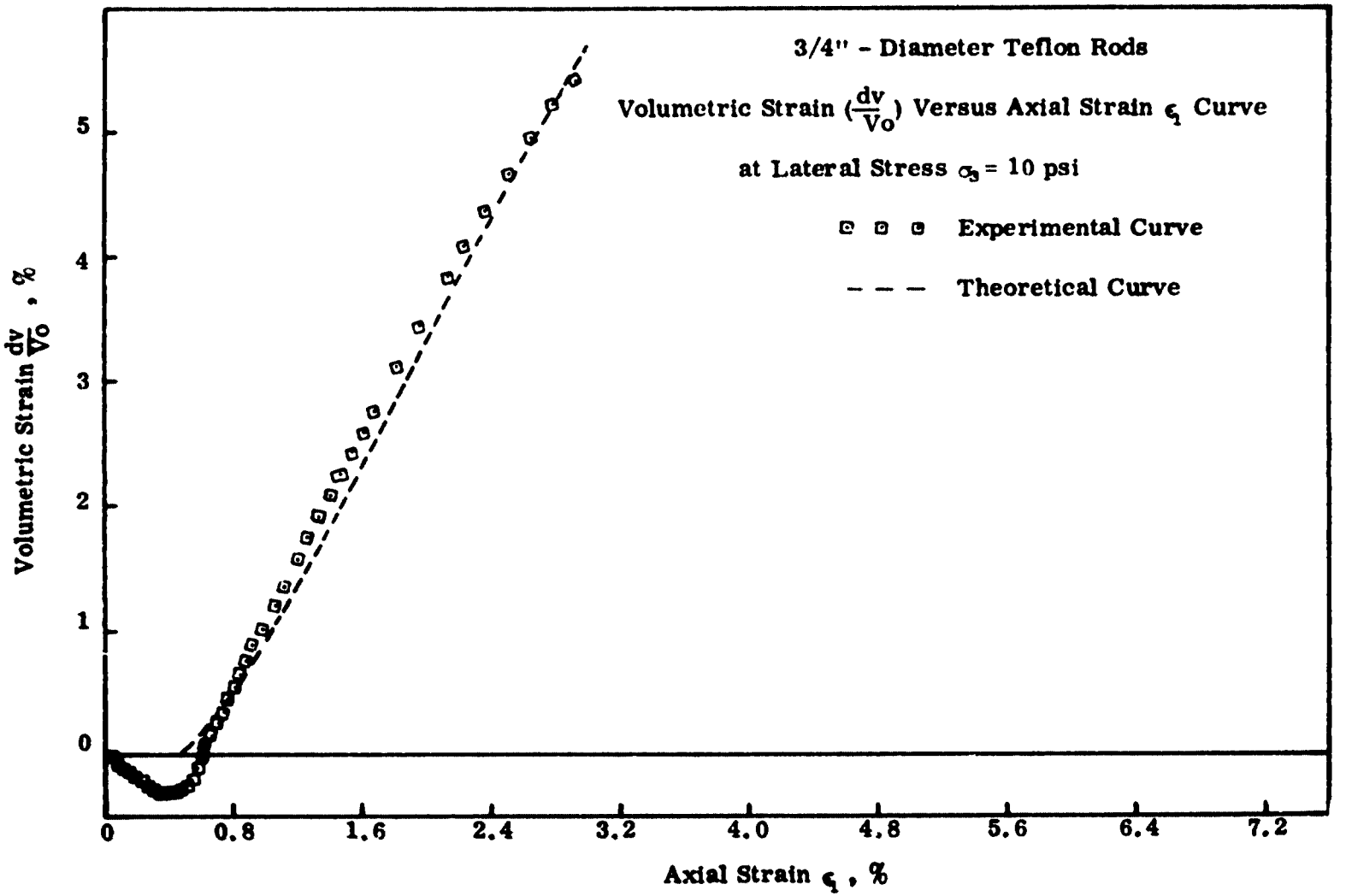
3/4" - Diameter Teflon Rods
Volumetric Strain (dv/Vo) Versus Axial Strain ε1 Curve
at Lateral Stress σ3 = 10 psi
Experimental Curve
Theoretical Curve
Volumetric Strain dv/Vo , %
Axial Strain ε1 , %
0
1
2
3
4
5
0
0.8
1.6
2.4
3.2
4.0
4.8
5.6
6.4
7.2

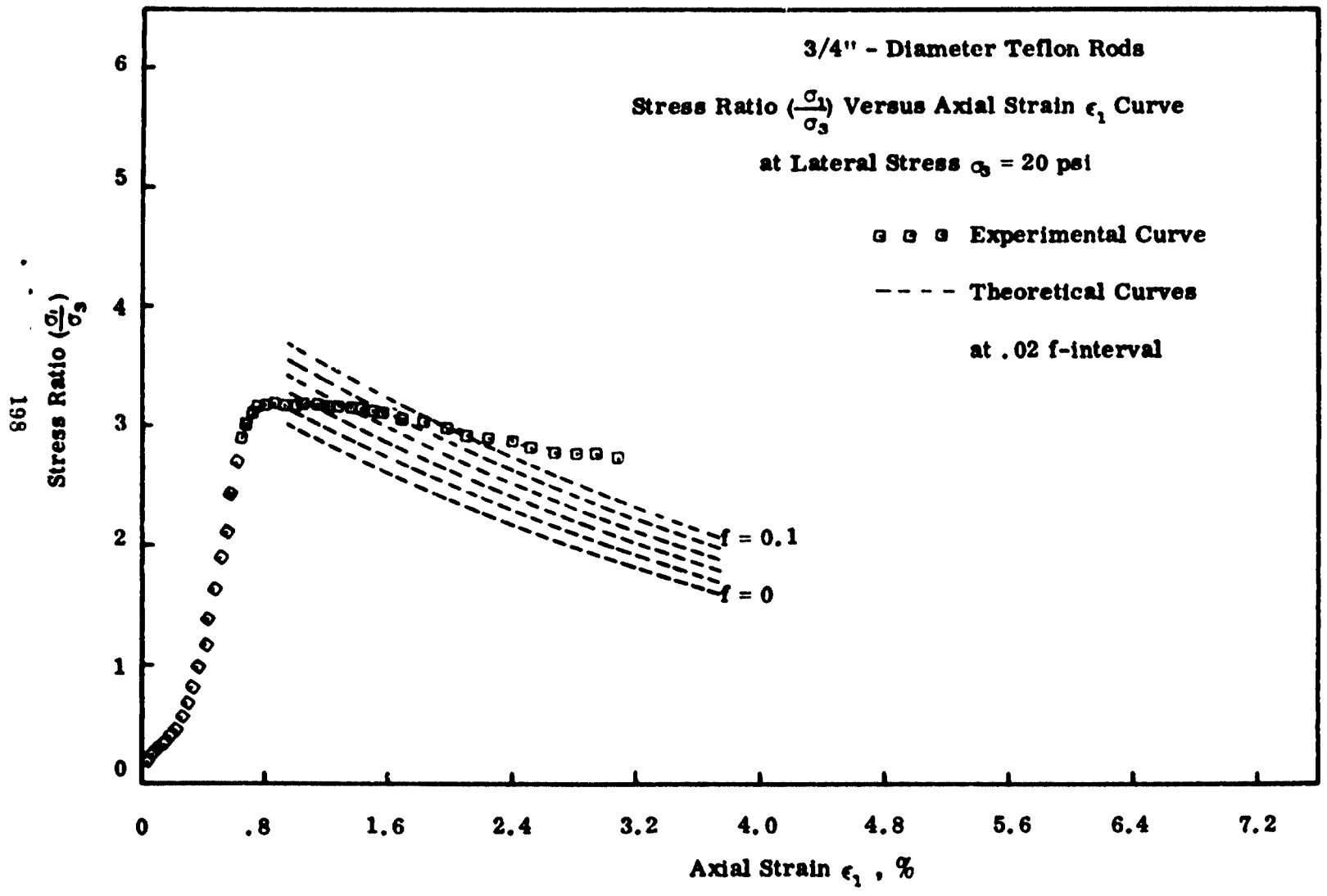
3/4" - Diameter Teflon Rods
Stress Ratio ($\frac{\sigma_1}{\sigma_3}$) Versus Axial Strain ϵ_1 Curve
at Lateral Stress σ_3 = 20 psi
Experimental Curve
Theoretical Curves
at .02 f-interval
f = 0.1
f = 0
Stress Ratio ($\frac{\sigma_1}{\sigma_3}$)
Axial Strain ϵ_1 , %
0
1
2
3
4
5
6
0
.8
1.6
2.4
3.2
4.0
4.8
5.6
6.4
7.2

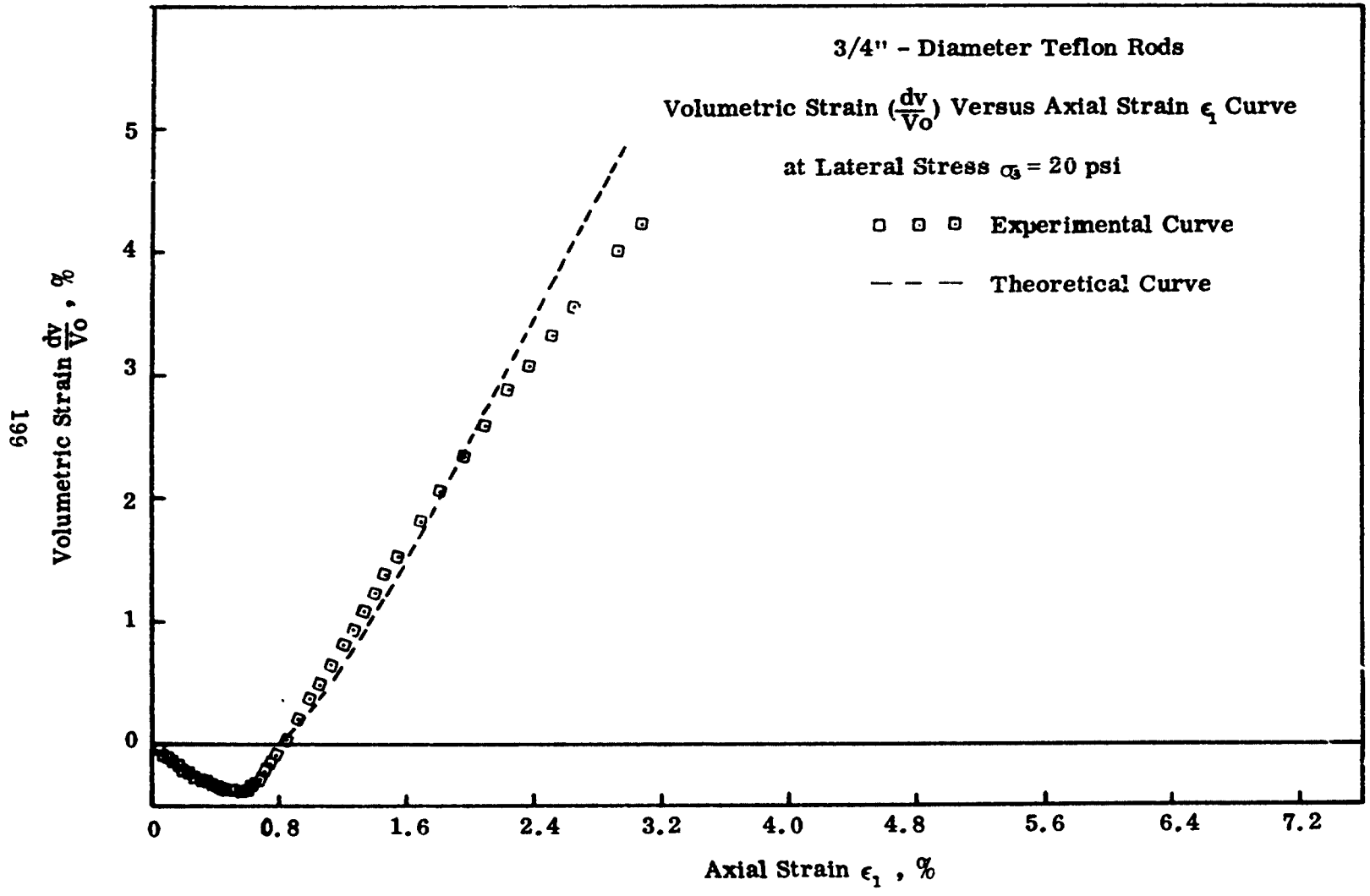
3/4" - Diameter Teflon Rods
Volumetric Strain (dv/Vo) Versus Axial Strain ε1 Curve
at Lateral Stress σ3 = 20 psi
Experimental Curve
Theoretical Curve
Volumetric Strain dv/Vo , %
Axial Strain ε1 , %
0
1
2
3
4
5
0
0.8
1.6
2.4
3.2
4.0
4.8
5.6
6.4
7.2

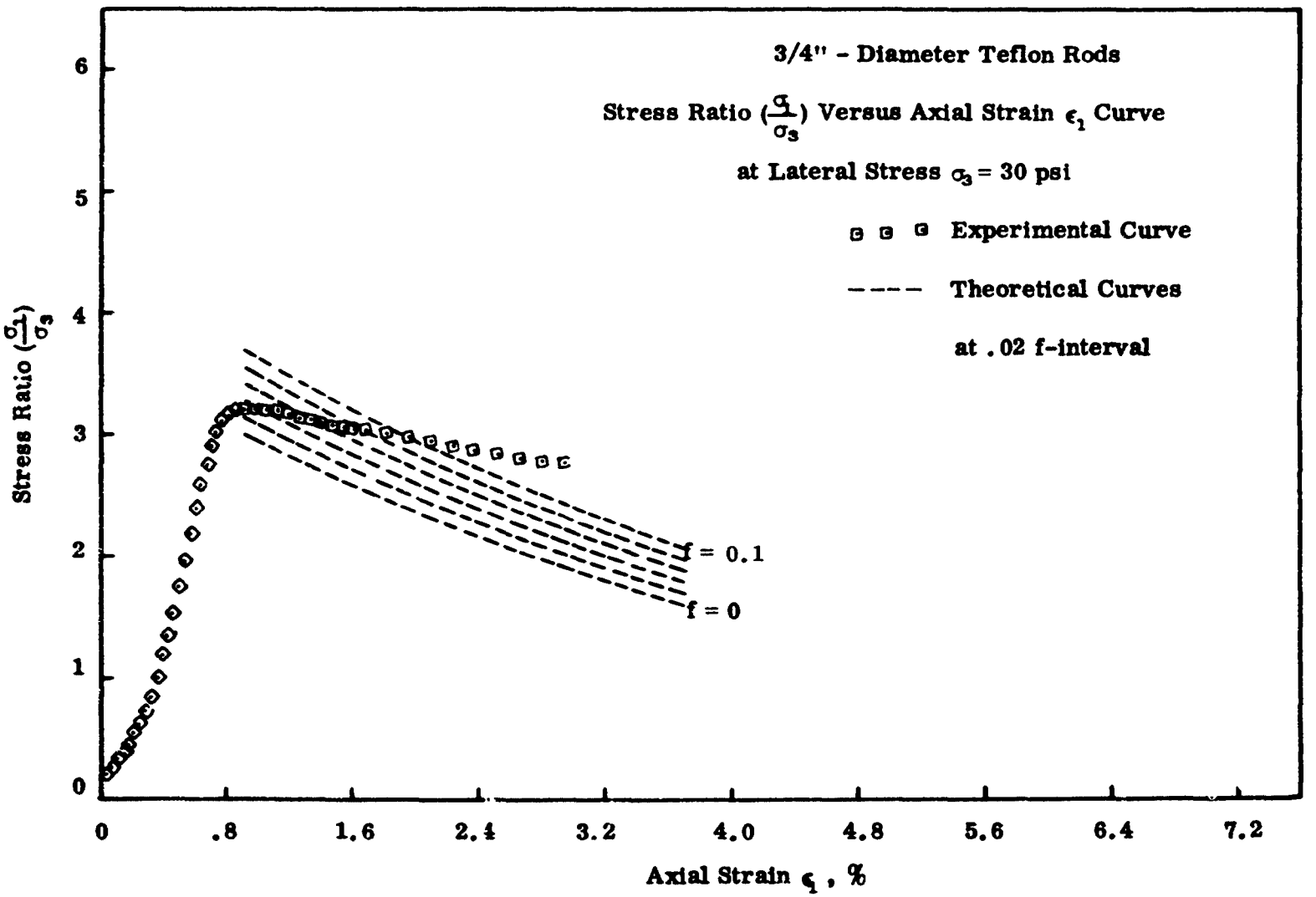
3/4" - Diameter Teflon Rods
Stress Ratio ($\frac{\sigma_1}{\sigma_3}$) Versus Axial Strain ϵ_1 Curve
at Lateral Stress σ_3 = 30 psi
Experimental Curve
Theoretical Curves
at .02 f-interval
f = 0.1
f = 0
Stress Ratio ($\frac{\sigma_1}{\sigma_3}$)
Axial Strain ϵ_1, %
0
1
2
3
4
5
6
.8
1.6
2.4
3.2
4.0
4.8
5.6
6.4
7.2

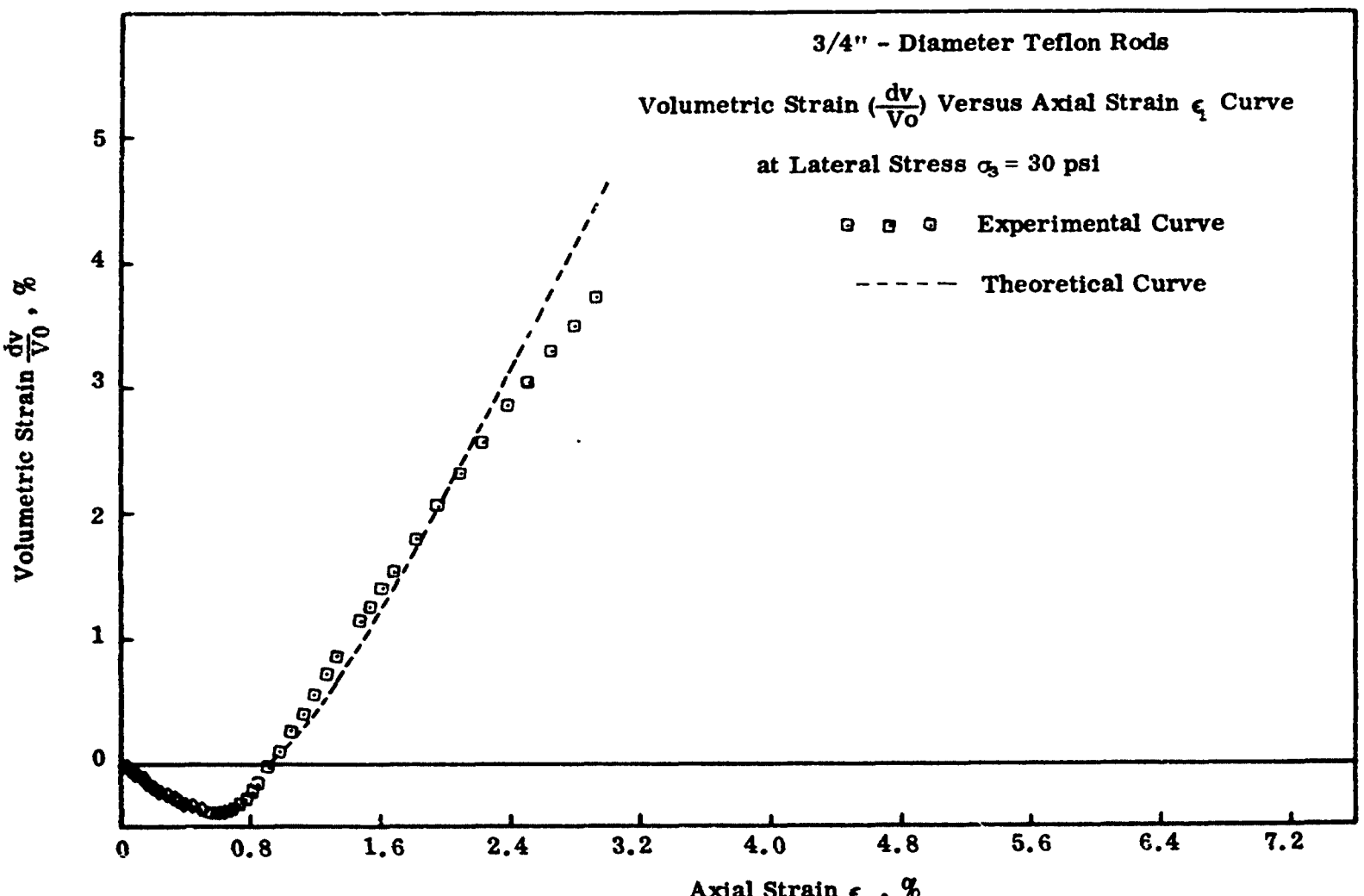
3/4" - Diameter Teflon Rods
Volumetric Strain (dv/Vo) Versus Axial Strain ε1 Curve
at Lateral Stress σ3 = 30 psi
Experimental Curve
Theoretical Curve
Volumetric Strain dv/V0 , %
Axial Strain ε1 , %
0
1
2
3
4
5
0
0.8
1.6
2.4
3.2
4.0
4.8
5.6
6.4
7.2

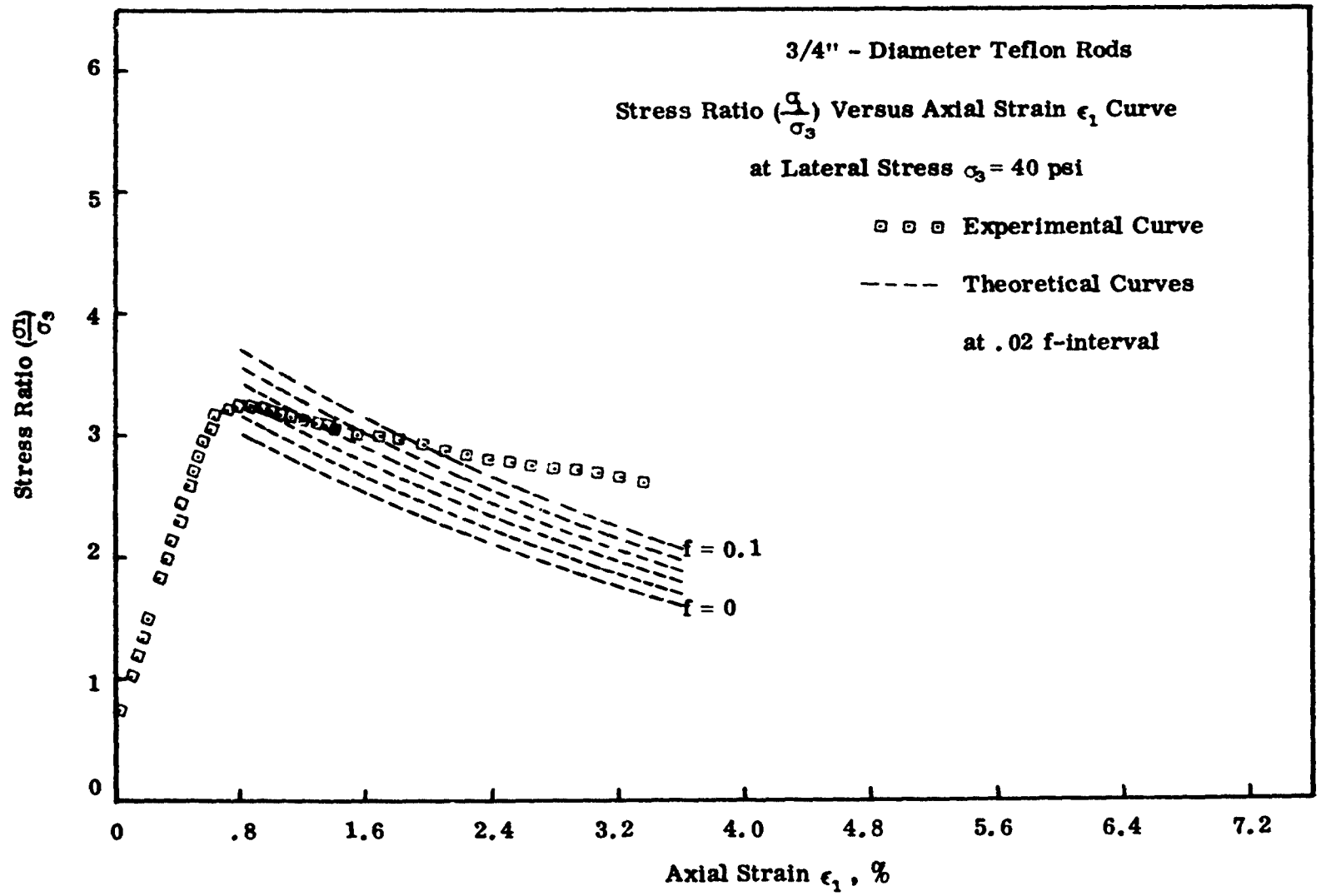
3/4" - Diameter Teflon Rods
Stress Ratio ($\frac{\sigma_1}{\sigma_3}$) Versus Axial Strain ϵ_1 Curve
at Lateral Stress σ_3 = 40 psi
Experimental Curve
Theoretical Curves
at .02 f-interval
f = 0.1
f = 0
Stress Ratio ($\frac{\sigma_1}{\sigma_3}$)
Axial Strain ϵ_1, %
0
1
2
3
4
5
6
0
.8
1.6
2.4
3.2
4.0
4.8
5.6
6.4
7.2

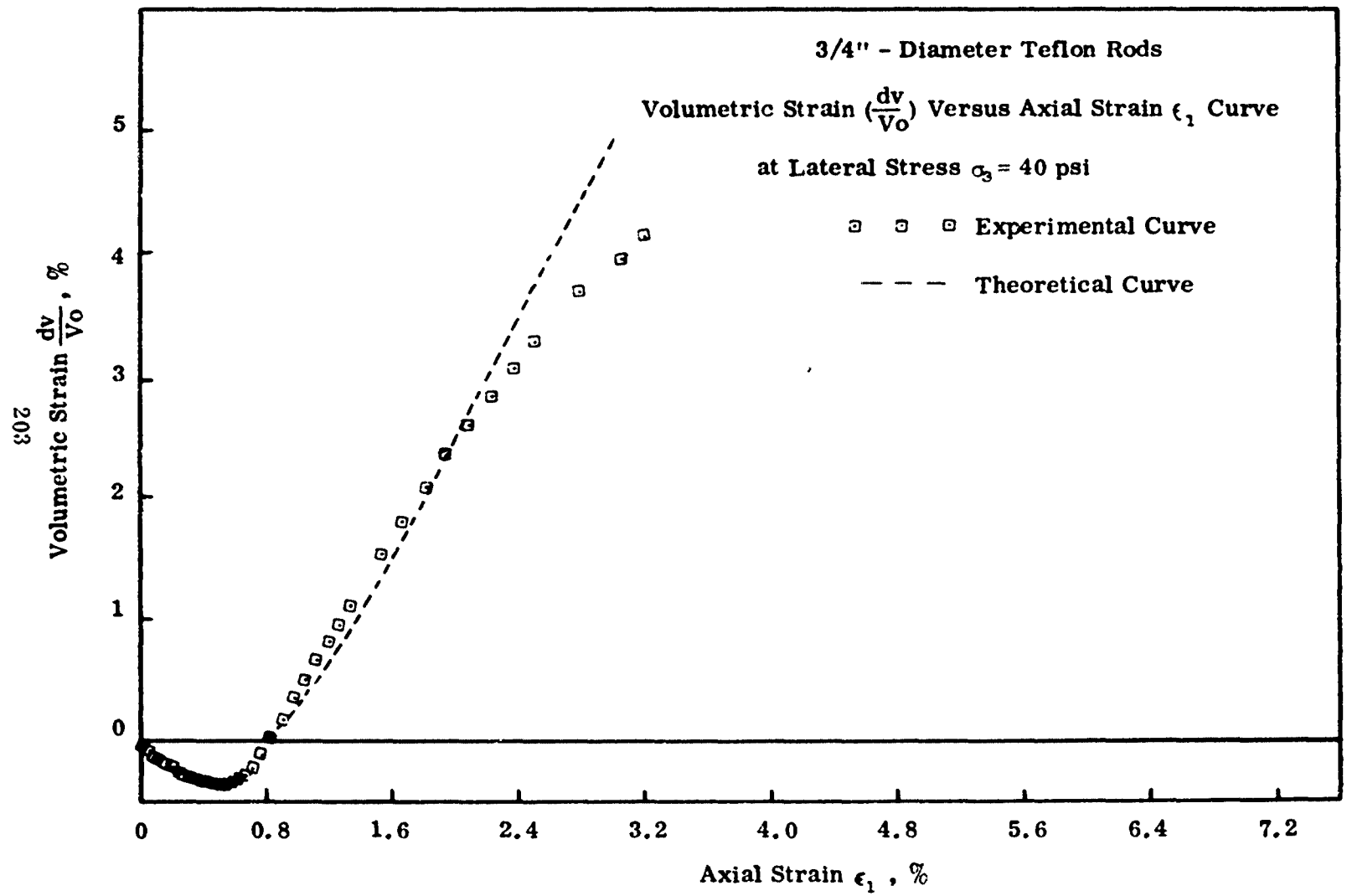
3/4" - Diameter Teflon Rods
Volumetric Strain (dv/Vo) Versus Axial Strain ε1 Curve
at Lateral Stress σ3 = 40 psi
Experimental Curve
Theoretical Curve
Volumetric Strain dv/Vo, %
Axial Strain ε1, %
0
1
2
3
4
5
0
0.8
1.6
2.4
3.2
4.0
4.8
5.6
6.4
7.2

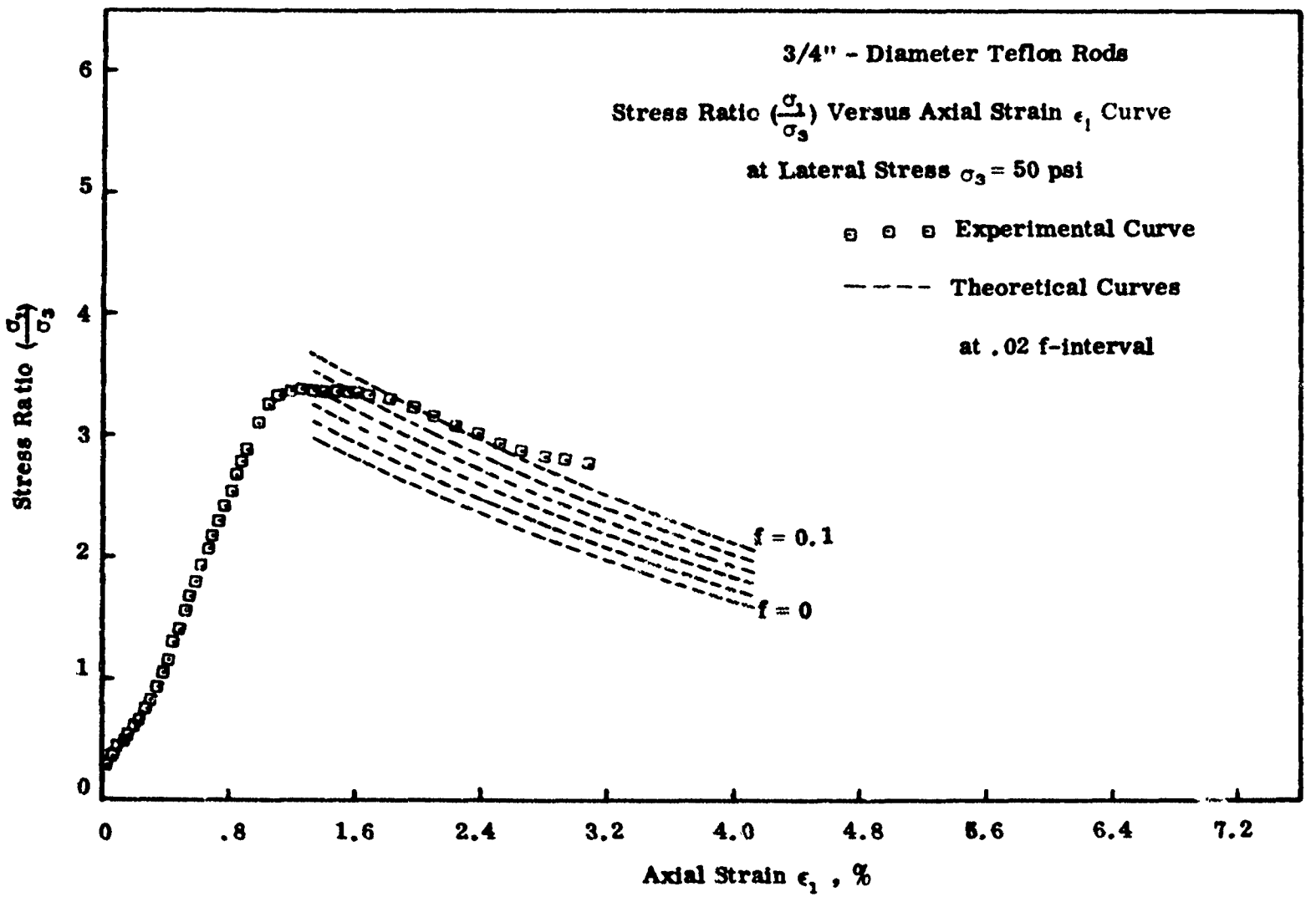
3/4" - Diameter Teflon Rods
Stress Ratio $(\frac{\sigma_1}{\sigma_3})$ Versus Axial Strain ϵ_1 Curve
at Lateral Stress σ_3 = 50 psi
Experimental Curve
Theoretical Curves
at .02 f-interval
f = 0.1
f = 0
Stress Ratio $(\frac{\sigma_1}{\sigma_3})$
Axial Strain ϵ_1 , %
0
1
2
3
4
5
6
0
.8
1.6
2.4
3.2
4.0
4.8
5.6
6.4
7.2

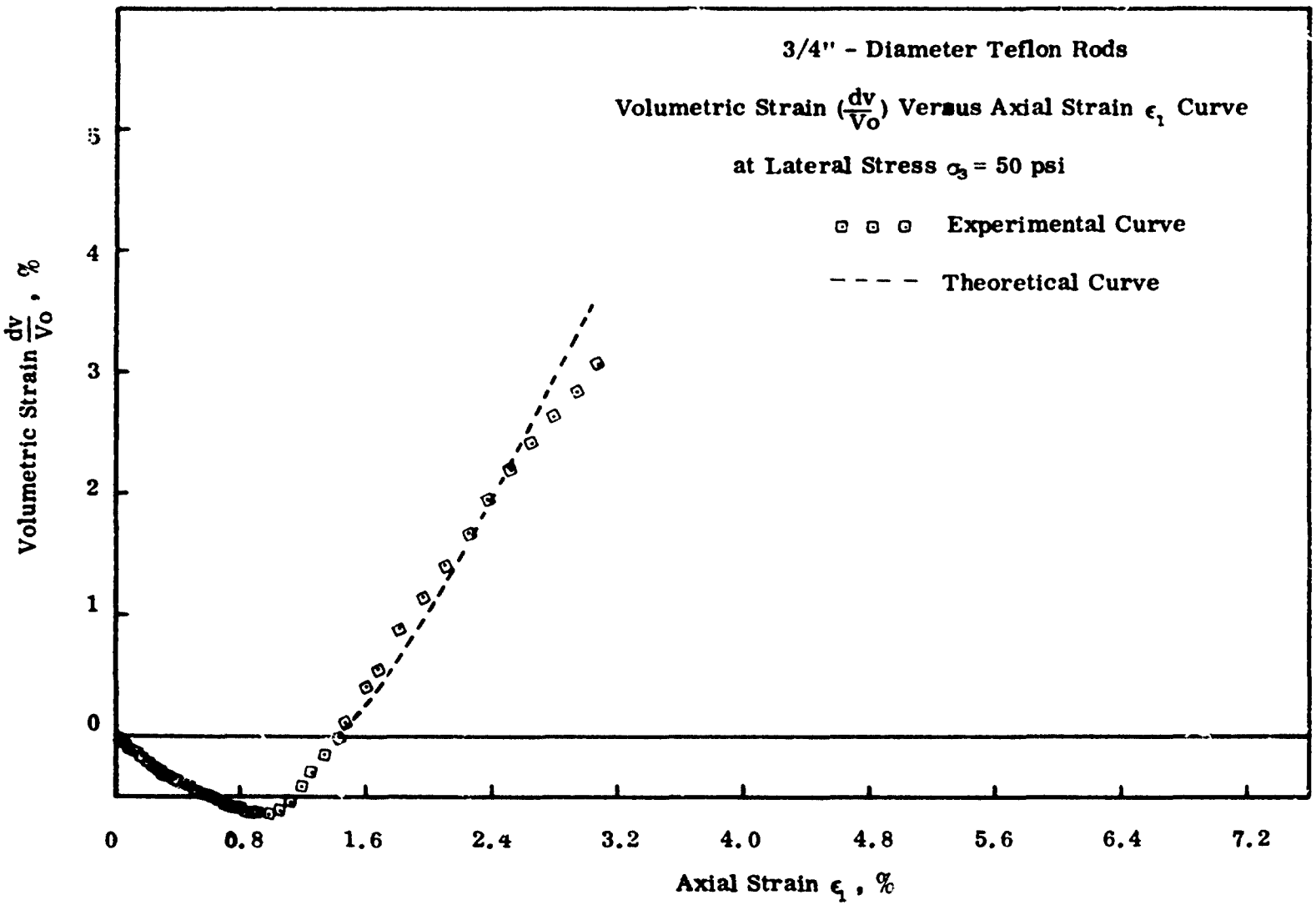
3/4" - Diameter Teflon Rods
Volumetric Strain (dv/Vo) Versus Axial Strain ε1 Curve
at Lateral Stress σ3 = 50 psi
Experimental Curve
Theoretical Curve
Volumetric Strain dv/Vo , %
5
4
3
2
1
0
0
0.8
1.6
2.4
3.2
4.0
4.8
5.6
6.4
7.2
Axial Strain ε1 , %